l'université nantes angers le mans
COMMUNAUTÉ D'UNIVERSITÉS ET ÉTABLISSEMENTS

UNIVERSITÉ DE NANTES

Thèse de Doctorat

Laëtitia SALOU

Mémoire présenté en vue de l'obtention du
grade de Docteur de l'Université de Nantes
sous le label de L'Université Nantes Angers Le Mans

École doctorale : *Biologie-Santé*

Discipline : *Biologie, médecine et santé*
Spécialité : *Biomatériaux*
Unité de recherche : *Inserm UMR 957*

Soutenue le *08/09/2015*
Thèse N° : …

New bioactive surfaces for titanium implants

Research, characterisation and industrial development

JURY

Rapporteurs :	**Stéphane DESCAMPS,** PUPH, CHU Clermont-Ferrand, France **Ståle Petter LYNGSTADAAS**, Pr, Faculty of dentistry, University of Oslo, Norway
Invité(s) :	**Valérie DUMAY,** CEO, Biomedical Tissues SAS, France
Directeur de Thèse :	**Pierre LAYROLLE**, DR, Inserm U957, Lab. Pathophysiologie de la résorption osseuse, Nantes, France
Co-directeur de Thèse :	**Guy LOUARN,** Pr, CNRS –Institute of Materials Jean Rouxel, Nantes, France

ACKNOWLEDGEMENTS

This thesis was carried out in CIFRE contract with Biomedical Tissues, a start up in biomaterials science. This work would not be possible without the collaboration of the Inserm 957, the Laboratory of Pathophysiology of Bone Resorption and bone tumors (LPRO) and the Institute of materials Jean Rouxel of Nantes (IMN-CNRS). This three years gave me two great opportunities to discover both the creativity and curiosity of research world and the financial reality of the business world that found really attractive. The most rewarding was the human relationship, positive and negative, which remain a good personal and professional experience. For all of this, I would like to thank all the people who have contributed for this thesis work.

First of all, I would like to thanks my two supervisors, Pierre LAYROLLE and Guy LOUARN. A special thank for their availability, heplful knowledge and relevant advices during my research. I also would like to thank them for their support during difficult moments and to have been able to resist my strong personality.

Then, I would like to thank Valérie DUMAY for giving me the opportunity to do the pHd work in her company, Biomedical Tissues. A great thank for her support, especially during the last weeks!

I also extend my thanks to each jury member: Stephane DESCAMPS, who honor me reporting my work, and Stå le Petter LYNGSTADAAS for agreeing to come from Norway to be part of the jury.

To finish, I would like to acknowledge some others persons...

- My comity of thesis, Pr Philipp ROSSET, PU PH in Orthopedic and Mireille RICHARD PLOUET, researcher at IMN, who followed my thesis evolution each year. A special thanks to them for all discussion about research and news perspectives.

- Professor Dominique HEYMAN, PU-PH and head of Inserm UMR957, who gave me the opportunity to do my pHd in his laboratory.
- Engin VRANA and Protip company for their collaboration on one part of my thesis topic.
- The surgeons, Alain HOORNAERT, Julien STANOVICCI and Sylvain BRIAND, for their contribution on animale experimentation and article's proofreading.
- Jérome AMIAUD, for his help in histology technics and ImageJ software.
- Yann BORJON-PIRON and Nicolas STEPHAN for all slot and helpful advices for the SEM analysis.
- Anne PISCITELI who gave me the opportunity to use the little-know L.I.B.D. technics in Subatech laboratory.
- Jean-Michel BATARD for his advices and responsiveness. I also want to offer my condolences to Origin MP company.
- Christian GAUTHIER and Thierry ROLAND of Institut Charles Sadron in Strasbourg, who performed some mechanical tests on my sample.
- The biomedical tissues team in particular Cyril D?ARROS, for his scientific reflexion and single support he provided me when I needed it !!
- The LPRO team, for their warm welcome, good mood and also their cakes-Thursday! Thanks to Regis, Kévin, Romain, Marie, Audrey, Camille,? every one !
- My familly and friend... and more specifically, my cousin, Pierre SALOU, for his precious help on LaTeXsoftware.

The last word is not a thank you, but forgiveness. Sorry to all those I have forgotten to mention.

Thank you !

VALORIZATION OF THESIS WORK

Publications

Laëtitia Salou, Alain Hoornaert, Guy Louarn , Pierre Layrolle
Book chapter 20, Bone apposition on nanoporous titanium implants
Handbook of Nanoceramic and Nanocomposite Coatings and Materials
Elsevier
Invitation for writing a book chapter, In Press

Laetitia Salou, Alain Hoornaert, Julien Stanovici, Sylvain Briand, Guy Louarn and Pierre Layrolle
Comparative bone tissue integration of nanostructured and micro-rroughened dental implants
Nanomedicine, 10(5), 741-751 (2015)

Laëtitia Salou, Alain Hoornaert, Guy Louarn, Pierre Layrolle
Enhanced osseointegration of titanium implants by nanostructured surface: an experimental study in rabbits
Acta Biomaterialia, 11, 494-502 (2015)

Rui Xing, **Laetitia Salou**, Sebastien Taxt-Lamolle, Janne Reseland, Stale Haugen Havard Lyngstadaas
Surface hydride on titanium by cathodic polarization promotes human gingival fibroblast growth
Biomedical materials research, 102(5), 1389-98 (2014)

Publication in collaboration

Elisabeth Rieger, Agnes Dupret-Bories, **Laetitia Salou**, Marie-Helene Metz-Boutigue, Pierre Layrolle, Philippe Lavalle, Christian Debry, Nihal Engin Vrana
Controlled implant/soft tissue interaction by nanoscale surface modifications of 3D porous titanium implants
Nanoscale, 7(21), 9908-9918 (2015)

Presentation in congress

2013

Laetitia Salou, Alain Hoornaert, Guy Louarn and Pierre Layrolle. *«Enhanced osseointegration of titanium implants by nanostructured surface area: an experimental study in rabbits»*. **Oral communication at the 25th European Society on Biomaterials – ESB** (Madrid, Spain – September 2013)

Laëtitia Salou, Alain Hoornaert, Guy Louarn and Pierre Layrolle. *«Nanoporous surface of titanium enhances implant osseointegration»*. **Poster communication at Congress "European Association of Osseointegration" – EAO** (Dublin, Ireland – October 2013)

2014

Laëtitia Salou, Alain Hoornaert, Guy Louarn and Pierre Layrolle. *«Bone apposition on nanoporous titanium implants»*. **Oral communication at the 22nd meeting of the European orthopedic research society – EORS** (Nantes, France – July 2014)

Laetitia Salou, Alain Hoornaert, Stanovici Julien, Guy Louarn and Pierre Layrolle. *«Histomorphometric analysis of Ti dental implant osseointegration in a rabbit model: Nanostructured Surface sand-blasted versus acid-etched surface»*. **Poster communication at Congress "European Association of Osseointegration" – EAO** (Roma, Italy – September 2014)

2015

Selected for an **Poster communication at the the 27th European Society on Biomaterials – ESB** (Kraków, Poland – September 2015) : Laëtitia Salou, Engin Vrana, Anne Piscitelli, Pierre Layrolle, Guy Louarn, Valérie Dumay. *«Innovative nanostructured medical devices - A risk of nanoparticles release»*.

CONTENTS

LIST OF ABBREVIATIONS

AFM: Atomic Force Microscopy
ALP: Alkaline Phosphatase
BIC: Bone Implant Contact
BG: Bone Growth
BMP: Bone Morphogenetic Proteins
BS/TS: Bone Surface around Titanium Surface
BSE: Backscattered Electron
CA: Contact Angle
CIFRE: Industrial agreements on Training through research
CTA: Connective Tissue Attachment
CV: Coefficient of Variation
E. Coli:Escherichia coli
EDS: Energy Dispersive X-ray spectrometry
ELI: Extra Low Interstitials
EG: Ethylene Glycol
ENT: Ear Nose Throat
FEG: Field Emission Gun
DMSO: Dimethylsulfoxide
HCl: Hydrochloric acid
HF: hydrofluoric acid
ICP-MS: Inductively Coupled Plasma & mass spectroscopy
JE: Junctional Epithelium
LB: lysogeny broth
LIBD: Laser Induced Breakdown Detection
MEC: Extracellular Matrix (MEC)
MIC: Minimum Inhibitor Value
MO: Metal Oxide
MSC: Mesenchymal Stem Cell
NaCl: Sodium chloride
NT: Non-treated PBS: Phosphate Buffered Saline
PFA: Paraformaldehyde
PTFE: Polytetrafluoroethylene
SLA: Sand blasted with Large grit and Acid-etched

SE: Secondary Electron
SEM: Scanning Electro Microscope
SD: Standard Deviation
TA6V: Titanium allows, Ti + 6% Al + 4% V
Ti cp: Titanium commercial pur
VEGF: Vascular Endothelial Growth Factors
WC: Worst Case
XPS: X-ray Photoelectron Spectroscopy

RESUMÉ

L'implantologie médicale est constamment en croissance et représente un défi majeur dans le domaine de la santé. En France, environ 243 000 implants dentaires, 111 000 arthroplasties de hanche et 71 000 prothèses totale de genou en 2011 ont été implantées d'après des données de 2007, 2011 et 2012. [1, 2, 3]. Le dynamisme de ce marché s'explique par de nombreux facteurs tels que le vieillissement de la population, de nouvelles connaissances dans le traitement des pathologies et de nouvelles exigences en termes de qualité de vie exigeant des dispositifs médicaux de plus en plus performants.

Le titane (ex : Ti cp grade 4) et ses alliages (ex : TA6V) sont largement utilisés comme biomatériaux en raison de leurs bonnes propriétés mécaniques, et une densité moindre par rapport aux autres métaux utilisés dans le médical (ex : Chrome-cobalt, Acier inox 316). Néanmoins, ces propriétés mécaniques varient en fonction de la structure cristalline du matériau : alpha, beta ou une combinaison des deux phases. Le titane possède également une grande résistance à la corrosion naturellement procurée par sa couche d'oxyde native de 2-6 nm, qui se forme instantanément au contact avec l'air ambiant. Cette couche d'oxyde confère également une stabilité chimique, empêchant la libération d'ions métalliques et assurant ainsi la biocompatibilité du titane dans l'environnement du corps humain.

Bien que l'implantation de titane n'entraîne pas de réaction de rejet, le titane est inerte et ne participe pas de manière active à l'intégration tissulaire. Il est alors nécessaire d'attendre trois à six mois pour obtenir une intégration osseuse autour des implants en titane. Cette durée est bien évidement patient-dépendante et varie en fonction de la qualité de l'os [4, 5].

Malgrè un fort taux de succès en implantologie, des problèmes de manque

d'intégration tissulaire (ex : prothèse de trachée) ou d'infection de l'implant peuvent survenir au court et le long terme [6, 7, 8, 9, 10]. Ces infections sont considérées comme la complication la plus grave puisque qu'elles sont difficilement remédiables sauf par le retrait de l'implant (surface contaminée). Ces problèmes concernent aussi bien les implants dentaires (ex : péri-implantites) que les implants orthopédiques (ex : staphylocoque doré pour les fixateurs percutanés).

Dans le cadre des implants intra-osseux, la bonne intégration du tissu osseux avec la surface de l'implant semble être pertinente pour le succès clinique et la durée de vie de l'implant. Plusieurs facteurs peuvent jouer un rôle sur cette intégration: la géométrie de l'implant, mais aussi la nature du matériau, sa surface, la préparation du site d'implantation, la technique chirurgicale utilisée ou même les conditions de mise en charge de l'implant [5]. Depuis le début des années 1980, des études ont porté sur les traitements de surface afin d'améliorer l'ostéointégration des implants métalliques. Différents travaux ont montré que les propriétés de surface telles que la rugosité, la mouillabilité, la charge électrique ou la composition chimique et pouvaient moduler l'adhérence, la prolifération et la différenciation des cellules [11, 12, 13, 14, 15]. Plusieurs traitements de surface ont été développés et sont actuellement commercialisés : la projection plasma, l'anodisation colorée ou spark (ex : $TiUnite^{®}$, Nobel Biocare), le sablage (ex : la surface $TiOblast^{TM}$, Astra Tech), le mordancage acide (ex : la surface $Osseotite^{®}$, Biomed 3i) ou bien encore une combinaison des deux derniers procédés de sablage et de mordançage (ex : $SLA^{®}$, Straumann).

La majorité de ces traitements de surface produisent une rugosité micrométrique uniquement perceptible à l'échelle cellulaire. Avec le développement des nano-technologies, de nouveaux procédés permettent une modification de la surface à l'échelle des protéines. Ainsi les protéines de la matrice extracellulaire telles que intégrines peuvent contrôler l'adhésion des points focaux de la cellule et entrainer un certain nombre de changements au niveau de la morphologie cellulaire et de l'expression des gènes [16, 17, 18]. La modulation de protéines kinases associées à Rho (ROCK), médiateur des la tension interne du cytosquelette, conduit à la génération de la force contractile de la cellule. Celles-ci impliquent la régulation de l'expression du gène de la matrice extracellulaire et donc la différenciation des cellules souches mésenchymateuses (CSM) en cellules spécifiques. Ce phénomène appelé mécanostranduction a par ailleurs été démontré dans plusieurs publications scientifiques utilisant des nano-surfaces [19, 20, 21, 22].

Actuellement, plusieurs approches pour modifier la surface à l'échelle nanométrique sont possibles : les méthodes lithographiques, le traitement hydrothermale, l'anodisation, les dépôts de nanoparticules ou encore le greffage moléculaire.

Dans cette thèse, nous nous intéressons principalement à l'élaboration de structure de nanotubes et nanopores de TiO_2 via un procédé simple et dit "rentable": l'anodisation. L'objectif global de cette thèse concerne l'étude du potentiel de cette surface en nid d'abeille en terme d'applications médicales. Ce manuscrit se dessine alors en 3 étapes que sont : la caractérisation physico-chimique de la surface, la caractérisation biologique (ici, *in vivo*) et son application directe sur des dispositifs médicaux (DM) tels que les implants dentaires et les prothèses de trachée. Ce projet de thèse a été réalisé dans le cadre d'un financement CIFRE (Conventions Industrielles de Formation par la REcherche) au sein de l'entreprise Biomedical Tissue à Nantes.

Pour réaliser ce projet, nous avons adapté le protocole d'anodisation utilisé pendant la précédente thèse de Sandrine Lavenus, également inspiré d'une publication de Seughan Oh de 2009 [23]. Ce procédé utilise un mode potentiostatique et une solution électrolytique de première génération qu'il a fallu adapter afin de ne pas empiéter sur des brevets de concurrents direct [24, 25]. L'anodisation en présence de suffisamment de fluorure permet à la fois la formation et la dissolution chimique de la couche de TiO_2. Un bon équilibre entre ces deux phénomènes conduit à la création d'une couche de TiO_2 en structure d'éponge ou bien même une structure tubulaire respectivement appelés nanopores et nanotubes. Le principal inconvénient de l'anodisation est que la structure formée est amorphe et donc thermodynaniquement instable. Le recuit est alors utilisé afin de transformer cette phase amorphe en phase d'anatase, de brookite, de rutile ou d'une combinaison de ces phases. L'état de l'art du procédé de nanostructuration a été publié dans un chapitre de livre publié par Elsevier et présenté dans le premier chapitre de cette thèse.

La réalisation de ces structures a été opérée sur des échantillons de composition diverses (Ti cp, TA6V) et géométries variées : pastilles, implants prototypes, implants dentaires, prothèses de trachée et leur gabarits. L'analyse de la nano-surface de titane a sollicité l'utilisation de diverses caractérisations de surface (MEB, AFM CA, XPS, RAMAN). Elle a nécessité aussi des techniques spécifiques aux nano-surfaces tel que le nanoscratch test et la nanotribologie pour caractériser l'adhésion mécanique des revêtements. Enfin des caractérisation avancées ont été mises en oeuvre tels que le LIBD, capable de détecter des colloïdes de 5 nm en solution faiblement concentrée (ppt). Les principes de ces techniques sont détaillées dans le chapitre 2.

La caractérisation physico-chimique est présentée dans le chapitre 3. A l'échelle macroscopique, le traitement d'anodisation nanostructurée entraine une coloration par phénomène d'interférences constructives. A l'échelle submicroscopique, les analyses révèlent un diamètre de pores facilement contrôlable de 30 à 100 nm par modification de la tension d'anodisation appliquée. Les

nanotubes de TiO_2 formés à 20 V sur les pastilles de titane présentent une bonne uniformité avec une épaisseur d'environ 150 nm. Une tension d'anodisation plus faible de 10 V permet d'obtenir un réseau de nanopores tout aussi homogène et présentant un comportement hydrophile en terme de mouillabilité. Bien que le traitement consiste en une attaque chimique de la surface, les résultats ne montrent aucune modification de la rugosité initiale de la surface de titane. Néanmoins, la structure initiale de la surface (composition alpha, beta, ou mixte) joue un rôle majeur sur l'homogénéité de la surface. La phase β, présente dans les alliages de TA6V, ne réagit pas de la même manière à l'anodisation que la phase α. Dans nos conditions expérimentales, la phase beta ne forme pas de nanoporosité créant ainsi une double structure micro- et nano- modifiée.

Concernant l'étape de recuit, l'étude de la température de recuit (de 300 à 600 ˚ C), du temps de recuit (de 0.5 à 2 h) et de la surface traitée (Ti cp, TA6V) ont montré avoir un impact sur la morphologie des nanotubes et la structure cristalline résultante. La structure initialement amorphe, est transformée à basse température (de 300 ˚ C à 450 ˚ C) en phase anatase qui est elle-même progressivement transformée en phase rutile. La conversion s'effectue plus ou moins rapidement suivant le temps de recuit, le type de nanostructure et le type de substrat. Néanmoins pour des températures supérieures à 550 ˚ C, la structure devient complètement composée de phase rutile entrainant la formation de cristaux de rutile émergeant en surface et détériorant ainsi la nanostructure.

Enfin, les analyses XPS nous ont permis de confirmer une absence de contaminants de surface liée aux acides utilisés lors du procédé électrochimique d'anodisation. Les résultats montrent également une présence d'ions fluorure provenant de l'électrolyte et ayant migré à travers la couche poreuse de dioxyde de titane lors du procédé.

La seconde partie de cette thèse a concerné la caractérisation des effets biologiques de la nanostructure de TiO_2. Une étude *in vivo* a été effectuée afin de comparer l'ostéoingration de notre nano-surface avec d'autres surfaces plus rugueuses : une surface brute d'usinage (MA), une surface type SLA® de Straumann (MICRO) et une surface nanostructurée via le procédé d'anodisation (NANO). Après traitement, les implants prototypes ont été implantés dans les deux épiphyses fémorales de lapin. Après quatre semaines d'implantation, des essais de traction et la caractérisation des tissus environnant ont été réalisés pour caractériser l'ostéointégration des différentes surface d'implants. Les résultats ont montré que l'ancrage osseux de la surface NANO était similaire à celle des implants MICRO, alors que la rugosité était 3 fois plus faible (0,5 vs 1,5 μm). La surface NANO présente également une meilleure apposition osseuse (Contact os-implant (BIC) et formation osseuse dans la cavité de l'implant (BG)) que les deux autres surfaces, mais les résultats ne sont pas statistique-

ment significatifs. Cette étude a été publié dans le journal Acta biomaterialia l'article N° 1 de la thèse.

Enfin la dernière partie de la thèse, concerne l'application du traitement de surface directement sur des dispositifs médicaux : les implants dentaires et les prothèses de trachée. L'anodisation d'implants dentaires a été réalisée avec succès et révèle des effets biologiques similaires lors de l'implantation dans le même modèle chez le lapin. Les résultats de l'étude *in vivo* sont visibles dans l'article N° 2 publié dans le journal Nanomedecine. Par ailleurs, le procédé unitaire a été validé en 2013 par un organisme agréé (G-MED) pour le traitement de surface d'implants dentaires et orthopédiques. Néanmoins, ce procédé unitaire ne peut difficilement s'appliquer en l'état dans le cadre de lot très important comme dans le cas des implants dentaires. Il nécessite alors un "scaling up". Des premiers résultats ont montré une bonne homogénéité de surface lors du traitement de 12 implants simultanément en mode galvanostatique (intensité fixée), néanmoins ce changement d'échelle nécessite davantage de recherche vis-à-vis de sa complexité (agitation, température du bain, taille de la cuve, etc).

L'utilisation des nanostructures pour l'intégration de surface avec les tissus mous a également été exploré dans le cadre d'un application ORL sur des prothèses de trachée. Des résultats *in vitro* et *in vivo* en sous-cutané chez le rat ont montré une meilleure adsorption des protéines et un meilleure prolifération tissulaire pour les implants nanostructurés que pour le groupe non traités. Ces résultats ont été publié dans le journal Nanoscale, article N° 3 de la thèse. Néanmoins, la même problématique de "scaling up"a été observée pour l'application aux prothèses de trachée dont la taille est plus importante et dont la géométrie est plus complexe que les implants dentaires. Bien que l'obtention d'un traitement de surface relativement homogène, sur les gabarits de prothèse de trachée, on observe un phénomène de délamination de la nanostructure. Elle s'effectue par nanotubes individuels mais aussi par plaques ou agrégats. La délamination est visble en surface de l'échantillon mais également dans le bain de rinçage (eau distillée) utilisé pour nettoyer l'implant post-anodisation. Après avoir épluché la littérature, très censurée sur ce genre de phénomène, la délamination proviendrait des ions fluorures présent dans la nanostructure. Ces ions qui pourraient être un atout pour la cicatrisation osseuse, forment avec le titane une espèce chimique soluble dans l'eau ($[TiF_6]^{2-}$) et, qui part sa dissolution, va fragiliser l'adhésion la nano-surface [26]. Le rinçage à l'eau a donc été remplacé par un rinçage à l'éthanol pur. Le recuit à 500 $^\circ$C permet également de réduire la concentration en fluorure réduite par évaporation de TiF_4 [27]. Néanmoins, les résultats LIBD révèlent toujours la présence de nanoparticules relarguées lors de l'immersion de la prothèse dans une solution physiologique.

En présence de fluides biologiques, la prothèse est donc susceptible de relarguer des nanoparticles. Des essais mécaniques de scratch test ne révèlent aucune différence de tenue mécanique entre les surfaces obtenues sur les implants dentaires et celle des gabarits de prothèse de trachée. Néanmoins les résultats à l'usure sont plus faibles que ceux présenté par la littérature, pour un même procédé appliqué sur des implants orthopédiques [28].

D'un point de vue réglementaire, ces problématiques de nanoparticules relarguées est un sujet actuel puisque la nouvelle réglementation européenne sur les dispositifs médicaux incorporant des nanomatériaux va entrer en vigueur courant 2015. Ainsi, les dispositifs incorporant des nanomatériaux intégreront la classe III, DM à haut risque. Bien que la tenue mécanique peut être améliorée, la réglementation va entrainer quelques difficultés supplémentaires pour proposer ces nano surfaces aux industriels du milieu médical. Par exemple, les implants dentaires initialement de classe IIb, qui passeront alors en classe III avec la présence de nanostructure en surface et entrainant alors davantage de contrainte réglementaire pour le fabriquant.

En conclusion, ce travail a permis de démontrer l'intêret des surfaces nanostructurées pour améliorer l'intégration tissulaire des implants. Les perspectives possibles concernent l'optimisation de la nanostructure. L'anodisation permet de réaliser des nanostructures de morphologies différentes (nanopores, nanotubes). Or, il a été montré que le design de la nano-surface pouvait induire un comportement cellulaire différent [29]. Il serait alors intéressant de comparer l'impacte de ces deux structures (nanopores, nanotubes) sur l'intégration osseuse et tissulaire. De plus, La structure cristalline formée lors du recuit entraine la formation d'une phase stable (rutile) ou métastable (anatase, brookite) qui peuvent améliorer la bioactivité de la surface par rapport à une surface amorphe [30, 31]. Néanmoins, une étude sur la composition cristalline idéale serait une piste d'optimisation de la surface. Par ailleurs, Kim et al. ont également montré que le potentiel zéta des nanotubes de TiO_2 pouvait varier suivant le pH de l'électrolyte utilisé [32]. Pour un électrolyte de troisième génération, la surface est chargée positivement pour un pH 3 alors que pour un pH plus basique la charge de la surface devient négative. Ainsi, en créant une surface d'implant chargée négativement pourrait permettre d'attirer les cations nécessaires pour la formation osseuse (ex : calcium Ca^{2+}, phosphate ${PO_4}^{2-}$, magnésium Mg^{2+}, Zinc Zn^{2+}). Dans cette thèse, il est également discuté d'utiliser ces nano-surfaces comme support pour le relargage d'agent antibactérien comme le zinc. Cet élément combine à la fois une activité antibactérienne et des effets anabolisants sur le métabolisme osseux [33, 34, 35]. Ainsi la combinaison de la morphologies de la nanostructure, la composition cristalline, la charge de surface et l'incorporation d'agent anti-bactérien pourraient permettre de créer

une surface prometteuse pour des applications médicales.

GENERAL INTRODUCTION

Medical implantology is a major challenge for health and is a field enjoying continuous growth. In France, around 243,000 dental implants have been implanted per year in 2007, 111,000 hip joint replacements in 2011 and 71,000 total knee prosthesis in 2012 [1, 2, 3]. The dynamics of this market are driven by many factors including population ageing, new knowledge in pathology treatment and new demands in terms of quality of life requiring more successful medical devices. Titanium is a widely-used biomaterial because of its mechanical properties, corrosion resistance and biocompatibility: it does not provoke a rejection reaction. However, titanium is inert, meaning it is then necessary to wait three to six months before obtaining full bone tissue-integration around titanium implants. This delay depends on bone quality and other patient conditions. This bone-tissue integration appears to be a relevant factor in clinical success and implant life time [36]. Despite a high rate of success in implantology, we have noted persistent problems in the long term: peri-implantitis, for dental implants [37], infection, for intra-osseous orthopaedic implants[9] or poor integration with soft tissue for tracheal prostheses.

Several works have shown that surface properties such as roughness, wettability, electric charge or chemical composition may modulate adhesion, proliferation and cell differentiation[11, 12, 13, 14, 38]. Since the beginning of the 1980s, studies have focused on surface treatments as a means of enhancing the osseointegration of metal implants.

Most surface treatments produce random, micrometric roughness and can only play a role at the cellular scale. With the development of new nanotechnologies, surface treatments are being proposed that modify the surface at the protein scale. In this way, proteins in the extracellular matrix (ECM), such as integrins, may control focal cell adhesion and alter a number of metabolic

changes and cellular morphology. Modulation of Rho-associated kinase (ROCK), the principal mediator of cytoskeletal tension, leads to contractile force generation and involves regulation of extracellular matrix gene expression and thus differentiation of mesenchymal stem cells (MSC). Several studies prove this mechanostranduction phenomenon and have shown higher cell attachment and MSC differentiation into osteoblasts using nano-surfaces [19, 20, 21, 22].

The objective of this thesis is to propose a new bioactive nano-surface for industrial applications in order to respond to current demands in biomedical devices. These nano-surfaces may be created by different means, but the simplest and most cost-effective process is anodisation. The biological effects of nano-porous surfaces have already been studied in our laboratory and others [23, 39, 40, 41, 42]. However, only a few publications have applied this surface treatment directly to medical devices [28, 43, 44]. Our work focuses on the preparation of nanostructuration of titanium implants by anodisation, and their physicochemical and biological characterisation. All this work have been supported financially by the company Biomedical Tissues and the "Association Nationale de la Recherche et de la Technologie"(ANRT).

The first chapter of this manuscript is an opportunity to establish a state of the art of knowledge of titanium and the biomedical questions it raises, the use of surface treatments and the impact of a change at the nanoscale on cell behaviour. This first part allows us to place the theoretical basis and context of the thesis topic.

In the second chapter, we develop the materials and methods used. The work carried out during this thesis largely concerns the development of the anodisation process to create nano-modifications, as well as the use of various methods for characterising surfaces at the nanometer level. The mechanical equipment and particle analyser used in our experiments will then be exposed. To conclude, the biological tools used to qualify the biocompatiblity of our nano-surfaces are described.

The third chapter is devoted to both physical and chemical characterisation, and quantifying the biological effect of custom-made implants. Most of the characterisation of the titania nanotubes was carried out using nano or surface techniques, analysis of the chemicals, and structural composition. Osseointegration on custom-made titanium implants with our nano-surface was then compared to other types of surface.

A fourth chapter presents the medical applications of this nano-surface treatment using our anodisation process. The results obtained with dental implants

in an *in vivo* study in rabbits are given. The validation of the process according to the EN ISO 13485 directive applied to medical devices is then exposed. Extrapolation of the process to an industrial scale is mentioned for batches with several implants, large size or complex-shaped implants (*e.g.* tracheal prostheses) leading to a number of issues regarding reproducibility and the delamination of the nano-porous layer.

To conclude, the incorporation and release of elements such as zinc are approached as an alternative method for implant treatment requiring both tissue integration and antibacterial effects. The last topic addressed in this thesis deals with the new European regulation regarding medical devices incorporating nanomaterials. As many concerns are related to the safety of nanomaterials on surface implants, the regulatory approval for human use may be difficult to obtain. Finally, a summary of the results of our research and development is given briefly. The short and long term perspectives of optimisation of the honey comb surface in medicine are discussed.

CHAPTER

1

STATE OF THE ART: SURFACE TREATMENTS FOR MEDICAL APPLICATIONS

Biomaterials are defined as "non viable materials used in medical devices intended to interact with biological systems"(Consensus conference in 1986). This field involves medicine, materials science and multi-scale characterisation, as well as materials in biological environments (**Figure 1.1**).

Biomaterials are commonly used as elements for reconstructing, helping or replacing tissues damaged, weakened or failing as a result of age, accident or disease. Biomaterials can be used to restore different types of tissue such as bone, cartilage, ligament, tendon, and skin, and thus have a vast number of applications in the cardiovascular field, ophthalmology, dentistry, stomatology, and various types of surgery such as plastic, orthopaedic or general.

There are two different yet important key notions. **Biocompatibility** is the ability of a material to perform with an appropriate host response, and thus to not induce rejection (inert) of the implant by the host in a specific application. **Biointegration** is the ability of a material to be colonised by living cells and tissues. Bioactive materials can be inserted into the human body and become fixed and stable in the surrounding natural soft or bone tissues. A biocompatible material is not necessarily biointegrated in certain types of application (i.e. urinary catheters).

Different materials are used for implants. These include polymers, ceram-

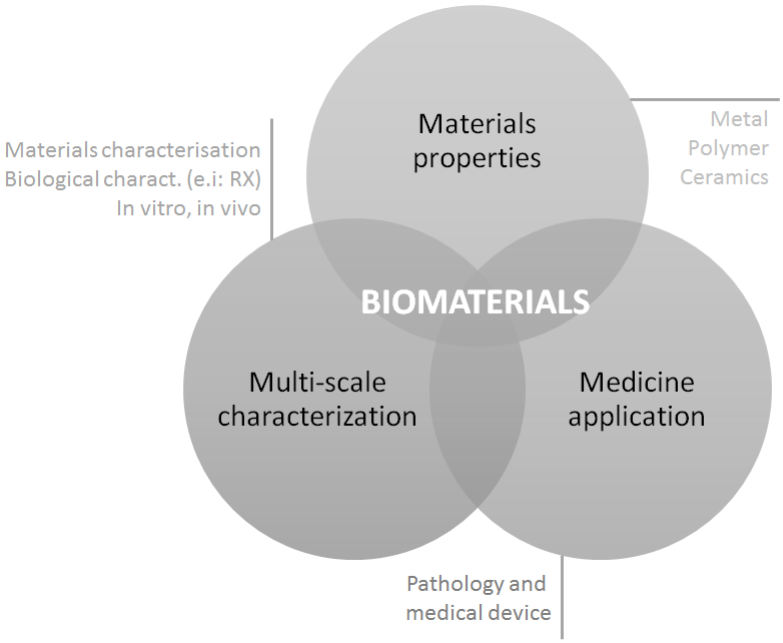

Figure 1.1: Materials in medical applications

ics, metals, composites and natural products. Each material has interesting properties that are useful for certain specific medical applications [45]. The **natural materials** used in implantology are logically biocompatible due to their biological origin. This not only concerns he transplants (i.e. autografts, allografts, xenografts) but also collagen-derived products. Other natural materials are currently in development, such as polysaccharides, cellulose, and coral. Research is also focusing on **hybrid biomaterials** composed of a material matrix incorporating cultured stem cells or growth factors for tissue regeneration.

Numerous **polymers** are used as biomaterials: thermoplastic polyether ether ketone polymer (PEEK) in spinal surgery, polymethyl methacrylate (PMMA) in bone cements, polytetrafluoroethylene (PTFE) in vascular grafts or polyethylene terephthalate (PET) fibres for ligament prostheses, etc. Some of them have the particularity of being resorbable, others demonstrate excellent primary fixation with bone, however, monomers may give rise to inflammation, or increase the risk of polymer degradation.

Ceramics are widely used in hip prostheses using inert alumina (Al_2O_3) or zirconia (ZrO_2), which have advantageous mechanical properties in compression. Other bioactive ceramics which mimic the chemical composition of bone such as hydroxyapatite ($Ca_5(PO_4)_3OH$) or tricalcium phosphate ceramics ($Ca_3(PO_4)_2$) can also be used to coat hip prostheses or scaffolds to fill bone defects. The mechanical and biological properties of bioceramics depend on

many factors during synthesis (sintering temperature, powder purity and particle size distribution) which may lead to large variations in the biological and clinical performances of the materials.

Metallic materials are in some ways the "ancestors"of biomaterials as they were the first generation of biomaterials to be introduced in the mid-twentieth century. Most of the metal implants used are 316L stainless steel. Although it has high mechanical strength, stainless steel is sensitive to corrosion in the body fluids through oxidation, and its wear resistance is poor in comparison with other metal implants. Cobalt-chrome alloys are mainly used in cardiovascular and orthopaedic surgeries. Although there is high corrosion resistance, implant wear leads to metallic ions being released into the surrounding area of the prosthesis. Other metallic materials are used, including NiTi which is a shape memory alloy, and also some noble metals (Au, Ag) for orthodontic applications. The last but not the least - metallic materials used in implantology is titanium and its alloys. They are widely used as biomaterials in dental implants as well as in certain orthopaedic applications. As this material is the centre of interest of this thesis, its characteristics and properties are developed in the following section.

1.1 Titanium and alloys in medicine

Titanium and it alloys are widely used in medicine due to their characteristics and properties which are more suitable than other previously-mentioned implant metals.

Mechanical properties and material density – Titanium exists in two different forms: alpha, which is a stable phase with poor mechanical properties but more resistant to oxidation than the second type, the beta phase, formed over 882 $^{\circ}$C (Figure 1.2). The alpha phase mainly composes pure titanium also known commercially as pure titanium (cp Ti). There are several grades of purity, characterised by the amount of oxygen, carbon and iron contained in the titanium. Titanium Grades 1 to 4 only concern pure titanium, the other grades are alloys. In medical applications, Ti Grade 4 is used for dental implants while Ti-40 (Grade 2) is used here for tracheal applications.

Beta type titanium alloys, such as Ti-13Nb-13Zr, Ti-15Mo or NiTi, are stronger and have low Young's modulus, making them favourable for homogeneous stress transfer between implant and bone (i.e. bone plates and screws), while also having limited ductility that reduces the capacity for shaping [46]. NiTi materials are useful in orthodontic applications as they have super-elastic

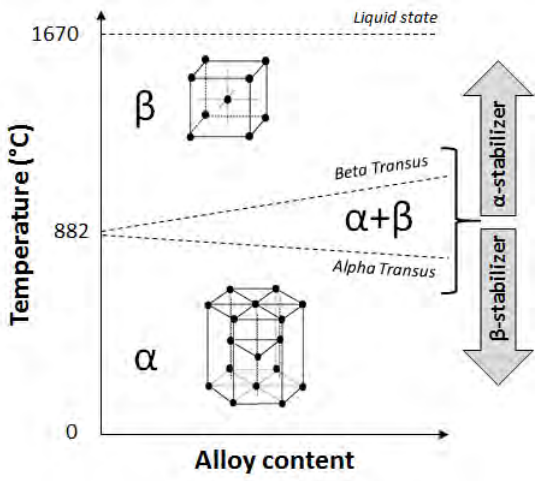

Figure 1.2: Binary diagram for titanium and alloys with neutral element. In presence of alpha-phase stabilizer or beta-phase stabilizer, alpha-transus and beta-transus are shifted.

behaviour and shape memory effects. Mixed alpha and beta phase alloys, such as TA6V or TiZr, are interesting due to improved fatigue properties compared to pure metal. TA6V alloy, made of 6 % aluminum and 4 % vanadium, is the most common type of titanium used in medicine as Grade 5 and 23. The phase stability of this alloy depends on the alloying element ratio. It has been established that vanadium, molybdenum, niobium and tantalum act as *beta*-stabilisers while aluminium acts as an α-stabiliser. However, these elements can have undesirable effects at the biological level. Aluminium and vanadium are respectively classified to form a capsule or scar tissue, and prevent cell division. Both elements can display mutagenicity and cytotoxicity, and cause allergic reactions.

The mechanical properties of titanium and its alloys are compared to other biomaterials in **Table 1.1**. The metal titanium is known for its biomechanical properties (Young's modulus, tensile strength, ductility, fatigue life, and wear resistance) and relatively low material density. Ti 6Al-4V ELI (Extra Low Interstitials) contains reduced levels of oxygen, nitrogen, carbon and iron and these lower interstitials provide improved ductility and tensile strength.

Biocompatibility and corrosion resistance – Titanium is naturally covered by a thin layer of amorphous titania or titanium oxide (TiO_2) 2 - 6 nm thick. This passivation film forms spontaneously in contact with air. Titania

Table 1.1: Mechanical properties of materials used for bone implants [47, 48, 49, 50]

Materials	Phase Structure	Density	Tensile strenght MPa	Elastic modulus GPa	Yield strenght MPa
Bone	-	1.6-2	90-140	10-40	
Polyethylene	-	0.9-1.2	30-35	<1	15-43
Steel 316	Austenitic	7.5-8	465-950	200	170-750
Cobalt alloys	-	8.5	209	1000	145-270
Ti cp Grade 1	α		240		170
Ti cp Grade 2	α	4.5	340	100-115	275
Ti cp Grade 3	α		450		380
Ti cp Grade 4	α		550		480
TA6V	$\alpha + \beta$	4.9	960-1000		850-900

has a high affinity for organic contaminants and carbon. The oxide layer also confers chemical stability, prevents bio-corrosion and the release of metal ions, thus ensuring the biocompatibility of implants in a human body environment.

The titania layer is mainly composed of initially amorphous TiO_2 but may also exist in a crystalline phase: the tetragonal anatase phase (**Figure 1.3(a)**) is metastable and formed at an early temperature (around 208 $^\circ$C) and it transforms irreversibly into a stable rutile phase at higher temperatures (**Figure 1.3(b)**). A final crystalline form of titanium dioxide is called brookite. This metastable phase with an orthorhombic structure is less described in the literature than the others (**Figure 1.3(c)**). This nucleation-growth type of phase transition is not instantaneous, leading to a mixture of phases [51].

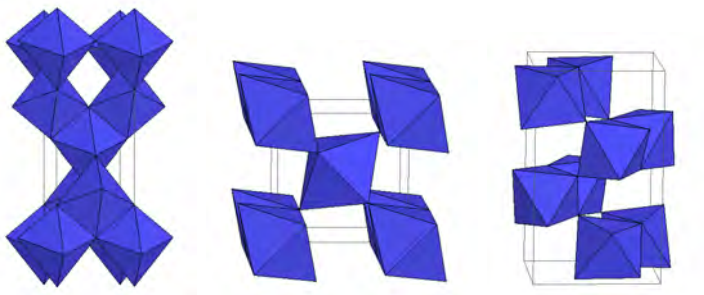

(a) (b) (c)

Figure 1.3: The different crystal structures of titanium dioxide : (a) anatase, (b) rutile et (c) brookite (source : http://www.ruby.colorado.edu)

1.2 Biological tissue integration: successes and failures

In the case of intra-osseous implants, the main objective is to obtain a direct bone-implant contact. The biological processes in tissue healing around implants are briefly described in this part.

First of all, soft tissue includes tendons, ligaments, fascia, skin, fibrous tissues, fat, and synovial membranes (also called connective tissue), as well as muscles, nerves and blood vessels (which are not connective tissues). Connective tissue is essentially composed of fibroblast cells in extracellular matrix. These fibroblast cells differentiate from a multipotent mesenchymal stem cell (MSC) that could also contain other specific cells (i.e. adipocytes, chondroblasts, osteoblasts and myoblasts). The main function of fibroblasts is to produce collagen fibres giving high resistance to connective tissues.

Bone tissue is composed of an mineral component at 65 % and of an organic element 35 % (i.e. type-I collagen, non collagenic proteins and growth factors). The mineral present is essentially composed of **hydroxyapatite crystals** or amorphous calcium phosphate.

Bone is also composed of different cells: osteoblasts, osteocytes and osteoclasts. Osteoblast cells have the particularity of actively synthesizing bone matrix. Osteocytes result from the maturation of osteoblasts and are embedded into the bone tissue made of mineralised collagen fibres. Osteocytes synthesize collagen fibres and regulate and moderate bone formation by controlling the activity of osteoclasts, the cells that resorb bone tissue. Bone is a living tissue that follows a continuous cycle of formation and destruction. This phenomenon is called **"bone remodelling"**. There are two types of bone: compact bone, characterised by cylindrical bone lamellae concentrically arranged around the Haversian canal, and cancellous bone which consists of ramified trabeculae between which bone marrow and vessels are found.

1.2.0.a Concepts of osteointegration

In the early 1950s, Professor Per-Ingvar Brånemark of the University of Lund in Sweden discovered that bone can integrate with titanium components [52]. The **concept of osseointegration** was introduced for titanium implants. It is now defined as the direct structural and functional connection between living bone and the surface of a load-bearing artificial implant.

The placement of an implant requires several distinct stages before osseointegration is obtained (**Figure 1.4**) [16, 17, 18]. When the implant is inserted, biological fluid (i.e. blood) with various constituents, such as proteins, mineral ions, glucids, and lipids, enters into contact with the surface. RGD components

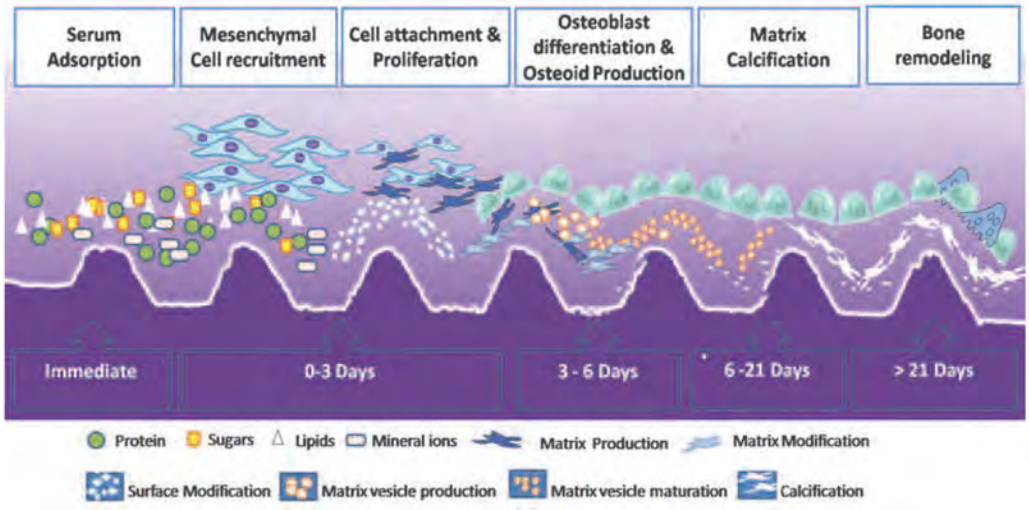

Figure 1.4: Chronology of the various steps towards osseointegration [53]

containing the Arg-Gly-Asp pattern are adsorbed on to the implant surface and allow the adhesion of cells **integrins** [54]. It makes possible the connection between the cell and extracellular matrix (fibronectin or laminin), leading to cell adhesion, proliferation or migration. Moreover, platelets from blood attract MSC by using growth factor release. Thus, during the first 3 days of implantation, cells attach to the implant surface and proliferate. Cells may be already differentiated (i.e. osteoblasts) or primitive cells that can differentiate into osteoblasts or osteocytes, which is called osteocondution. After 6 days of healing, osteoid tissue is synthesized by osteogenic cells. After two weeks, a neo-bone formation is obtained by calcification of the extracellular matrix. Three weeks after the placement of an implant, the bone remodelling process occurs. Nevertheless, none of these steps are fixed and may change as in the case of immediate implant loading.

As reported by Raghavendra, **primary stability** corresponds to the mechanical anchorage of the implant (**Figure 1.5**) [55]. This stability gradually decreases during the bone remodelling process. During the healing process, bone remodelling forms new bone in direct contact with the surface of the implant leading to **secondary or biological stability**. The healing process is complete when the biological stability entirely replaces the initial mechanical stability.

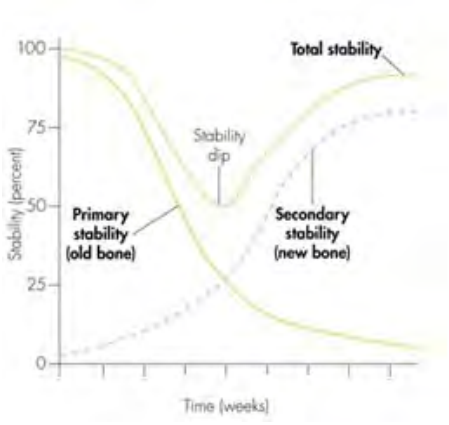

Figure 1.5: Primary and secondary stability curves as shown by Raghavendra *et al.* [55] (source : http://straumann.ca)

1.2.0.b Limitations and needs

The placement of titanium implants has a high clinical success rate, notably in dental implantology with a rate of 95 % according to authors [6, 7, 56, 57]. Clinical success is based on early integration of the implant. Several factors may play a role in this integration: the nature, surface and geometry of the implant, the preparation of the implant site, the surgical technique used or even the condition of the implant-loading [5].

As titanium and alloy surfaces are bio-inert, they cannot actively stimulate the initial bone formation on the surface at an early stage of implantation. As soft tissue healing grows faster than hard tissue formation, it may interact on implant surface integration [58]. Implant encapsulation by fibrous tissue may isolate the implanted material from the surrounding bone and lead to implant instability and premature loosening. In the case of dental implantology, most implant failures occur in the critical early period between weeks 2 and 4 [55].

If the bone formation process is initiated earlier, it is possible to dramatically improve the total stability of the implant. Thus, the surface of an implant requires optimisation of its bioactivity with tissues. Several factors may play a role in titanium integration. Authors have shown the impact of surface modification (mechanical, physical, chemical) that may modulate cell behaviour with the implant surface [11, 12, 13, 14]. Thus, surface treatments or modifications have been developed and are currently used with the aim of enhancing the clinical performance of titanium implants. This subject is exposed in the next section of this chapter.

1.3 Titanium surface technology

Bioactivity may be stimulated by surface parameters such as roughness, wettability or chemical composition which modulate cell adhesion, proliferation and/or differentiation (**Figure 1.6**) [11, 12, 13, 14, 15].

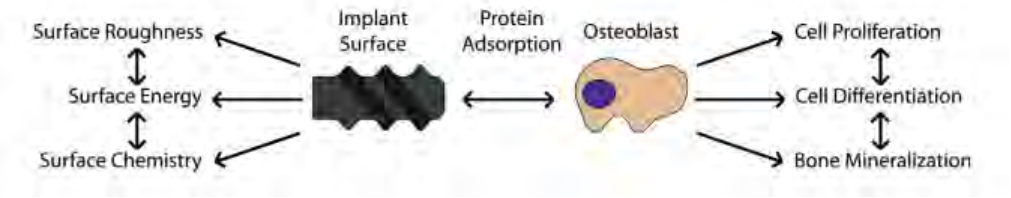

Figure 1.6: Diagram of interactions between surface properties (i.e. surface roughness, surface energy, surface chemistry) and biological events, such as protein adsorption and thus osteoblast response (i.e. proliferation, differentiation, bone mineralisation)[15]

The initial surface of an implant is usually turned or machined. This surface is relatively smooth and only has a few micrometric machining streaks (**Figure 1.7**). The polishing process (i.e. electro-polishing) makes it possible to reduce the machining traces resulting in polished mirror surface roughness at the range of 0.1 μm. The main advantage of polished surfaces is the aesthetic surface and the inhibition of plaque accumulation [59], while giving less stimulation of human gingival fibroblasts than machined surfaces [60]. Machined smooth surfaces have been shown to increase the risk of failure when implanted in a low quality bone site while increasing fibroblast adhesion and spread, and thus soft tissue proliferation more than rough surfaces [4, 61, 62].

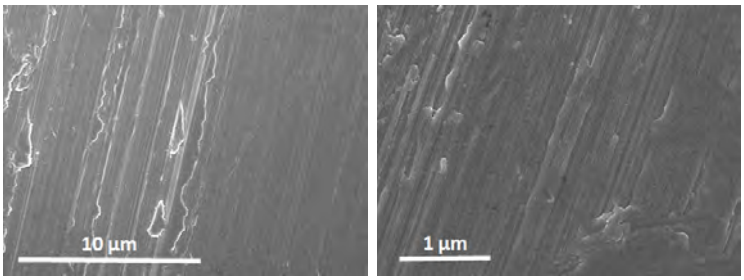

(a) (b)

Figure 1.7: SEM observation of the morphology of a TA6V machined surface at two magnifications ($\times 5,000$ and $\times 20,000$)

Macro-rugosity obtained thanks to the "spire/screw shape"makes it possible to anchor intra-osseous implants into the bone (i.e. dental implants, osteosynthesis screws). Moreover, modifications to the microscopic roughness (1-10 μm) have been shown to positively influence bone integration into the surface [63, 64, 65]. In addition, Hara *et coll.* reveal higher alkaline phosphatase on rough than on smooth surfaces [66]. In addition, roughness increases the contact area between the titanium implant and bone tissue. Currently, no one knows the ideal micro-roughness and thus various surface roughnesses are manufactured. However an excessively rough surface up to Sa = 1 à 1.4 μm could increase the risk of surface corrosion, bacteria colonisation and could also be difficult to clean up in case of bacterial decontamination [67, 68, 69]. Recent studies have shown that nano-surface modification (from 1 to 100 nm) may modulate protein adsorption and enhance cell adhesion, osteoblast proliferation and osseointegration [12, 22, 41, 70, 71]. Nano-structured surfaces have been shown to enhance cell adhesion and osteogenic parameters better than traditional turned surfaces *in vitro* [72] as well as bone anchorage *in vivo* [43]. Recently, Lu and Webster have also shown that nano-surfaces reduced pro-inflammatory cytokine release as well as submicron titanium surfaces compared to a flat surface [73]. Other authors showed that combining surface patterning techniques at both at the micrometer and nanometer scale may lead to enhanced osteoblast activity [74].

Methods have been developed to improve the clinical surfaces of titanium implants, known as surface treatments. Surface treatments can be additive, creating a chemical coating or increasing the implant surface using an electrochemical process, or subtractive, removing material thus increasing the contact area without changing the chemical composition of the surface (i.e. blasted, acid etched). Some implants could have a hybrid surface with both a smooth portion for soft tissue adhesion and a second portion that is rough for titanium osseointegration with bone (i.e. dental implants with gingival tissue and alveolar bone).

Titanium integration with biological tissues is evaluated by observing the surrounding tissues and quantifying elements such as percentage of bone implant contact (% BIC) or bone formation surrounding the implant surface (% BS).

The first part of this section presents the main method for surface treatment and the associated commercialised brands. Thesecond part introduces a new approach to surface modifications at the nanoscale. The formation of a honeycomb nanostructure via anodisation is then reviewed in chapter 20, "Bone Apposition on Nanoporous Titanium Implants"published by Elsevier.

1.3.1 Commercialised surfaces for implants

For around ten years, studies have been carried out in both enhancing clinical performances with tissues (hard or soft) and marketing. Several surface modifications have been developed and are currently commercialised. They make it possible to modify both the roughness and/or chemical composition of the surface. There are various applications, from dental implants to spine or hip prostheses, etc.

This part presents the process and some results regarding the biological performance of titanium surface treatments such as grit-blasting, acid-etching, porous sintering, oxidising, plasma-spraying (titanium or hydroxyapatite-coating) and laser techniques. There are other treatments, such as physical vapour deposition (PVD) and chemical vapour deposition (CVD) for organic or inorganic coatings, but they will not be developed in the section below.

1.3.1.a Grit blasted surface (i.e. $Tioblast^{TM}$, Astra Tech)

Grit-blasting is a subtractive treatment which consists in air spraying particles on to the titanium surface. Impaction of the particles creates micrometric roughness in the range of 0.5 to 6 μm depending on the type of material and particle sizes used, as well as other treatment conditions (pressure, projection time, etc) [75]. The particles mainly used for these surface treatments are aluminium oxide powder (Al_2O_3). The method leads to particles being retained in the titanium surface and may interact on tissue integration [76, 77]. Titanium dioxide (TiO2) can also be used to avoid this external contamination (i.e. the $TiOblast^{TM}$ surface from Astra Tech newly Dentsply Implant, see **Figure 1.8**). A third technique called "clean sand blasting"consists in blasting using calcium phosphate ceramic particles such as tricalcicium phosphate beta (Beta TCP) or hydroxyapatite (i.e. MTX^{TM} surface, Zimmer dental). The ceramic can dissolve into nitric acid after treatment leading to a "clean"titanium surface. Then, a new blasted surface with anti-bacterial properties is manufactured by Medicoating using hydroxyapatite powders containing silver particles.

1.3.1.b Acid etched surfaces (i.e. $Osseotite^{®}$, Biomed 3i)

The etching method consists in attacking the surface with corrosive acids. The corrosion is not uniform and thus produces micrometric roughness or cavities that are interesting for bone formation and anchorage. The interest is twofold because the native oxide layer is also removed leading to surface decontamination. The Biomed 3i corporation proposes a dual acid-etched surface into an aqueous solution of hydrochloric acid and small amount of hydrofluoric acid called $Osseotite^{®}$ surface (**Figure 1.9**) [78].

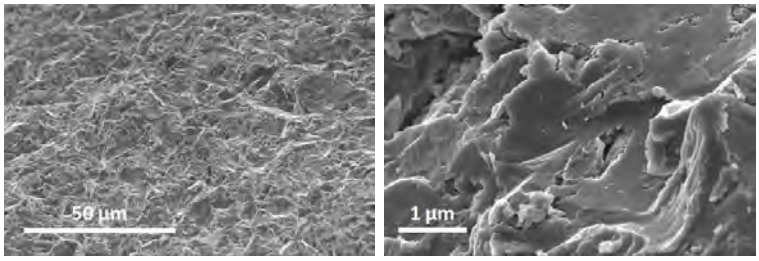

(a) (b)

Figure 1.8: SEM observation of the morphology of grit-blasted surfaces of $TiOblast^{TM}$ (Astra Tech, newly Dentsply Implant) at two magnifications: (a) $\times 1,000$ and (b) $\times 20,000$)

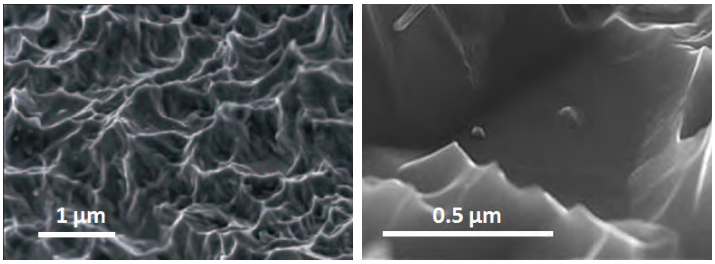

(a) (b)

Figure 1.9: SEM observation of the morphology of the acid-etched surface of Osseotite (Biomed 3i) at magnification (a) $\times$ 20,000 and (b) $\times$ 100,000 (sources : http://biomed3i.com and http://www.mdtmag.com)

1.3.1.c Grit blasted and acid etched surface (i.e. $SLA^{®}$, Straumann)

The combination of both grit-blasting and dual acid-etching is the standard surface method used in dental implantology. Grit-blasting using Al_2O_3 particles 250-500 μm in diameter followed by a warm hydrochloric and sulphuric acid attack makes it possible to both remove sandblasting residue and produce 1 to 2 μm random micrometric cavities. These surfaces are developed by Straumann SLA (**Figure 1.10**).

$SLAactive^{®}$ is produced by rinsing in an N_2 atmosphere. It is then submerged in an isotonic NaCl solution following acid-etching to avoid contact with molecules from the atmosphere. SLA surface is widely published and is known as a reference surface in dental implantology. Frialit by Dentsply and Osseospeed by Astra Tech are also prepared following this blasted and acid etched method.

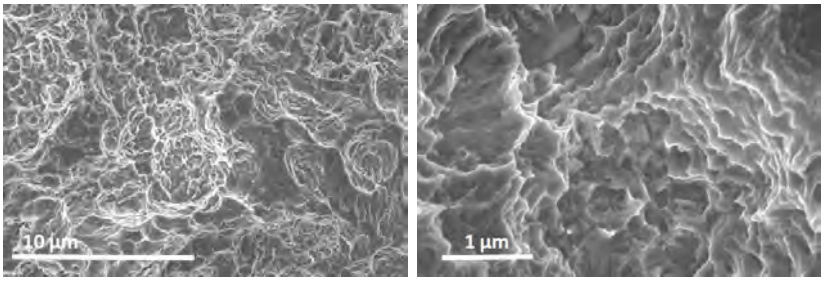

(a) (b)

Figure 1.10: SEM observation of the morphology of a SLA surface (Straumann) at double magnification :(a) $\times 5,000$ and (b) $\times 20,000$)

1.3.1.d Oxidized (i.e. $TiUnite^{®}$, Nobel Biocare)

Anodic oxidation is widely used and mastered on metal to increase its oxide layer. It may be either additive or subtractive, depending on the electrochemical parameters used. Currently, the use of this technique on titanium surfaces makes it possible to produce 3 kinds of surface.

A colour anodizing surface is obtained from the reaction between metal ions with oxygen in an electrochemical cell, and forms a compact metal oxide (MO) layer. The thickness of this oxide layer on the titanium substrate leads to a colour-coding surface treatment, through a light constructive interference phenomenon caused by a difference in reflective index. This coloured surface can be used for the identification of medical instrumentation. In addition to this marketing asset, the thick oxide layer increases biocompatibility by preventing corrosion and decreasing metallic ion release from the titanium surface.

Under high electrochemical conditions (i.e. 100-300 V), the thickness of the oxide layer is greatly increased, leading to electrical resistance of the surface during the anodising treatment. Thus, dielectric breaks with sparks occur at the titanium surface causing the melting of the oxide layer [33]. This method produces 1 to 10 μm porosity. This treatment is called as spark anodisation and is commercialised by Nobel Biocare under the name of TiUnite (**Figure 1.11**).

During this spark anodisation process, a compact oxide layer is also formed under the microporous outer oxide layer. The first compact oxide layer has been shown to increase the fatigue strength and to reduce wear from friction on the titanium surface. It is currently proposed by KKS as TioDark treatment.

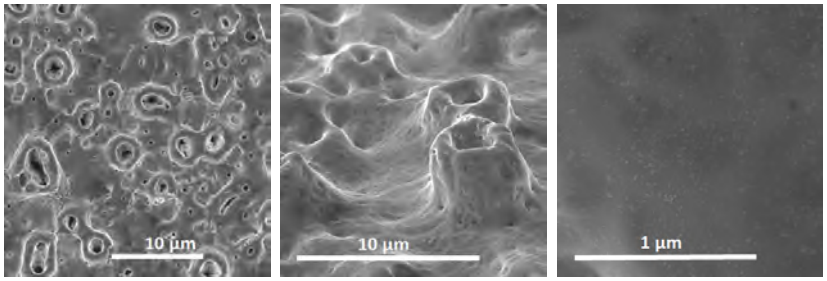

(a) (b) (c)

Figure 1.11: SEM observation of the morphology of a TiUnite surface (Nobel Biocare) at three differente magnifications : (a)$\times 2,000$, (b) $\times 5,000$ and (c) $\times 20,000$

1.3.1.e Titanium and HAP plasma sprayed surface (i.e. TSP coating, DOT)

The titanium plasma spray process, also called the plasma torch process, is one of the main additive surface treatments leading to coating from 50 to 200 μm in thickness. It consists in spraying a material at high temperature which adheres to the titanium substrate and forms a coating. This process makes it possible to create a globular and porous coating by spraying titanium powder or titanium hydride, increasing the roughness of the surface (**Figure 1.12**). It could also increase the bioactivity of the surface by using a coating whose chemical properties are osteoconductive, such as hydroxyapatite ($Ca_{10}(PO_4)_6(OH)_2$).

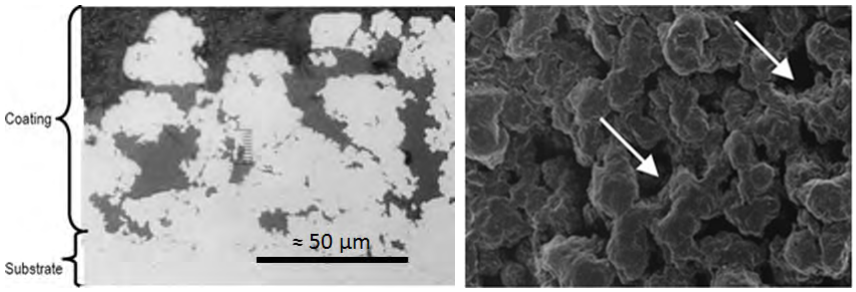

(a) (b)

Figure 1.12: SEM observation of the morphology from (a) the top and (b) the section of a titanium plasma sprayed surface, magnification $\times 5,000$ (source : http://www.exac.com)

The white calcium phosphate ceramic is known for its bioactive properties. This hydroxyapatite surface dissolves in contact with biological fluids leading

to the release of calcium and phosphate ions into the peri-implant region and the precipitation of a biological apatite on to the implant surface. This apatite layer makes it possible to retain proteins and cells that produce the bone matrix directly on the titanium surface.

Although the surface can be blasted beforehand to increase the mechanical anchorage of the coating, the cooling generates internal stress and cracks. Thus, the coating still adheres to bone tissue while detaching the coating from the surface, leading to weak implant anchorage in the long term. This surface was suspended from the market in 2001 by AFSSAPS (*l'Agence Nationale de Sécurité du Médicament et des produits de santé*). Other process treatments synthesized hydroxyapatite on to the surface by biomimetic precipitation (**Figure 1.13 (a)**), ion sputtering, sol-gel (NanoTite, 3i) but they are not as developed as the plasma-sprayed technology and will not be describe in this manuscript.

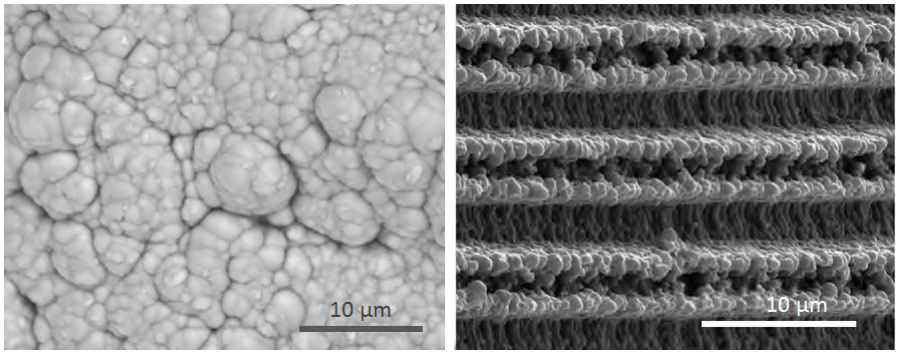

(a) (b)

Figure 1.13: SEM observation of the morphology of a biomimetic hydroxyapatite formed by precipitation and a Laserlok surface produce under Laser ablation (BioHorizons). Magnification : (a)$\times 5,000$, (b) $\times 7,000$ (source: http://fr.biohorizons.com/laserlok.aspx)

1.3.1.f Laser ablation surface (i.e. *Laser-Lok*®, BioHorizons)

Laser ablation, also called Laser peeling is a subtractive technology which consists of laser beam bombardment of the surface with high intensity (5-15 GW/cm^2) nanosecond pulses (10-30 ns) causing small indentations or dimples. These microstructures greatly increase hardness, corrosion resistance, and provide a high degree of purity with a standard roughness and thicker oxide layer on the titanium surface.

This surface treatment is currently manufactured for dental applications such as Laser-Lok by BioHorizons (Birmingham, Alabama, USA). The Laser-Lok surface produces a grooved surface at the cell scale (**Figure 1.13 (b)**). Biological performances were evaluated for the Laser-Lok surface and were shown to orientate osteoblast cell attachment and control the direction of ingrowth [79].

Other laser techniques are also commercialised with the same principle as the plasma-sprayed surface, such as laser pulsed depositing and the laser microfusion technique, also called Direct Laser Metal Forming (*i.e.* Tixo, leader-italia).

1.3.2 New approach for nanoscale modification via anodisation

The surface treatments presented above produce randomly micrometric surfaces. Although this rough surface increases tissue intergration as compared to a non-treated surface, it has been shown that nano-surface modification of titanium also provides a high biological response. Several authors are currently studying the nano-surface approach, producing randomly ordered nano-surfaces such as nano-grass, nano-needle, nano-pits, nano-porous surface for medical applications. These nanopatterned surfaces are created in the same way as those used for surface micropatterning, such as lithographical methods, hydrothermal treatment, anodising, depositing nanoparticles or grafting, etc. As previously discussed, new bone formation includes complex processes that produce the different micro-, submicro- and nanoscales on titanium surfaces (**Figure 1.14**) [15].

Immediate implant insertion leads to protein adsorption at the surface nanoscale and is used for cell adhesion through integrins. Nano-modification may regulate the type, number, spacing and distribution of the focal adhesion ligands for cells on the titania surface (**Figure 1.15**). This changing also changes the location and spacing of transmembrane intergrins leading to cytoskeletal tension in the actin filaments of the adhered cells. The resultant stress on the cytoskeleton of the cells may regulate its behaviour regarding proliferation and differentiation.

In the case of TiO_2 nanotube surfaces, it has been shown that MSC and osteoblast cells may proliferate if of different pore size but highly differentiate or stimulate on larger 70-100 diameter nanotubes while higher cell adhesion was observed for lower diameters (**Figure 1.16**). This modification of the cell behavious is due to the phenomenum of mechanotransduction, already published by serveral authors[19, 20, 21, 22, 20, 41, 81].

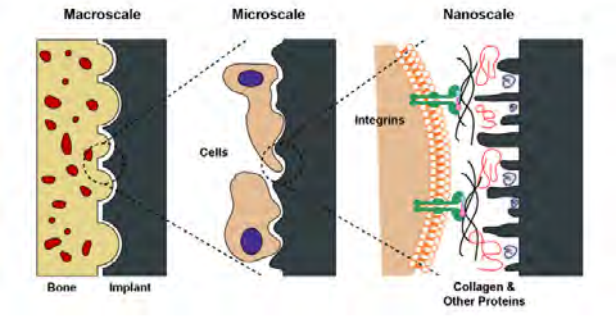

Figure 1.14: Interactions between bone and the implant surface at different length scales : At the macroscale, the implant shape provides a good mechanical fixation with bone; at the microscale, microroughness can directly interact with osteoblasts and mesenchymal stem cells. At the nanoscale, cell membrane receptors, such as integrins, can recognize proteins adsorbed on the surface [80]

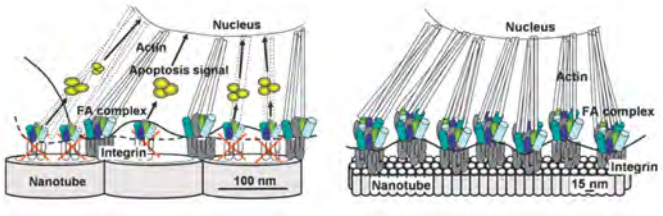

Figure 1.15: Interactions between proteins, intergrines of cells on nanotubular surface with different pore sizes [22]

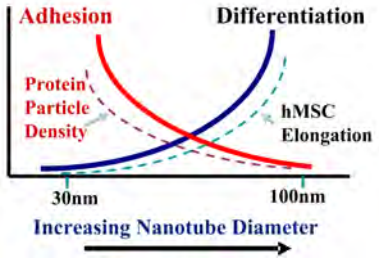

Figure 1.16: Schematic illustration of the effect of diameter of nanoporous structure on hMSC after a 24-h culture : for lower diameter, cell adhesion and growth without differentiation while for higher diameter, elongation of hMSC are observed leading differentiation [23]

Thus, incorporating some types of nanoscale surface features on to the surface with a combination of microscales is a way of mimicking the bone's hier-

archical structure and inducing better tissue integration. Nano-modification of the surface using ordered nanotubes and nanoporous array are the subject of this thesis. These nano-surfaces are more developed in a book chapter published by Elsevier which reviews the formation of the TiO_2 honey comb structure and its biomedical applications.

1.3.2.a Book chapter : Bone apposition on nanoporous titanium implants

CHAPTER 20

Bone Apposition on Nanoporous Titanium Implants

Laëtitia Salou[1,2,3], Alain Hoornaert[4], Guy Louarn[3], Pierre Layrolle[1]
[1]Inserm U957, Lab. Pathophysiology of bone resorption, University of Nantes, Nantes, France
[2]Biomedical Tissues SAS, IRSUN, Nantes, France
[3]Institute of Materials Jean Rouxel, CNRS, University of Nantes, Nantes, France
[4]CHU Nantes, Nantes, France

Chapter Contents

1. INTRODUCTION

Titanium and its alloys are widely used for manufacturing dental and orthopedic implants because of their good biocompatibility. Surface properties of titanium implants are key factors for rapid and stable bone tissue integration [1]. Upon implantation in the body, titanium implant surfaces interact with proteins, cells, and tissues in the nanometer range. Nanotechnologies may produce surfaces with controlled topography and chemistry that would help in understanding biological interactions and developing novel implant

Handbook of Nanoceramic and Nanocomposite Coatings and Materials
http://dx.doi.org/10.1016/B978-0-12-799947-0.00020-1

surfaces with predictable tissue-integrative properties [2–4]. Various surface treatments such as templating, hydrothermal processing, and electrochemical anodization may be applied to the surfaces of dental and orthopedic implants to produce controlled features at the nanometer scale. These nanostructured surfaces exhibit titania nanotubes of various sizes and distributions.

Basic research on the self-organization of nanostructures made by Zwilling and coworkers showed that the porous surface of titania could be formed electrochemically in fluorinated electrolytes by an anodization process [5]. Two years later, Gong and coworkers [6] first reported the observation of the growth of highly ordered self-assembled TiO_2 nanotube arrays via anodic oxidation of titanium in a hydrofluoric (HF) electrolyte. This new titania structure was shown to improve properties compared with any other form of titania making some interest for different applications such as photocatalysor [7,8], sensors [9,10], and photovoltaic applications [11,12] and in the biomedical field [13–15] including drug delivery [16–19].

Titania nanotubes may be highly relevant to biomedical applications, particularly in dental and orthopedic implants. The optimal surface may be screened by using high-throughput biological assays *in vitro*. For instance, specific protein adsorption, cell adhesion, and differentiation of stem cells should be studied in relation to the surface properties. Following *in vitro* screening, nanostructured surfaces may then be verified in animal models to validate hypotheses in a complex *in vivo* environment. This approach may define the ideal surface for a specific biological response such as bone tissue integration.

In this chapter, the different methods to produce titania nanotubes and their application in the biomedical field will be reviewed.

2. METHODS OF FABRICATION OF TITANIA NANOTUBES

Titanium metal is naturally covered by a thin layer of titania or titanium oxide (TiO_2). This layer is a few nanometers thick and generally amorphous. This passivation film forms spontaneously when titanium is exposed to air. In the biological environment, this titanium oxide layer is very stable and prevents biocorrosion and the release of metal ions ensuring the biocompatibility of implants. However, the oxide layer surface is often contaminated with hydrocarbon components from the environment. Indeed, Ogawa and colleagues have shown that the bioactivity and osteoconductivity of titanium degrade over time after surface processing [20]. In general, manufacturers of implants do not control the formation and properties of the titanium oxide layer in the nanometer range. Several groups have demonstrated that nanostructured titanium surfaces have a great impact on the fate of cells and may ultimately control

the integration of implants in bone tissue. Among other nanostructures, titania nanotubes have received much attention. Titania nanotubes and nanotube arrays can be produced using various routes. One of the important ways is a template-assisted method that was used by Hoyer [21]. It consists of forming TiO_2 nanotubes by using alumina templates [21–24]. Other methods for fabricating TiO_2 nanotubes using hydrothermal [25,26] or anodization processes have been described [27–29]. These different methods to produce titania nanotubes are presented hereafter. The advantages and drawbacks of the different methods are reported in Table 1.

Table 1 Advantages and disadvantages of the different fabrication methods for TiO_2 nanotubes

Technique	Advantage	Disadvantage
Positive template-assisted method	Dimension control of TiO_2 nanotubes by the template	Not uniform in length and open ends Only large tubes and small wall Complicated fabrication process Not applicable to complex-shaped implants
Negative template—sol-gel technique	Ordered array of TiO_2 nanotubes with uniform diameters	Large tubes Risk of contamination during dissolution Time of pre- and postprocessing, difficult to scale up in industry
Hydrothermal treatment	Good crystallinity (anatase) Titania fiber/tube 100 nm to micron	Nonreproducibility of nanostructures Long reaction time ($\approx$20 h) Highly concentrated NaOH used Individual free nanotubes Numerous critical parameters
Anodization	Simple and cost-effective process applicable to different implants Well-ordered and vertically aligned nanotubes Wide range of nanotube dimensions Directly attached on substrate	Amorphous nanotubes Requires a postannealing step Highly expensive fabrication apparatus for large batches (Pt electrode)

2.1 Template-Assisted Methods

The template-assisted method utilizes a pattern transfer made of porous alumina. The alumina template is generally made of anodic aluminum oxide (AAO). The length or diameter of the TiO_2 nanotubes directly depends on template dimensions. Two types of template, positive and negative, are described in the literature.

In the positive template method, an anodic alumina mask is placed on the titanium surface. The AAO film serves as a mold for a polymer on which TiO_2 is electrochemically deposited. Then, the polymer mold is dissolved and reveals TiO_2 nanostructures corresponding to the AAO pattern. This technique was explored by some authors [22,30] but it does not produce uniform length nanotubes.

The negative template method consists of a sol-gel technique. An anodic alumina mask is placed on the titanium substrate and then dipped into a $Ti(OR)_4$ solution that penetrates through the AAO film. After calcination of over 400 °C, the template is removed by chemical dissolution and reveals an ordered array of TiO_2 nanotubes with uniform diameter [23,24].

However, these template-assisted methods are not easily applicable to complex-shaped medical devices such as dental and orthopedic implants. Furthermore, their scalability for industrial production is also difficult.

2.2 Hydro-/Solvothermal Processes

This method is based on the self-assembly of TiO_2 nanoparticles or powder treated into a NaOH solution that deposits on the surface of titanium implants. Following the hydrothermal process at temperatures ranging from 100 to 150 °C, the Ti-O-Ti bond breaks out to Ti-O-Na or Ti-OH, leading to the formation of a nanostructured layer. Chemical acid treatment in HCl converts this layer into nanotubes by removing electrostatic charges of the sodium salt [25,26]. This procedure may be applicable to medical devices. However, the obtained nanostructures are not easily controlled as they depend on multiple parameters (e.g., size of titanium oxide, concentration of NaOH, temperature, and neutralization).

2.3 Electrochemical Anodization Method

Anodization of titanium implants is widely used in the medical device industry for color coding of products. It is a relatively simple and cost-effective process that does not change the tolerances of implants. However, the anodization is usually performed without any control of the nanostructure of the titanium oxide layer.

A self-assembly or "bottom-up" technique has been described to produce nanomodifications of the titanium oxide surface by the electrochemical process of anodization with or without fluoride ions. By using specific electrochemical parameters, an array of oxide nanotubes aligned perpendicularly to the surface can be formed. Some authors have described self-standing nanostructured membranes by detaching the titanium oxide layer from the surface [31]. Dimensions of the nanotubes can be precisely controlled. A large variety of sizes from 20 up to 100 nm in pore diameter, length from 50 to 6000 nm, and a wall thickness ranging from 7 to 34 nm can be produced. [27,32].

In the following paragraph, the mechanism and the influence of the different electrochemical parameters on the properties of this self-assembled TiO_2 nanotube array are discussed. Their application in the biomedical field as a new surface treatment for implants with or without biologically active molecules is then presented.

3. TiO_2 NANOTUBE FORMATION UNDER ANODIC POLARIZATION

As shown in Figure 1, the electrochemical process of anodization consists of applying a potential (potentiostatic method) or a current (galvanostatic method) between the titanium implant and a counter electrode in an electrolyte solution. The titanium implant acts as an anode and a platinum inert electrode as a cathode. When applying a current, an oxidation reaction occurs at the titanium surface. Depending on the anodizing conditions, four behaviors are possible. At first, there is a continuous solvation of metal ions due to electrocorrosion and the process is known as electropolishing. Metal ions can also react with oxygen and form a compact metal oxide (MO) layer. This process is used as a color-coding surface treatment, by phenomenon of constructive and destructive interference with light. The colored surface can be used for decorating or for the identification of medical instrumentation. Under high electrochemical conditions (i.e., 100-300 V), the thickness of the oxide layer is greatly increased, leading to dielectric breaks with sparks that cause the melting of the oxide layer [33]. In the latter conditions, two layers are formed: a compact oxide layer and a microporous outer oxide layer. The first layer has shown to increase the fatigue strength and to reduce wear of friction. During anodization, the competition between solvation and growth of the oxide layer forms a nanoporous array of dioxide layer. By using more specific parameters, these nanopores self-organize into oxide

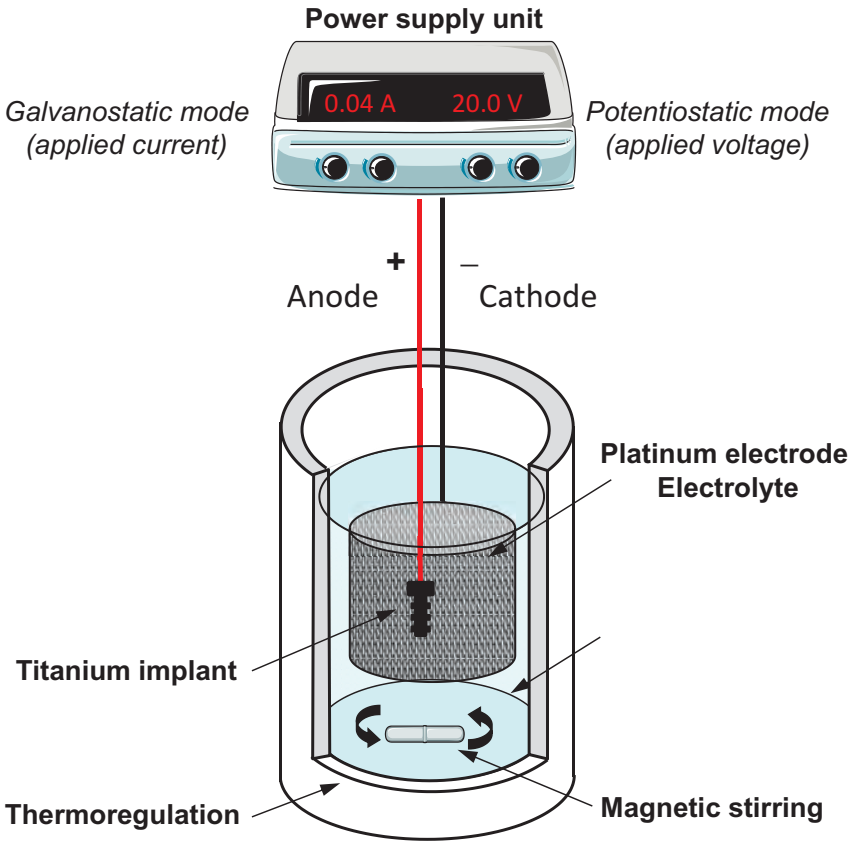

Figure 1 Experimental setup of the electrochemical anodization process for the formation of nanoporous TiO_2 on a titanium implant surface.

nanotubes, perpendicularly aligned on the metal surface. This nanostructure formation has been demonstrated and mainly developed at first not only on aluminum substrate but also on titanium, niobium, tantalum, zirconium, and a large range of other transition metals and alloys. These materials are called "valve metals" because of their dense, stable, well-attached electrical insulating oxide layer. In the following paragraphs, the mechanism of the formation of a nanotubular titanium dioxide film, the influence of the electrochemical condition, and the mean thermodynamic stabilization are discussed.

3.1 Mechanism of TiO_2 Nanotube Formation

The mechanism of TiO_2 nanotube formation is illustrated in Figure 2. During the anodization process, a chemical reaction corresponding to water decomposition appears at the cathode and produces dihydrogen gas according to Equation (1):

$$2H^+ + 2e^- \rightarrow H_2 \quad (1)$$

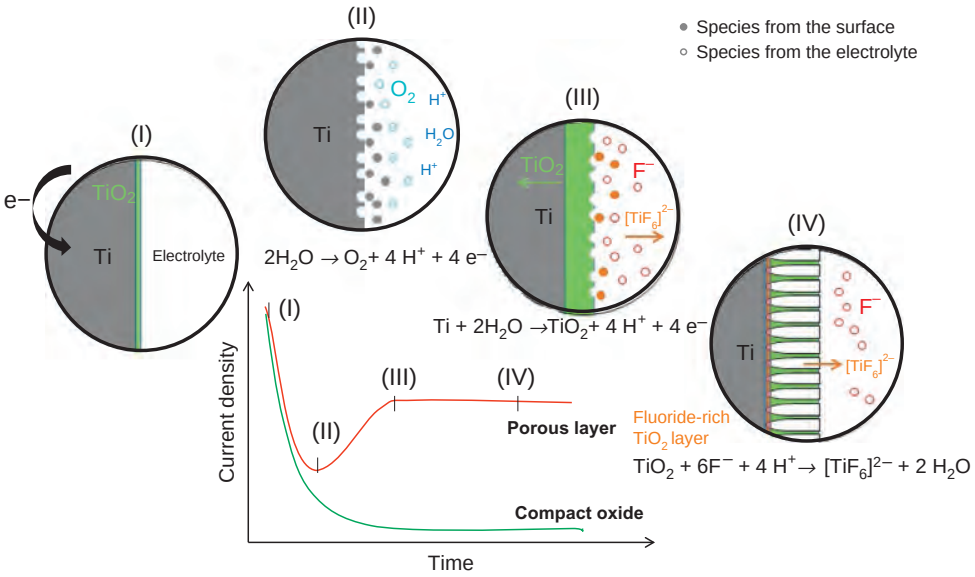

Figure 2 Mechanism of the electrochemical anodization process of titanium implant surfaces into TiO_2 nanotubes with ring used for species from the electrolyte and full circle for species from the surface.

At the anode interface, metal oxidation (Eq. 2) and decomposition of water take place and generate dioxygen gas (Eq. 3):

$$M \rightarrow Mn^{n+} + ne^- \tag{2}$$

$$2H_2O \rightarrow O_2 + 4H^+ + 4e^- \tag{3}$$

In the case of titanium substrate, anodization follows the same scheme, titanium ion (Ti^{4+}) formations that react with O^{2-} originating from water deprotonation to form the oxide layer (Eq. 4). The thickness of the oxide layer increases with the applied current, leading to current resistance.

In the presence of sufficient fluoride in the bath, a water-soluble species $[TiF6]^{2-}$ is formed on the substrate surface (Eq. 5). Chemical dissolution of the oxide layer by the electrolyte creates pitting corrosion on the surface. Difference in the oxide thickness and thus electrical conductivity leads to the preferential passage of current. Therefore, the competition between oxide formation and Ti^{4+} solvatization creates etching at some point forming a nanopit array. The resistance of the oxide layer decreases the current density in other locations. A good balance between specific electric power, oxide formation, and chemical dissolution can form a nanoporous or nanotube array:

$$Ti + 2H_2O \rightarrow TiO_2 + 4H^+ + 4e^- \tag{4}$$

$$TiO_2 + 6F^- + 4H^+ \rightarrow [TiF_6]^{2-} + 2H_2O \tag{5}$$

Fluoride rapidly migrates into the oxide layer and accumulates at the oxide-metal interface and at grain boundaries [29]. This fluoride-rich layer seems to play a role in the transition from a porous hexagonal structure to a tubular structure due to a preferential chemical dissolution between pores forming individual nanotubes. Examples of TiO_2 nanopores and nanotubes are shown in Figure 3. These nanostructures uniformly cover the surface of titanium. Depending on experimental conditions, the size of the pores may vary from 20 to 110 nm in diameter. The thickness of the TiO_2 nanotube layer may be adjusted from few tens to several hundred nanometers by increasing the processing time but is generally around 150 nm in thickness. As shown in the cross section, columnar nanotubes are oriented perpendicular to the titanium surface.

Nanoanodization is applicable to complex-shaped medical implants, and either nanopores or nanotubes have been uniformly produced on dental implants, orthopedic implants, or spine fusion devices. The main disadvantage of nanoanodization is that the formed nanotubes are amorphous and so thermodynamically instable. Annealing from 280 to 580 °C transforms the amorphous structure into crystalline phases. The tetragonal anatase phase is metastable and formed at lower temperatures (around 280 °C) and transforms irreversibly to rutile at higher temperatures (Figure 4). This nucleation-growth type of the phase transition is not instantaneous but is time-dependent [34]. Depending on the nanotubular structure, crystallized rutile phase grows up from the surface, destroying the nanotubular morphology at higher temperatures than 600 °C [28,35].

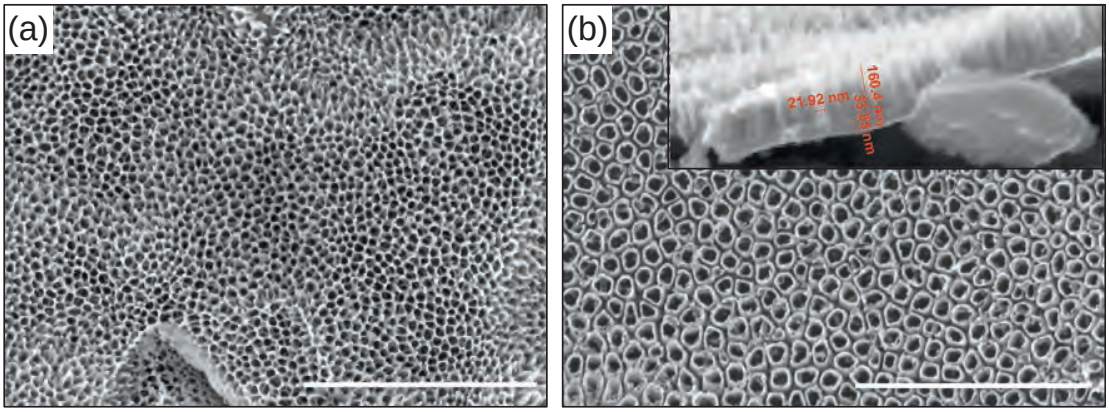

Figure 3 Scanning electron microscopy images of TiO_2 porous structures formed by anodization in 1 wt% HF and 1 M CH_3COOH at (a) at 10 V nanopores and (b) at 20 V nanotubes are formed. Inset shows the thickness of the layer of nanotubes (≅160 nm).

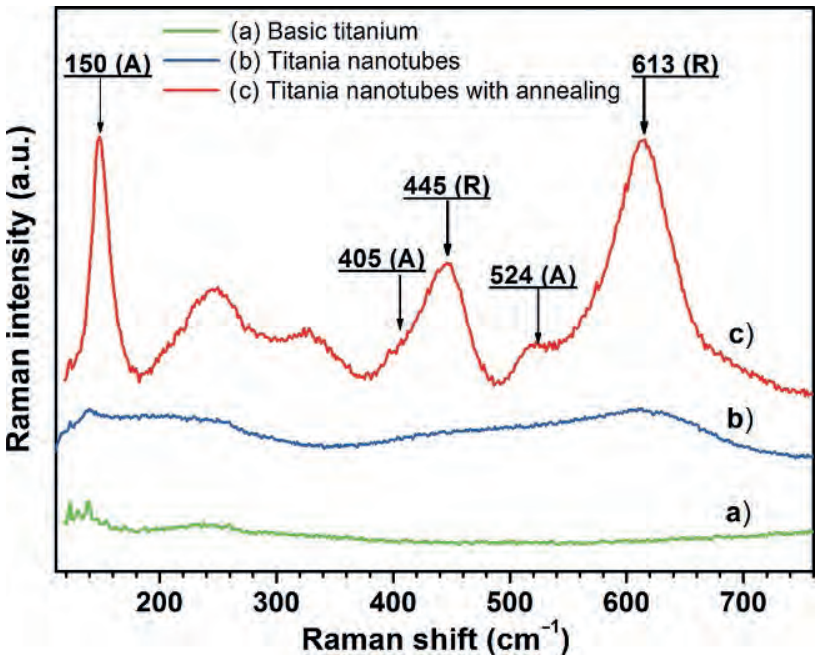

Figure 4 FT-Raman spectra of the titanium surfaces before and after the anodization process with or without annealing at 500 °C (A: anatase; R: rutile).

3.2 Importance of the Electrolyte in the Nanoanodization Process

Since the TiO_2 nanotubes have been discovered, a large number of articles have studied the electrochemical parameters that can modulate nanotube morphologies such as length, pore size, and ordering. However, the electrolytes govern both the formation and dissolution rates of the oxide layers and subsequently may be the most important parameter for nanopore formation and control. Four different generations of electrolytes have been reported in the literature. The first generation was used at the beginning with Gong and his coworkers [6] and is based on an aqueous dilute HF electrolyte. Because of the low pH value ($pH < 5$), the length of nanotubes is limited to approximately 500 nm. Therefore, a second generation of electrolytes was used in buffered aqueous solution at higher pH. By using these solutions, the nanotube lengths could be increased to microns. For example, Sreekantan et al. obtained nanotubes of 3 μm in length by using an electrolyte solution at pH 7 [36]. Other authors have investigated the use of a the third generation electrolyte containing a polar organic electrolytes, such as dimethyl sulfoxide (DMSO) and ethylene glycol (EG), together with or without water (1-3%). These organic electrolytes enabled the production of long nanotubes from 18-220 mm [37,38] to 1000 mm [39,37,36,35]. Finally, some studies have proposed a fourth generation of electrolytes to prepare titania nanotube

arrays fabricated in a non-fluoride-based electrolyte that contains an acidic sulfate solution. Other electrolyte parameters that have been found to influence the titania nanotube arrays are the viscosity, the water content and the fluoride concentration, the bath temperature, etc. [29].

3.3 Influence of the Electrochemical Parameter on Titania Nanotube Arrays

3.3.1 Electrophysical Parameters

The literature mainly reports about experiments carried out under constant voltage (potentiostatic) conditions, whereas only few studies have used a constant current (galvanostatic) condition that should be easily transposed to the industrial surface treatment of medical devices. The electrochemical characteristic curve depends on the mode used (Figure 2). However, in both cases, the reaction time and dissolution rate define nanotube lengths. Under the potentiostatic condition, the diameter of nanotubes grows proportionally with voltage. Constant voltage produces straight nanotubes, while a sweeping voltage forms conical structures. By increasing the magnetic stirring and current density, the production of hydrogen gas bubbles increases. Unfortunately, the formation of hydrogen gas could cause current fluctuations [40]. In the characteristic curve of the galvanostatic condition, the voltage increases linearly with reaction time until stationary regime at which a porous oxide layer is formed. Current densities from 10 to 30 mA cm^{-2} in HF aqueous solutions promote titania nanotubes from 50 to 200 nm in diameter.

3.3.2 Electrode Surface

In electrochemistry, both the anode and cathode influence the anodization process. The main material used as cathode is a conductive material, platinum, due to its high stability. Nevertheless, some authors [41] have used different cathode systems to develop alternatives to the platinum-based electrode as it is quite expensive. Therefore, various cathode materials such as Ni, Pd, Fe, Co, Cu, Ta, W, C, Al, and Sn were used for producing TiO_2 nanotubes. Only the Ni, Pd, and C cathodes have produced similar homogen nanotubular structures as Pt. However, nickel shows lower stability than the two other materials. Instable materials could lead to element contamination, which should be problematic in biomedical application.

In our case, titanium implants or alloys are used as anode. The chemical composition of the surface could vary from alpha phase or both alpha and beta phases. Those two titanium phases have found to form nanostructure

under different conditions and thus give microheterogeneity into the nanotubular array as observed in [42,43]. It has also been shown that a more uniform and regular nanotube array is obtained after a second anodization [44]. Nanoanodization with a short treatment time does not modify the initial surface roughness of the titanium surface. Therefore, the nanostructuration of implants is compatible with microroughened surfaces obtained by grit blasting or polished surface. As the developed surface of the implant increases, the current rises proportionally. This increase of surface area and current could modify bath temperature and thus the oxide layer characteristics [28]. In general, this electrochemical processing enables to treat complex geometries (Tullio Monetta 2013). However, in the case of masked area from the cathode, the equilibrium between the formation and dissolution of the oxide layer can be broken, which can lead to heterogeneity of structures.

4. BIOMEDICAL APPLICATIONS OF NANOSTRUCTURED TITANIUM DIOXIDE COATING

Surface properties play a determinant role in biological interactions. In particular, the nanometer-sized roughness and the chemistry have a key role in the interactions of surfaces with proteins and cells. These early interactions will in turn condition the late tissue integration. In this prospect, nanostructuration of the TiO_2 layer may be beneficial for enhancing bone healing around titanium implants.

The nanoanodization is applicable to complex-shaped medical implants, and either nanopores or nanotubes have been uniformly produced on dental implants, orthopedic implants, or spine fusion devices. Anodization is a method commonly used to obtain nanoscale oxides on metals including titanium. By adjusting the anodization condition such as voltage, time, and shaking, nanoscale properties can be controlled. Shankar et al. [38] had reported that the diameters of the nanotubes could be adjusted to a range from 20 nm up to 100 nm by modifying voltage conditions. On the other hand, Kang et al. [45] found that TiO_2 nanotube arrays were more uniform on electropolished titanium than machined titanium.

4.1 Medical Device Applications and Biocompatibility

During surgery, blood vessels are injured and thus, implant surfaces interact with blood components. Various plasma proteins get adsorbed on the material surface within a minute. Platelets from the blood interact also with the

implant surface. Plasma proteins modify the surface, while activated platelets are responsible for thrombus formation and blood clotting. Subsequently, various cell types will after migration to the surface interact with the modified surface through membrane integrin receptors. These early events occur prior to peri-implant tissue healing.

Following blood clotting around implants, several cells interact with surfaces for tissue healing. Mesenchymal stem cells (MSCs) attracted to the injured site by chemotactic factors have a determinant role in peri-implant tissue healing. Numerous studies have shown that nanometer-sized features on surfaces direct stem cell fate through protein adsorption and cell signaling pathways [2,46,47]. MSCs are multipotent cells that are present in the bone marrow, peripheral blood, and other tissues in very low levels. These cells are attracted to the peri-implant healing site by cytokines and are able to migrate through the blood clot to colonize the implant surface. Depending on their microenvironment, MSCs can differentiate into different lineages such as osteoblasts (bone), chondrocytes (cartilage), adipocytes (fat), or fibroblasts (skin).

The surface properties of implants may control the differentiation of MSCs and thus the type of peri-implant tissue. Nevertheless, this hypothesis has mainly been validated *in vitro*. For instance, it has been shown that cytoskeleton tensions modulate gene expression through the Ras homologue gene family, member A (RhoA) molecular pathway and regulate stem cell lineage commitment [48]. Dalby et al. have shown that random nanostructured surfaces induce the osteoblastic differentiation of MSCs, even without osteogenic supplements [49]. Titania nanotubes obtained by anodization have been shown to control the adhesion and osteoblastic differentiation of MSCs [50,51]. These studies have demonstrated that nanotubes measuring 30 nm in diameter favor cell adhesion, whereas larger nanopores of 70-100 nm induce cell elongation, cytoskeletal stress, and selective differentiation into osteoblastic cells. It has been shown that TiO_2 nanotubes on Ti improved the activity of alkaline phosphatase (ALP) by MSCs. Since ALP is a marker of osteogenic differentiation, these surfaces may demonstrate enhanced bone tissue-integrative properties. We have indeed demonstrated a correlation between the osteoblastic cell differentiation and bone tissue integration of nanostructured titanium implants [14].

In a more recent study, we have compared the bone tissue integration of machined (MA), standard microroughened (MICRO), and nanostructured (NANO) titanium implants by implantation into the femoral epiphysis of rabbits. After 4 weeks of healing, all types of implants appeared well

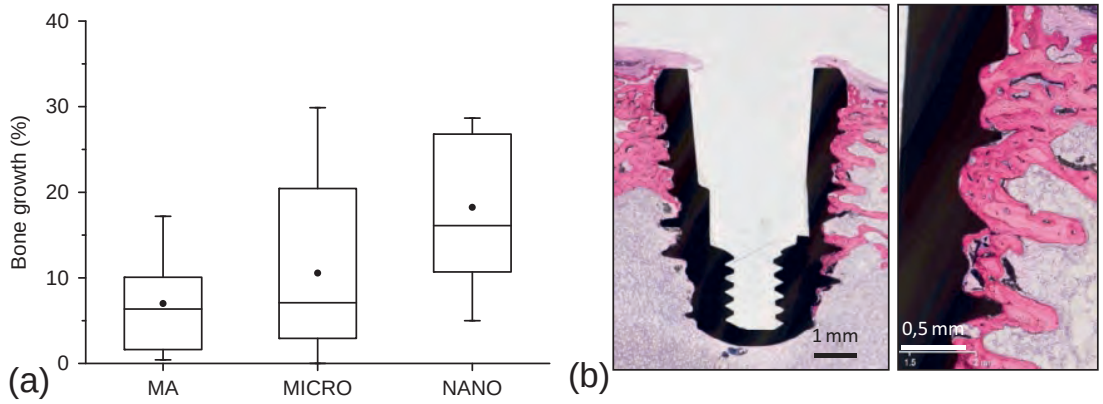

Figure 5 (a) Bone growth into titanium implants after 4-weeks implantation in femoral epiphyses of rabbits with three different surface treatments: machined (MA), grit-blasted and acid-etched creating micro-roughness (MICRO) and anodizing in HF electrolyte creating nanotubes array on the titanium surface (NANO) (* if $p < 0.05$). (b) Nondecalcified histology sections of dental implant inserted in bone tissue at 4 weeks (basic fuchsine and methylene blue staining; original magnifications $\times 1$ and $\times 10$).

integrated into the bone without macroscopic signs of osteolysis. As shown in Figure 5, the quantitative assessment of the bone growth was higher for the NANO implants than for the MICRO and MA implants. The histological sections corroborated bone tissue healing around the implants (Figure 5). Newly formed bone apposition was visible at the cortical and trabecular levels. The quantity of bone around the implants appeared comparable for the three types of implant surfaces. At high magnification, a thin, fibrous tissue gap between the bone and the MA implants was observed, whereas direct bone-to-implant contact was seen on both NANO and MICRO implants.

4.2 Immobilization of Biologically Active Molecules in the Coatings

Titania nanotubes have an ideal size for many biomolecules, and therefore, these nanotubes are particularly attractive for local drug delivery. For instance, nanotubes may be loaded with growth factors and act as reservoirs for delivering molecules that would trigger tissue repair in the peri-implant region. In this perspective, Neupane et al. have successfully incorporated gelatin-stabilized gold nanoparticles into titania nanotubes by simple vacuum drying. Since gelatin is a thermally denatured form of collagen, it represents a good substrate for cell adhesion [52]. These authors have consequently studied the adhesion and proliferation of osteoblastic cells on standard and modified Ti plates with polished Ti, nanotubes, or

AuNPs-gelatin. After only 1 day of culture, an elongated flattened cell morphology was observed, suggesting a rapid cell spreading on the nanotubes loaded with AuNPs-gelatin surface. Furthermore, they observed a significantly higher osteoblastic cell adhesion and proliferation on the AuNPs-gelatin surface as compared with other groups.

Titanium implants are widely used clinically but postsurgical infections lead to serious complications. During surgery, and particularly in oral implantology, microorganisms may colonize the surface of implants and hamper the tissue integration. It becomes especially difficult for the immune system to clear robustly adherent antibiotic-resistant biofilm infections on medical devices. In addition, the expansion of bacterial antibiotic resistance is a growing problem today. For many years, it has been known that silver ions exhibit strong inhibitory effects towards a broad spectrum of bacterial strains. However, Ag^+ is also toxic for mammalian cells at high concentrations. In a recent paper, Zhao et al. have loaded titania (TiO_2) nanotubes with silver nanoparticles. After anodization, titanium implants were simply soaked in $AgNO_3$ solution, followed by ultraviolet light irradiation. Due to the outstanding photocatalytic properties of TiO_2, reduction of Ag^+ occurred and nanoparticles of Ag adhered tightly to the wall of the TiO_2 nanotubes. The amount of Ag introduced to the nanotubes could be easily varied by changing processing parameters such as the $AgNO_3$ concentration and immersion time. Depending on loading conditions, the release of Ag^+ was in the range of 0.05-0.5 ppm for up to 2 weeks, a relatively low concentration compatible to cell viability. They showed that the TiO_2 nanotubes loaded with Ag nanoparticles were effective against bacteria growth and in preventing bacterial adhesion on the implant surface without obvious decline for 30 days. This time span is long enough to prevent postsurgical infection in the early and intermediate stages and perhaps even late infection around dental implants. The authors have also studied the cytotoxicity of silver-loaded nanotubes using osteoblasts. They found limited cytotoxicity of leached samples that could be reduced by controlling the Ag^+ release rate [53]. In conclusion, using TiO_2 nanotubes as release systems to fight together with controlled biological response and accelerated tissue integration may rapidly become an attractive solution for dental and orthopedic implants. This simple method used by Zhao et al. [53] may be an interesting strategy in order to prevent peri-implantitis, one of the major drawbacks in the growing market of dental implants. Future work should examine preclinical models for studying the osseointegration of implants in infected sites.

5. CONCLUSION

Nanotechnology may produce surfaces with controlled topography and chemistry that help to improve our understanding of biological interactions and help to develop novel implant surfaces with predictable tissue-integrative properties. In this perspective, nanotopographies were created, particularly titania nanotubes, by a simple electrochemical anodization of Ti implants. TiO_2 nanotubes grow perpendicularly to the surface, forming a regular array of nanopores with controllable dimensions. It has been shown by several groups that these nanotubes control the fate of MSCs and promote differentiation to osteoblastic lineage. Consequently, many studies have shown that nanostructured Ti implants were similar or even faster and better integrated into bone tissue than untreated ones or with other surface modifications [15,43,54].

6. FUTURE PERSPECTIVES

TiO_2 nanotubes applied on orthopedic or dental implants are potent carriers of proteins that can trigger adhesion, proliferation, or differentiation of cells. The control of cell responses by nanotechnology is a fast-growing field of research as it potentially opens new directions in peri-implant tissue healing. The technology of nanotubes may be introduced to other medical devices such as cardiovascular stents that locally release antithrombotic drugs or growth factors.

REFERENCES

[1] L. Le Guéhennec, A. Soueidan, P. Layrolle, Y. Amouriq, Surface treatments of titanium dental implants for rapid osseointegration, Dent. Mater. 23 (7) (2007) 844–854.
[2] L. Bacakova, E. Filova, M. Parizek, T. Ruml, V. Svorcik, Modulation of cell adhesion, proliferation and differentiation on materials designed for body implants, Biotechnol. Adv. 29 (6) (2011) 739–767.
[3] M.J. Dalby, Topographically induced direct cell mechanotransduction, Med. Eng. Phys. 27 (9) (2005) 730–742.
[4] H.W. Liwen Lin, Enhanced osteointegration of medical titanium implant with surface modifications in micro/nanoscale structures, J. Orthop. Transl. 2 (1) (2014) 35–42.
[5] V. Zwilling, M. Aucouturier, E. Darque-Ceretti, Anodic oxidation of titanium and TA6V alloy in chromic media. An electrochemical approach, Electrochim. Acta 45 (6) (1999) 921–929.
[6] D. Gong, C.A. Grimes, O.K. Varghese, W. Hu, R.S. Singh, Z. Chen, et al., Titanium oxide nanotube arrays prepared by anodic oxidation, J. Mater. Res. 16 (12) (2001) 3331–3334.

[7] D. Guan, P.J. Hymel, C. Zhou, Y. Wang, Engineering bamboo-type TiO_2 nanotube arrays to enhance their photocatalytic property, J. Nanosci. Nanotechnol. 14 (6) (2014) 4541–4550.
[8] R. Yuan, B. Zhou, D. Hua, C. Shi, L. Ma, Effect of metal-ion doping on the characteristics and photocatalytic activity of TiO_2 nanotubes for the removal of toluene from water, Water Sci. Technol. J. Int. Assoc. Water Pollut. Res. 69 (8) (2014) 1697–1704.
[9] P.X. Yunhuai Zhang, Carbon monoxide annealed TiO_2 nanotube array electrodes for efficient biosensor applications, J. Mater. Chem. 19 (7) (2009) 948–953.
[10] Z.-D. Gao, J. Guo, N.K. Shrestha, R. Hahn, Y.-Y. Song, P. Schmuki, Nickel hydroxide nanoparticle activated semi-metallic TiO_2 nanotube arrays for non-enzymatic glucose sensing, Chem. Eur. J. 19 (46) (2013) 15530–15534.
[11] H.M.A. Javed, W. Que, Z. He, Anatase TiO_2 nanotubes as photoanode for dye-sensitized solar cells, J. Nanosci. Nanotechnol. 14 (2) (2014) 1085–1098.
[12] X. Zhen, D. Yu, F.-Q. Xiong, M. Li, Z. Yang, J. Zhu, et al., Controlled growth of semiconductor nanofilms within TiO_2 nanotubes for nanofilm sensitized solar cells, Chem. Commun. (Camb.) 50 (33) (2014) 4364–4367.
[13] K.S. Brammer, C.J. Frandsen, S. Jin, TiO_2 nanotubes for bone regeneration, Trends Biotechnol. 30 (6) (2012) 315–322.
[14] S. Lavenus, V. Trichet, S. Le Chevalier, A. Hoornaert, G. Louarn, P. Layrolle, Cell differentiation and osseointegration influenced by nanoscale anodized titanium surfaces, Nanomedicine 7 (7) (2012) 967–980.
[15] Y.-T. Sul, Electrochemical growth behavior, surface properties, and enhanced *in vivo* bone response of TiO_2 nanotubes on microstructured surfaces of blasted, screw-shaped titanium implants, Int. J. Nanomedicine 5 (2010) 87–100.
[16] P. Chennell, E. Feschet-Chassot, T. Devers, K.O. Awitor, S. Descamps, V. Sautou, *In vitro* evaluation of TiO_2 nanotubes as cefuroxime carriers on orthopaedic implants for the prevention of periprosthetic joint infections, Int. J. Pharm. 455 (1–2) (2013) 298–305.
[17] Y. Hu, K. Cai, Z. Luo, D. Xu, D. Xie, Y. Huang, et al., TiO_2 nanotubes as drug nanoreservoirs for the regulation of mobility and differentiation of mesenchymal stem cells, Acta Biomater. 8 (1) (2012) 439–448.
[18] T. Shokuhfar, S. Sinha-Ray, C. Sukotjo, A.L. Yarin, Intercalation of anti-inflammatory drug molecules within TiO_2 nanotubes, RSC Adv. 3 (38) (2013) 17380–17386.
[19] Y.-Y. Song, F. Schmidt-Stein, S. Bauer, P. Schmuki, Amphiphilic TiO_2 nanotube arrays: an actively controllable drug delivery system, J. Am. Chem. Soc. 131 (12) (2009) 4230–4232.
[20] N.H. Wael Att, Time-dependent degradation of titanium osteoconductivity: an implication of biological aging of implant materials, Biomaterials 30 (29) (2009) 5352–5363.
[21] P. Hoyer, Formation of a titanium dioxide nanotube array, Langmuir 12 (6) (1996) 1411–1413.
[22] C. Bae, H. Yoo, S. Kim, K. Lee, J. Kim, M.M. Sung, et al., Template-directed synthesis of oxide nanotubes: fabrication, characterization, and applications, Chem. Mater. 20 (3) (2008) 756–767.
[23] J. Qiu, W. Yu, X. Gao, X. Li, Fabrication and characterization of TiO_2 nanotube arrays having nanopores in their walls by double-template-assisted sol-gel, Nanotechnology 18 (29) (2007) 295604.
[24] M. Zhang, Y. Bando, K. Wada, Sol-gel template preparation of TiO_2 nanotubes and nanorods, J. Mater. Sci. Lett. 20 (2) (2001) 167–170.
[25] N. Liu, X. Chen, J. Zhang, J.W. Schwank, A review on TiO_2-based nanotubes synthesized via hydrothermal method: Formation mechanism, structure modification, and photocatalytic applications, Catal. Today 225 (2014) 34–51.

[26] C.L. Wong, Y.N. Tan, A.R. Mohamed, A review on the formation of titania nanotube photocatalysts by hydrothermal treatment, J. Environ. Manage. 92 (7) (2011) 1669–1680.
[27] A.W. Tan, B. Pingguan-Murphy, Review of titania nanotubes: fabrication and cellular response, Ceram. Int. 38 (6) (2012) 4421–4435.
[28] G.K. Mor, O.K. Varghese, M. Paulose, K. Shankar, C.A. Grimes, A review on highly ordered, vertically oriented TiO_2 nanotube arrays: fabrication, material properties, and solar energy applications, Sol. Energy Mater. Sol. Cells 90 (14) (2006) 2011–2075.
[29] P. Roy, S. Berger, P. Schmuki, TiO_2 nanotubes: synthesis and applications, Angew. Chem. Int. Ed. 50 (13) (2011) 2904–2939.
[30] J.-H. Lee, I.-C. Leu, M.-C. Hsu, Y.-W. Chung, M.-H. Hon, Fabrication of aligned TiO_2 one-dimensional nanostructured arrays using a one-step templating solution approach, J. Phys. Chem. B 109 (27) (2005) 13056–13059.
[31] G. Liu, K. Wang, N. Hoivik, H. Jakobsen, Progress on free-standing and flow-through TiO_2 nanotube membranes, Sol. Energy Mater. Sol. Cells 98 (2012) 24–38.
[32] S. Minagar, C.C. Berndt, J. Wang, E. Ivanova, C. Wen, A review of the application of anodization for the fabrication of nanotubes on metal implant surfaces, Acta Biomater. 8 (8) (2012) 2875–2888.
[33] M.V. Diamanti, M. Ormellese, Anodic titanium oxide as immobilized photocatalyst in UV or visible light devices, J. Hazard. Mater. 186 (2–3) (2011) 2103–2109.
[34] D.A.H. Hanaor, C.C. Sorrell, Review of the anatase to rutile phase transformation, J. Mater. Sci. 46 (4) (2011) 855–874.
[35] P. Xiao, D. Liu, B.B. Garcia, S. Sepehri, Y. Zhang, G. Cao, Electrochemical and photoelectrical properties of titania nanotube arrays annealed in different gases, Sens. Actuators B Chem. 134 (2) (2008) 367–372.
[36] S. Sreekantan, Z. Lockman, R. Hazan, M. Tasbihi, L.K. Tong, A.R. Mohamed, Influence of electrolyte pH on TiO_2 nanotube formation by Ti anodization, J. Alloys Compd. 485 (1–2) (2009) 478–483.
[37] S. Sreekantan, K.A. Saharudin, Z. Lockman, T.W. Tzu, Fast-rate formation of TiO_2 nanotube arrays in an organic bath and their applications in photocatalysis, Nanotechnology 21 (36) (2010) 365603.
[38] K. Shankar, G.K. Mor, H.E. Prakasam, S. Yoriya, M. Paulose, O.K. Varghese, et al., Highly-ordered TiO_2 nanotube arrays up to 220 μm in length: use in water photoelectrolysis and dye-sensitized solar cells, Nanotechnology 18 (6) (2007) 065707.
[39] M. Paulose, H.E. Prakasam, O.K. Varghese, L. Peng, K.C. Popat, G.K. Mor, et al., TiO_2 nanotube arrays of 1000 μm length by anodization of titanium foil: phenol red diffusion, J. Phys. Chem. C 111 (2007) 14992–14997.(cité 5 déc 2014). Disponible sur: http://wenku.baidu.com/view/5dd6824a852458fb770b5603.
[40] Y.C. Satoshi Kaneco, Fabrication of uniform size titanium oxide nanotubes: impact of current density and solution conditions, Scr. Mater. 5 (2007) 373–376.
[41] N.K. Allam, C.A. Grimes, Effect of cathode material on the morphology and photoelectrochemical properties of vertically oriented TiO_2 nanotube arrays, Sol. Energy Mater. Sol. Cells 92 (11) (2008) 1468–1475.
[42] C. Pérez-Jorge, A. Conde, M.A. Arenas, R. Pérez-Tanoira, E. Matykina, J.J. de Damborenea, et al., *In vitro* assessment of Staphylococcus epidermidis and Staphylococcus aureus adhesion on TiO_2 nanotubes on Ti-6Al-4V alloy, J. Biomed. Mater. Res. A 100A (7) (2012) 1696–1705.
[43] L. Salou, A. Hoornaert, G. Louarn, P. Layrolle, Enhanced osseointegration of titanium implants with nanostructured surfaces: an experimental study in rabbits, Acta Biomater. 11 (2015) 494–502.
[44] Y. Lai, J. Gong, C. Lin, Self-organized TiO_2 nanotube arrays with uniform platinum nanoparticles for highly efficient water splitting, Int. J. Hydrog. Energy 37 (8) (2012) 6438–6446.

[45] S.H. Kang, H.S. Kim, J.-Y. Kim, Y.-E. Sung, An investigation on electron behavior employing vertically-aligned TiO_2 nanotube electrodes for dye-sensitized solar cells, Nanotechnology 20 (2009) 355307.
[46] K. Cai, J. Bossert, K.D. Jandt, Does the nanometre scale topography of titanium influence protein adsorption and cell proliferation? Colloids Surf. B: Biointerfaces 49 (2) (2006) 136–144.
[47] S. Lavenus, J.-C. Ricquier, G. Louarn, P. Layrolle, Cell interaction with nanopatterned surface of implants, Nanomedicine 5 (6) (2010) 937–947.
[48] R. McBeath, D.M. Pirone, C.M. Nelson, K. Bhadriraju, C.S. Chen, Cell shape, cytoskeletal tension, and RhoA regulate stem cell lineage commitment, Dev. Cell 6 (4) (2004) 483–495.
[49] M.J. Dalby, N. Gadegaard, R. Tare, A. Andar, M.O. Riehle, P. Herzyk, et al., The control of human mesenchymal cell differentiation using nanoscale symmetry and disorder, Nat. Mater. 6 (12) (2007) 997–1003.
[50] J. Park, S. Bauer, K. von der Mark, P. Schmuki, Nanosize and vitality: TiO_2 nanotube diameter directs cell fate, Nano Lett. 7 (6) (2007) 1686–1691.
[51] S. Oh, K.S. Brammer, Y.S.J. Li, D. Teng, A.J. Engler, S. Chien, et al., Stem cell fate dictated solely by altered nanotube dimension. Proc. Natl. Acad. Sci. 106 (7) (2009) 2130–2135, http://dx.doi.org/10.1073/pnas.0813200106.
[52] M.P. Neupane, I.S. Park, T.S. Bae, H.K. Yi, M. Uo, F. Watari, et al., Titania nanotubes supported gelatin stabilized gold nanoparticles for medical implants, J. Mater. Chem. 21 (32) (2011) 12078–12082.
[53] L. Zhao, H. Wang, K. Huo, L. Cui, W. Zhang, H. Ni, et al., Antibacterial nanostructured titania coating incorporated with silver nanoparticles, Biomaterials 32 (24) (2011) 5706–5716.
[54] L.M. Bjursten, L. Rasmusson, S. Oh, G.C. Smith, K.S. Brammer, S. Jin, Titanium dioxide nanotubes enhance bone bonding *in vivo*, J. Biomed. Mater. Res. A 92 (3) (2010) 1218–1224.

1.4 Conclusion

This first chapter establishes the state of the art of this multidisciplinary thesis. It makes it possible to present the properties and context of application of the titanium materials used. This chapter also makes it possible to briefly introduce biology with tissue composition and behaviour in case of implant integration. But the most important aspect is the presentation of the surface treatments currently being commercialised, which only modify the surface at the micrometric scale while nano-scale modification may be a promising way to increase the clinical success of implants.

OBJECTIVES OF THE THESIS

Our interets concern the nano surface treatement of titanium surface. Currently, several approaches enable to modify the surface at the nanometer scale. In this thesis, we focused on the synthesis of TiO_2 nanotubes and nanopores structure via a cost effective process of anodisation. Athought, the biological effects of nano-porous surfaces have been already studied by authors [23, 39, 40, 41, 42], only a few publications has applied this new bioactive surface treatment directlty on medical devices [28, 43, 44].

The objective of this thesis work is to develop a new bioactive nano-surface intended for industrial application to enhance soft and hard tissue integration. To study of the potential of this honeycomb surface in terms of medical applications, we perfomed 3 main step:

- The synthesis and physico-chemical characterization of the nano-surface on titanium implant.
- The biological characterization of this nano-surface as compared to a commonly commercialized micrometric surface.
- The transposition this surface treatment to medical devices (DM) such as dental implants and tracheal prosthesis.

This PhD project was carried out as part of a financing CIFRE (industrial agreements on training through research) within the company Biomedical Tissue in Nantes.

CHAPTER

2

MATERIALS AND METHODS

This chapter introduces our experimental methods for nanotubular titanium dioxide formation using an electrochemical anodisation process. Then, the principles of certain experimental techniques will be briefly exposed. First of all, various surface characterisations such as MEB, the topographical method, and contact angle will be described. The mechanical characterization, element release and nanoparticle detachment will be presented in two other parts. Last part but not least, we will present the methods used for the characterisation of the biological effects *in vivo*, histomorphometric calculations and its statistical analysis.

2.1 Preparation of TiO2 nanotubes array

The anodising protocol used in this thesis, based on the synthesis of titania nanotubes, was taken and adapted from S. Lavenus et al. [82] themselves inspired by the Seughan Oh publication in 2009 [23]. This process used a first generation electrolyte composed of diluted HF based on an aqueous solution. The thickness of the titania nanostructure is relatively limited (<500 nm) and may thus minimise the risk of exfoliation.

2.1.1 Titanium substrate

In this work, the samples used were supplied by MicroPrecis for the Ti-6Al-4V ELI and by Createct for the Ti cp grade 2. Various geometries were used: coin-

shaped, cylindrical shaped implants, dental implants or tracheal prostheses. All the sample used are displayed in **Figure 2.1**.

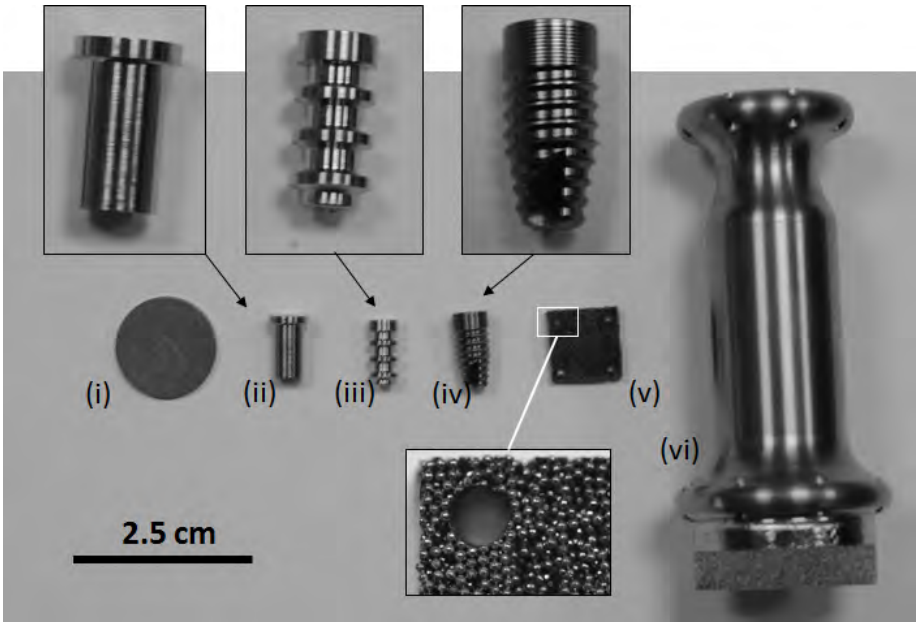

Figure 2.1: Macroscopic images of samples used in this thesis: **(i)** titanium disks (Ti cp and TA6V, machined and blasted) used for surface characterisation; **(ii)** cylindrical implants with an apical bone growth chamber (Ti cp, machined) used for an *in vivo* study published in Article N° 1; **(iii)** cylindrical implants shape with circular bone chamber (TA6V, machined and blasted) used for surface characterisation; **(iv)** dental implants (Tip, TA6V, machined and blasted) used for process valitation and in an*in vivo* published in Article N° 2 ; **(v)** 3D porous titanium disks (Tip, sintered) used in an *in vivo* published in Article N° 3 and **(v)** tracheal prothesis (Tip, finished and sintered) used for surface characterisation

In addition to the different chemical composition, these alloys present different structural compositions. Pure titanium is only composed of an alpha phase, while the TA6V microstructure is a mixture of alpha/beta. This beta phase is present from a range of 5 to 20 %. The titanium microstructure may be revealed by surface etching using Kroll's reagent (an aqueous solution containing HF and $HN0_3$) and optical microscope observation. The chemical composition of the sample is presented in **Table 2.1**.

Substrate preparation – The original surfaces were either machined, slightly polished or sand blasted using alumina particles. In order to obtain a homogeneous and adherent deposit, the substrate must be free of impurities

Table 2.1: Chemical composition of the titanium alloys Wt.%

Alloys	C	N	O	Al	Ti	V	Fe
Ti-6Al-4V ELI	0.0004	0.002	0.13	5.92	89.91	3.86	0.17
Ti T40 Grade2	0.022	0.012	0.11	-	99.82	-	0.040

(physical debris, fat traces) from manipulations. Thus, Titanium pellets were cleaned by successive immersion in acetone, 70 % alcohol and distilled water for 10 minutes each and then dried in air.

2.1.2 Process configuration

Electrochemical mounting – The anodisation process consists of applying a potential (potentiostatic method) or a current (galvanostatic method) between a standard two or three electrode process (**Figure 2.2**). The treated metal plays the role of anode and a platinum inert electrode is a cathode or working electrode. This Pt electrode cylinder is made of wire gauze with a wire diameter 0.15 mm × 360 mesh per cm^2. The current flow in the cell is achieved through the counter electrode. A KCl saturated calomel reference electrode could also be added to the bulk electrolysis cell in order to record evolution in the current-time or voltage-time curve during anodisation process. It is possible to measure cyclic polarisation and impedance using specific instrumentation. The oxidation reaction occurs at the metal interface. The homogeneous distribution of electric charge as well as the dispersion of the gas produced at the surface of the counter electrode is provided by a magnetic bar stirring.

2.1.3 Experimental protocol

Typical anodising conditions – The composition of the first generation electrolyte by Seughan Oh [23] was slightly modified in order to adapt to new requirements in terms of protection of intellectual property (**Table 2.2**). Competing firms working on other surface treatments have filed patents with large claims [24, 25]. Thus, our electrolyte composition was adjusted at 1 wt.% of hydrofluoric acid in water. According to the HF-based aqueous solution, the thickness of the titania nanostructure is relatively limited (<500 nm) and may then minimise the risk of exfoliation. The acetic acid is added to the solution as in the Seughan Oh protocol [23]. Its addition has been shown to improve the mechanical robustness of the nanotubes without changing their dimension [83].

Rinsing step – A basic and simple step that takes all its importance in our surface treatment process. At the beginning of this work, rinsing was carried

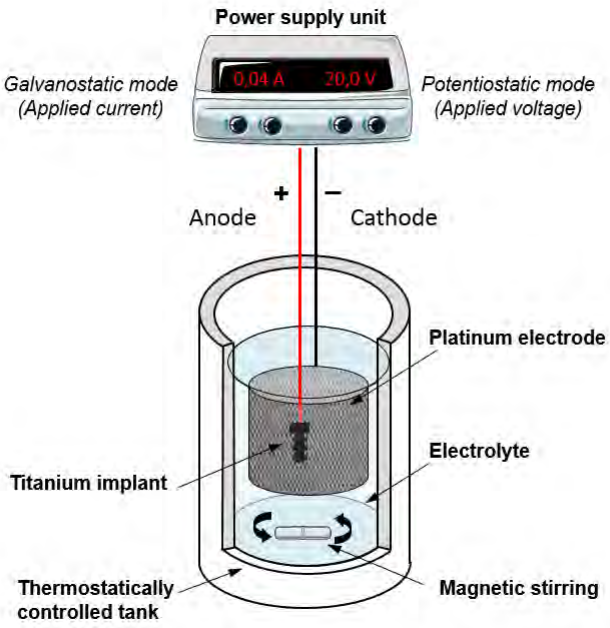

Figure 2.2: Diagram of the electrochemical anodisation mounting for TiO_2 nanoporous or nanotube formation on titanium implant surfaces.

out by soaking the sample in distilled water. Recently, over time the role of water on titania nanotubes detachment was discovered and was replaced by soaking in pure ethanol solution. Moreover, the rinsing bath was shown to give surface heterogeneity due to solution-runs during drying. To avoid it, a second wash-out was carried out in a fast volatile solvent: acetone.

Stabilisation by annealing – The samples were then heat treated for 1 to 2 hours in muffle furnace equipment already preheated to 500 °C. Thereby the amorphous dioxide layer transformed into a more thermodynamically stable crystalline structure (*i.e.* anatase, brookite, rutile).

Precautions to be taken during anodisation – The electrochemical anodisation process enable to control both the nanostructure formation but also visual rendering (uniform colouring). In order to obtain the reproducibility of the results, some precautions must be taken:

- The cell should be designed to maintain a fixed distance between the electrodes themselves and with agitation but also in order to make it easier to handle

Table 2.2: Typical operating conditions for preparing films with a TiO_2 nanostructure using the anodisation process

Parameters	Value
HF concentration	1
Acetic acid conc.	1M
Voltage	$10 - 20$ V
Treatment duration	$10 - 20$ min
Agitation	350 rpm

- The sample size or anode surface developed must be defined and reproducible. Thus some holder units for the titanium coins, cylindrical, dental implants and tracheal prostheses were machined.
- The solution must have a fixed invariable composition during the test. In our case, pH measurements were carried out before and after using.
- The use of a large capacity bath is necessary to dilute the reaction products which can pass into solution
- The temperature bath should be kept constant because it can play a role in the efficiency of other parameters or in the surface treatment itself.
- To ensure an acceptable reproducibility of the results, the tests were repeated at least 3 times for each experiment.

Sterilisation − The samples used for biological evaluation (in vivo) need to be devoid of any microbiological organisms. Thus sterilisation of these surfaces was effected by autoclaving at 121 ˚ C for 20 minutes in individual bags provided for the purpose.

2.2 Surface characterisation

2.2.1 Scanning electron microscope and quantification

The scanning electron microscope (SEM) is designed for surface morphology studies. In our work, this equipment was used to size nanotube length and porosity but also for imaging in histomorphometric analysis. Principle of this technique is described in Appendix A.

Specimen preparation for surface observation − Although a compact titanium dioxide is an electrical insulator, the titania porous structure is a

sufficiently electrical conductor to avoid the charge accumulation phenomenon. It is thus not necessary to use the preparation by metalisation with platinum or gold-paladium before analysis.

Specimen preparation for thickness measurement – Titanium is a very ductile metal and has a tendency for mechanical deformation. The use of a basic cutting process did not make it possible to observe the nanotube profile. A specific preparation of nanotube cross sections was developed. A deep scratch was made in the sample in order to weaken it and the nanotube thickness was measured at the breakage of the sample.

Equipment – Basic surface observations were made using a "Benchtop SEM" TM 3000 (Hitachi, Japan). The acceleration voltage used was 5 kV and most of the other working parameters were automatically defined. Surface observations to higher magnification and high resolution (sub-nanometer) were performed by using SEM-FEG (Field Emission Gun), Merlin brand (Carl Zeiss, Germany) for scanning the sample with a thinner beam. The working parameters were a probe current of 80 pA, a 5 kV accelerating voltage and a working distance of between 4 and 6 mm.

Image analysis via ImageJ – SEM images were taken from $\times 150$ to $\times 100,000$ magnification and analysed using ImageJ, a free open source image processing programme. Calculation of the dimension of the nanoporosity (diameter, circularity) was performed using the particle tracking mode. Other image analyse modes were also used for histomorphometric quantification and are explained in section 2.4.2).

2.2.2 Topography analysis

Topography analyses were carried out in order to characterise the roughness parameters of a surface initially very rough using the Roughness tester or a relative flat by Atomic Force Microscopy. Principles of those two techniques are described in Appendix A. Several surface parameters could be evaluated using these two topographical techniques. Some of them have been correlated to tissue integration in literature. The most interesting parameters are presented in the following **Table 2.3**. Notation of the data from 3D images is noted as Sa, St, ... etc.

Equipment & protocol of Atomic force microscopy – Measurements were made using a Nanosurf easyScan AFM (nanoScience Instruments, Phoenix, US) on a vibration insulation holder (Accurion). Data were acquired using

Table 2.3: Basic topographical parameters for 2D analysis

Name	Description
Ra	**Arithmetic mean deviation** of the surface
Rq	**Root Mean Square deviation** of the surface (Similar to Ra but calculated differently: this parameter is more sensitive to flaw within surface texture than Ra)
Rt	**Total height** of the surface (Heigh between the highest peak and the deepest hole)
Rz	**Maximum Height** of the surface (Ten point height of the surface, calculated by the mean)
RSm	**Average width of periodic patterns** It has no sense on a random roughness surface)
Rku	**Kurtosis** is a measure of the **distribution of spikes** above and below the mean line (Sku>3 indicate sharp peaks and valleys while Sku<3 indicate lack thereof)
Rsk	**Skewness** is a **measure of the asymmetry** of the profile about the mean line (Ssk>0 indicate peaks topography while Ssk<0 indicate a profile with composed of valleys)

nanosurf easy scan 2 software. Topography measurements were made in dynamic mode (tapping mode) with a TAP 190-G candilever. Before the analysis, integral gain (I-gain), proportional gain (P-gain) and the scanning speed were adjusted to obtain an overlay of scanned back and forth. Two to three analyses were carried out on one sample of each surface group with an image width of 40 $\mu m-$ 20 μm and 256 points per line. Gwyddion software made it possible to analyse AFM images and calculate topographical parameters (see section 2.2.2)

Equipment & protocol of surface roughness tester – Measurements were made by Sonats society using an INTRA 2 Roughness tester (Tayor Hobson, England) with a 2 μm conial standard diamond as tip. The length of measurement was 4mm with a speed measurement of 0.25 mm/sec and a cut-off of 0.25 mm (maximum bending of the tip). Measurements were made on one sample per group and three measurements were made on each surface.

2.2.3 Wettability by contact angle

Basic work principle – See Appendix A.

Equipment & protocol – Measurements were made with OCA-206F equipment and SCA software for the acquisition and treatment of data. Typical contact angles were carried out by water sessile drops. The outline of the drops were analysed using a semi automatic Young-Laplace model at the rate of 5 to 10 measures depending on the available on specimens with n=1 for each type of treatment.

2.2.4 X-ray photoelectron spectroscopy

Basic work principle – See Appendix A.
Equipment & protocol – In our work, X-ray photoelectron spectra were recorded with Nova XPS (Kratos) using a monochromatic Al source. First a spectrum covering the energy range of the source (around 1400 eV) was made to identify element regions of interest. Then other spectra were carried out for each element identified for a detailed analysis of its orbital (*e.g.* O, C, F, V, Zn, Al, Ti). XPS profiles obtained by combining ion erosion were made under argon gas with a titania etching rate of 14.7 nm per minute. Atomic percentages of each element were quantified by taking into consideration the sensitivity factors which may differ from XPS instruments (**Table 2.4**).

Table 2.4: Relative Sensitivity Factors (RSF)

	C	O	Ti	F
RSF	1	2.93	7.81	4.43

2.2.5 Raman spectroscopy

Basic work principle – See Appendix A.
Equipment & protocol – Our analysis were done with a Renishaw (InVia) with the following acquisition parameter: laser wavelength of the argon ionized gas : 514,5 nm (green); objective × 50; power 10 % ; Network 2400 stroke/mm and acquisition time of 60 s.

2.3 Nanoparticles released & Mechanical adhesion

In this work, we observed that some nanostructure peel off from the titania surface creating nanoparticule realised. Currently, few analytical methods are

capable of this type of detection in "extreme" conditions such as low sizes (nanoparticles, element) and/ or low concentrations (up to ppt). Thus, Laser Induced Breakdown Detection method was used to verify a possible release of nanoparticles after optimisation of the process.

The mechanical properties of a surface applied to a field such as medical devices are of paramount importance as they can play a role in its efficacy or lead a health risk. The methods aim to characterise the adhesion of our titania nanotubes to the substrate by a scratch test, and wear behaviour will be deducted from the tribology assay.

2.3.1 Laser induced breakdown detection

Basic work principle – Laser Induced Breakdown Detection (LIBD) is a powerful tool for the analysis of weakly concentrated colloidal solutions based on the Laser-Induced Breakdown Spectroscopy (LIBS) principle. A laser pulse beam is focused on a measuring cell containing the solution to analyse (**Figure 2.3**). A specific beam energy makes it possible to generate plasma only if a particle passes through the beam at the focal point. This phenomenon is called a breakdown phenomenon. Thus plasma detection may be carried out using the acoustic method (propagation of a shock wave) or the optical method (light emission). In our case, the detection is made using the acoustic method and we obtain an “s”shaped curve giving the laser energy a function of the probability of breakdown. Thus, the threshold and the slope of the curve give repectively the particle size and concentration. This analysis makes it possible to determine particles down to about 5 nm at low concentrations (up to ppt).

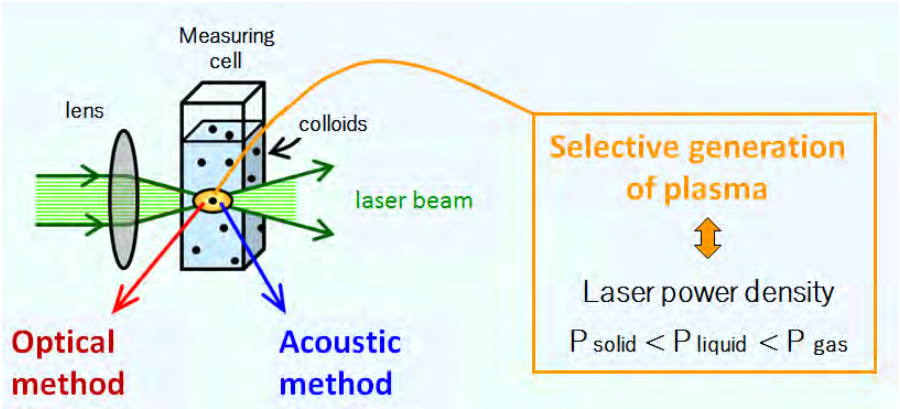

Figure 2.3: Schematic principle of Laser Induced Breakdown Detection (LIBD)

Equipment & protocol used – Analyses were performed with custom-made

equipment from the Subatech laboratory at the EMN (Ecole des Mines de Nantes) under the responsibility of Dr Anne Piscitelli. The wavelength of the laser used is 532 nm and the power beam scan in the range from 10^8 to 10^{10} W/cm^2. Results were based on two analyses at a rate of two specimens per type of sample.

2.3.2 Nano scratch test

Basic work principle – The nanoscratch tester is dedicated to characterising the adhesion properties of thin films or coatings with thicknesses less than 800 μm. The scratch test consists in scratching the surface with a sphero-conical diamond tip, in which is usually applied a gradually controlled normal force. A force control loop makes it possible to apply force independently of the surface profile within the limits of a height of 1 mm. This scratch leads to the occurrence of one or more specific types of damage (cracking, spalling, delamination ...) that are subject to an optical diagnosis (microscopy) to determine the critical load for damages. From a technical point of view, the occurrence of such defects is strongly dependent on the geometry of the tip used and its radius of curvature. The choice of the tip depends on the parts and surfaces to be studied. Moreover, the critical load results depend strongly on thickness. In a comparative study, it is better to have layers of equivalent thicknesses.

Equipment & protocol used – Nanoscratch tests were carried out by CSM Instruments (Anton Paar) and Prof. Thierry Roland of the Charles Sadron Institute (ICS, University of Strasbourg, France). Analyses were performed at the rate of 3 strips of 500 μm per sample tested. The gradient force was from 0.3 mN to 25 mN at 1 mm/min and a slope of 50 mN/min. Thus analysis made it possible to plot the increasing normal force and surface behaviour under load and residual depression. Finally, a comprehensive overview of the scratch for each zone by SEM analysis made it possible to provide confirmation of the results obtained and a distinction between cohesive and adhesive failure.

2.3.3 Nano-tribology

Basic work principle – The tribology analysis is used to determine the friction generated by the contact of two surfaces in movement. It makes it possible to evaluate a material's coefficients of friction and wear. The nano-tribology assay consists of applying to a surface a pin mounted on a cantilever with a controlled low strength. The friction coefficient is determined in real time by measuring the deflection of the cantilever arm. The wear rate of the

ball is assessed by calculating the volume eroded during the test. The pin could take two forms: ball (ball-on-disk) or advanced (pin-on-disc).

Equipment & protocol used – Analyses were carried out in the laboratory by Prof. Jamal Takadoum, FEMTO-ST Institute, University of Franche-Comté. The tests were performed using a CSM Instruments nano tribometer with a rubbing made of Si_3N_4 of 4 mm in diameter with a sliding speed of 1 mm/s. The wear resistance is estimated by calculating the volume of wear at the film after total number of cycles from 100 to 1000 cycles. Normal load varies from 5 to 100 mN. Analyses were performed of flat surfaces (*e.g.* disks) with n=1.

2.4 *In vivo* characterisation

The two animal experimentation and surgical procedures presented in this thesis were conducted according to European Community guidelines for the care and use of laboratory animals (2010/63/UE). The study protocol was submitted for approval to the regional animal care and safety committee. As the animals living conditions and the surgical procedures have been sufficiently described in two articles, the following section will briefly present the animal model and the method of histomorphometric quantification. Statistical tests are presented in the final section.

In October 2014, I graduated from Level 1 animal experimentation accreditation. In 2 weeks at the Veterinary School in Nantes, I learned about the regulations governing animal experimentation, project design and model choice, ethology and animal welfare-enrichment, pain management (anaesthesia and analgesia) and finally respectful killing for animal ethics.

2.4.1 Animal model

The two experiments were performed using adult female New Zealand White (NZW) rabbits provided by a certified breeder (Charles River Laboratories, USA or Hypharm, Roussay, France). Female rabbits (body weight 3.5 kg, age 16-20 weeks) were used because they are less aggressive by nature compared to males. In articles 1 and 2 presented in this work the implantation site was located in the femoral epiphysis of rabbits as shown in **Figure 2.4**. Titanium implants were inserted bilaterally following a permutation implantation. The number of animals was calculated using statistical power to obtain a hypothetical effect of 20 %. An average of 6 animals per group was found to obtain statisticly exploitable results. The animals were operated on under general

anaesthesia. All the surgical steps are described in the articles. Post-operative analgesics were used and after a healing period of 2 to 4 weeks, the animals were euthanised in accordance with ethical guidelines.

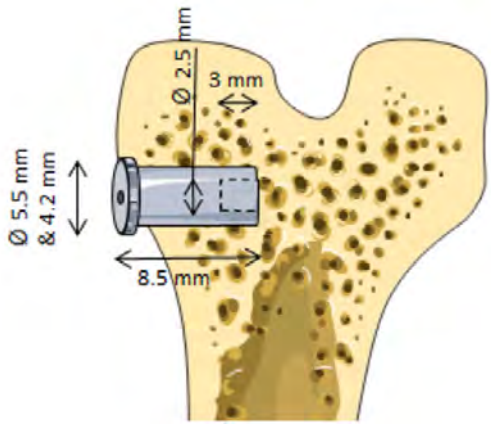

Figure 2.4: Diagram of the implantation site: custom-made implants with a bone growth cavity inserted into rabbit femoral epiphyses

2.4.2 Histomorphometric calculation

After a fixed healing period, the animals were euthanised in accordance with ethical guidelines. The implants were removed with the surrounding tissues and prepared according to a histological protocol: fixation in 4 % paraformaldehyde, dehydration in a gradient alcohol bath, impregnated with methyl methacrylate and finally embedded in a polymethyl methacrylate (PMMA) resin. Then the polymethyl methacrylate blocks were cut using a diamond saw microtome (Leica Sp 1600; Leica, Solms, Germany) in the central longitudinal direction of the implant. Thin sections were stained with basic fuchsine and toluidine blue following a specific protocol [84] and observed using a slide scanner (NanoZoomer 2.0RS and NDP view software, Hamamatsu, Japan). Continuous images at magnification of $\times 50$ were obtained on blocks in back scattered electron mode (BSEM, 2.2.1).

The composite image depicting the titanium implant (white), the new bone (grey) and the resine (dark grey) was used for histomorphometry calculation with ImageJ software. All these calculations were based on methods developed at the UMR957 laboratory of D. Heymann and were adapted and written as macros to a semi-automatic quantification. The following histomorphometry data calculations were polled into a single macro available in the Appendix B. All the measurements were repeated at least three times.

Bone growth (BG) was determined by the threshold of the bone formed in a cavity of the implant in which no bone was initially present. In our first article, this chamber was situated at the apical extremity of the implant.

The Bone-to-implant contact (BIC) was determined over the entire length of the implant inserted into the bone for implant of same size or only at 2 mm-depth corresponding to the average thickness of human cortical bone which gives the homogeneity of the surrounding tissues in case of different implant sizes. This area is called the region of interest (ROI). The calculation consists in dividing the length of the mineralised bone in direct contact with the implant surface and the perimeter of the implant in the ROI, and was expressed as a percentage.

Bone surface (BS/TS 0.5mm) indicates the quality of the environment and/or the osteocondution of the surface by determining the percentage of bone at a distance of 0.5 mm from the implant divided by the total surface (TS) of the ROI. BS/TS 0.5 mm was expressed as a percentage.

2.4.3 Statistical analysis

In this work, samples were statistically expressed using basic descriptive statistics (mean, standard deviation or median, minimum and maximum value) and analysed with specific statistical tests such as Dixon's Q and the non-parametric tests of Mann Whitney test or Kruskal Wallis.

Dixon's Q statistic test is used to identify and reject outliers from a data series. It consists in calculating the ratio between the absolute difference between the outlier in question and the closest number to it, and the extent of the results compared to the critical values ($Q_{critical}$) provided in tables depending on the desired level of confidence, and the number of data in the series. If the calculated value of Q is greater than the value of $Q_{critical}$ selected, the data can be eliminated.

Non-parametric statistical analyses were performed on a low number of samples which not did not make it possible to have a normal distribution of the population. Mann Whitney and Kruskal Wallis are based on observation of the ranks of the results for two or more groups respectively and the result is considered significant for $p < 0.05$ (OriginPro.8 software).

2.5 Conclusion

This chapter is devoted to a detailed description of the various experimental methods used in this thesis work. We optimised the anodisation process on titanium implants and used different methods to characterise the surface treatment

from several points of view: dimensional, composition, mechanical, nanoparticle and biological. We will now report the results obtained from these surface characterisations and the application of this treatment directly on medical implants.

CHAPTER

3

PHYSICAL, CHEMICAL AND BIOLOGICAL CHARACTERISATION OF TITANIA NANOSTRUCTURES

In this chapter, we present first the synthesis and characterisation of titania nanoporous array, then the biological evaluation in rabbits. The results obtained are discussed to correlate surface properties and biological behaviour. The effect of applying current, bath temperature, annealing or other synthesis conditions on nanopore architecture (diameters, length, wall thickness) and properties has already been published in several papers [85, 86, 87]. However during anodisation, the two most important parameters are electrolyte composition and the surface treated. It plays a critical and sensitive role on the synthesis condition which regulates TiO_2 formation. Thus surface characterisation should be performed for each new experimental protocol. In addition, the biological characterisation of titania nanoporous array is widely performed using *in vitro* study or flat and non-complex samples but *in vivo* studies are required to assess the bone tissue integration of implants.

This chapter presents the experimental results of various surface characterisations of our honeycomb titania surface from nanotube morphologies, their properties and the structural and chemical composition. Although our anodic treatment changed the surface at the sub-microscopic scale, the change of colour

was also investigated. And then, to complete this first section, the results of an alternative surface using zinc incorporation to avoid bacterial infection on implants surface is introduced

The second section of this chapter exposes the results of the osseointegration of a nano versus a micro-surface on custom-made and more complex implants in a rabbit model presented in an article in the journal Acta biomaterialia.

3.1 Characterisation of the nanostructured surface

3.1.1 Nanostructured surface formation

Titania nanostructures were synthesized following Sandrine Lavenus' protocol. Anodisation was performed at 20 V (potentiostatic mode) for 20 minutes. The electrolyte solution used was composed of 1 wt.% hydrofluoric acid and 1 M acetic acid with a final pH of about 3.5 at room temperature.

From a macroscopic point of view, typical coloration was observed on the anodised surface. The titanium oxide layer formed on the anodised substrates, and through light interferences, could display various colours. **Figure 3.1** shows the macroscopic aspect of the surface before and after our nano-anodic treatment. The initial surface is grey-mat coloured while the anodic treated surface presented a glossy blue colour. Colour intensity depended on the output current obtained at a voltage of 20 V. This current was proportional to the immerged surface. Thus, the titanium wire used as the sample holder should be masked to obtain an output current for the treated sample only. The second advantage of the masked holder was the fact that the presence of titanium at the electrolyte and air interface seemed to lead to fluctuation in the current density as observed [88]. For example, in **Figure 3.1**, the darker blue sample was treated without masking the titanium wire holder ($I = 0.12A \pm 0.14$) while the other sample was treated with a masked titanium wire ($I = 0.04A \pm 0.01$). The output current was stable and the implant colour was more homogeneous for this last sample.

Sub-microscopic changes are presented by SEM images in **Figure 3.2**. This figure shows titanium surfaces before and after anodic treatment. The initial surface used was a gross machined and sand blasted surface 3.2(a). It presented randomly microscopic large roughness. The surface processed by our anodising protocol showed the regular size and geometry of nanoporosity from the top view 3.2(b) and (c). Diameters were measured around 60 nm with a minimum of 25 nm and a maximum value of 115 nm. Even though the colour changes are observed for the same anodisation conditions, it did not lead to much difference

in terms of nanoporosity. However, as the nanostructures were more uniform in (b) than in (c), experimental conditions that masked the Ti wire were used for continuity in the work.

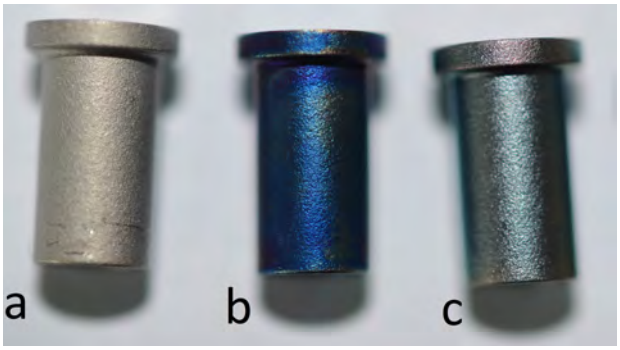

Figure 3.1: Optical micrographs of custom made implants: (a) machined and sand-blasted prior to anodisation, (b) anodised using a non-masked titanium holder (I= 0.12 A), (c) anodised using a masked titanium holder (I= 0.04 A)

The differences in the colours result from the thickness of the oxide layer, as explained by Van Gils *et coll.* [89]. Others authors explored the possibility of calculating thickness by colour observation [90, 91] if the refractive index of the different layers, $n_1 > n_2 > n_3$ or $n_1 < n_2 < n_3$, and thus the light interferences and especially the constructive interference of thin films, can be studied using the following equation. Parameters m, λ, n, d and θ are the diffraction order (an integer), the wave length of light (nm), the refractive index, the thickness of the film and the incident angle respectively.

$$m\lambda = 2nd\sin(\theta) \qquad Bragg's\ law \tag{3.1}$$

The 20 V-anodised samples were both blue in colour. The average wavelength was 460 nm. The refractive index of the TiO_2 film varied depending upon its structure and composition. An average value of n= 2.4 was thus used, in accordance with Yang's publication [91]. By using $\theta = 0$, and m = 1, the thickness of the oxide layer was calculated up to 100 nm. In the case of the blue-grey colour, its wavelength was higher than the indigo wavelength. Thus, the oxide layer thickness should be slightly higher. These results were confirmed by cross section analysis. As depicted in Figure 2 of Article N° 1 presented 3.2.1, it shows columnar growth on a compact barrier layer. The total thickness (columnar growth + barrier layer) of the layer is about 150-170 nm. The thickness of the barrier layer is around 30 to 50 nm.

Differences in coloration for the same anodisation experiment suggest that current density plays a significant role in nanostructure formation. Only a few

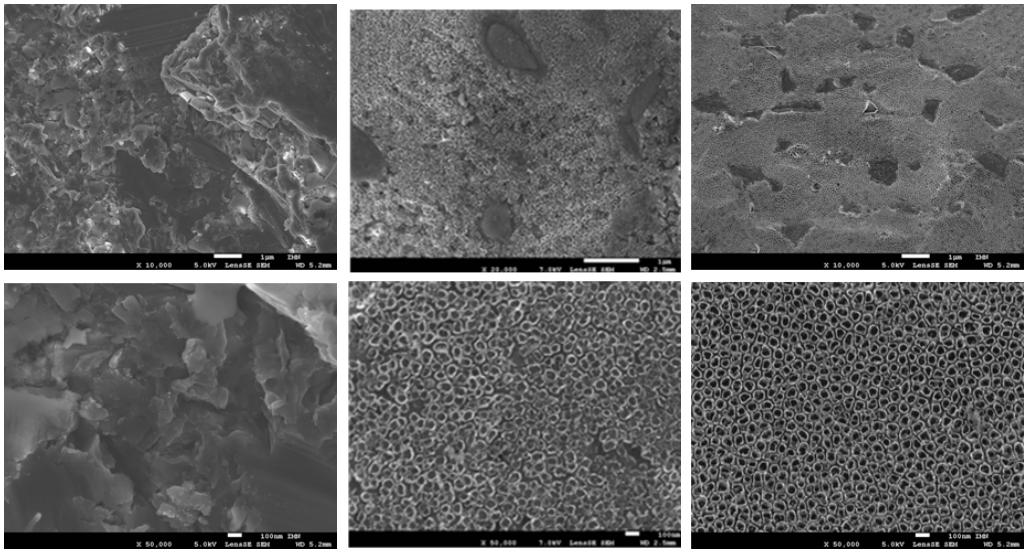

(a) (b) (c)

Figure 3.2: SEM micrographs (top view) at 2 different magnifications ($\times 10,000$ and $\times 50,000$) of the specimen before and after the anodisation process: (a) initial sand-blasted surface presenting randomly microscopic large roughness, (b) TiO_2 nanostructure formed under 20 V and presenting a nanotubular morphology using a non-masked titanium holder, (c) TiO_2 or a masked titanium holder

publications deal with the possibility of using a constant-current mode, which is easier for industrial processes. Kaneco Satoshi *et al.*, formed nanotubes of 30 nm to 145 nm with current densities of 10 to 30 mA/cm^2 in 1 wt.% HF [88]. By calculation, the current densities in constant-voltage mode were about 20 mA/cm^2. However, our results, obtained in galvanostatic mode, gave only nanoporous structures and no nanotubular layers. For the continuity of this work, we remained in constant-voltage mode, while keeping in mind that the galvanostatic mode would be better for scaling up.

3.1.2 Effect of anodic conditions

In this part, the anodic parameters such as voltage, time of treatment and stirring were studied in order to determine their effect on the nano-surface, and in order to optimise the process for industry. Many publications have already dealt with these anodic condition effects, such as electrode material, voltage, time of treatment, agitation, solution etc. and have been used to discuss the results.

First of all, anodisation voltage was studied. It varied from 2 to 25 V. SEM images of some of the surfaces obtained are shown at 3 different magnifications in **Figure 3.3**. It clearly shows that the voltage applied affects the surface morphology. By applying a voltage of 5 V, nano-pits were created on the surface while nanopore array was generated for a voltage of 10 V. Self-organised nanotubes with regular patterns were obtained at high voltages of 20 V. Slightly above this value (22-25 V), the nanotubes were damaged. At the same time, voltage that was too low led to acid etching of the surface. This observation is consistent with the results of other publications [92, 85]. Our main interest and focus for the continuity of this work was a nanostructure array composed of nanopores or nanotubes.

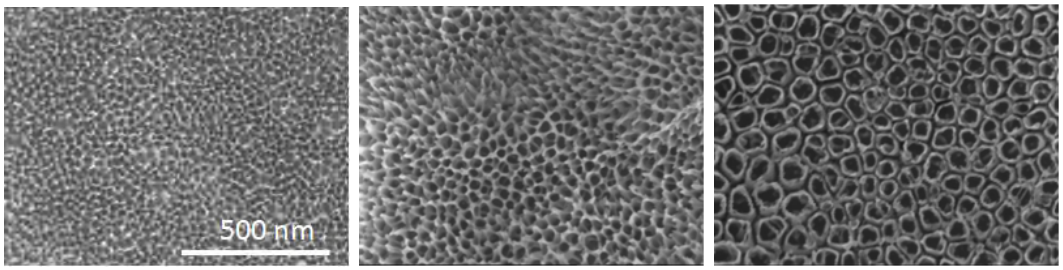

(a) (b) (c)

Figure 3.3: SEM micrographs (top view) of a TiO_2 nanostructure with significantly different morphology and diameter created at potentials ranging between 5 V (a), 10 V (b) and 20 V (c) at 3 different magnifications: $\times 5,000$, $\times 20,000$ and $\times 100,000$.

Measuring wettability is a basic characteristic when carrying out a surface treatment. In our case, we calculated the surface wettability by sessile drop. **Figure 3.4** presents the profile of the drops on different surfaces. The initial surface prior to anodisation was hydrophobic with a contact angle of 81 $^\circ$. In the same position, nanotubular structures give a higher contact angle of 105 $^\circ$. This drop behaviour resembles that observed for the lotus leaf. Unlike the other two surfaces, the nanopores led to higher hydrophilicity with a contact angle down to 62 $^\circ$. Thus, these two surfaces whose manufacturing processes are very similar, have different properties. This is interesting for biological applications. The wettability of the surface has often been studied in cell integration, tissue and also as an antibacterial surface [11, 38, 93, 94].

The second anodic parameter studied was the time of treatment. It varied from 2 min to 60 min. SEM analysis revealed that with 10 to 60 minutes of treatment there was no change in either surface coloration or nanoporosity (shape and size). However, with shorter times (1 to 2 min) we observed only

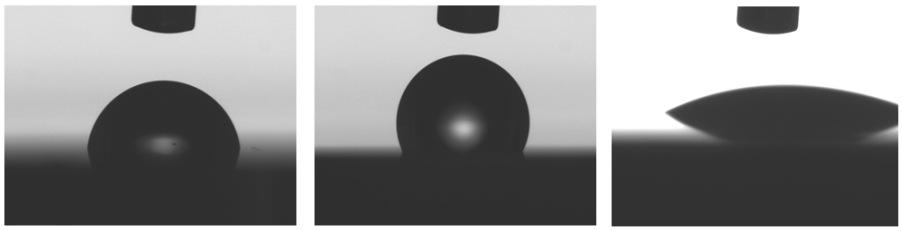

(a) (b) (c)

Figure 3.4: Sessile drop of 5 μL water on different surfaces: initial surface prior to anodisation (a) and with TiO_2 nanostructure created at 10 V (nanopores) (b) and 20 V (nanotubes) (c)

the beginning of nanostructure formation. These same results were obtained by Antony *et al.* [95]. As described by Yu *et coll.*, at a constant applied voltage and anodisation time, oxide layer thickness also increases in the beginning, and reaches a plateau after a certain period of reaction time [90]. The dimensions of the implants were measured using a Vernier calliper prior to and after anodisation. The results show that our anodisation process is a subtractive surface treatment due to the acidic solution. Approximately 43($\pm$10) microns of material were thus etched per hour. Time treatment from 10 to 20 minutes ($<$ 27($\pm$8) microns/hour) was chosen as a balance between manufacturer tolerance (usually round 50 μm) with regard to the dimensions of the implant, and the formation of the nanostructure.

The final parameter studied was solution stirring. Stirring is generally a fixed parameter in studies. Lavenus *et al.* used a stir speed of 350 rpm. We studied the effect of increasing or decreasing stir speed, from 0 to 500 rpm. **Table 3.1** shows the different current values as a function of the stir rate. Without stirring, the current drops, while higher currents were obtained with vigorous agitation. Mixing the solution made it possible to increase the ion exchange and thus accelerate the reaction. As seen previously, current density is important for nano-formation and stirring plays an important role in the electrochemical process.

Table 3.1: Current values as a function of stirring for a unit treatment of cylindrical implant

Stirring (rpm)	0	350	500
Current (A)	$<$0.01	0.04	0.06

3.1.3 Effects of the titanium substrate

Anodising parameters are often tested on a given substrate. However, it seems that only a few publications evoke the effects of varying the initial surface [96, 97].

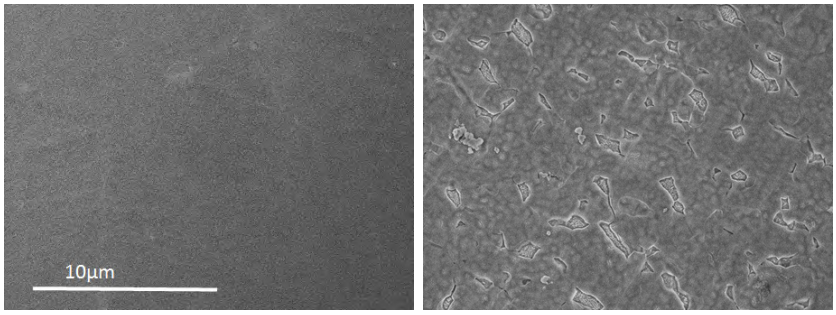

(a) (b)

Figure 3.5: SEM micrographs (top view) of TiO_2 nanostructured layer created at potentials ranging of 20 V of (a) pure titanium surface (Ti cp) and (b) titanium alloy (TA6V) (magnification 5,000)

Figure 3.5 opposite shows the surface appearance obtained after anodising a pure titanium surface and TA6V alloy. The differences in the surface are visible at a low magnification of 5,000. Flat micrometer dark particles were observed in nano-porous array on the alloy surface, while completely homogeneous structures were obtained for pure titanium. These particles or areas correspond to the body-centred cubic β phase grains naturally present in certain alloys annealed above a temperature of 890 $^\circ$ C and hardened. The nanostructure array formed alpha phase structure which mainly compose pure titanium implants. However some other have published the total nanostructuration of beta alloys [87]. These two structures can be revealed by a Kroll reaction as shown in Figure 2(a) of the article N^o 1 presented in part 3.2.1.

3.1.4 Effect of annealing on crystal structure

The main disadvantage of titania nanostructuration by means of the anodic process is the formation of an amorphous structure. This structure is thermodynamically unstable. Annealing treatment is used to convert the amorphous phase into a crystalline phase of TiO_2: anatase, rutile or brookite. Brookite is a metastable structure like anatase which was less explored in the literature until recently and which will thus not be explored in detail in this section. As

presented in chapter 1, the composition of the crystalline structure may play a role in surface biocompatibility in comparison to a non-crystalline surface. Our objective was to characterise the chemical structure in relation to synthesis parameters or the initial surface. The end objective was to propose an annealing process making it possible to obtain a stable nanostructure with the crystal structure offering the best biocompatibility.

In our work, TA6V samples were heated from 300 to 600 ° C in air for 0.5 to 2 hours. Titania nanotubes were observed by SEM to determine the effect of the annealing temperature on nanotube morphology, and by Raman spectroscopy to determine the resulting crystal structure.

Table 3.2: Raman vibrational modes for TiO_2 phases

Phase	Peack (cm^{-1})					
Anatase	144 (E_g)	197 (E_g)	399 (B_{1g})	513 (A_{1g})	519 (B_{1g})	639 (E_g)
Rutile	143 (B_{1g})	447(B_{1g})	612(B_{1g})	826 (B_{1g})		
Brookite	156 (A_{1g})	245 (A_{1g})	287 (B_{3g})	320 (B_{1g})	365 (B_{2g})	637(A_{1g})

Figure 3.6 shows the composition of the titania structures before ("unstreated") and after anodising ("anodised"), with annealing ("A + conditions of annealing"), and in relation to the annealing temperature and time of thermal treatment for nanoporous structures formed at 10V. **Figure 3.7** also shows the effect of annealing parameters on the crystal structure formed by annealing of the nanotubular structure formed at 20V. The peak corresponding to the Raman vibrational modes of the TiO_2 phases described in Table 3.2 were also indicated on the graph with vertical full or dotted lines.

First of all, the results show an amorphous structure for the TiO_2 before and after anodisation without annealing. Heat treatment with varying temperature and time parameters made it possible to obtain different structures. At low temperatures (from 300 ° C to 450 ° C) the conversion of the amorphous titania nanotubes into a mixture of anatase and rutile phases was observed. As reported in the literature, anatase is known to progressively transform into rutile. At temperatures of more than 550 ° C, the TiO_2 crystal phase was composed of only the pure rutile form.

Regarding the effect of annealing time on crystalline structure formation, it played a role in phase transformation from amorphous to anatase, and from anatase to rutile. Annealing at 500 ° C for 0.5 hour thus made it possible to obtain the same structure as obtained at 450 ° C for 2 hours.

Analyses carried out on the nanotubular surfaces revealed slighly different results. The structures obtained at 450 and 500 ° C were mainly composed of

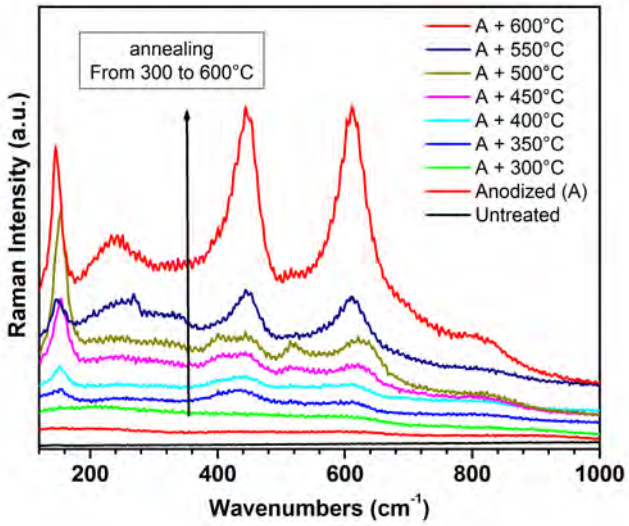

(a)

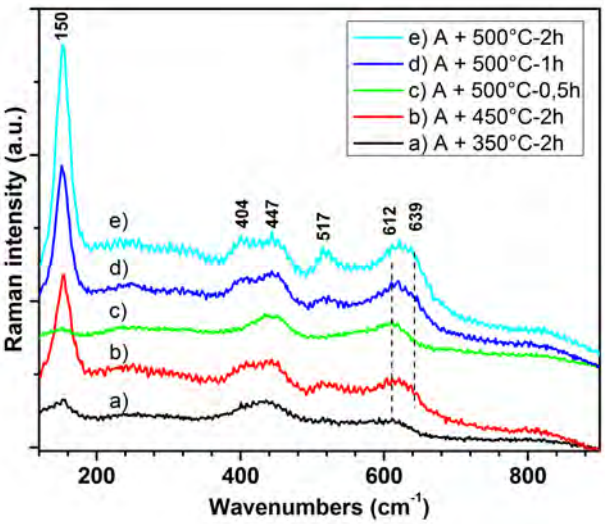

(b)

Figure 3.6: Raman spectroscopy showing evolution in titania crystalline structure in relation to the annealing temperature (a) and time (b) obtained on nanopores formed at 10V for 20 min

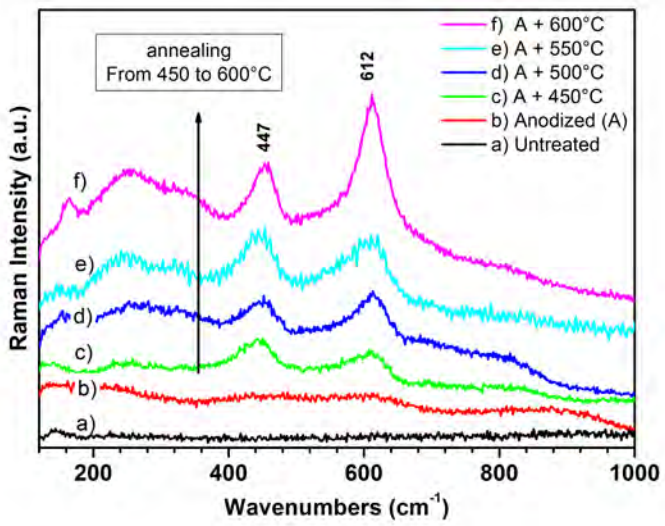

(a)

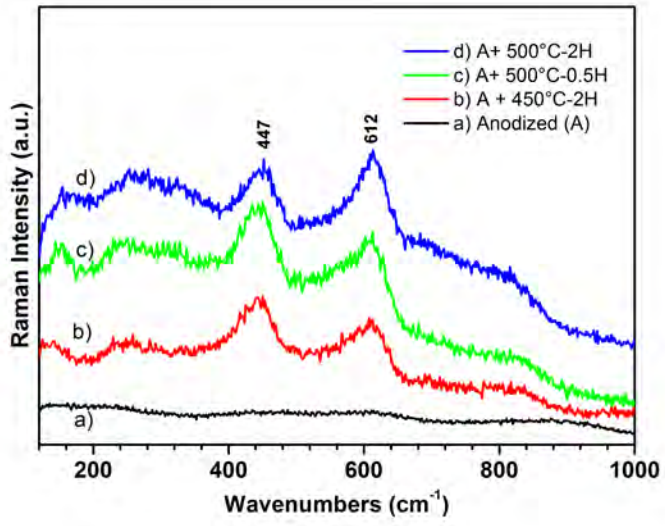

(b)

Figure 3.7: Raman spectroscopy showing the evolution of titania crystalline structure in relation to annealing temperature (a) and time (b) obtained on nanopores formed at 20 V for 20 min

rutile, while a mixture of anatase and rutile was observed for the nanoporous structures. Morphology or the anodising process must play a role in TiO_2 phase formation. These results, when compared to the literature, show that the amorphous and crystalline phases of titania nanostructures vary with the synthesized conditions (10V, 20V) and annealed conditions (temperature and duration) [98, 85]

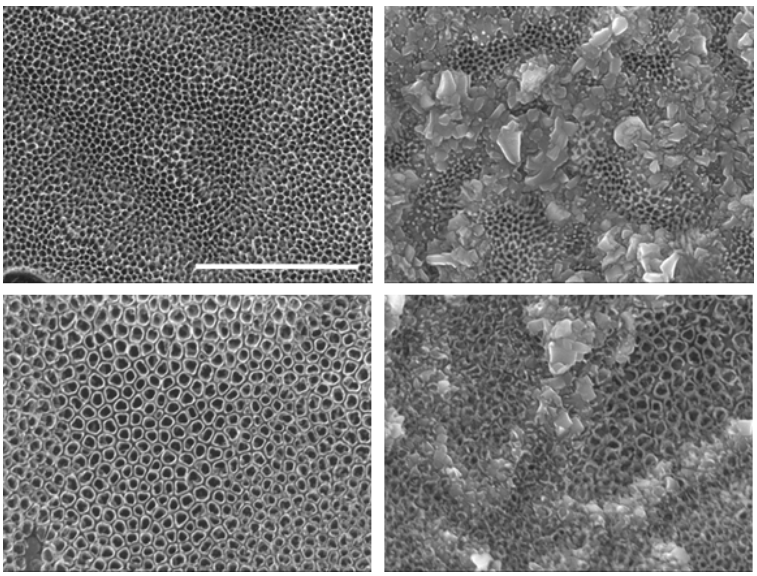

Figure 3.8: Top view SEM images of titania nanopores and titania nanotubes array heated at 500 and 600 ˚ C for 2 hours: intact structures are obtained at low annealing temperature while the nanostructure diminished with temperatures up to 550 ˚ C due to the growth of rutile crystals.

The second part of this section is based on SEM evaluation of the morphology changes and stability of titania nanostructures grown in aqueous HF electrolyte and annealed in air. **Figure 3.8** shows titania nanotubes heat treated in ambient air at 500 and 600 ˚ C. No significant changes in morphology were observed up to 500 ˚ C for either nanostructure, as shown in the SEM micrographs. However, above an annealing temperature of 600 ˚ C it was shown that the surface retained a nanotube-like structure but did not appear to be homogeneous. The nanostructure partially collapsed by beginning to sinter together with crystal formation overlying the nanotube array. As explored by Jaroenworaluck *et al.* in 2010, the anatase phase developed between 200 and 300 ˚ C and crystallite increased with annealing temperature [99]. The rutile phase started to occur at the Titanium-titania nanostructure interface around 430 ˚ C without affecting the architecture of the nanostructures. The collapse

was the consequence of rutile protrusions emerging in the anodic layer due to oxidation and grain growth in the titanium support at high temperatures.

As reported in the literature, the crystalline titania phase nanostructure increased cell proliferation viability and mineralization more than the amorphous structure. However, the rutile phase was only shown to diminish apatite deposits and higher biocompatibility was obtained for anatase-rutile phase surfaces than for pure anatase surfaces. A balance between these two surfaces may be a way to improve the biocompatibility of the nanostructured titania surface. A semi-quantitatve phase analysis is possible by calculating the mass proportion of the rutile phase (W_R) as presented by Zhang *et al.* in 2006 [100].

After calculation, **Table 3.4** shows the rutile phase proportion that makes up the titania nanostructure synthesized at 10 V (nanopores) and annealing at 350, 400, 450, 500 and 550 ° C. Titania nanotube structures presented a high increase of rutile ratio from 500 to 550 ° C. These results confirm that the crystal phase obtained by the annealing process. It have shown to depend on the structure diameter or anodic synthetic conditions [98].

Table 3.3: Weight fraction of anatase/rutile using both peacks at 395 cm^{-1} (anatase) and at 445 cm^{-1} (rutile) [100]

Temperature (° C)	350	400	450	500
Weight fraction W_A/W_R	2.33	1.13	0.86	0.4

Finally, the effects of the annealing process were also studied in different surface compositions: pure titanium or alloys (e.g.: Ti-Al 6%-V 4%). **Figure 3.9** shows the crystalline composition of titania nanotube structures formed at 20 V for 10 min in two different substrates and annealing at 500 ° C for 2 hours. The results showed a presence of both anatase and rutile phases in the pure titania structures, whereas the anatase phase was totally absent from the titanium alloys. This result proved that the composition of the alloys (i.e. Ti or TA6V) as well as the anodisation conditions (i.e. 10 V or 20 V) are a critical and sensitive parameter with regard to the effect of the annealing process.

In conclusion, according our results and in accordance with the literature, the anodising process produces an initial amorphous nanostructure which is needed to transform into a crystalline phase: anatase or rutile. The composition obtained depends on various parameters: the chemical composition of the substrate, the nanostructured surface formation (diameter, type of structure, thickness, chemical composition of the layer) and also the annealing conditions

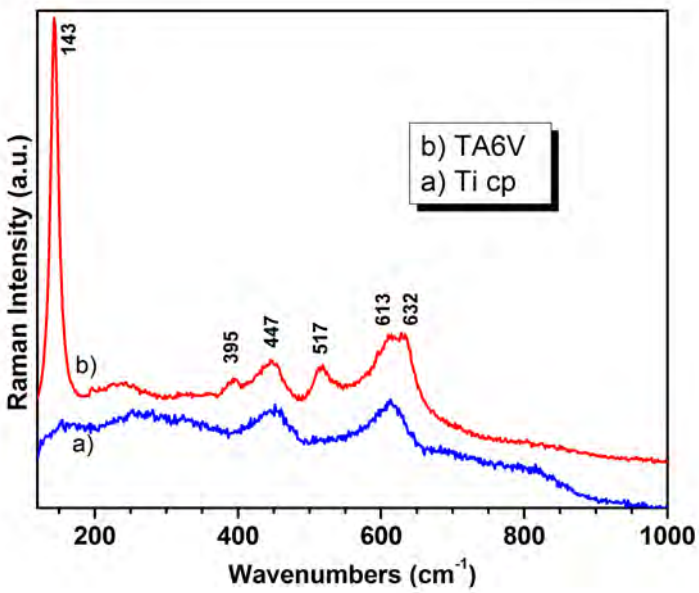

Figure 3.9: Raman spectroscopy showing the evolution of titania crystalline structures with annealing time obtained on nanopores formed at 20V during 10 min and annealed at 500 ° C for 2 hours

(temperature, slope, time, gas used) [85, 86, 87]. In case of industrialisation of the process, adjustments will need to be made in order to obtain the desired crystalline and more biocompatible structure.

3.1.5 Chemical composition of the nanostructure

The anodisation process makes it possible to increase the natural oxide layer from 2-6 nm to further micrometer thicknesses with specific architecture. The change in the chemical composition, and thus the refractive index, produced the colours on the surface by light interferences through the oxide layers on the titanium. From a marketing point of view, this coloration is useful for colour-coding medical implants in order to recognise the instrumentation. Another important point in biomedical devices and integration is surface contamination. However, the anodisation process uses electrolytes containing dangerous acidic solutions such as hydrofluoric acid. Therefore, for quality control, it is necessary to control the absence of any trace of acid.

Wide scan energy spectrum were acquired using a monochromatic Al K_α source and is presented in **Figure 3.10**. High-resolution X-ray photoelectrons

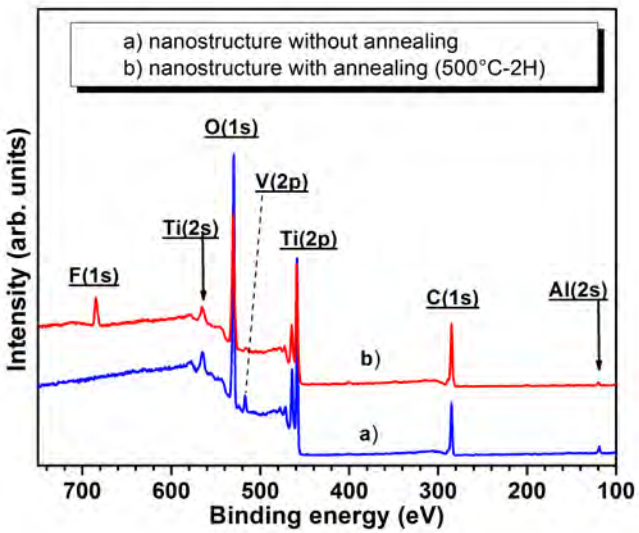

Figure 3.10: wide scan energy spectrum of a nanostructured surface with and without annealing : Peak of F 1s is only presents on non-annealing sample

(XPS) were recorded before and after anodising for Ti 2p, O 1s, C 1s and F 1s are shown in **Figure 3.11, 3.12, 3.13** and **3.14** respectively. Decomposition of the spectrum of each sample using different curves, Gaussian or Lorentzian, corresponds to the different binding statements of the element.

Table 3.4: Samples composition

	Ti	O	C	F
Initial surface	12.9 (±1.4)	40.3 (±1.9)	46.3 (±3.5)	0.7 (±0.6)
After anodisation	15.2 (±2.7)	40.0 (±2.0)	30.0 (±3.5)	14.8 (±8.1)
After annealing	17.9 (±0.1)	52.3 (±0.1)	29.3 (±0.2)	0.4 (±0.1)

The two characteristic peaks of Ti 2p $\frac{1}{2}$ and Ti 2p $\frac{3}{2}$ were usually apparent at 465 eV and at 459.2 eV respectively. According to the literature, the peak at 451-452 eV can be assigned to Ti metal (Ti^0) originating from the substrate. Titanium is naturally covered with a 2-6nm oxide layer, and XPS analysis is about 2 to 10 nm deep. By deconvolution of the Ti 2p $\frac{3}{2}$ spectrum, we can observe spin orbit components. Binding energies at 459, 457 and 456 eV were assigned as Ti^{4+} (TiO_2) and a reduction state of Ti^{3+} ($TiOOH$) and Ti^{3+}

(unsaturated) respectively.

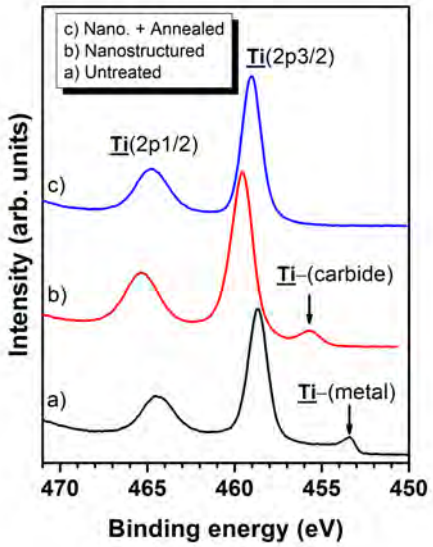

Figure 3.11: High resolution Ti 2p spectra for surface untreated, anodized at 20 V for 20 min, and both anodised and annealed at 500 ° C for 2 hours

Stoichiometric TiO_2 consists of Ti^{4+} and also O^{2-} ions. The different types of oxygen species are presented by the deconvolution of the binding energies of the O 1s spectra. The peak positions around 530 eV had a higher intensity corresponding to lattices of oxygen as in $Ti^{4+} - O$, while other peaks were also observed at 533, 532 and 528.5, 527 eV, corresponding to both oxygen atom oxidation and reduction. The latter originate in surface pollution from oxygen reduction including O_3 formation. Oxygen near an oxygen vacancy such as in $Ti^{3+} - O$ binding is characterised by peaks at 531−532 eV and $Ti - OH$ at 532−533 eV. These results are in adequacy with other XPS analyses on synthesised self-aligned titanium dioxide nanostructures found in the literature [95]. In case of titanium alloys such as TA6V, aluminium (Al 2s) at 118 eV and vanadium at 512 eV could be also detected in the oxide layer.

High-resolution C (1s) spectra (**Figure 3.13**) revealed high carbon peaks at 284.8 eV, which was used for the entire spectra calibration in order to adjust the energies offset. The analyses also revealed high carbon and carbide adsorption (281-283 eV) which disappeared with the anodic process. This carbon is due to absorption of atmospheric contamination. Titanium and especially TiO_2 is known to have the particularity of adsorbing any element or compound around it and thus it is used as a catalyst or decontaminant. Acid traces such as acetic

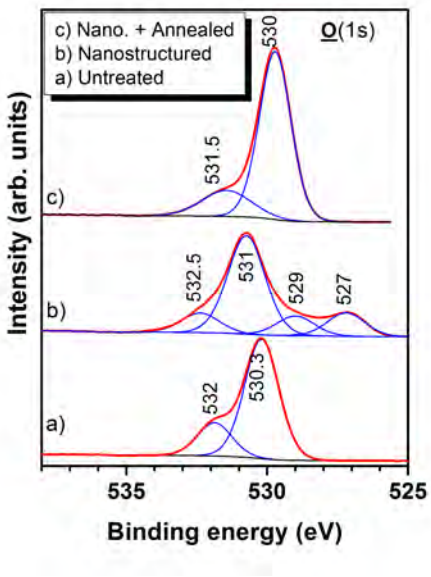

Figure 3.12: High resolution O 1s spectra for surface untreated, anodized at 20 V for 20 min, and both anodised and annealed at 500 ° C for 2 hours

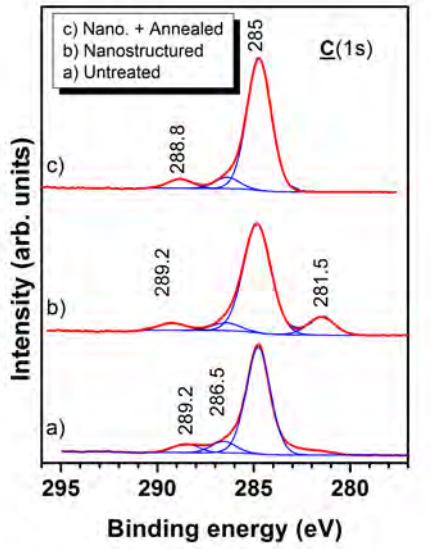

Figure 3.13: High resolution C 1s spectra for surface untreated, anodized at 20 V for 20 min, and both anodised and annealed at 500 ° C for 2 hours

acid (CH_3COOH) could be characacterised by the carboxyl links ($-COOH$) visible at 289 eV. An atomic percentage of 4-5% was observed in the reference sample at 8-12% in the sample without the cleaning and annealing step. Rinsing or annealing reduced the presence of $-COOH$ links on the surface.

Figure 3.14 shows the F 1s XPS spectra and the impact of different synthesis conditions on its fluoride composition: anodisation process, rinsing bath and annealing treatment. Traces of fluor were already present in the reference surface due to adsorption or chemical pollution from sample machining. The presence of fluorine was detected after anodisation with or without rinsing. The binding energy value of 685 and 683 eV correspond to adsorbed fluoride ions or forming compounds of $TiOF_2$ or F-Ti-O. Chemical composition was also recorded in depth by combining X-ray photoelectron (XPS) analysis and ionic erosion. **Figure 3.15** shows the presence of fluoride in depth, along the oxide layer. Fluoride ions are very small and compete with O_2 migration through the TiO_2 lattices to the oxide-metal interface. They migrate at a rate twice as high as O_2 leading to accumulation at the metal-oxide interface. The presence of fluorides form water-soluble $[TiF_6]^{2-}$ species [26].

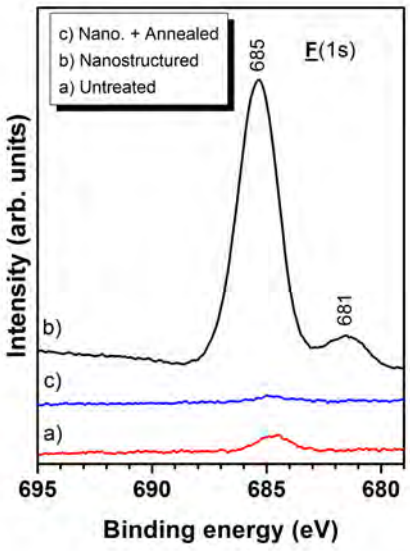

Figure 3.14: H
igh-resolution XPS spectra for the F 1s regions]High resolution F 1s spectra for surface untreated, anodized at 20 V for 20 min, and both anodised and annealed at 500 ° C for 2 hours

The presence of a $H-F$ link could be characterised at 689 eV. Thus the absence of acetic acid could be confirmed at rates above 2 per 1000. Fluoride

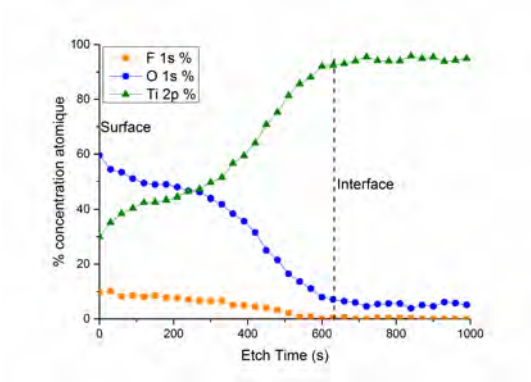

Figure 3.15: X-ray photoelectron (XPS) concentration profiles obtained on nanotubular array formed at 20V for 20 min

composition is completely lost from the surface. This is due to TiF_4 evaporation by heating at high temperature [100]. Although this fluoride is widely used in toothpaste with various beneficial effects, it is currently controversial due to dental problems (fluorosis linked to fluoride overdoses during the mineralisation period) or bone hypercalcification which makes it brittle. Annealing is then required to avoid any problems with fluoride composition.

Using the erosion rate, the XPS profile made it possible to calculate the thickness of the oxide layer. The etching rate of TiO_2 has been calculated at about 14.7 nm per minute. Thus the thickness of the oxide layer formed at 20V for 20 min is a 150 nm long Titania layer

3.2 Biological characterization of the nanostructured surface

Titane is widely used for biomedical devices such as in dental or orthopaedic applications. One of the current challenges in implantology is to obtain rapid osseointegration and thus immediate-loaded implants. It is postulated that intimate bone-implant contact could prevent bacteria colonisation along implants and that is particularly relevant for dental implants. Improving the interface of the materials with biological tissues is thus a way to increase the clinical success and long life of implants. Studies have shown the importance of the relationship between surface properties and tissue healing [11, 12, 13, 14]. Many different surface treatments with micro or nano-modifications have been developed and commercialised (see chapter 1). The three main surfaces are the plasma spray hydroxyapatite coating for orthopaedics and a grit-blasted and/or acid-etched

surface treatment in dental applications. However, these surface treatments produce a roughness in the micrometer range while biological objects interact at the nanometer scale.

It known that nano-modified surfaces can interact with the biological environment at the scale of proteins [81, 22]. Honeycomb titania surfaces may induce cell elongation, cytoskeletal stress and selective differentiation into osteoblastic cells by mechanostranduction as presented in chapter 1 [22, 41]. Recent *in vitro* studies have shown higher osteoblastic differentiation and mineralisation [40]. These results were correlated by *in vivo* studies in rabbits or other animals, in which better anchorage or bone apposition were observed [101, 102]. However, many of these studies were performed using titanium disks or wire geometry samples and compare to a non-treated surface.

The objective of this section is to biologically characterise this honeycomb titania surface in a rabbit femur model. This study was performed using cylindrical custom-made implants with growth chamber geometry. The osseointegration of three different types of surface were compared: machined surface (MA), nanostructured (NANO) implants and “homemade”standard alumina grit-blasted and acid-etched (MICRO) implants, also called SLA-like (See Chapter 1). The specimens were implanted into the femoral condyles of New Zealand White rabbits. After 4 weeks, a pull out strength test and histolomorphometry analysis with calculation of both bone-to-implant contact and bone growth values were determined.

The results of this study were published in article n N^{o} 1 accepted in the journal Acta biomaterialia and titled "Enhanced osseointegration of titanium implants with nanostructured surfaces: an experimental study in rabbits".

3.2.1 Article N^{o} 1 : Enhanced osseointegration of titanium implants with nanostructured surfaces: an experimental study in rabbits

Acta Biomaterialia 11 (2015) 494–502

Contents lists available at ScienceDirect

Acta Biomaterialia

journal homepage: www.elsevier.com/locate/actabiomat

Enhanced osseointegration of titanium implants with nanostructured surfaces: An experimental study in rabbits

Laëtitia Salou [a,b,c], Alain Hoornaert [d], Guy Louarn [c], Pierre Layrolle [b,*]

[a] Inserm UMR957, Laboratory of Pathophysiology of Bone Resorption, Faculty of Medicine, University of Nantes, Nantes, France
[b] CNRS—Institute of Materials, University of Nantes, Nantes, France
[c] Biomedical Tissues, Nantes, France
[d] CHU Nantes, Faculty of Dental Surgery, University of Nantes, Nantes, France

ARTICLE INFO

Article history:
Received 13 June 2014
Received in revised form 15 September 2014
Accepted 15 October 2014
Available online 23 October 2014

Keywords:
Titanium
Nanostructure
Bone-to-implant contact
Osseointegration

ABSTRACT

Titanium and its alloys are commonly used for dental implants because of their good mechanical properties and biocompatibility. The surface properties of titanium implants are key factors for rapid and stable bone tissue integration. Micro-rough surfaces are commonly prepared by grit-blasting and acid-etching. However, proteins and cells interact with implant surfaces in the nanometer range. The aim of this study was to compare the osseointegration of machined (MA), standard alumina grit-blasted and acid-etched (MICRO) and nanostructured (NANO) implants in rabbit femurs. The MICRO surface exhibited typical random cavities with an average roughness of 1.5 μm, while the NANO surface consisted of a regular array of titanium oxide nanotubes 37 ± 11 nm in diameter and 160 nm thick. The MA and NANO surfaces had a similar average roughness of 0.5 μm. The three groups of implants were inserted into the femoral condyles of New Zealand White rabbits. After 4 weeks, the pull-out test gave higher values for the NANO than for the other groups. Histology corroborated a direct apposition of bone tissue on to the NANO surface. Both the bone-to-implant contact and bone growth values were higher for the NANO than for the other implant surfaces. Overall, this study shows that the nanostructured surface improved the osseointegration of titanium implants and may be an alternative to conventional grit-blasted and acid-etched surface treatments.

1. Introduction

Titanium dental implants are widely used in dentistry for single- or multiple-tooth prosthetic rehabilitation [1,2]. The surface properties of titanium implants are key factors for rapid and stable bone tissue integration [3–5]. At present, the surfaces of most dental implants are grit-blasted and acid-etched to improve osseointegration. Well-documented and successful examples of such surface treatments for dental implants are the Straumann SLA® and SLA active® [6,7]. Physical modification by grit-blasting produces a rough surface at the micrometer level which, to a certain extent, increases its mechanical interlock with bone tissue [8,9]. Chemical etching in strong acids creates micrometer pits on the implants that increase the surface energy, protein adsorption, cell adhesion and finally osseointegration [10–12]. Several studies have shown that an average surface roughness of between 0.5 and 2 μm, achieved by means of grit-blasting and/or acid-etching, is the optimal topography for the osseointegration of dental implants [13,14]. However, this type of rough surface has random and uncontrolled microstructures, while proteins and cells interact with the implant surface in the nanometer range. It has recently been shown, by our group and by others, that nanostructures on titanium implants significantly enhance the adhesion and osteoblastic differentiation of mesenchymal stem cells [15–20]. Particular surface topographies with regular depressions of <100 nm may induce cell elongation, cytoskeletal stress and selective differentiation into osteoblastic cells by mechanostranduction [21–23]. Nanostructured surfaces consisting of a regular array of columnar titanium dioxide (TiO_2) nanotubes have been produced simply by the anodization of titanium implants [16,17,24]. In line with in vitro results in which osteoblastic cell differentiation was observed, the apposition and fixation of the bone were enhanced by nanostructured titanium wires implanted into rat tibias in comparison with a control surface [24]. In this context, a smooth, nanostructured surface that may enhance osseointegration at a rate similar to that of the standard grit-blasted acid-etched surface may be relevant for clinical use. This nanomodified surface may

* Corresponding author at: Inserm UMR957, Laboratory of Pathophysiology of Bone Resorption, Faculty of Medicine, University of Nantes, 1 rue Gaston Veil, 44035 Nantes, France. Tel.: +33 2 72 64 11 43; fax: +33 2 40 41 28 60.
E-mail address: pierre.layrolle@inserm.fr (P. Layrolle).

http://dx.doi.org/10.1016/j.actbio.2014.10.017
1742-7061/

also avoid bacterial attachment or biofilm formation on the implant surface [25–28]. Moreover smoother nanostructured surfaces may be more conveniently decontaminated in case of peri-implantitis than the classical micro-rough surfaces [29,30].

The aim of this work was to compare the osseointegration of nanostructured surfaces with standard grit-blasted, acid-etched and machined titanium alloy implants. Three types of surface, machined (MA), alumina grit-blasted and acid-etched (MICRO), and nanostructured (NANO), were prepared and characterized using profilometry, scanning electron microscopy and Raman spectroscopy. These three groups of implants were bilaterally inserted into rabbit femoral epiphyses. After a healing period of 4 weeks, the pull-out test, bone-to-implant contact and newly formed bone were measured and compared. Simple cylindrical implants were used instead of threaded implants in order to directly compare the effect of surface on the kinetics of bone integration [31].

2. Materials and methods

2.1. Implant preparation

Titanium alloy implants (TA6V) were specially designed for this study. Cylindrical implants with a diameter of 4.2 mm and a length of 7.5 mm were machined (ALTA Industries SARL, Arnage, France). A hole was drilled to hold the implant during surface treatments, surgical implantation and mechanical pull-out testing. In order to reproduce the depth of insertion in rabbit femurs, the neck region of the implants had a rim of 1 mm with an outer diameter of 5.5 mm. An apical bone growth chamber of 3 mm in diameter and 2.5 mm in depth was machined along the vertical axis of the implants. The following groups were prepared and characterized: machined implants (MA), alumina grit-blasted and acid-etched (MICRO), and nanostructured (NANO) surfaces. The machined (MA) implants were used as received. The MICRO implants were grit-blasted with alumina particles with an average size of 110 μm. The implants were placed in a sand-blasting chamber (Sanduret 3 K, MW Dental, Germany) and rotated along their vertical axis at 100 rpm. The implants were then blasted using an air pressure of 5 bar at a working distance of 1 cm. After blasting, the implants were washed with water and etched in a mixture of hydrochlorhydric acid (37 wt.%), sulfuric acid (95 wt.%) and demineralized water in a volume ratio of $HCl/H_2SO_4/H_2O$ 2:1:1 at 80 °C for 5 min. After acid-etching, the implants were rinsed with demineralized water and air-dried. For the NANO implants, columnar TiO_2 nanotubes were manufactured by electrochemical anodization as previously described [16,24,32]. Briefly, the machined implants were cleaned for 15 min in acetone, ethanol 70% and demineralized water and then air-dried. The implants were anodized in an electrolyte consisting of 1 M acetic acid (Prolabo) and 0.5 wt% hydrofluoric acid (HF; Sigma, St Quentin Fallavier, France). The titanium implant served as the anode while a platinum electrode (Kitco, Canada) served as the cathode. Both were connected to a power generator (HQ Power, PS3010) and immersed in the electrolyte solution with stirring at room temperature. A tension of 10 V was applied for 20 min. After anodization, the implant was rinsed in demineralized water and annealed at 500 °C for 2 h in a furnace (Nabertherm, L1/12/R6). Following the surface treatments, the implants were cleaned in ultrasonic baths with acetone, 70% ethanol and deionized water for 10 min. Finally, the three groups of implants were packaged in double-sealed bags and sterilized in an autoclave at 121 °C for 20 min.

2.2. Characterizing the implant surfaces

The surface topography was analyzed using a contact profilometer (Intra 2, Taylor Hobson) (n = 3 implants/group). The surface of the implants was observed by field-emission scanning electron microscope (FE-SEM; Carl Zeiss, Merlin). Microanalysis was performed by energy-dispersive X-ray analysis (EDX; Oxford Instruments, model XMAX 80 mm2). In order to reveal the α and β phase domains on the titanium alloy, machined implants were etched for 30 s with Kroll's reagent (100 ml demineralized water, 2 ml HF 40 wt.%, 4 ml HNO_3 65 wt.%) prior to FE-SEM observations. The thickness of the nanotube film was measured by FE-SEM after machining and fracturing the substrate. The internal diameter and circularity of the nanotubes were determined on the NANO surface using FE-SEM images at a magnification of ×50000 and image analysis software (ImageJ). To assess the reproducibility, four FE-SEM images taken on three representative NANO implants were used. Raman spectroscopy (Rénishaw InVia reflex spectrometer) was done to analyze the phases (amorphous, anatase, rutile) on the surface of the implants.

2.3. Surgical procedure

All animal handling and surgical procedures were conducted according to European Community guidelines for the care and use of laboratory animals (2010/63/UE). The study protocol was submitted for approval to the regional animal care and safety committee. The experiments were conducted at the Faculty of Medicine, University of Nantes in approved experimental facilities. The experiments were performed using 10 adult female New Zealand White rabbits (NZW; body weight 3.5–3.75 kg, 16–18 weeks old) provided by a certified breeder (Charles River Laboratories). The animals were housed in individual cages, with freely available water and food, and an artificial day/night cycle of 12 h/12 h in an air-conditioned room. The animals were allowed to acclimate for at least 10 days prior to surgery. All the animals were operated under general anaesthesia performed by intramuscular injection of a mixture of xylazine (5 mg kg^{-1}, Rompun 2%, Bayer) and ketamine (35 mg kg^{-1}, Imalgene 1000, Merial). Possible post-surgical infections were prevented by a subcutaneous injection of prophylactic antibiotic (Marbocyl, 2 μg kg^{-1}, 1 μg ml^{-1}) at the time of surgery and in the following 3 days. The posterior limbs were shaved and disinfected with iodine solution (Betadine 10%, Meda) and draped with a hollow sterile sheet (Foliodrape, Hartmann). A local anaesthetic (1 ml, Septanest® N Articaine HCl 4% with 1:200,000 epinephrine) was injected into the surgical area. A lateral 3 cm incision in the skin and muscle was made to expose the proximal epiphyses of the femur. A bone defect of 4 mm in diameter and 6 mm in depth was centred on the lateral side of the femoral condyle through the cortical and trabecular bone. The defects were made under saline irrigation using a series of three dental burrs with increasing diameters (1, 2, 3 and 4 mm) mounted on a dental implant micromotor (NSK surgic XT). After drilling, the cavity was thoroughly rinsed with physiological saline solution. The implants were press-fit inserted into the defects as far as the rim. The wound was tightly closed in two layers using degradable sutures (Vicryl 5/0, Ethicon). After surgery, the animals were observed daily for possible wound complications, and post-surgical pain was controlled by intramuscular injection of buprenorphine (50 μg kg^{-1} day^{-1} for 3 days, Buprecare 100 μg ml^{-1}). After a healing period of 4 weeks, the rabbits were put under general anaesthesia with an intramuscular injection of xylazine/ketamine as previously described, and killed by intracardiac injection of an overdose of sodium pentobarbital (2 ml, Dolethal®, Vetoquinol, France). The femoral condyles with the implants were dissected and any abnormal signs of healing were recorded. After harvesting, the samples were immediately stored at -80 °C. The femoral condyles were X-rayed in order to localize the implant and verify the absence of peri-implant osteolysis (Faxitron MD20).

2.4. Mechanical pull-out test

After warming the samples at room temperature, the osseointegration of the implants was measured by tensile pull-out force testing (Zwich Roell 72.5). A specially designed screw was inserted into the implant and fixed to the crosshead device. The proximal region of the femoral condyle was held by a fixture in order to align the long axis of the implant with the vertical axis of the crosshead device. A load cell (Zwich Roell 8125) with a maximum force of 200 N and an accuracy of 0.1 N was used. The uniaxial tensile test was carried out using a crosshead speed of 1 mm min^{-1}. The force–displacement curve was obtained by using the software Xpert II. The maximum pull-out force was recorded for each sample. After pull-out testing, the implants were put in 4% neutral formaldehyde fixative and further processed for non-decalcified histology.

2.5. Histology and histomorphometry

After fixation for 7 days, the specimens were rinsed in water, dehydrated in a graded series of ethanol (from 70% to 100%), impregnated in methyl methacrylate and finally embedded in polymethylmethacrylate resin. Polymerization was performed by adding a radical initiator and propagator in a vacuum at 4 °C in order to prevent the formation of bubbles. After resin hardening, each implant was longitudinally sectioned in the middle with a diamond circular saw (Leica SP1600, Germany). Tissue/implant sections of ~30 μm in thickness were sawn, glued to a glass slide and polished using a series of SiC papers on a polishing machine (Buelher Metaserv 2000). After polishing, the semi-thin sections were stained in methylene blue/basic fushin. The tissue/implant sections were digitized and visualized using a virtual microscope (Hamamatsu, NanoZoomer 2.0RS and NDP view software). On the stained sections, bone tissue appeared purple while soft tissue was coloured in blue. Both remaining blocks surrounding the section were polished and used for backscattered electron microscopy (BSEM; Hitachi, Tabletop TM3000) in order to quantify the bone around the three groups of implants. Contiguous photographs of the whole implant and surrounding bone tissue were taken at a magnification of ×50 using a motorized programmable stage (model). On these BSEM images, the titanium implant appeared in light grey, mineralized bone in grey and non-mineralized tissue in black. Histomorphometry was carried out using a custom-made programme developed with image-processing software (ImageJ). On each image, the percentage of direct contact between the mineralized bone and titanium surface (BIC) was calculated by using a semi-automatic binary treatment. The bone surface at a distance of 0.5 mm around the implant (BS/TS 0.5 mm) was also measured. Finally, bone growth (BG) was determined in each bone growth chamber at the apical extremity of the implant. All the measurements were repeated at least three times.

2.6. Statistical analysis

The physicochemical characterization of the prepared implants was done in triplicate ($n = 3$/group). Seven samples each for the MICRO and NANO groups ($n = 7$) and six samples for the MA group ($n = 6$) were implanted following a permutation implantation scheme in both femoral epiphyses of 10 rabbits. This design prevented possible lateral bias. In this study, all data are expressed as an average ± standard deviation, apart from the pull-out, BIC, BS/TS and BG data, which are shown in the form of a median with minimal and maximal values or quartile. Prior statistical analysis of the data and critical values were detected using the Dixon test with significance levels of 95%. The non-parametric Kruskal–Wallis one-way analysis of variance (ANOVA) test was used for statistical analysis between all groups. The Mann–Whitney non-parametric *U*-test was used to compare the effect of the surface treatment between two groups. Differences were considered significant for *P*-values of <0.05. All data were plotted and statistically analyzed using commercial software (OriginPro 9.1).

3. Results

3.1. Surface properties

The three types of implant surfaces differed drastically in topography on both the micro- and nanometer scales. The surface roughness and spatial parameters are shown in Table 1. For instance, the average surface roughness (Ra) was 0.6, 1.5 and 0.5 μm for the MA, MICRO and NANO surfaces, respectively. However, surface spacing parameters, such as surface kurtosis (Sku), surface skewness (Ssk) and the spacing between peaks (Rsm), were similar for all three types of surface. As observed by FE-SEM and shown in Fig. 1, the control MA surface exhibited a relatively smooth surface with machining stripes. As shown in Fig. 2A, the titanium alloy was composed of α and β phases that were revealed after Kroll's reagent etching. The MICRO surface, observed at low magnification, showed a random, rough microstructure with large cavities dozens of microns in diameter, resulting from the alumina grit-blasting. At high magnification, these depressions contained microstructures resulting from the acid-etching. The machined implants were anodized in fluorhydric and acetic acids, and then heated at 500 °C, resulting in a thin film of TiO_2 nanotube arrays (NANO). The FE-SEM images showed that most of the NANO surface was covered by a regular array of nanotubes. However, nanotubes were not present on the β phase domains as previously reported [32,33]. As indicated in Table 2, EDX analysis confirmed the segregation of the two phases. A high proportion of vanadium was found on the microdomains corresponding to the β phase as this element is a *β*-phase stabilizer in titanium alloys [32,34]. At high magnification, the nanotubes were found to have a mean inner diameter of 37 ± 11 nm ranging from 12 to 109 nm maximum and an average circularity of 0.44 ± 0.15. As shown in the cross-section view (Fig. 2), the NANO film had a thickness of ~160 nm and was composed of a columnar structure grown on a dense oxide layer of 30 nm. Raman spectroscopy indicated that the positions of the peaks between the MA and MICRO groups were similar and typical of an amorphous titanium oxide layer (Fig. 3). After the anodizing process, the NANO surface was still amorphous as confirmed by Raman spectroscopy. Annealing at 500 °C converted the amorphous titanium oxide film into crystalline anatase and rutile phases (calculated WA/WR ratio ≈0.2 [35]).

Table 1
Topographic measurements of the three types of surface.

	Ra (μm) Arithmetic mean deviation	Rz (μm) Maximum height	Rsm (μm) Spacing between peaks	Ssk Factor asymmetry	Sku Factor flattening	n
MA	0.6 ± 0.2	2.9 ± 0.2	82.3 ± 9.1	0 ± 0.3	2.4 ± 0.2	3
MICRO	1.5 ± 0.1	10.4 ± 0.8	58.6 ± 10.6	−0.2 ± < 0.1	3.0 ± 0.4	3
NANO	0.5 ± < 0.1	2.5 ± 0.3	76.4 ± 9.1	0 ± 0.1	2.9 ± 0.4	3

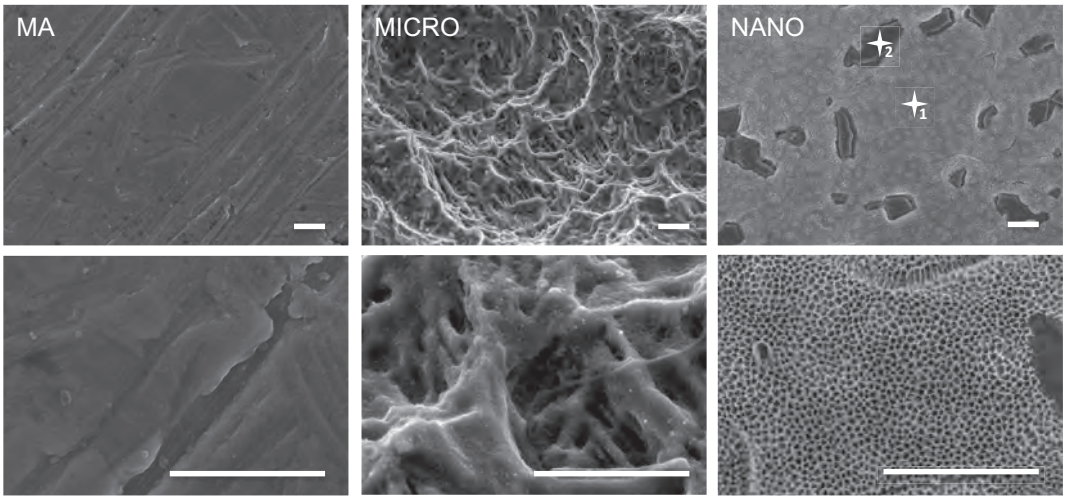

Fig. 1. FE-SEM images of the three types of titanium surface: machined (MA), alumina grit-blasted and acid-etched (MICRO) and nanostructured (NANO) (magnifications ×10000 and ×50000, scale bar: 1 μm). Stars indicate the X-ray analysis on the NANO surface.

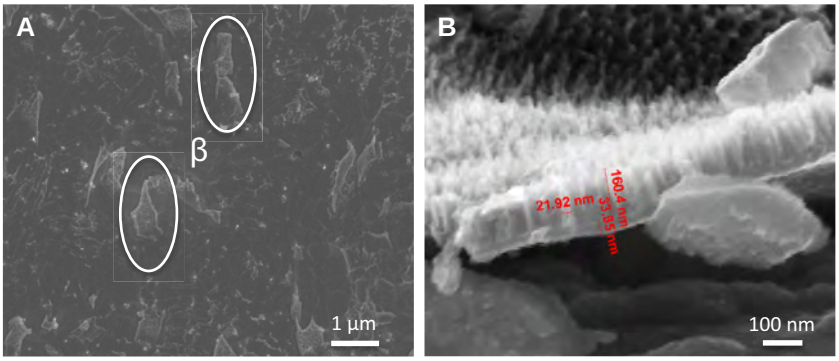

Fig. 2. FE-SEM characterization of (A) the titanium alloy implant surface showing the β phase in circles and (B) a cross-section of the nanotube array film showing its thickness.

Table 2
Elemental composition of the NANO-surface.

Analyzed zone	% atm.					Description
	O	F	Al	Ti	V	
1	23.7	6.8	4.3	73.2	5.0	Nanotube array
2	16.7	8.3	5.0	62.0	7.9	Micro domains

3.2. Comparing the osseointegration

All the animals recovered quickly from implant surgery, and neither clinical signs of inflammation nor infections were observed. As illustrated in Fig. 4, the surface-treated cylindrical implants were all inserted in the femoral epiphysis of rabbits. All types of implants appeared well integrated into the bone after 4 weeks without macroscopic signs of osteolysis on the X-rays. The histological sections corroborated bone tissue healing around the implants (Fig. 5). Newly formed bone apposition was visible at the cortical and trabecular levels. The quantity of bone around the implants appeared comparable for the three types of implant. At high magnification, a thin, fibrous tissue gap between the bone and the MA implants was observed, whereas direct bone-to-implant contact was seen on the MICRO and NANO implants. Newly formed bone was also observed in the apical bone growth chamber of the NANO implants, while limited amounts were seen in the MICRO and MA implants. These results were corroborated by

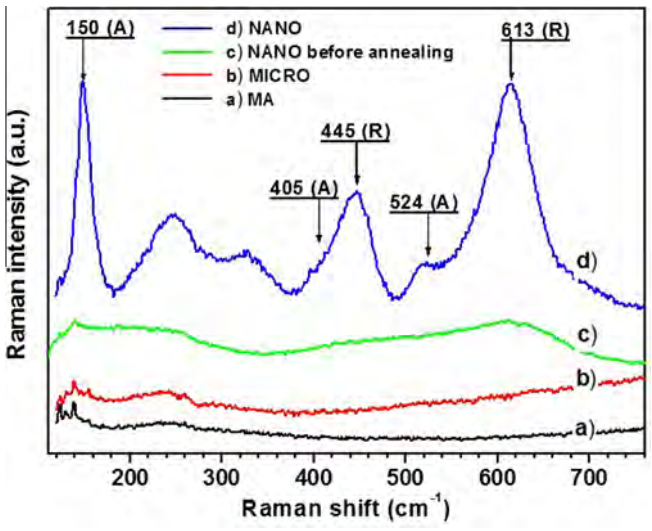

Fig. 3. FT-RAMAN spectra of the three types of titanium surface: machined (MA), alumina grit-blasted and acid-etched (MICRO) and nanostructured (NANO), before annealing and after heat treatment at 500 °C (A, anatase; R, rutile).

the BSEM images shown in Fig. 6. Mineralized bone tissue was observed in the peri-implant region of the different groups. Thin trabeculae of mineralized bone—characteristic of newly formed

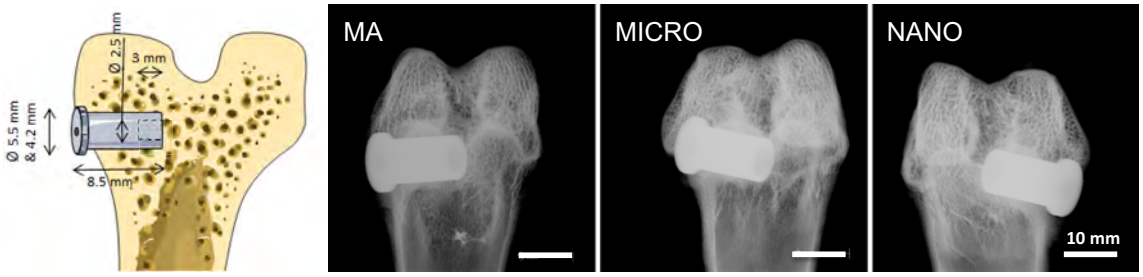

Fig. 4. Implantation site and X-rays of rabbit femoral epiphyses with implants from each group after 4 weeks: (A) machined (MA), (B) alumina grit-blasted and acid-etched (MICRO) and nanostructured (NANO) surfaces.

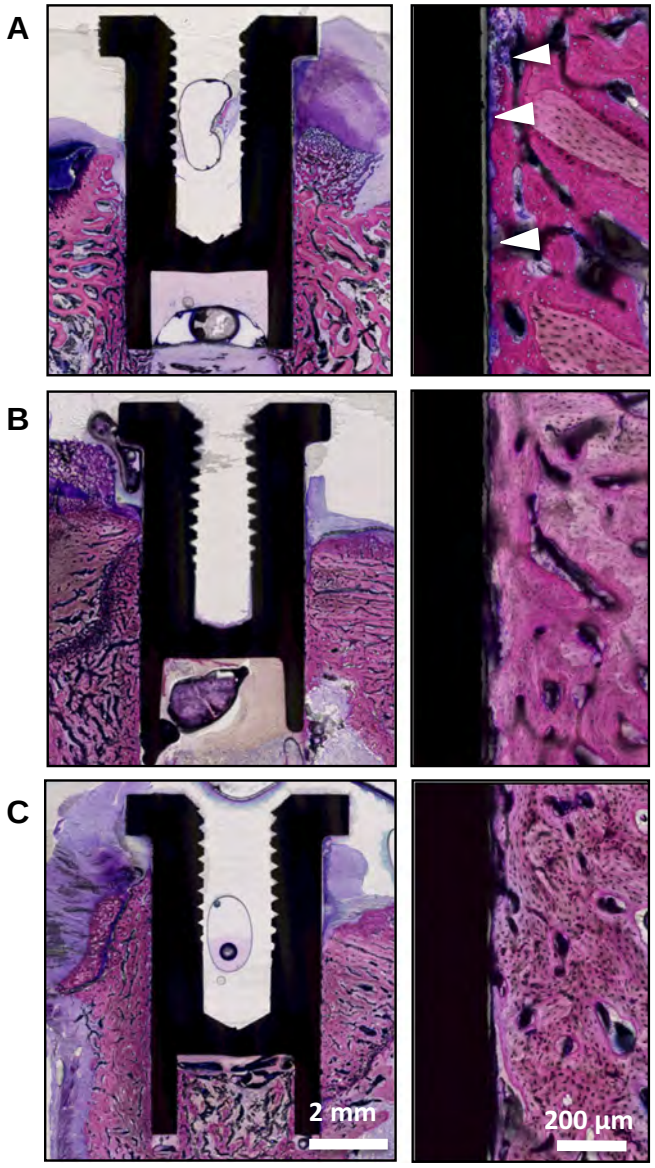

Fig. 5. Non-decalcified histology sections of implant and bone tissue at 4 weeks after implantation in rabbits: (A) machined (MA); (B) alumina grit-blasted and acid-etched (MICRO) and (C) nanostructured (NANO) surfaces. White arrowheads show fibrous tissue. Basic fuchsin and methylene blue staining. (Original magnifications ×1 and ×10.).

bone—were visible around the implants. The apical chambers of the NANO implants contained more bone than in the other groups. These qualitative histological observations were confirmed by quantitative mechanical and histomorphometry results (Table 3, Figs. 6 and 7). The pull-out forces were higher for the MICRO and NANO than for the MA implants (Fig. 7). Bone anchorage in the MICRO and NANO implants was comparable despite the average surface roughness of the MICRO being 3 times greater than for the NANO (Table 1). However, statistical differences between the three groups could not be demonstrated due to wide variability in the data. As shown in Fig. 7, quantitative assessment of the bone surfaces at a distance of 0.5 mm around the implants (BS/TS 0.5 mm) was slightly higher for the NANO than for the MICRO and MA implants. The quantity of bone in the apical chambers of the NANO implants (median: 16%) was also greater than the MICRO (7%) and MA (6%) implants, although the differences were not statistically different between the groups (Fig. 8). In line with the pull-out test results, the bone-to-implant contact of the NANO and MICRO surfaces were significantly higher than for the control MA surface.

4. Discussion

In this study, the osseointegration of three types of implant surface were compared in the femoral epiphyses of NZW rabbits. Overall, the results indicated that the NANO surface was better integrated into the bone than the standard MICRO surface, and even more for the MA control surface after 4 weeks of healing. Although significant differences could not be demonstrated between the groups, the study illustrated the importance of the surface physical and chemical properties of the implants in their integration into bone tissue. In this work, three types of surface on titanium implants were carefully prepared and characterized prior to implantation in rabbit femurs. The osseointegration of implants is due to both primary and secondary stability, which are related to mechanical anchoring to bone and biological bone apposition, respectively. As the design of the implant (e.g. conical shape, screw) has a considerable impact on primary bone-anchorage, simple cylindrical titanium alloy implants were designed and manufactured by machining (MA) and used as the control. Several studies have demonstrated that blasted and acid-etched surfaces integrate better into bone than conventional smooth, blasted or only acid-etched surfaces [12,36]. For these reasons, in the present study, a classic, alumina grit-blasted and acid-etched surface with a random microstructure (MICRO) was prepared on titanium implants and used as the reference implants. As nanometer-sized features have been shown to influence the osteoblastic differentiation of human mesenchymal stem cells (hMSCs) in vitro [15,16], a nanostructured (NANO) surface was prepared by anodization on titanium implants and their bone integration was studied here. As shown in Fig. 1, the anodization produced a regular array of titanium oxide nanopores growing on the α phase domains. This observation was confirmed after Kroll's reagent etching of the surface of the titanium alloy (Fig. 2A). In addition, EDX analysis confirmed the highest quantity of vanadium in β phase domains

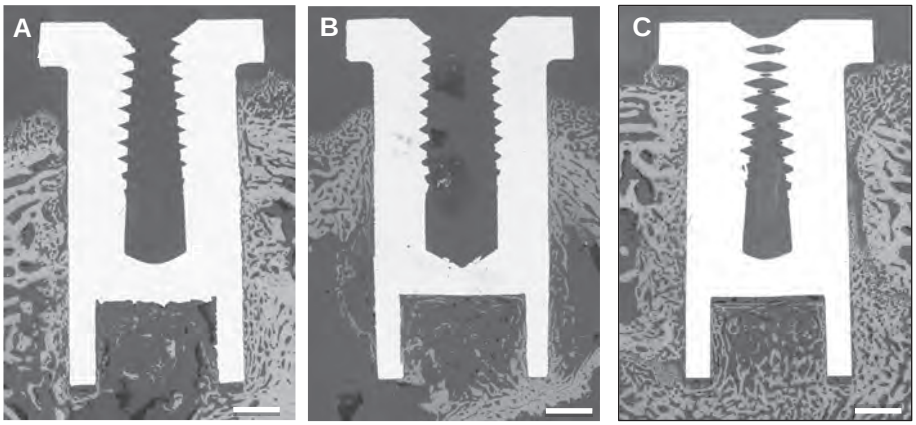

Fig. 6. BSEM images of the three types of titanium surface: machined (MA), alumina grit-blasted and acid-etched (MICRO) and nanostructured (NANO) (magnification ×50, scale bar: 1 mm).

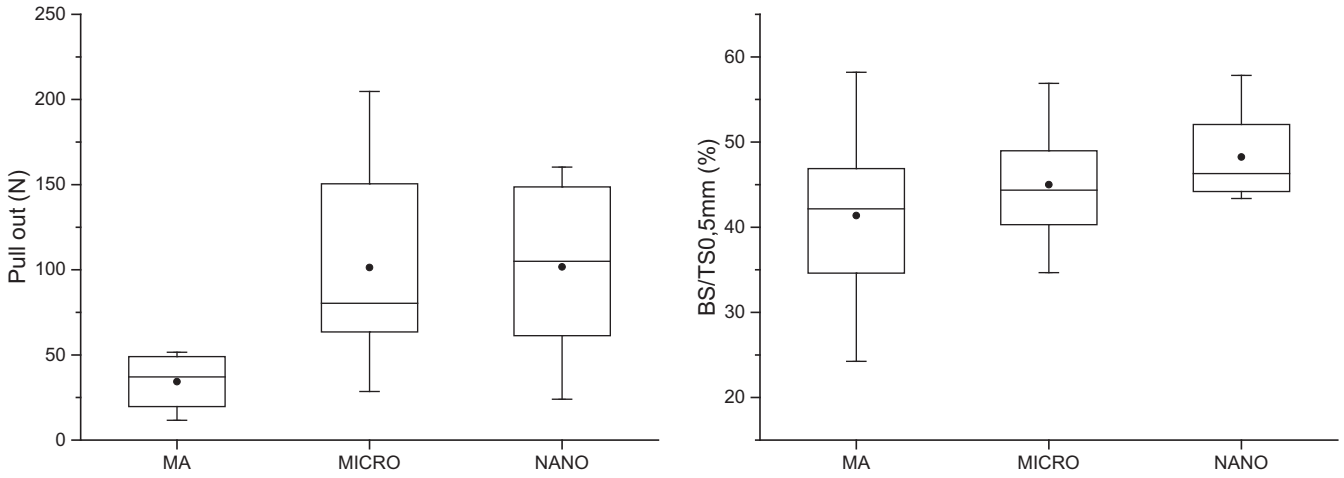

Fig. 7. Whisker plots of pull-out force and percentage of bone surface at 0.5 mm (BS/TS 0.5 mm) around the implants for the three types of titanium implant at 4 weeks after implantation in rabbit femoral epiphyses (*$P < 0.05$).

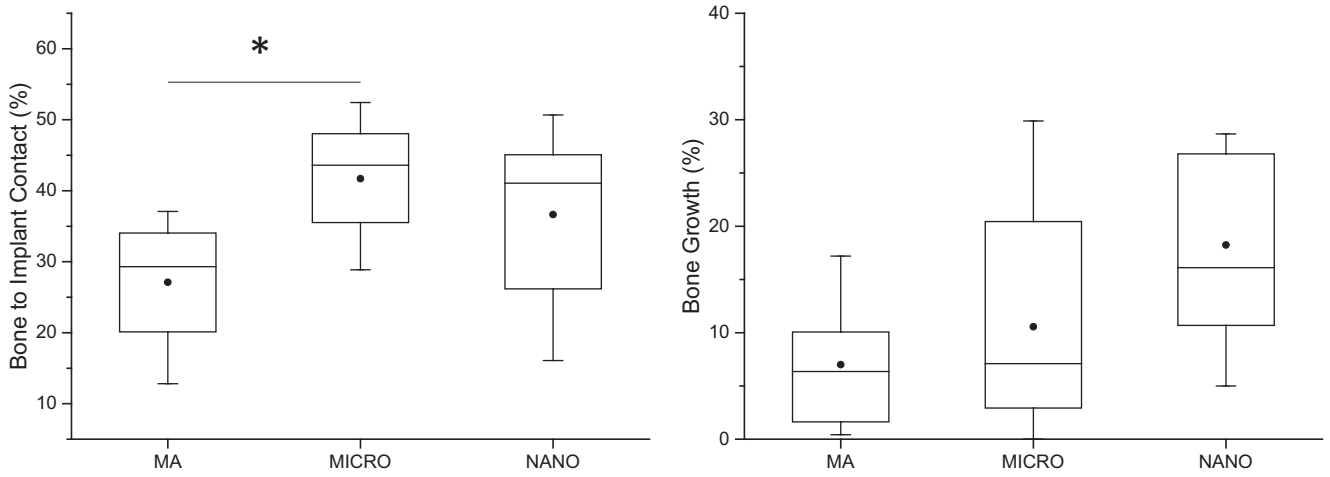

Fig. 8. Whisker plots of the percentage of bone–implant contact (BIC) and bone growth (BG) in the apical chamber for the three types of titanium implant at 4 weeks after implantation in rabbit femoral epiphyses (*$P < 0.05$).

(Table 2). The proportion and position of the α and β phases was in good correlation with the partial coverage of implants with nanotubes. The formation of an inhomogeneous layer composed of both nanotubes and microdomains of dense titanium oxide resulted from the different electrochemical oxidation rates of the two phases as already observed in other publications [32,33,37]. After annealing at 500 °C, this thin oxide layer converted to a mixture of anatase and rutile (Fig. 3), in line with other studies [35].

Table 3
Median proportions of pull-out and histomorphometry results of the three types of implant inserted into the femoral condyles of NZW rabbits for 4 weeks: median [min; max].

	Pull out (N)	BIC (%) Bone-to-implant contact	BS/TS 0.5 mm (%) Bone surface at 0.5 mm	BG (%) Bone growth in apical the chamber	n
MA	37 [12;52]	29 [13;35]	42 [24;58]	6 [0;17]	6
MICRO	80 [28;205]	44 [29;52]	44 [34;57]	7 [0;30]	7
NANO	105 [24;160]	41[16;51]	46 [43;58]	16 [5;29]	7

Anodization is a relatively simple process that is applicable to complex-shaped implants, while the internal diameter of the nanotubes can easily be controlled via the applied tension [16,32,38].

Recently, it has been demonstrated that the nanoscale environment is a critical factor for both the cellular behaviour and the bone tissue integration of implants [15,16]. However, to our knowledge, no study has compared the osseointegration of NANO implants with classic grit-blasted, acid-etched MICRO implants. We have shown previously that nanostructured surfaces with nanotubes 20, 30 and 50 nm in diameter enhanced early bone tissue apposition as well as higher bone implant anchorage in comparison to smooth titanium wires after implantation in rat tibias for 1 and 3 weeks [24]. Fan et al. [39] also demonstrated that titanium dioxide nanotubes resulted in a higher push-out force when compared with machined implants after implantation in dog femurs for 3 months. Another study evaluating the BIC of implants placed in the frontal skulls of domestic pigs showed a significantly higher value for the 50, 70 and 100 nm groups than the machined controls [40]. Similarly, a significant increase in BIC and gene expression levels was found in the bone attached to implants with titanium dioxide nanotubes, especially 70 nm diameter nanotubes, compared with machined titanium implants in minipigs [41]. Another study demonstrated that after 4 weeks of implantation in rabbit tibias, pull-out testing was nine times higher for implants with TiO_2 nanotubes than with TiO_2 grit-blasted surfaces [42]. In a similar animal model of rabbit femoral condyles, it was found that titanium dioxide nanotubes significantly increased torque strengths (41 vs. 29 N cm^{-1}; $P = 0.008$) and new bone formation (57.5% vs. 65.5%; $P = 0.008$) ($n = 8$) in comparison to grit-blasted, moderately rough dental implants after 6 weeks [43]. Torque value is one of the indicators of both primary and secondary stability of implants in bone. However, the strength of the mechanical anchorage of screwed implants in bone varies with the implantation site, the healing rate, the roughness of the implant and the bioactivity of the implant surface [14]. In our study, the pull-out force was measured on cylindrical implants of similar shape in order to avoid possible bias with different implant designs. The roughness of the surface has also been shown to play an important role in bone implant integration. Smooth surfaces promote fibroblast and epithelial cell adhesion, whereas rough surfaces increase osteoblastic proliferation [44]. In agreement, more fibrous tissue was observed on the MA implants than in other groups where bone tissue apposition was present after 4 weeks (Fig. 5). It is well known that fibrous tissue proceeds faster than bone apposition during peri-implant healing. Quantitative assessment of bone to implant contact (Fig. 8) corroborated this qualitative result. Nevertheless, our study showed that the NANO surface produced a similar pull-out value to the MICRO surface, even though its roughness was 3 times greater than that of the NANO implants. Some studies have shown a correlation between surface roughness and bone–implant contact. Positive asymmetry distribution (skewness, Ssk), with sharp peaks (kurtosis (Sku) > 3) and large spacing between peaks such as Rsm, positively affect bone retention by the implants [45]. In our study, all these surface roughness parameters, apart from the average roughness Ra, were similar in all groups. Therefore, the anodization process did not modify the initial roughness or surface spacing parameters of the machined implants (Table 1).

Surface chemistry plays also a major role in the osseointegration of implants as it determines the adsorption of proteins from body fluids. In this study, the surfaces of the different implants were primarily composed of titanium oxide. Raman spectroscopy indicated that either the natural titanium oxide layer found on titanium implants or those processed by anodization were amorphous (Fig. 3). After heating at 500 °C, the NANO surface crystallized into a mixture of rutile and anatase but the effect of these phases on the osseointegration of implants was not investigated here. As derived from the hydrofluoric acid treatment of titanium alloy implants, the NANO surface also contained some fluoride, aluminium and vanadium (Table 2). Since aluminium and vanadium elements were also present in the control titanium alloy implants in similar proportions, their effect on osseointegration could not determined. On the other hand, fluoride ion modification of implants has been shown to enhance osteoblastic differentiation and interfacial bone formation [46]. The relatively better osseointegration of the NANO implants may result from the incorporation of fluoride in the titanium oxide layer.

The osseointegration of grit-blasted and acid-etched MICRO surfaced implants has been widely documented in pre- and clinical studies [6,47–50]. However, micro-rough surfaces are less suited to efficient bacterial decontamination in case of peri-implantitis than smooth surfaces. Micro-rough surfaces (Ra = 1.5 μm) favour both the entrapment of bacteria and biofilm attachment, even though mechanical devices such as brushes or air flow are used to decontaminate infected implants [29,51]. In addition, it has recently been demonstrated that nanostructured titanium prevents bacterial attachment compared to conventional titanium surfaces [52]. The photocatalytic properties of the titanium dioxide nanotube array could even be used to decontaminate implants using ultraviolet light [53]. In a recent study, it has been shown that nanotube surfaces reduce fibrotic capsule thickness after implantation in rat abdominal walls more than control implants, indicating a better soft tissue response [54]. The nanotube surface may also improve the gingival tissue integration of dental implants, thus preventing the invasion of bacteria along their surface.

5. Conclusion

In this study, the osseointegration of a surface composed of anodized titanium dioxide nanotubes (NANO) was compared to machined (MA) implants or those with a classic grit-blasted and acid-etched surface (MICRO). After implantation for 4 weeks in rabbit femoral condyles, the bone anchorage of the NANO surface was similar to that of the MICRO implants, whereas its roughness was 3 times lower. The NANO surface presented higher but not significant bone integration than the other two surfaces regarding BIC and apical BG values.

6. Disclosure

A.H. and P.L. are founders of the spin-off company Biomedical Tissues that sponsored this experimental study.

Acknowledgements

Authors are grateful to Jerome Amiaud for his technical assistance in non-decalcified histology of samples. N. Stephant, Y. Borjon-Piron and the electronic microscopy centre of IMN are acknowledged for their technical help. L.S. is a PhD student at the University of Nantes financially supported by the company Biomedical Tissues and the Association Nationale de la Recherche et de la Technologie (ANRT).

Appendix A. Figures with essential colour discrimination

Certain figures in this article, particularly Figs. 2–5 are difficult to interpret in black and white. The full colour images can be found in the on-line version, at http://dx.doi.org/10.1016/j.actbio.2014.10.017.

References

[1] Papaspyridakos P, Mokti M, Chen C-J, Benic GI, Gallucci GO, Chronopoulos V. Implant and prosthodontic survival rates with implant fixed complete dental prostheses in the edentulous mandible after at least 5 years: a systematic review. Clin Implant Dent Relat Res 2013. http://dx.doi.org/10.1111/cid.12036.
[2] Gokcen-Rohlig B, Yaltirik M, Ozer S, Tuncer ED, Evlioglu G. Survival and success of ITI implants and prostheses: retrospective study of cases with 5-year follow-up. Eur J Dent 2009;3:42–9.
[3] Le Guéhennec L, Soueidan A, Layrolle P, Amouriq Y. Surface treatments of titanium dental implants for rapid osseointegration. Dent Mater Off Publ Acad Dent Mater 2007;23:844–54.
[4] Stanford CM. Surface modifications of dental implants. Aust Dent J 2008;53(Suppl 1):S26–33.
[5] Junker R, Dimakis A, Thoneick M, Jansen JA. Effects of implant surface coatings and composition on bone integration: a systematic review. Clin Oral Implants Res 2009;20(Suppl 4):185–206.
[6] Buser D, Broggini N, Wieland M, Schenk RK, Denzer AJ, Cochran DL, et al. Enhanced bone apposition to a chemically modified SLA titanium surface. J Dent Res 2004;83:529–33.
[7] Schwarz F, Herten M, Sager M, Wieland M, Dard M, Becker J. Bone regeneration in dehiscence-type defects at chemically modified (SLActive) and conventional SLA titanium implants: a pilot study in dogs. J Clin Periodontol 2007;34:78–86.
[8] Rønold HJ, Ellingsen JE. Effect of micro-roughness produced by TiO2 blasting–tensile testing of bone attachment by using coin-shaped implants. Biomaterials 2002;23:4211–9.
[9] Rønold HJ, Lyngstadaas SP, Ellingsen JE. A study on the effect of dual blasting with TiO2 on titanium implant surfaces on functional attachment in bone. J Biomed Mater Res A 2003;67:524–30.
[10] Schliephake H, Aref A, Scharnweber D, Bierbaum S, Sewing A. Effect of modifications of dual acid-etched implant surfaces on peri-implant bone formation. Part I: organic coatings. Clin Oral Implants Res 2009;20:31–7.
[11] Novaes Jr AB, de Souza SLS, de Barros RRM, Pereira KKY, Iezzi G, Piattelli A. Influence of implant surfaces on osseointegration. Braz Dent J 2010;21:471–81.
[12] Ross AP, Webster TJ. Anodizing color coded anodized Ti6Al4V medical devices for increasing bone cell functions. Int J Nanomed 2013;8:109–17.
[13] Schwartz Z, Nasazky E, Boyan BD. Surface microtopography regulates osteointegration: the role of implant surface microtopography in osteointegration. Alpha Omegan 2005;98:9–19.
[14] Wennerberg A, Albrektsson T. Effects of titanium surface topography on bone integration: a systematic review. Clin Oral Implants Res 2009;20(Suppl 4):172–84.
[15] Lavenus S, Berreur M, Trichet V, Pilet P, Louarn G, Layrolle P. Adhesion and osteogenic differentiation of human mesenchymal stem cells on titanium nanopores. Eur Cell Mater 2011;22:84–96.
[16] Oh S, Brammer KS, Li YSJ, Teng D, Engler AJ, Chien S, et al. Stem cell fate dictated solely by altered nanotube dimension. Proc Natl Acad Sci 2009;106(7):2130–5.
[17] Oh S, Daraio C, Chen L-H, Pisanic TR, Fiñones RR, Jin S. Significantly accelerated osteoblast cell growth on aligned TiO2 nanotubes. J Biomed Mater Res A 2006;78A:97–103.
[18] Sirivisoot S, Yao C, Xiao X, Sheldon BW, Webster TJ. Greater osteoblast functions on multiwalled carbon nanotubes grown from anodized nanotubular titanium for orthopedic applications. Nanotechnology 2007;18:365102.
[19] Yao C, Slamovich EB, Webster TJ. Enhanced osteoblast functions on anodized titanium with nanotube-like structures. J Biomed Mater Res A 2008;85(1):157–66.
[20] Popat KC, Leoni L, Grimes CA, Desai TA. Influence of engineered titania nanotubular surfaces on bone cells. Biomaterials 2007;28:3188–97.
[21] Dalby MJ. Topographically induced direct cell mechanotransduction. Med Eng Phys 2005;27:730–42.
[22] Park J, Bauer S, von der Mark K, Schmuki P. Nanosize and vitality: TiO2 nanotube diameter directs cell fate. Nano Lett 2007;7:1686–91.
[23] Bacakova L, Filova E, Parizek M, Ruml T, Svorcik V. Modulation of cell adhesion, proliferation and differentiation on materials designed for body implants. Biotechnol Adv 2011;29:739–67.
[24] Lavenus S, Trichet V, Le Chevalier S, Hoornaert A, Louarn G, Layrolle P. Cell differentiation and osseointegration influenced by nanoscale anodized titanium surfaces. Nanomed 2012;7:967–80.
[25] Ercan B, Taylor E, Alpaslan E, Webster TJ. Diameter of titanium nanotubes influences anti-bacterial efficacy. Nanotechnology 2011;22:295102.
[26] Ercan B, Kummer KM, Tarquinio KM, Webster TJ. Decreased Staphylococcus aureus biofilm growth on anodized nanotubular titanium and the effect of electrical stimulation. Acta Biomater 2011;7:3003–12.
[27] Kummer KM, Taylor EN, Durmas NG, Tarquinio KM, Ercan B, Webster TJ. Effects of different sterilization techniques and varying anodized TiO_2 nanotube dimensions on bacteria growth. J Biomed Mater Res B Appl Biomater 2013;101:677–88.
[28] Puckett SD, Taylor E, Raimondo T, Webster TJ. The relationship between the nanostructure of titanium surfaces and bacterial attachment. Biomaterials 2010;31:706–13.
[29] Subramani K, Wismeijer D. Decontamination of titanium implant surface and re-osseointegration to treat peri-implantitis: a literature review. Int J Oral Maxillofac Implants 2012;27:1043–54.
[30] Wu Y, Zitelli JP, TenHuisen KS, Yu X, Libera MR. Differential response of Staphylococci and osteoblasts to varying titanium surface roughness. Biomaterials 2011;32:951–60.
[31] Coelho PG, Granjeiro JM, Romanos GE, Suzuki M, Silva NRF, Cardaropoli G, et al. Basic research methods and current trends of dental implant surfaces. J Biomed Mater Res B Appl Biomater 2009;88:579–96.
[32] Minagar S, Berndt CC, Wang J, Ivanova E, Wen C. A review of the application of anodization for the fabrication of nanotubes on metal implant surfaces. Acta Biomater 2012;8:2875–88.
[33] Pérez-Jorge C, Conde A, Arenas MA, Pérez-Tanoira R, Matykina E, de Damborenea JJ, et al. In vitro assessment of Staphylococcus epidermidis and Staphylococcus aureus adhesion on TiO2 nanotubes on Ti–6Al–4V alloy. J Biomed Mater Res A 2012;100A:1696–705.
[34] Eisenbarth E, Velten D, Müller M, Thull R, Breme J. Biocompatibility of β-stabilizing elements of titanium alloys. Biomaterials 2004;25:5705–13.
[35] Zhang J, Li M, Feng Z, Chen J, Li C. UV Raman spectroscopic study on TiO2. I. Phase transformation at the surface and in the bulk. J Phys Chem B 2006;110:927–35.
[36] Koh J-W, Yang J-H, Han J-S, Lee J-B, Kim S-H. Biomechanical evaluation of dental implants with different surfaces: removal torque and resonance frequency analysis in rabbits. J Adv Prosthodont 2009;1:107–12.
[37] Tsuchiya H, Macak JM, Ghicov A, Schmuki P. Self-organization of anodic nanotubes on two size scales. Small 2006;2:888–91.
[38] Liu G, Wang K, Hoivik N, Jakobsen H. Progress on free-standing and flow-through TiO2 nanotube membranes. Sol Energy Mater Sol Cells 2012;98:24–38.
[39] Fan X, Feng B, Liu Z, Tan J, Zhi W, Lu X, et al. Fabrication of TiO2 nanotubes on porous titanium scaffold and biocompatibility evaluation in vitro and in vivo. J Biomed Mater Res A 2012;100:3422–7.
[40] Von Wilmowsky C, Bauer S, Roedl S, Neukam FW, Schmuki P, Schlegel KA. The diameter of anodic TiO2 nanotubes affects bone formation and correlates with the bone morphogenetic protein-2 expression in vivo. Clin Oral Implants Res 2012;23:359–66.
[41] Wang N, Li H, Lü W, Li J, Wang J, Zhang Z, et al. Effects of TiO2 nanotubes with different diameters on gene expression and osseointegration of implants in minipigs. Biomaterials 2011;32:6900–11.
[42] Bjursten LM, Rasmusson L, Oh S, Smith GC, Brammer KS, Jin S. Titanium dioxide nanotubes enhance bone bonding in vivo. J Biomed Mater Res A 2010;92:1218–24.
[43] Sul Y-T. Electrochemical growth behavior, surface properties, and enhanced in vivo bone response of TiO2 nanotubes on microstructured surfaces of blasted, screw-shaped titanium implants. Int J Nanomed 2010;5:87–100.
[44] Boyan BD, Dean DD, Lohmann CH, Cochran DL, Sylvia VL, Schwartz Z. The Titanium-bone cell interface in vitro: the role of the surface in promoting osteointegration. Titan. Med., Berlin: Springer Verlag; 2001; 561–85.
[45] Lamolle SF, Monjo M, Lyngstadaas SP, Ellingsen JE, Haugen HJ. Titanium implant surface modification by cathodic reduction in hydrofluoric acid: surface characterization and in vivo performance. J Biomed Mater Res A 2009;88A:581–8.
[46] Cooper LF, Zhou Y, Takebe J, Guo J, Abron A, Holmén A, et al. Fluoride modification effects on osteoblast behavior and bone formation at TiO2 grit-blasted c.p. titanium endosseous implants. Biomaterials 2006;27(6):926–36.
[47] Cochran DL, Buser D, ten Bruggenkate CM, Weingart D, Taylor TM, Bernard J-P, et al. The use of reduced healing times on ITI implants with a sandblasted and acid-etched (SLA) surface: early results from clinical trials on ITI SLA implants. Clin Oral Implants Res 2002;13:144–53.
[48] Cochran DL, Jackson JM, Bernard J-P, ten Bruggenkate CM, Buser D, Taylor TD, et al. A 5-year prospective multicenter study of early loaded titanium implants with a sandblasted and acid-etched surface. Int J Oral Maxillofac Implants 2011;26:1324–32.
[49] Buser D, Schenk RK, Steinemann S, Fiorellini JP, Fox CH, Stich H. Influence of surface characteristics on bone integration of titanium implants. A

histomorphometric study in miniature pigs. J Biomed Mater Res 1991;25:889–902.
[50] De Sanctis M, Vignoletti F, Discepoli N, Zucchelli G, Sanz M. Immediate implants at fresh extraction sockets: bone healing in four different implant systems. J Clin Periodontol 2009;36:705–11. http://dx.doi.org/10.1111/j.1600-051X.2009.01427.x.
[51] Subramani K, Jung RE, Molenberg A, Hammerle CHF. Biofilm on dental implants: a review of the literature. Int J Oral Maxillofac Implants 2009;24:616–26.
[52] Durmus NG, Webster TJ. Nanostructured titanium: the ideal material for improving orthopedic implant efficacy? Nanomed 2012;7:791–3.
[53] Ahn S-J, Han J-S, Lim B-S, Lim Y-J. Comparison of ultraviolet light-induced photocatalytic bactericidal effect on modified titanium implant surfaces. Int J Oral Maxillofac Implants 2011;26:39–44.
[54] Smith GC, Chamberlain L, Faxius L, Johnston GW, Jin S, Bjursten LM. Soft tissue response to titanium dioxide nanotube modified implants. Acta Biomater 2011;7:3209–15.

3.2.2 Additional discussion

In this study, we compared the osseointegration of machined (MA), standard alumina grit-blasted and acid-etched (MICRO) and nanostructured (NANO) implants in rabbit femurs. A micro surface is composed of typical random cavities with an average roughness of 1.5 μm quite similar to the SLA surface. On the other hand, the NANO surface consisted of a regular array of titanium oxide nanopores 37 nm in diameter and 160 nm thick. The results showed that after 4 weeks, the anchorage of the NANO surface was higher than for the other groups while its roughness was three times lower than the MICRO surface (0.5 vs 1.5 μm). Histology analysis showed a direct apposition of bone tissue on to the NANO surface. Hismorphometric calculations were in accordance with the bone-to-implant contact and bone growth values. Both displayed higher values for the NANO than for the other implant surfaces. This study thus showed by using "homemade"samples in a rabbit model that the nanostructured surface improved the osseointegration of titanium implants and may be an alternative to conventional surface treatments.

Although these results are satisfactory, the study deals only with the integration of a structure composed of a network of nanopores. It would have been interesting to study a fourth group of surfaces composed of regular nanotubes aligned perpendicularly to the surface. Indeed, results of surface characterisation obtained in the beginning of this chapter show different surface properties between nanopores and nanotubes (i.e. contact angle and crystalline structures after annealing). So far, not a single publication has clearly demonstrated the bioactivity effect of these two types of nanostructure, but only considers the size. For a same electrolyte, the nanopores formed are generally smaller than the nanotubes. Divya Rani *et coll.* have published a study on the effect of different nanostructure morphologies on osseointegration [29]. They compared nanotube, nanoscaffold, nanoleaf and nanoneedle surfaces produced by anodisation or hydrothermal methods. The authors found that nanoleaves, which are a network of vertically aligned, non-periodic, fibre structures, provide higher protein adsorption, and osteoblast cell proliferation and differentiation. However, the results for protein adsorption on nanoleaves were closely followed by nanotubular and nanoneedle structures after 1 hour and levelled out after 2 hours. Moreover, some of the gene expression in primary osteoblasts was missing for the nanotubular structure. Thus, the nano-architecture should be investigated in greater detail to be able to draw clear conclusions with regard to its effect on tissue integration.

In 2014, Kang *et coll.* published a comparative study in rabbits on the osseointegration of titanium implants with various diameters of nanotube [102]. Nanotubes with similar porosity size of 30 nm and made using the same proto-

col as in our study were compared to 70 nm and 100-nm-large nanotubes. This study confirmed the results of Brammer and Oh, that is, that 30 nm and 70 nm nanotubes may positively affect osseointegration healing [23, 41]. Recently, Yi *et coll.* also published a comparative study in rats using the same implant geometry [103]. They compared different surface groups with nanopores of 30 nm and nanotubes of 70 nm. After 4 and 12 weeks of healing, the authors did not find any difference between the groups, but they only took into consideration nanoporosity size without taking into account the difference in nanostructure.

As shown at the beginning of this chapter, nanopores and nanotubes may produce different crystalline structures (i.e. amorphous, anatase, rutile, brookite) after a single annealing treatment. Similar results were also observed by Liu *et al.* who compared crystalline structures in relation to nanostructure size, shape and annealing temperature for solar cell applications. The crystalline titania structure is widely put forward as improving biocompatibility more than an amorphous titania structure [104]. Several studies affirm that a crystalline structure composed of both anatase and rutile is more bioactive than an only anatase structure, while a pure rutile phase would induce cell apoptosis [30, 105]. So far, not a single publication has clearly studied an optimal crystalline structure for a better surface bioactivity effect. In this thesis, we tried to study this topic *in vitro* but were confronted with difficulties in the implementation of the protocols on titanium disks and not only on culture plates.

Another point not developed in the discussion of this article is the fluoride contained in the surface after anodising. Titania nanostructure formation usually requires electrolytes containing a fluorinated substance which leads to fluoride incorporation during oxide layer growth. This fluoride ion has been recognised as an important trace element in bone and dental health [106, 107]. It has been found that fluoride may play a role in tissue generation, as dentistry [108, 109]. However, inadequate or excess fluoride may cause tooth enamel damage and skeletal fluorosis after prolonged exposure [110].

To conclude, this study makes it possible to demonstrate the osseointegration of nanoporous surfaces with both mechanical anchorage and analysis of surrounding tissue. The surface could be optimised with a crystalline structure. Although there are several publications in the field, no one has identified either the most biocompatible crystalline structure or the different effects of nanopores and nanotubes.

3.3 Conclusion

This third chapter deals with the synthesis and characterisation of nanostructured surfaces in both materials science and the biological field. Our anodising surface treatment makes it possible to propose colourful titanium implants with an oxide layer presenting nanopore or nantube architecture, with a controllable crystalline structure (anatase, rutile, brookite). Annealing treatments at 500 °C reduce fluoride insertion and eliminate acid traces adsorbed on to the surface but may risk modification of the titania nanostructures morphology due to the crystal growth of rutile. The first article shows promising results in terms of biocompatibility as it is similar to conventional grit-blasted and acid-etched surfaces. The direct application of this surface treatment on intraosseous implants (dental implants) and soft tissues contact (tracheal prostheses) are reported in the next chapter.

CHAPTER

4

MEDICAL APPLICATIONS

As life expectancy increases, there is a need for better quality of life. General medical progress has led to a widespread increase in the use of implantable medical devices to assist or replace an organ or tissue. Some replacements may be due to a minor accident requiring simple implantation into healthy tissue. However, other devices are required in cases of serious disease (*e.g.* cancer) in order to regain a certain degree of aesthetics or functionality in a given organ in not necessarily healthy tissue. Surgery is performed on patients who have already undergone a number of violent treatments (such as chemotherapy) or other surgeries. They are thus more fragile physically and are more mentally frail than a healthy person. The best thing for them is to limit the number of surgical procedures. For instance, the surgery for throat and /or trachea carcinoma may require tracheal prostheses to restore normal breathing function (**Figure 4.1**).

It should be noted that despite significant progress in the field of implant surgery, and a global success rate after five to ten years or less following the operation, implants nevertheless need to be replaced. The possible causes of failure in the short or middle term, and in the long term, are diverse. In all the setting-up phase for prostheses, the success of an operation above all depends on the patient's condition, pathology, and lifestyle, the surgical technique used, and post-operative activity. In the longer term, problems are related to the implant itself (material, geometry, surface) and how it binds to the surrounding tissues.

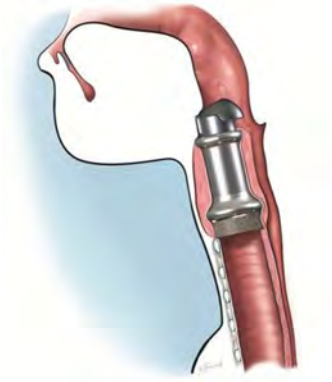

Figure 4.1: Diagram of implantation of a tracheal prosthesis (source: http://www.protipmedical.com)

In the case of dental implants, peri-implantitis (similar to parodontitis - loosening of bone surrounding a tooth) may be observed around the implant (**Figure 4.2**). This problem occurs due to bacterial colonisation of the tissue-implant interface [10]. Orthopaedic prostheses are also subject to bacterial infiltration [8, 9]. In the case of other orthopaedic joints, the main cause of long term failure is the emission of debris/fragments due to friction [111]. Finally, in the case of tracheal prostheses, patients are often subject to fistulas due to poor tissue integration. Therefore, the life of implants needs to be extended and depends on many factors. However, the high quality and bioactivity of implant surfaces makes it possible to obtain optimal implant tissue integration, ensuring full implant function, and may act as a barrier to bacteria, while avoiding any element release capable of causing other pathologies.

In this context, chapter 4 considers the medical applications of new surface treatments. The ultimate objective of this thesis is to elaborate a surface treatment for dental implants and tracheal prostheses that satisfies the various specifications inherent to the biomedical domain:

- Biological Performance (*e.g.* bone or soft-tissue integration);
- Security (*e.g.* manufacturer, user, patients);
- Aesthetics (*e.g.* colour, reproducibility);
- Functional (*e.g.* respect of tolerances, mechanical);
- Regulatory (*e.g.* ISO 13485,...).

The surface treatment used in this section was based on the results obtained in chapter 3. All the steps and problems encountered for the medical application

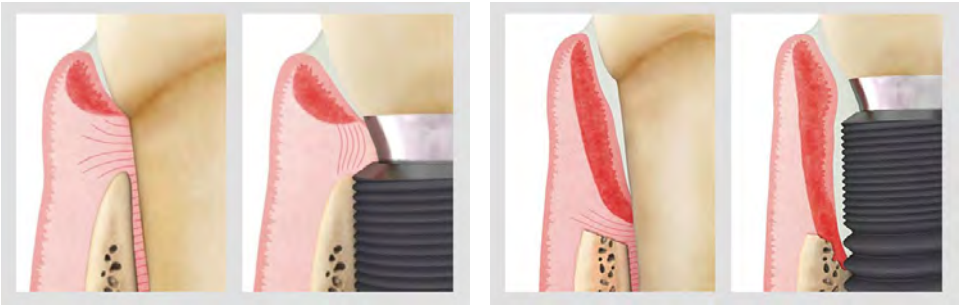

(a) (b)

Figure 4.2: Cases of inflammation (dark pink) of the gingival tissue around a tooth and implant(a) that does not touch the bone (reversible); (b) that goes deep into the tissue and destroys the bone around the tooth (parondotitis) or the implant (peri-implantitis) (Source: http://www.wandji-parodontie.com/les-maladies-peri-implantaires/)

were presented in the latter chapter. The first part concerns the use of nano-surfaces for the osseointegration of dental implants. This part is introduced by a general presentation of dental implants followed by the results of an *in vivo* study of osseointegration in a rabbit model. We end this part with the results of the validation of the titanium nanostructuring process obtained in September 2013 from a certified organisation (G-MED) and an initial approach to industrial scaling up to handle a larger number of implants in one batch. The second section relates to the use of nano-surfaces for soft tissue integration in applications with tracheal prostheses. Although the treatment obtained is homogeneous on the tracheal prosthesis, the results indicate the problem of nanotube film adhesion and the release of nanometer particles.

4.1 Nanostructured surfaces on dental implants

4.1.1 Context and generalities concerning dental implants

Dental implantology is a special field in dentistry that has dealt with the rehabilitation of damaged chewing apparatus due to the loss of natural teeth for more than 30 years. Missing teeth can be replaced by dental implants or bridges (for tooth groups), which are inserted instead of natural tooth roots into the mandible or maxilla. According to the report published by the French High Authority for Health (HAS) in 2007, the number of implants placed in France in 2007 was more than 243,000 (study by the Millennium Research Group) while more than 5 million are inserted each year in the United States. As an

average of 2 to 3 implants are used per patient, it can be estimated that about 100,000 patients are concerned by oral implantology in France [3]. However, not everyone can afford this surgical procedure as the cost for dental implants is high. Some patients go to other countries to find proper affordable dental and medical work.

Dental implants are composed of three main parts:

- The implant body, which defines the shape of the implant and contains the thread which provides the primary stability;
- The collar/col is the upper part of the implant and the junction zone between the actual dental implant and the abutment. Its surface is generally flat without thread for the contact with the soft tissues of the oral cavity;
- The apex, which ends the body of the implant and can be either be pointed or rounded;

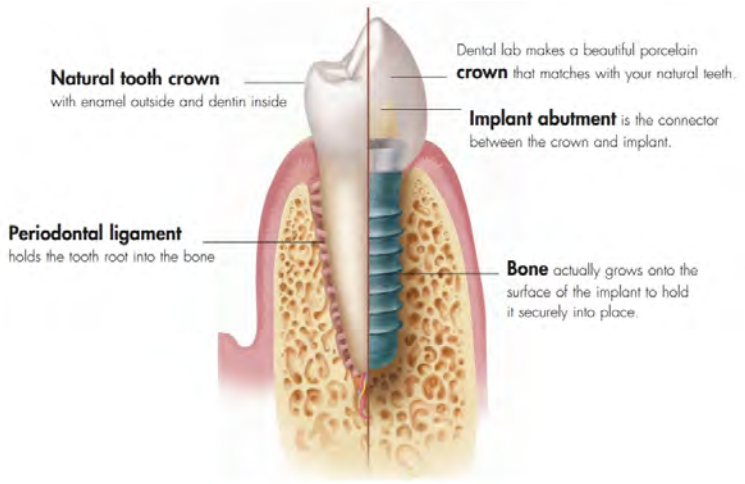

Figure 4.3: Dental implant diagram (Source: http://dunadentalbudapest.com/service/dental-implants/)

As shown in the diagram 4.3, dental implants are associated with two other elements: the abutment and the crown. The abutment is a connecting element which is not necessarily made of the same material as the dental implant. More modern abutments are now also made from zircona ceramics. It serves as a fixation by either a screwed-in or cemented crown. This element is the only part seen in the mouth giving artificial teeth their natural appearance.

When implants are inserted into the mouth, they are directly immersed in biological fluids such as blood, providing protein adsorption. Soft tissues such

as junctional epithelium (JE) and connective tissue attachment (CTA) develop promptly around it. The latter is composed of approximately 80 % collagen fibres, 13 % fibroblasts and 4 % vascular structures. The connective tissue forms a "biological barrier"about 3 mm thick which protects the bone-implant interface against dental plaque and the oral cavity [112]. However, the success and long-term prognosis for implant prosthetic therapy depends primarily on the anchorage of the implant in the jawbone: the **osseointegration**. It takes a relatively long time (1 to 3 months) before the implant can be loaded and 3 to 6 months to obtain total integration of the implant.

Despite a global success rate that exceeds 95 % in implantology today, a number of implant failures still persists and causes loss of the implant. In up to 30 % of cases, these failures may be due to an infection resulting from bacterial penetration at its interface. An inflammatory reaction ensues and causes the loss of the supporting bone in the tissues surrounding the implant. This phenomenon is called **peri-implantitis** [112]. The reaction can start soon after the operation but takes several years (average 5 years) to develop before we can detect the destructive peri-implantitis sites. The process of peri-implantitis is not yet well-known but studies make it possible to understand certain factors behind the malfunction: patient predisposition, lifestyle, environment, surgical procedures, type of implant, etc...

There are a large number of implant systems (around 250 types of implant in 2014 in France). The choice of an implant (geometry, implant surface) is made in particular in relation to the clinical situation. There are three key changes that have a significant impact on implant practice: implant shape (cylindrical or conical), size (diameter and length), and surface conditions. Implant shape mainly varies in relation to the choice of dental implant brand. Implant size is related to bone anatomy and the space available, but can vary from 3 to 5 mm in diameter and 6 to 18 mm in length. In cases where the bone defect is too large, a bone substitute covered or not with a dental membrane can be used to increase the bone volume. And finally, the surface properties of the implant can be standard or enhanced by using specific surface treatments.

Today, much effort is devoted to the design, synthesis and manufacture of Ti or alloy dental implants in order to obtain long term success and secure anchoring to the bone. One hypothesis states that the speed and quality of integration could be improved by a surface treatment, obtaining effective sealing at the implant-tissue interface. Some research aims to improve soft-tissue integration at the abutment [113]. The implant surface effectively does not produce the same kind of connection with the surrounding soft tissues as natural teeth. Discontinuous tissues with different spatial orientation or poor blood irrigation are some anomalies found at the implant interface [63]. These de-

fects make bacterial colonisation possible on the implant abutment surface and consequently contribute to peri-implantitis. However, much research aims to obtain early bone integration of the titanium dental implant. Nowadays there are a wide range of dental implants with different surface treatments. The most widely used commercial techniques for surface treatment of titanium are sand-blasting and acid-etching. Manufactured implants often have a surface with a range extending from the nanometre to the millimetre scales. The focus of this thesis is to characterise *in vivo* the application of nano scale modification by anodisation directly on dental implants in order to enhance osseointegration.

4.1.2 Comparative study in rabbit femurs

Titanium or alloys (TA6V, TiZr, etc) are widely used for manufacturing dental implants. Because these materials are inert while dental implants require a bioactive surface to enhance early bone integration, surface treatments have been developed. Nowadays, there are a wide range of dental implants (250 different dental implants in France) with different surface treatments from the nanometre to the millimetre scales with or without coating with a specific chemical composition. The standard techniques for the surface treatment of titanium are blasting or acid-etching methods. The most widely used commercial method for surface treatment is the surface developed by Straumann that is Sand-blasted with Large grit and Acid-etched (SLA).

The current challenges in dental implantology are two-fold and concern biocompatibility and innovation. Many works on new bioactive surface treatments have been presented in the literature. However, they are done on one sample disk or a "home-made"implant and its homogeneity has never really been studied for complex implants. Only a few articles have studied surfaces and compared them to the biocompatibility of actual manufactured surfaces. Moreover, although by obtaining rapid osseointegration and thus immediate-loaded implants we could increase the implant success rate, we will still be confronted with biological limitations. Treatment providing the same performances as the Straumann SLA surface, while innovative in terms of structure and the process used, can be interesting for a manufacturer to set itself apart from the market.

The objective of this section is quite similar to the article N° 1 **??** which presents the results of the biological characterisation of this honeycomb titania surface implanted into a rabbit model. The difference with the previous article N° 1 is that the study was performed using real dental implants from Biotech Dental with two groups of nanostructured surfaces (S-NANO and R-NANO) and Straumann implants with the standard grit-blasted and acid-etched (SLA) surface, referred to as MICRO in our work. After 2 to 4 weeks of implantation

into the femoral condyles of New Zealand white rabbits, histomorphometry calculations were carried out to compare the bone integration of NANO vs MICRO dental implants.

The results of this study were published in article n N° 2 with the invitation in the journal, Nanomedecine and titled "Comparative bone tissue integration of nanostructured and micro-roughened dental implants".

4.1.2.a Article N° 2: Comparative bone tissue integration of nanostructured and micro-roughened dental implants

Research Article

Nanomedicine

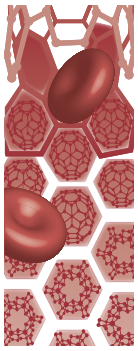

Comparative bone tissue integration of nanostructured and microroughened dental implants

Aim: The aim was to compare osteointegration of nanostructured implants to a microsurface widely used for titanium dental implants. **Materials & methods:** Commercial titanium dental implants with smooth or microroughened surfaces were nanostructured. Implants were inserted into the femoral condyles of rabbits. After 2 and 4 weeks, histomorphometry calculation was performed. **Results:** Nanotubes measuring 60 nm in diameter were observed on both S-NANO (roughness: 0.05 μm) and R-NANO (roughness: 0.40 μm) surfaces. The MICRO surface exhibited typical random cavities (roughness: 2.09 μm). At 4 weeks, bone-to-implant contact values were significantly higher for the R-NANO than for the MICRO surface while no differences were observed at 2 weeks. **Conclusion:** Overall, this study shows that the nanostructured surfaces improved osteointegration similar or higher than the MICRO.

Keywords: bone-to-implant contact • dental implant • nanostructure • osseointegration • titanium

Laëtitia Salou[1,2,3], Alain Hoornaert[4], Julien Stanovici[1], Sylvain Briand[1,5], Guy Louarn[3] & Pierre Layrolle*[,1]

[1]Inserm U957, Lab. Pathophysiology of Bone Resorption, Faculty of Medicine, University of Nantes, France
[2]Biomedical Tissues, Nantes, France
[3]CNRS – Institut des Matériaux, Nantes, France
[4]CHU Nantes, Faculty of Dental Surgery, Nantes, France
[5]CHU Nantes, Department of Orthopaedic Surgery, University Hospital of Nantes, Nantes, France
*Author for correspondence:
Tel.: +33 2 72 64 11 43
Fax: +33 2 40 41 28 60
pierre.layrolle@inserm.fr

Titanium and its alloys are widely used for manufacturing dental implants because of their good biocompatibility. Soft tissue adhesion onto implant abutment is important in order to prevent bacterial infiltration along the implant. Direct bone-to-implant contact is necessary for biomechanical anchoring of the implants. The surface properties of dental implants are key factors for rapid and stable bone tissue integration [1]. Dental implant surfaces that promote bone tissue integration are microroughened by anodization, grit blasting and acid etching. These surfaces have random micrometer-scale features that increase the mechanical interlock with bone tissue, and thus the primary stability of dental implants. Well-documented and successful examples of such microroughened surfaces on dental implants are the Straumann SLA® and SLA active® (Straumann AG, Basel, Switzerland) [2,3]. Nevertheless, the biological integration of implants into bone involves a series of events that takes place at the nanometer scale [4]. Immediately after implantation, surfaces are fully covered by nanoobjects such as FN proteins that serve as adhesion sites for cells. These microtopographies may, however, be suboptimal for the rapid attachment and proliferation of osteoblastic cells leading to bone tissue apposition on dental implants [5]. Microroughened surfaces may also be more difficult to decontaminate in cases of bacteria attachment and biofilm formation than smooth surfaces on dental implants [6,7].

Numerous studies have shown that nanometer-sized features on surfaces direct stem cell fate through protein adsorption and cell signaling pathways [4,8,9]. Mesenchymal stem cells (MSCs) are multipotent cells that are present in bone marrow, peripheral blood and other tissues to very low levels. These cells are attracted to the periimplant healing site by cytokines and are able to migrate through the blood clot to colonize the implant surface. Depending on their microenvironment, MSCs can differentiate into different lineages such as osteoblasts (bone), chondrocytes (cartilage), adipocytes (fat) or fibroblasts (skin). The surface properties

Future Medicine part of fsg

of implants may control the differentiation of MSCs, and thus the type of peri-implant tissue. Nevertheless, this hypothesis has mainly been validated *in vitro*. For instance, it has been shown that cytoskeleton tensions modulate gene expression through the *RhoA* molecular pathway and regulate stem cell lineage commitment [10]. Dalby *et al.* have shown that random nanostructured surfaces induce the osteoblastic differentiation of MSCs, even without osteogenic supplements [11]. Titania nanotubes obtained by adonization have been shown to control the adhesion and osteoblastic differentiation of MSCs [12,13]. These studies have shown that nanotubes measuring 30 nm in diameter favor cell adhesion, whereas larger nanopores of 70–100 nm induce cell elongation, cytoskeletal stress and selective differentiation into osteoblastic cells. We have also demonstrated a correlation between the osteoblastic cell differentiation and bone tissue integration of nanostructured titanium implants [14]. However, this study was conducted on titanium discs and wires, which are far less complex in geometry than dental implants. Of the other methods used to create nanostructures on titanium, anodization is a relatively simple electrochemical process that produces columnar titania nanotubes. By controlling voltage and the electrolytes, the anodization method makes possible the formation of a regular array of pores with diameters ranging from a dozen of nanometer to a little more than 100 nm [15]. This nano-structuration of titanium should be applicable on commercially available dental implants with smooth or microroughened surfaces.

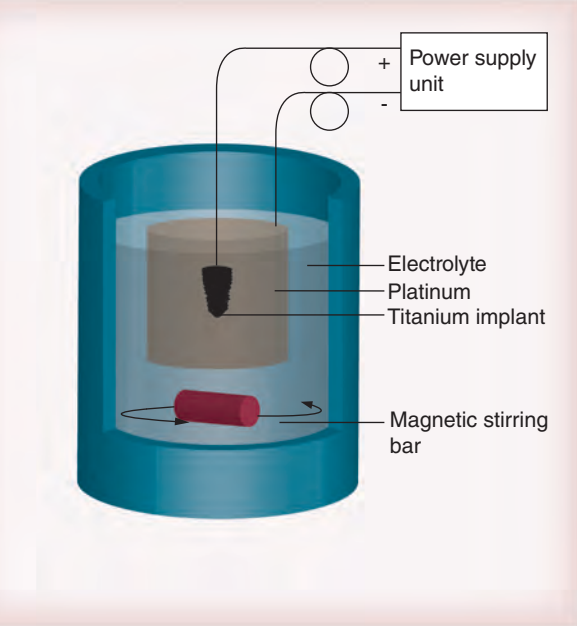

Figure 1. Experimental setup used for the anodization process and preparation of nanostructured R-NANO and S-NANO surfaces on dental implants.
For color figures, please see online at www.futuremedicine.com/doi/full/10.2217/NNM.14.223

The aim of this study was to compare bone tissue integration of nanostructured implants, smooth (S-NANO) and microroughened (R-NANO), with standard microroughened titanium dental implants (MICRO) by implantation into the femoral epiphysis of rabbits. After a healing phase of 2 or 4 weeks, both the quantity of bone surrounding the implants, and the direct bone apposition on the surfaces, were determined by histomorphometry.

Materials & methods

Dental implant preparation

Commercially available dental implants from Biotech Dental and Straumann were used for this study. As shown in Figure 1, the geometries of the implants differed by their shape (cylindrical or conical), screw design and dimensions, which varied from 3.6 to 4.2 mm in diameter and 6–11 mm in length. The implants were divided into three groups, depending on their surface characteristics. According to the manufacturer (Straumann AG), the implants were machined out of Ti grade 4. The microroughened surface SLA was obtained by sandblasting the implant with 250 µm alumina particles and acid-etched it in a warm acidic solution with a ratio of $HCl/H_2SO_4/H_2O$ 2:1:1. The SLA surface on dental implants (Bone level®, Straumann AG) was used as the control surface (MICRO). The two other groups comprised dental implants (Kontact®, Biotech Dental, Salon-de-Provence, France) that were nanostructured by anodization in order to form titania TiO_2 nanotubes on their surface. These implants were machined out of titanium alloy Ti-6Al-4V grade 5. Before nano structuration, the dental implants had their initial machined smooth (S-NANO) or grit-blasted rough (R-NANO) surfaces. Although Straumann and Biotech Dental implants were made out of Ti grade 4 or titanium alloy Ti-6Al-4V grade 5, these alloy compositions only affect the mechanical properties of the implant and not their early bone tissue integration. The implants were first cleaned for 15 min in acetone, ethanol 70%, and demineralized water and then air-dried. As shown in Figure 2, the nanostructuration of the dental implants was conducted by electrochemistry in a PTFE beaker containing a platinum ring cathode and a screw-holder to fix the implant in the center of the system. The anodization was carried out in an electrolyte composed of 1 M acetic acid (CH_3COOH 100%, Merck, Darmstadt, Germany) and 1% wt. hydrofluoric acid (HF 48%, Merck) in demineralized water. The tension was maintained at 20 V for 20 min with magnetic stirring at 350 rpm at room temperature. The samples

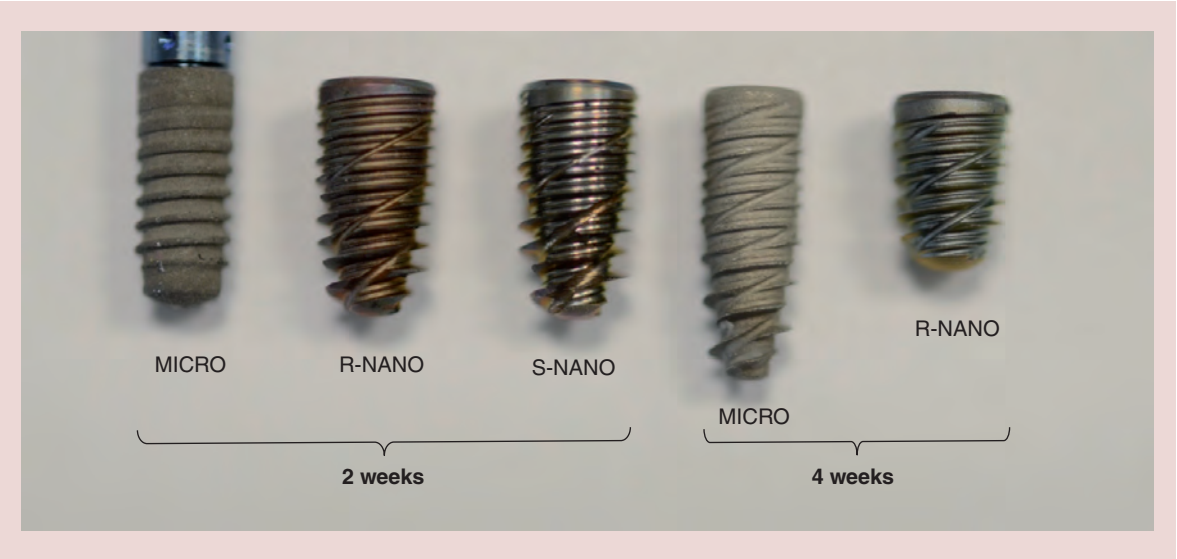

Figure 2. Dental implant groups. Photograph of the different dental implants with the three types of surface used for comparative bone tissue integration at 2 and 4 weeks: alumina grit-blasted and acid-etched (MICRO), grit-blasted and nanostructured (R-NANO) and machined and nanostructured (S-NANO) surfaces.

were immediately rinsed with demineralized water and heated at 500°C for 2 h in an oven (L1/12/R6, Nabertherm, Lilienthal, Germany). Finally, the three groups of dental implants were packaged in double-sealed bags and sterilized by γ-irradiation at 35 kGy prior to being used in the animal study.

Characterizing the implant surfaces

The three surfaces were carefully characterized in order to determine the physical and chemical parameters that may affect the kinetics of bone tissue integration. The topography was analyzed with a profilometer (Intra 2, Taylor Hobson, Leicester, UK ; n = 3 implants/group). The surfaces were observed using a field-emission scanning electron microscope (FE-SEM; Merlin, Carl Zeiss AG., Oberkochen, Germany). The internal diameter and circularity of the titania nanotubes were calculated on the FE-SEM images at a magnification of ×50,000 of the S-NANO and R-NANO surfaces, using a semi-automatic image analysis software (ImageJ). Energy-dispersive x-ray spectroscopy microanalysis (XMAX 80, Oxford Instrument, High Wycombe, UK) and RAMAN spectroscopy (InVia reflex spectrometer, Renishaw, Gloucestershire, UK) were carried out to determine the chemical and crystalline compositions of the surfaces.

Surgical procedure

Animal handling and the surgical procedures were conducted in accordance with European Community guidelines (2010/63/UE) and the study protocol was submitted for approval to the regional animal care and safety committee. The surgery was performed at the Experimental Therapeutic Unit, Faculty of Medicine, University of Nantes. Twenty-four adult female New Zealand white rabbits (NZW, body weight 3.5 kg, age 20 weeks) were purchased from a professional stock-breeder (Hypharm, Roussay, France). All rabbits were identified with a unique, ear-tattooed number. The animals were housed in individual cages with food and water *ad libitum* in an air-conditioned room, with an artificial 12-h day/night cycle. They were quarantined for a minimum period of 10 days after receipt for acclimation. The animals were operated on under general anesthesia by intramuscular injection of a mixture of ketamine/xylazine (35 mg/kg ketamine, Imalgène1000®, Merial and 5 mg/kg xylazine 2% Rompun®, Bayer). An intramuscular injection of analgesic (Buprenorphine, 20 µl/kg, Buprecare, AST Pharma, The Netherlands) was administered prior to surgery and daily for 4 days after. A prophylactic antibiotic (Marbofloxacin 6 mg/kg, Marbocyl FD, Vetoquinol) was also administered by subcutaneous injection at the time of surgery and every day for 4 days postoperatively. Both posterior limbs of the animals were operated on, and a dental implant from each group was inserted into both left and right femoral epiphyses using a permutation scheme (n = 8/group). The posterior limbs were shaved and disinfected with iodine solution and sterile gauzes, and covered with drape sheets. A local anesthetic (1 ml, 4% alphacaïne adrenaline), was injected at the implantation site. The lateral side of the femoral condyle was exposed by incision of the skin and the articular capsule. A hole was drilled in the femoral condyle with ascending series of dental burs (1.3, 2, 3, 3.6 and 4.2 mm in diameter) until the final diameter

and length of the dental implant. Bone drilling was performed under saline irrigation at 800 rpm using a dental surgery micromotor (Surgic XT Plus, NSK, Tochigi, Japan). After drilling through the cortical and trabecular bone, the cavity was thoroughly rinsed with physiological saline solution. The dental implants were screwed into the defect using the implant holder (speed 30 rpm, max. torque 50 N/cm). A cover screw was placed on the implant with the screwdriver. The articular capsule and skin were closed in two layers by suturing in X and U, respectively, with biodegradable sutures (Vicryl 5-0, Ethicon). After surgery, rabbits were observed daily with a control condition, appetite and mobility. After a healing period of 2 or 4 weeks, they were euthanized, in accordance with ethical rules, under general anesthesia by intracardiac injection of an overdose of sodium barbiturate (Dolethal, Vetoquinol). The femoral condyles with the implants were dissected and any abnormal signs of healing were recorded. After euthanasia, 48 epiphyses were removed, fixed in buffered 10% formaldehyde for histological analysis and stored at 4°C. The femoral epiphyses of the rabbits were x-rayed to determine the position of the implant (MX20, Faxitron, IL, USA).

Histology & histomorphometry

After fixation in formaldehyde for 48 h, the explants were dehydrated in successive ethanol baths at 50, 70, 80, 90 and 100% for 24 h. The explants were impregnated with methyl methacrylate for 2–3 days. The polymethyl methacrylate (PMMA) resin was polymerized at 4°C in a partial vacuum to remove air bubbles in the presence of an initiator and a radical polymerization catalyst. After complete hardening, the polymethyl methacrylate blocks were cut using a diamond saw microtome (Leica Sp 1600; Leica, Solms, Germany) in the central longitudinal direction of the implant. Sections of 15 microns in thickness were made, mounted on glass slides and stained with basic fuchsine and toluidine blue. The slides were digitized using a scanner for histological slides (NanoZoomer 2.0RS and NDP view software, Hamamatsu, Japan). The blocks were polished, cleaned with ethanol and dried prior to observation with scanning electron microscopy (TM3000, Hitachi, USA). Continuous images at magnification of ×50 were made in back scattered electron mode (BSEM). The composite image depicting the titanium implant (white) and the new bone (gray) was used for histomorphometry. As shown in Figure 3, the bone-to-implant contact (BIC) was determined in the region of interest (ROI), defined by the upper part of the implant with a rectangle of 2 mm in height corresponding to the average thickness of the cortical bone. The BIC was calculated by using image analysis software (Image J) by dividing the length of mineralized bone in direct contact with the implant surface and the perimeter of the implant in the ROI, and was expressed as a percentage. Bone growth was determined at a distance of 0.5 mm around the implant. Bone surface (BS) was divided by the total surface (TS) of the ROI and BS/TS 0.5 mm was expressed as a percentage. All the measurements were repeated at least three-times.

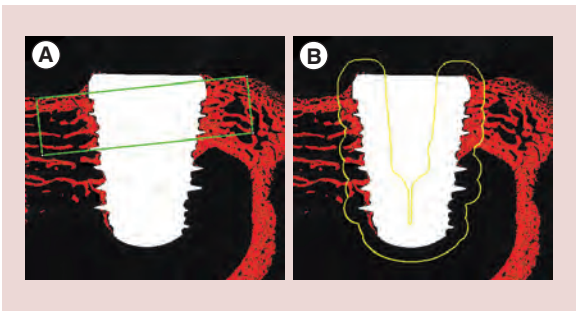

Figure 3. Method of calculation used in image analysis. **(A)** The percentage of bone-to-implant contact was calculated by measuring the length of bone (red) in direct contact with the implant (white), in the region of interest defined by 2 mm of cortical bone (green box). **(B)** Peri-implant bone healing was determined by dividing the bone surface by the total surface, defined at a distance of 0.5 mm from the implant (yellow contour).

Statistical analysis

Both physical and chemical characterization of each surface group were carried out at least in triplicate (n = 3/group). These data were expressed with mean and standard deviation values. Eight samples per group (n = 8/group) were implanted following a permutation implantation scheme in the two femoral epiphyses of 24 rabbits in order to prevent any lateral bias. As the number of samples was limited for ethical reasons, we assumed that data did not comply with normal distribution. In this study, all data from the histomorphometry analysis were expressed as a median, with minimal and maximal values or quartiles. Prior to any statistical analysis, critical values were detected using the Dixon test with significance levels of 95%. The nonparametric Kruskal–Wallis one-way analysis of variance test (ANOVA) was used for statistical analysis between groups. The effect of the surface treatment was statistically compared between two groups by using the Mann–Whitney nonparametric U test. The corresponding p-values were considered significant at less than 0.05. Statistical analysis and graphs were produced using commercial software (OriginPro 9.1).

Results

Nanostructuration of the dental implants was obtained by anodization in an electrolyte solution at a constant

Table 1. Roughness, porosity and crystalline composition of the three types of surface on dental implants.

Surface	Ra (µm; n = 3)					Porosity (n = 4)		Crystalline composition
	Ra	RMS	Rt	Ssk	Sku	Diameter (nm)	Circularity	
MICRO	2.09 (± 0.16)	2.63 (± 0.17)	14.72 (± 1.81)	-0.12 (± 0.12)	3.04 (± 0.39)	–	–	Amorphous titanium oxide
R-NANO	0.40 (± 0.02)	0.51 (± 0.03)	3.1 (± 0.37)	-0.25 (± 0.19)	3.16 (± 0.34)	56 (± 21)	0.58 (± 0.10)	Anatase/Rutile
S-NANO	0.05 (± 0.01)	0.07 (± 0,01)	0.61 (± 0.32)	0.63 (± 1.21)	3.15 (± 1.02)	51 (± 17)	0.59 (± 0.11)	Anatase/Rutile

Values are given as mean ± standard deviation.
Ra: Roughness; RMS: Root mean square; Rt: Maximum peak to valley height; Sku: Surface kurtosis; Ssk: Surface skewness.

voltage (Figure 1). During the anodization process, the natural titanium oxide layer was dissolved and regrown as columnar titania nanotubes. Machined, smooth as well as microroughened, grit-blasted dental implants can be nanostructured by anodization. The three types of surface on the different dental implants are shown in Figure 2. It should be noted that the dental implants differed in design by their cylindrical or conical shape, simple or complex threads as well as in their dimensions, with different diameters and lengths. The nanostructured implants were homogeneously colored by the anodization and annealing at 500°C. The S-NANO surface presented a shiny aspect, while the R-NANO had a mat surface, due to its initial microroughness. The surface roughness values and spacing parameters are shown in Table 1. Topography measurements indicated an average roughness (Ra) of 0.1, 0.4 and 2.0 µm for the S-NANO, the R-NANO and the MICRO control group, respectively. However, no significant differences were observed on the profile spacing parameters (i.e., surface kurtosis [Sku] and surface skewness [Ssk]) of the three types of surface. Interestingly, the nanostructuration of the titanium dental implants did not change the initial surface roughness at the micrometer level. Atomic force microscopy measurements of the roughness of the R-NANO surface prior and after anodization were 0.45 and 0.46 µm, respectively. FE-SEM images of the three types of surface at low and high magnification are shown in Figure 4. At low magnification, a typical random hilly topography with large cavities of several dozens of micrometers in diameter was observed on the microroughened implants (MICRO). Microroughness was also observed on the R-NANO but was less marked than the MICRO surface, while the S-NANO appeared relatively smooth. The observed microroughness of the MICRO and R-NANO resulted from alumina grit blasting. At high magnification, the MICRO surface exhibited random

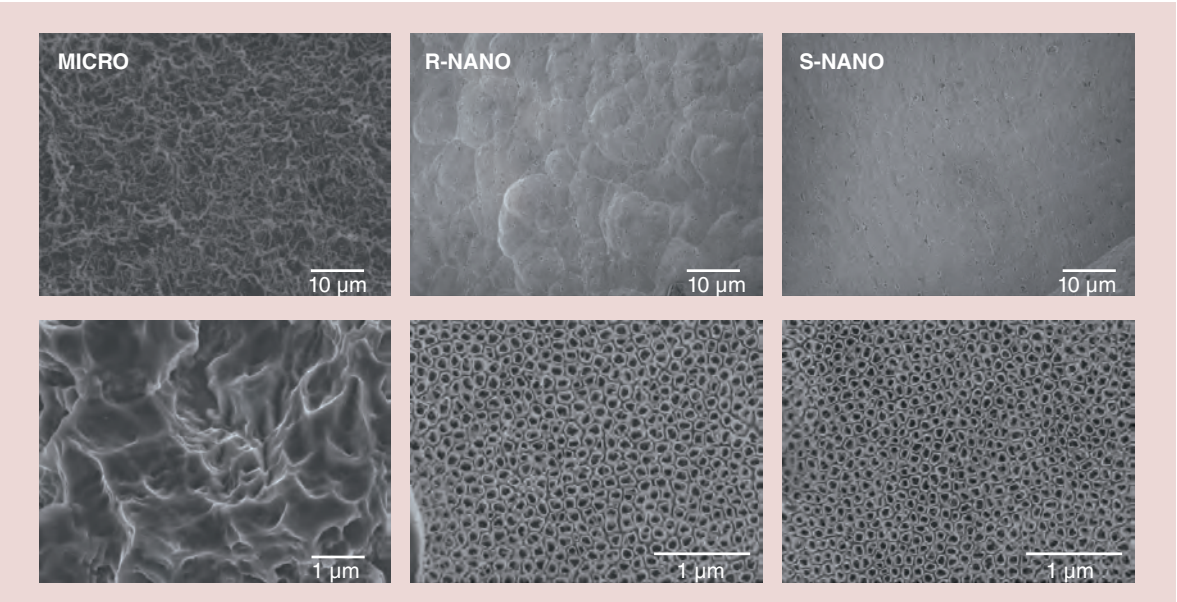

Figure 4. Field-emission scanning electron microscope images of the three types of titanium surface: alumina grit-blasted and acid-etched (MICRO), grit-blasted and nanostructured (R-NANO) and machined and nanostructured (S-NANO) surfaces (magnifications ×2000 and ×20,000 to ×50,000).

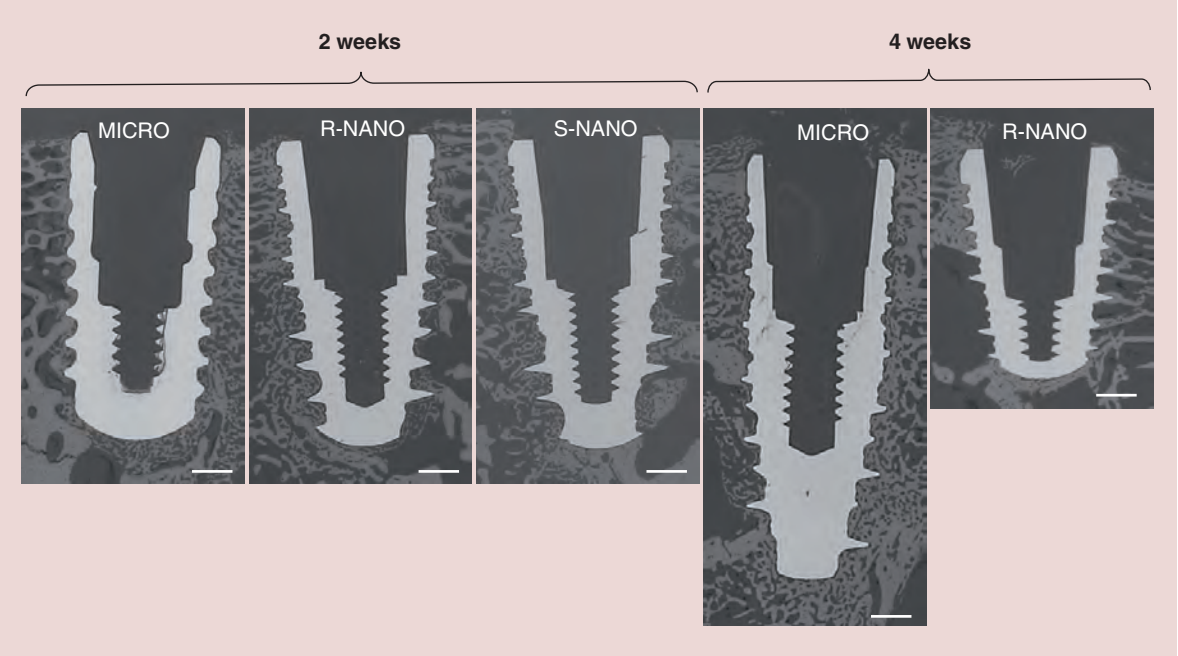

Figure 5. Back-scattered electron mode images of the three types of surface on dental implants inserted into the femoral epiphyses of rabbits for 2 and 4 weeks (magnifications ×50, scale bar: 1 mm).

microstructures resulting from the acid etching. Both S-NANO and R-NANO surfaces exhibited a regular array of nanotubes with a similar average inner diameter of 56 ± 21 and 51 ± 17 nm, and an average circularity of 0.58 ± 0.10 and 0.59 ± 0.11, respectively. Measurements of the cross-section of the oxide layer indicated a thickness of approximately 150 nm. The two nanostructured surfaces were composed in majority of titanium oxide, with about 1–3% of fluoride element: 2.1 ± 0.3 and 2.8 ± 0.9 atm.% for R-NANO and S-NANO, respectively. The anodization process caused the migration of fluoride ions from the solution to the oxide layer formed. Raman spectroscopy analysis indicated an amorphous titanium oxide for the MICRO surface. As a result of its thickening and annealing at 500°C, the titanium oxide crystallized into anatase and rutile on the R-NANO and S-NANO surfaces.

The bone tissue integration of the three types of surfaces on the dental implants was then compared in an experimental model in the femoral epiphyses of rabbits. All animals recovered well from surgery without complications and with normal load bearing. During the healing period of 2 and 4 weeks, neither clinical signs of inflammation nor infections were observed. The femoral epiphyses were x-rayed *post mortem* and none showed signs of osteolysis around the implants. BSEM images of the three groups of implants into the femoral epiphyses of rabbits after 2 and 4 weeks of healing are shown in Figure 5. After 2 weeks, newly formed bone with thin trabeculae was observed in direct contact with the dental implants. Bone appositions were even observed on the apical part of the implant, where less or no bone was initially present, indicating active healing in the peri-implant region. For the long dental implants, the apical portion was mainly housed in the trabecular part at 4 weeks. As the dental implants differed in size and shape, the BIC was only determined in the upper part of the implant corresponding to the thickness of the cortical bone (Figure 3). Bone healing was determined at a distance of 0.5 mm around the implant, as illustrated in Figure 3. The histomorphometric results are presented in Figures 6 & 7 for the delays of 2 and 4 weeks, respectively. After 2 weeks of implantation in the rabbit femurs, the BIC values were around 50% for the three surfaces. However, the BIC for the R-NANO surface was significantly lower than the value for the MICRO surface ($p = 0.04$). The quantity of bone surrounding the implants varied between 26 and 63% between groups and samples, but appeared higher for the MICRO than for the R-NANO and S-NANO surfaces. Nevertheless, significant differences in bone in the peri-implant region could not be evidenced between the groups at 2 weeks. As the S-NANO surface presented a significant lower BIC value at 2 weeks than the MICRO and R-NANO, this surface was excluded from the second implantation with a delay of 4 weeks. As shown in Figure 7, the BIC value in the cortical region for R-NANO was significantly higher than for the MICRO surface at 4 weeks ($p = 0.02$). Nevertheless, the quantity of bone in the peri-implant region appeared lower for R-NANO than for the MICRO surfaces. The histology sections presented in Figure 8 corroborated the BSEM images and

histomorphometry. The long MICRO implant was surrounded by cortical and trabecular bone, while the short R-NANO implant appeared integrated only into cortical bone. At high magnification, bone tissue was not always in direct contact with the MICRO surface in the cortical region. On the contrary, bone spans that went directly into the implant surface without fibrous tissue interposition were observed on the R-NANO at 4 weeks.

Discussion

In this study, the dental implants with smooth and rough nanostructured surfaces were prepared and characterized. The bone tissue integration of the nanostructured surfaces was then compared with those of a conventional microroughened surface obtained by grit blasting and acid etching. After 2 weeks of healing, the results showed that bone apposition was higher for this MICRO surface than for the R-NANO and S-NANO surfaces. However, a reverse trend was observed after 4 weeks of healing, where the bone in contact with the R-NANO was significantly higher than for the MICRO surface. These last few years, many studies, both *in vitro* and *in vivo*, have demonstrated the effect of surface properties on the biological response. To our knowledge, only a few studies have compared nanostructured surface treatments directly on dental implants with a well-documented and successful microroughened surface used in dental implantology.

The bone integration of a dental implant results from the addition of two phenomena: the primary stability brought by the mechanical anchorage of the implant in the bone and the secondary stability which is linked to biological bone apposition. The primary stability decreases with healing time whereas secondary bone apposition increases with time. Primary stability of a screwed implant depends on the thread geometry. A bioactivated surface accelerates bone apposition and compensates for the loss of primary stability, resulting in early achievement of total stability. Several studies have been shown that microroughened titanium surfaces such as grit-blasted, acid-etched or both, may integrate better with bone than smoother surfaces. In dental implantology, a surface treatment with large particle blasting and etching in strong acids makes it possible to create a microroughened surface with random cavities that is well documented and is considered as the reference surface for dental implants. For these reasons, this MICRO surface was used as a reference surface in this study.

Nanostructuration of the surface has been shown to influence MSC behavior by the phenomenon of mechanotransduction [9,12,16]. Anodization is a relatively simple process that can form a regular array of titanium dioxide nanotubes. This nanostructured surface when applied to titanium samples, has been widely studied at both physical and chemical and biological levels. In this study, the nanostructure was successfully made on commercial dental implants with initial smooth and rough surfaces. This NANO surface appeared in different colors, depending on the initial aspect of the surface (e.g., shiny-smooth or mat-rough), as well as the thickness of the oxide layer. This color coding could be useful for instruments and implant identification during surgery. Depending on anodization parameters such as voltage, time, temperature and composition of the electrolyte, the size of the nanotubes, as well as the thickness of the oxide layer, can be mastered. In our case, the differ-

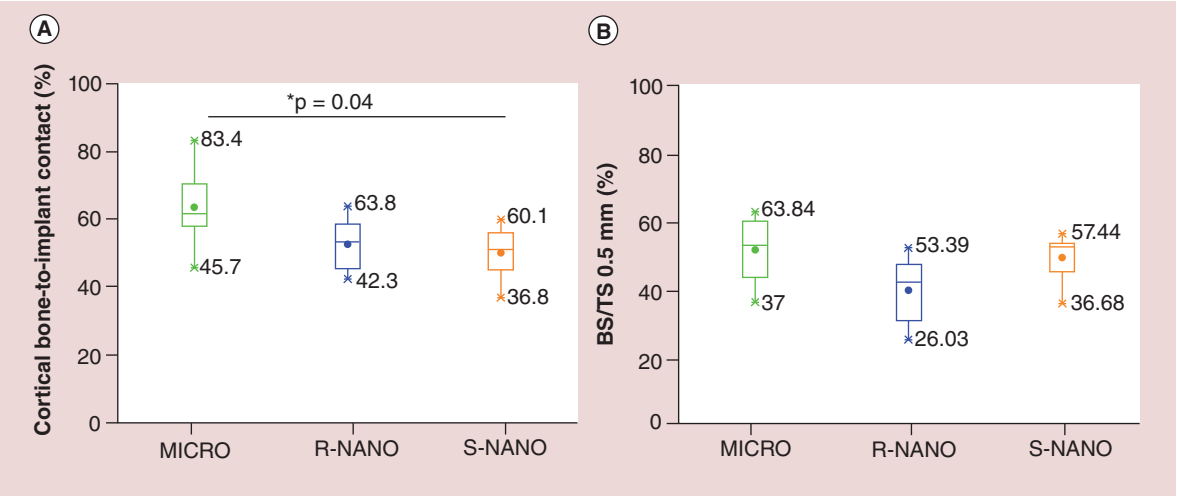

Figure 6. Bone tissue integration at 2 weeks. Whisker plots of bone-to-implant contact **(A)** and bone surface at 0.5 mm **(B)** around the implants for the three types of surfaces at 2 weeks after implantation in femoral epiphyses of rabbits (*if $p < 0.05$).
BS: Bone surface; TS: Total surface.

ent colors probably result from the length of the nanostructure in relation to the initial surface, as explained by Apolinário A *et al.* [17]. In case of anodization in an acidified solution (pH <5), the nano-oxide layer can have a thickness of more than 500 nm [18,19]. Nevertheless, the biological response with different lengths of nanotubes has not yet been studied. The postannealing treatment with various temperatures and times may also change the crystallinity of the oxide phase composed of amorphous, rutile or anatase, but its effect on cells and tissues was poorly investigated.

In previous works, we found that nanostructured surfaces of titanium with nanotubes from 20 to 50 nm in diameter enhanced osteoblastic differentiation of MSCs [20]. The bioactivity of the nanostructures was confirmed by early bone tissue apposition and higher anchorage compared with smooth titanium wires at both delays of implantation of 1 and 3 weeks in rat tibias [14]. More recently, we have shown that the nanoporosity of the titanium dioxide film may promote direct bone apposition in comparison to a machined smooth surface and increase bone formation in the growth chamber in a similar animal model. Another group confirmed that titanium dioxide nanotubes significantly increased new bone formation compared with grit-blasted dental implants (57.5 vs 65.5%; p-value of 0.008) after 6 weeks in rabbit femur. Two other studies conducted in large animals corroborated the bioactivity of nanotubes with significantly higher values for BIC than machined implants [21,22]. Nevertheless, none of these studies has compared nanostructured implants with the gold standard surface SLA as we have done here. Several studies have shown that an average surface roughness between of 0.5 and 2 µm is optimal for the bone integration of dental implants. In the present study, three different types of roughness, 0.1, 0.4 and 2.0 µm corresponding to the S-NANO, R-NANO and MICRO surfaces respectively, were compared. Interestingly, the nanostructuration did not modify the initial surface in the micrometer range. The beneficial effect given by microroughness to increase primary stability is therefore preserved after nanostructuration. Although microroughened surfaces are more difficult to decontaminate in case of infected implants, similar nanostructured surfaces have been shown to inhibit the growth of *Staphylococcus aureus* bacteria [23]. This antimicrobial property of the nanostructures could be particularly relevant for dental implants as there is periimplantitis in around 5–10% of cases after 5 years, and this figure seems to increase constantly.

This experimental study nevertheless has a certain number of limitations with regard to a strict comparison of the bone integration of nanostructured and microroughened surfaces on dental implants. The first limitation is related to the animal model that lacks repeatability in the implantation site. The bone environment in femoral condyles effectively varies from cortical to trabecular bone, including the osteochondral growth plate. These different environments may explain the lack of consistency between groups. Implantation in femoral diaphyses is also not representative of the septic environment of the mouth or the maxillary and mandibular bone structures that are normally encountered by dental implants. Nevertheless, this rabbit model has the advantage of being less costly than large animals such as dogs and pigs. Another drawback concerns the use of commercial dental implants of different designs, sizes, shapes and threads. As the bone defects were

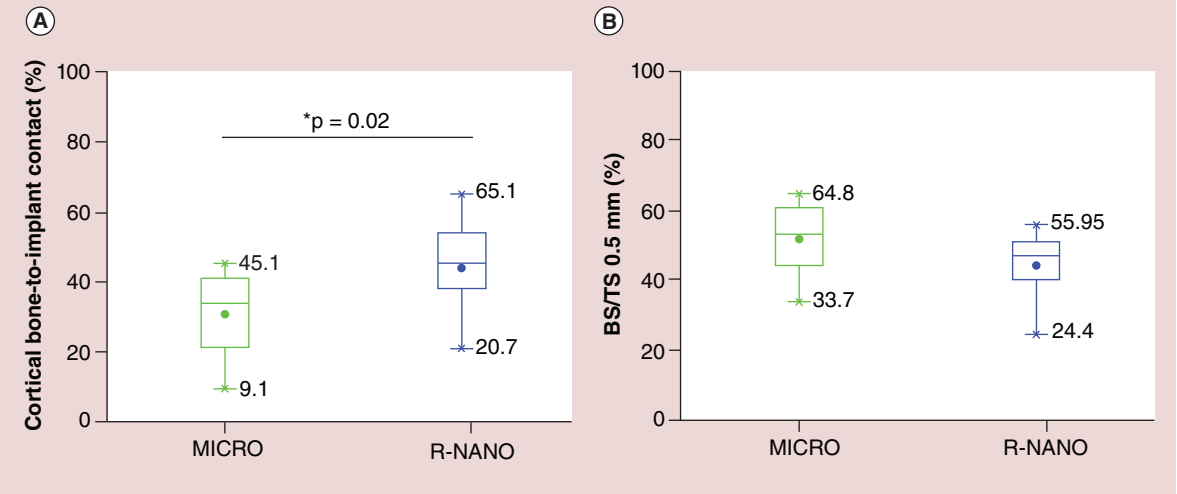

Figure 7. Bone tissue integration at 4 weeks. Whisker plots of bone-to-implant contact **(A)** and bone surface at 0.5 mm **(B)** around the implants for the three types of surfaces at 4 weeks after implantation in femoral epiphyses of rabbits (*if $p < 0.05$).
BS: Bone surface; TS: Total surface.

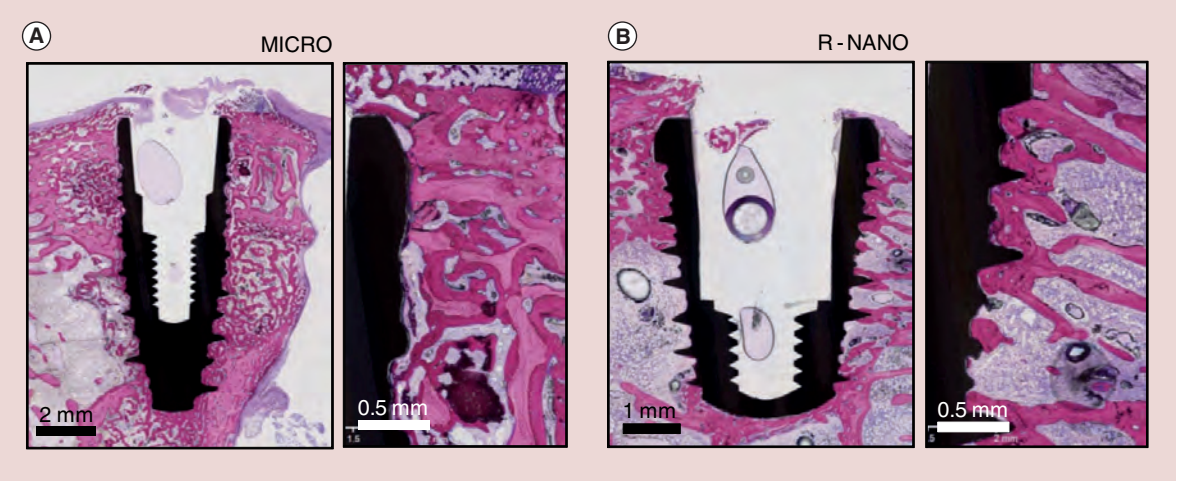

Figure 8. Nondecalcified histology sections of implant and bone tissue at 4 weeks after implantation in rabbits.
(A) Alumina grit-blasted and acid-etched (MICRO) and **(B)** alumina grit-blasted and nanostructured (R-NANO) surfaces. Basic fuchsine and methylene blue staining (original magnifications ×1 and ×10).

created using cylindrical drills, the apical part of the conical implants was not initially in contact with bone. The long dental implants that cross almost all of the femoral condyle may be stabilized in a way that differs from that of short implants. Nevertheless, these differences in implant design are inevitable when comparing commercial dental implants. In order to eliminate the variability between groups as much as possible, we standardized the histomorphometry method by measuring only BIC in the cortical region (Figure 3).

Conclusion

This study compares the bone–tissue integration of nanostructured surfaces with the conventional and well-documented microroughened surface of dental implants. After 2 weeks of healing, the MICRO surface gave the highest BIC value compared with R-NANO and S-NANO surfaces, in good correlation with their respective microroughness. The highest surface roughness of the MICRO resulted in better primary mechanical stability. After 4 weeks, more bone apposition was observed on the R-NANO than on the MICRO surface, indicating higher bioactivity for the former.

Future perspective

Several studies have demonstrated that nanostructured surfaces affect the shape of cells driving the lineage commitment of MSCs into osteoblasts. Implants with nanostructured surfaces may ultimately fasten and direct tissue integration. Manufacturers will provide implants with multi scaled surfaces from nanometre towards millimetre that would perfectly integrate into bone and gingiva at both biological and anatomical levels. Bacteria infections at the interface of medical devices are a growing problem especially in dentistry as the mouth is, by far, not a sterile environment. The infected area usually requires biofilm decontamination by surgery altering tissue integration of the implant. Nanostructured surfaces that would incorporate antimicrobial elements such as silver, zinc or copper, may prevent the contamination by bacteria as well as to facilitate tissue integration.

Acknowledgements

The authors are grateful to J Amiaud for his technical assistance in the nondecalcified histology of samples. N Stephant and Y Borjon-Piron from the electronic microscopy center at the IMN are acknowledged for their technical support.

Financial & competing interests disclosure

The company Biotech Dental provided the dental implants and certain surgical instruments, and supported this study financially. A Hoornaert and P Layrolle are founders of the spin-off company Biomedical Tissues that produced the nanostructuration on the dental implants. L Salou is a PhD student at the University of Nantes and is supported financially by the company Biomedical Tissues and the 'Association Nationale de la Recherche et de la Technologie' (ANRT). The authors have no other relevant affiliations or financial involvement with any organization or entity with a financial interest in or financial conflict with the subject matter or materials discussed in the manuscript apart from those disclosed.

No writing assistance was utilized in the production of this manuscript.

Ethical conduct of research

The authors state that they have obtained appropriate institutional review board approval or have followed the principles outlined in the Declaration of Helsinki for all human or animal experimental investigations. In addition, for investigations involving human subjects, informed consent has been obtained from the participants involved.

Executive summary

Background

- Dental implants have microroughened surfaces.
- Proteins and cells preferably interact with surfaces in the nanometer range.
- Nanostructured surfaces can control stem cell fate and possibly bone tissue integration.

Results & discussion

- Nano structuration applies to complex-shaped dental implants with smooth or rough initial surfaces.
- A regular array of titanium oxide nanotubes was uniformly produced by anodization on commercial dental implants.
- After an early implantation time, bone–tissue integration was higher for MICRO than NANO surfaces in agreement with their roughness.
- After 4 weeks of healing, the NANO surface shows significantly higher value than MICRO surface.

Conclusion

- Nanotubes can be applied to different dental implants by means of a simple anodization process.
- The NANO surface induced more of a secondary biological fixation to bone than a primary mechanical stability as was the case with the MICRO surface.
- Future studies should be conducted to optimize a combination of microstructure, nanostructure, composition and crystallinity provided by the anodized surface for better bone–tissue integration in both the short and long term.
- The antibacterial effect of nanotubes may be an advantage in the prevention of peri-implantitis and for ensuring the long-term success of dental implants.

References

Papers of special note have been highlighted as:
• of interest; •• of considerable interest

1 Le Guéhennec L, Soueidan A, Layrolle P, Amouriq Y. Surface treatments of titanium dental implants for rapid osseointegration. *Dent. Mater.* 23(7), 844–854 (2007).

• **Highly cited review of surface treatments for dental implants.**

2 Buser D, Broggini N, Wieland M *et al.* Enhanced bone apposition to a chemically modified SLA titanium surface. *J. Dent. Res.* 83(7), 529–533 (2004).

3 Schwarz F, Herten M, Sager M, Wieland M, Dard M, Becker J. Bone regeneration in dehiscence-type defects at chemically modified (SLActive) and conventional SLA titanium implants: a pilot study in dogs. *J. Clin. Periodontol.* 34(1), 78–86 (2007).

4 Lavenus S, Ricquier J-C, Louarn G, Layrolle P. Cell interaction with nanopatterned surface of implants. *Nanomedicine* 5(6), 937–947 (2010).

• **Review that describes the behavior of cells on nanostructured surfaces.**

5 Suzuki K, Aoki K, Ohya K. Effects of surface roughness of titanium implants on bone remodeling activity of femur in rabbits. *Bone* 21(6), 507–514 (1997).

6 Renvert S, Polyzois I, Claffey N. How do implant surface characteristics influence peri-implant disease? *J. Clin. Periodontol.* 38, 214–222 (2011).

7 Subramani K, Wismeijer D. Decontamination of titanium implant surface and re-osseointegration to treat peri-implantitis: a literature review. *Int. J. Oral Maxillofac. Implants* 27(5), 1043–1054 (2012).

8 Cai K, Bossert J, Jandt KD. Does the nanometre scale topography of titanium influence protein adsorption and cell proliferation? *Colloids Surf. B Biointerfaces* 49(2), 136–144 (2006).

9 Bacakova L, Filova E, Parizek M, Ruml T, Svorcik V. Modulation of cell adhesion, proliferation and differentiation on materials designed for body implants. *Biotechnol. Adv.* 29(6), 739–767 (2011).

• **Describes mechanotransduction.**

10 McBeath R, Pirone DM, Nelson CM, Bhadriraju K, Chen CS. Cell shape, cytoskeletal tension, and RhoA regulate stem cell lineage commitment. *Dev. Cell* 6(4), 483–495 (2004).

11 Dalby MJ, Gadegaard N, Tare R *et al.* The control of human mesenchymal cell differentiation using nanoscale symmetry and disorder. *Nat. Mater.* 6(12), 997–1003 (2007).

12 Park J, Bauer S, von der Mark K, Schmuki P. Nanosize and vitality: TiO_2 nanotube diameter directs cell fate. *Nano Lett.* 7(6), 1686–1691 (2007).

13 Oh S, Brammer KS, Li YSJ *et al.* Stem cell fate dictated solely by altered nanotube dimension. *Proc. Natl Acad. Sci. USA* 106(7), 2130–2135 (2009)

•• **First paper that demonstrated that nanotubes controlled differentiation of stem cells.**

14 Lavenus S, Trichet V, Le Chevalier S, Hoornaert A, Louarn G, Layrolle P. Cell differentiation and osseointegration influenced by nanoscale anodized titanium surfaces. *Nanomedicine* 7(7), 967–980 (2012).

•• **Study that correlated *in vitro* and *in vivo* results with nanostructures.**

15 Mor GK, Varghese OK, Paulose M, Shankar K, Grimes CA. A review on highly ordered, vertically oriented TiO_2 nanotube arrays: fabrication, material properties, and solar energy applications. *Sol. Energy Mater. Sol. Cells* 90(14), 2011–2075 (2006).

•• **Complete and synthetic review on nanotubes array on titanium.**

16 Dalby MJ. Topographically induced direct cell mechano-transduction. *Med. Eng. Phys.* 27(9), 730–742 (2005).

• **Complete study on mechanotransduction.**

17 Apolinário A, Sousa CT, Ventura J *et al.* The role of the Ti surface roughness in the self-ordering of TiO_2 nanotubes: a detailed study of the growth mechanism. *J. Mater. Chem. A* 2(24), 9067–9078 (2014).

18 Sreekantan S, Saharudin KA, Lockman Z, Tzu TW. Fast-rate formation of TiO_2 nanotube arrays in an organic bath and their applications in photocatalysis. *Nanotechnology* 21(36), 365603 (2010).

19 Mor GK, Varghese OK, Paulose M, Mukherjee N, Grimes CA. Fabrication of tapered, conical-shaped titania nanotubes. *J. Mater. Res.* 18(11), 2588–2593 (2003).

20 Lavenus S, Berreur M, Trichet V, Pilet P, Louarn G, Layrolle P. Adhesion and osteogenic differentiation of human mesenchymal stem cells on titanium nanopores. *Eur. Cell. Mater.* 22, 84–96; discussion 96 (2011).

21 Von Wilmowsky C, Bauer S, Roedl S, Neukam FW, Schmuki P, Schlegel KA. The diameter of anodic TiO_2 nanotubes affects bone formation and correlates with the bone morphogenetic protein-2 expression *in vivo*. *Clin. Oral Implants Res.* 23(3), 359–366 (2012).

22 Wang N, Li H, Lü W *et al.* Effects of TiO_2 nanotubes with different diameters on gene expression and osseointegration of implants in minipigs. *Biomaterials* 32(29), 6900–6911 (2011).

23 Ercan B, Taylor E, Alpaslan E, Webster TJ. Diameter of titanium nanotubes influences anti-bacterial efficacy. *Nanotechnology* 22(29), 295102 (2011).

•• **Complete study of bacteria on nanotubular array.**

4.1.2.b Additional discussion

In this study, we demonstrated a nanostructured implant surfaces capacity for bone integration in comparison with the conventional and well-documented micro-roughened surface of dental implants named SLA (Sand blasted, Large grit and Acid-etched, Straumann, Basel, Switzerland). This surface has a random and micrometric roughness that may increase primary bone anchorage. Nanostructured surfaces have been shown to enhance cell attachment and lead to MSC differentiation into osteoblasts by the phenomenon of mechanotransduction [19, 20, 21, 22, 81]. The results obtained in this study confirm this trend. A similar bone-to-implant contact was observed for the rough nanostructured surface (R-NANO) and for the micro-roughened (MICRO) surfaces on dental implants after 2 and 4 weeks of healing in a rabbit model. Direct bone apposition was observed, making it possible to act as a possible barrier against bacterial infiltration.

As discussed, the study has a certain number of limitations mainly related to the animal model. Our experiment was carried out by design of bilateral insertion of implants into the femoral epiphyses of rabbits. This animal model was selected because of its fast skeletal change and bone turnover which leads to rapid bone healing. However, it was difficult to extrapolate the results provided by the rabbit study on to the likely human clinical response. The bone structure of rabbits is different to human bone. Nevertheless, rabbits are commonly used and international standards have established that this species is suitable for testing the implantation of materials in bone, as are dogs, sheep, goats and pigs. The advantages of rabbits are that they are the largest animals in the small animal category and thus only require the approval of a local ethics committee for animal experiment. They are also the least phylogenetically developed animals available in sufficient quantity and easy to experiment prior to testing in a larger animal model [114].

The implantation site is located in the femoral epiphysis and implants were inserted perpendicularly to the length of the bone in the cartilage growth plate. In this position, bone is composed of both cortical and cancellous bone which prevents the cortical bone from splintering with implant insertion which could be observed in other areas [114]. This model was also used in other studies [115, 101, 116]. However, in our work, this model gives us a lack of repeatability in the implantation site due to insertion performed too close to the metaphysis and containing less cancellous bone. Many other studies inserted the implant into rabbit tibia. However, the bone is thinner in rabbit tibia and implants inserted would have to be small. There is also a risk of bone splintering with implant insertion [44, 117, 118, 119]. Sennerby *et al.* explained the use of the epiphysis of the femur in the knee-joint as a site resembling the more cancellous bone in

the maxilla, with the tibial methaphyses as sites resembling the more compact bone in the mandibula [120]. For us, the ideal location for implantation would be the intercondylar fossa between the distal tibia condyle (**Figure 4.4**). This location might be an alternative place for avoiding problems of repeatability of the implant position with a similar cortical and cancellous bone environment.

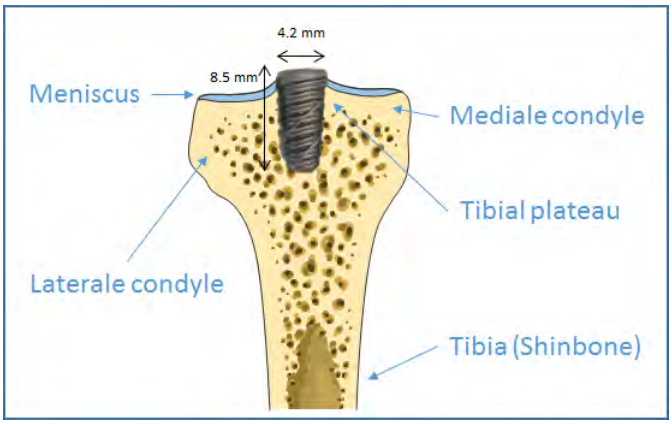

Figure 4.4: Scheme of implantation into the tibial plateau

In addition to the implantation site, another drawback concerns the use of commercial dental implants of different design, sizes, shapes and threads. The differences in implant design are inevitable when comparing commercial dental implants. Regarding implant size, the standard recommended implant size is of about 2 mm in diameter and 6 mm in length. A 6 mm diameter and 8 mm long implant could be used at the proximal side and thus the distal femoral condyle approach. The size of the implants that we used in our study was slightly higher with 3.6 to 4.6 mm in diameter and 6 to 11 mm in length. However other studies recently published used the large size in the femoral shaft [102].

To finish with the animal model, the implantation site does not provide representative implant healing regarding the septic environment of some implant types. The implant model of concern is an under the skin implant without contact with outside aggressions. However, in the oral cavity, different biological factors that are normally present (*e.g.* microbiota from the remaining teeth) may significantly influence osseointegration speed [121, 122]. As well as dental implantology, orthopaedic implants such as percutaneous prosthetic systems are subject to external aggression. For instance, superficial infections were the most common complication that occurred [8, 9].

A similar work was recently published in 2015 by Jea-Kwan Lee *et coll.* [44]. They studied osseointegration in rabbit tibia using dental implants with four different surfaces, including a machined surface, two other surfaces cor-

responding to the MICRO and R-NANO surfaces in our study, and the last corresponded to TiO_2 a nanotube array incorporating a BMP-2 growth factor.

As in our work, the study only focused on surface characterisation by SEM and histological analysis of the tissue surrounding the implant. The nano-surface was created in a third generation electrolyte containing ethylene glycol at 0.5 wt % NH_4F. This solution was chosen by the authors to produce thicker TiO2 nanotubes on the surface of the titanium for slower release of the BMP-2 growth factor. The nanostructures were obtained after two-step anodisation. The first nanostructure formed was removed by sonication and the final TiO_2 nanostructures were then manufactured by a second anodic oxidation at 60V for 60 minutes. It was demonstrated that two-step anodisation could be achieved to open-ended TiO_2 nanotube leading to new properties [123]. This two-step process also makes it possible to increase certain nanotube properties, such as photocatalytic properties. However, this technique required chemical etchants that dissolve only oxide NTs without dissolving the underlying substrate.

The nanostructures formed by the author are called "TiO_2 nanotubes"while their aspect corresponds to our nanoporous structure with the same size of nanoporosity of the nanotubes with 60-70 nm in average diameter [44]. As TiO_2 has nanosized holes, it is suggested that it could be of interest for drug loading and delivery. In their study, they incorporated BMP-2 growth factor using a dip-coating technique in a concentrated solution of 1.5 mg/mL. High concentrations of BMP-2 were used for the loading solution due to the effect of dilution by the blood surrounding the implant surface. However, the physiological efficiency dose of growth factor has been evaluated at about 100 ng/mL [124].

As compared to our work, Lee's study was carried out using only 3 rabbits and each received the four different types of implant [44]. The implantation site was located perpendicularly into the proximal tibia. After 8 weeks of healing, the percentages of bone contact and volume ratio were measured along and within the area of two threads. Higher mean bone-to-implant contact and bone volume ratios were obtained for both the nano-surfaces as compared to the machined and SLA surfaces. Growth factor loading in the nanotubes increased the biocompatibility of only the nanostructured surface. However, a weak point in this study was the small number of samples which precluded a statistical analysis. Descriptive statistics using non-parametric data would have been preferable using median and ranks.

As shown by Jea-Kwan Lee *et coll.*, an emerging alternative consisted in optimising the bioactivity of titania nanotubular surfaces through substance incorporation (dip-coating, functionalisation). Growth factors are secreted by osteoprogenitor cells and osteoblasts to induce osteoblastic differentiation dur-

ing osteogenesis [125]. The bone regeneration effect has already been reported using local delivery of growth factors such as bone morphogenetic proteins (BMPs). For instance, osteogenic growth factors such as BMP-2 (rhBMP-2) and BMP-7 (or osteogenic protein-1, rhOP-1) have been evaluated to improve osteoinductivity in numerous studies [126, 127, 128]. Its incorporation into nanostructures has been shown to stimulate osteoblast cells [44] while fibroblast adhesion and proliferation are promoted using fibroblast growth factor (FGFb) or connective tissue growth factor (CCN2) in case of regeneration of the periodontal ligament [129, 130].

As vascularisation plays a role in tissue regeneration, growth factor for angiogenesis could also be a means of improvement that has not yet been explored. It is regulated through a complex set of mediators and recent evidence shows that integrin $\alpha v\beta 3$ and vascular endothelial growth factors (VEGFs) play important regulator roles [131, 132]. By incorporating these substances into the titanium surface, we can suppose that substantial neo-vascularisation will be induced around the implant and thus faster and higher osseointegration [133]. Titania nanotubes could also be used as a reservoir for drug delivery such as inflammatory drugs [134]. Ibuprofen has been explored and revealed promising results [135, 136].

Although incorporating substances such as BMP-2 growth factor by dip-coating or functionalisation makes it possible to enhance the surface, these proteins are only one part of the cytokines found *in vivo*. Research was then carried out to see if it were possible to attach only the active part of the protein and link it to the surface. Peptidic or other molecules have been grafted by several authors [137, 138, 139].

To conclude, this study made it possible to demonstrate similar or higher bone integration of the nanostructured surfaces compared to the SLA surface after 2 and 4 weeks of healing in a rabbit model. Although this model can be discussed, a similar study was published at the same time. The trend of their results confirm our observation. Optimisation of this nano-surface was evoked by loading the growth factor. Although the compatibility of the surface is shown *in vivo* in rabbits, it seems necessary to observe these results in a more representative model in terms of environment of application (*e.g.* the oral cavity) as well as from a regulatory point of view.

4.1.3 Process validation for the surface treatment

This section presents the process validation of our new surface treatment n'TiOs for its industrial application on dental and orthopaedic implants. New surface treatments must comply with the ISO 13485 standard for commercial use in patients. The results of this process validation were audited by a certified

organisation, G-MED, in September 2013. The surface treatment consists of a 3-step process (cleaning, anodising and annealing) to form a honeycomb titania surface. The purpose of this surface treatment validation was to define the experimental conditions needed to obtain:

- Over 95% homogeneity of the nanostructure on the surface;
- Colour uniformity of the implant over 100%;
- The respect of the manufacturers dimensional tolerances;

Input datas – Firstly, the critical parameters were identified using previous results from R & D studies, patents (Astra Tech) [24], Nanovis [25]) and the literature on anodising treatments for bone implants [85, 104, 40]. The validation conditions were expanded as much as possible in order to adjust the service provided to the diversity of customer specifications, or the initial surfaces of the implants (roughness, composition). Each parameter was listed and its influence on the nano-surface of the implant was evaluated in an influence matrix (**Table 4.1**).

Risk analysis uses the FMECA (Failure Modes, Effects and Criticality Analysis) method to identify potential process failures before they occur. The ultimate intention is to eliminate or minimise the associated risks in the critical parameters of the process. The criticality index for each process parameter is analysed qualitatively and quantitatively in **Table 4.2**.

Process validation – The validation protocol was established on the basis of the input data. The protocol applies to the 3 steps in the process: the cleaning step prior to and after anodisation, the electrochemical process, and the annealing. The materials used for the validation process are detailed in **Figure 4.5**. Equipments (magnetic stirrer, current / voltage generator, oven) used were metrologically followed. All the documentation for the protocol and recording required for internal quality management systems were prepared in accordance with standard ISO 13485.

The validation process was designed in two parts. First the procedure was performed 3 times over 3 consecutive days following a standard protocol

Table 4.1: Influence matrix of variables and answers for the anodisation process

Characteristic of the implant						
Answers / Variables	Surface color	Formation of NS	Size of NS	Homogeneity of NS	Implant Dimensions	Trace of acids
Pre-cleaning	++	++	0	++	0	0
Electrolyte	0	+++	+++	0	+++	+++
Voltage	0	+++	+++	+++	0	0
Anodizing time	0	+++	0	0	+++	+++
Stirring	+++	++	0	+++	0	0
Annealing Temp.	0	+++	0	+++	0	+++
Annealing time	0	+++	0	+++	0	+++

NS = Nanostructure ; +++ = high ; ++ = moderate ; + = low ; 0 = null ; NA = non applicable

Table 4.2: Risk analysis: evaluation of the parameters of the surface treatment process of implants

Failure Mode and Effects Analysis (FMEA)						
Parameter	Influence	S	O	D	RPN	Criticality
Time of cleaning	Nanostructure (NANO) and color homogeneity	2	1	1	2	**NC**
Volume of cleaning	NANO and color homogeneity	2	1	1	2	**NC**
Electrolyte compostion	NANO formation (Fixed)	1	1	2	2	**NC**
Anodizing voltage	NANO formation	3	2	3	18	**C**
Anodizing time	Diminish the implant dimensions at high conditions	3	2	2	12	**C**
Anodizing stirring	Modify NANO and Surface colour	2	1	1	2	**NC**
Annealing temperature	Destruction of the NANO at high conditions	3	2	3	18	**C**
Annealing time	Destruction of the NANO at high conditions	3	2	3	18	**C**

S = severity of impact of the failure event

O = Frequency of occurrence of the failure event

D = Ability of the process control to detect the occurrence of failure events

Risk level: 3 = high ; 2 = moderate ; 1 = low

RPN: Risk priority number= $S \times O \times D$

Criticality index: if $RPN \geq 7 = critical(C)$; if $RPN < 7 = non - critical(NC)$

Implant	Dental implant
Number	n = 50
Dimension	L = 10.5; ϕ = 5
Manufacturer	Anthogyr
Batch	D4-110621-A2
Material	C. Pure titanium
Surface state	Machined

Figure 4.5: Characteristics of the implant used in the validation process

(RUNS). This first test made it possible to determine the reproducibility of the surface treatment. Two other tests were performed under extreme conditions (high and low), also called worst case (WC), to determine the range of use of the various process parameters. All the conditions in the 3 RUNS and the 2 WC (high and low) are displayed in **Table 4.3**.

	Standard conditions (runs)	Low worst case (WC N° 1)	High worst case (WC N° 2)
Anodising voltage (V)	15	5	22
Anodising time (min)	15	5	22
Temperature (° C)	500	475	525
Annealing time (min)	90	45	135

Table 4.3: Anodizing conditions used in the process validation

Several characterisations were performed during and after the entire process. A flow chart of the validation is presented in **Figure 4.6**. All data were recorded and used for statistical process analysis using descriptive statistics (mean, standard deviation, coefficient of variation, standard deviation of the mean, coefficient of variation of the mean) and the usual tests: Cochran, Student and Fisher with a risk of 5%.

Statistical evaluation − The results obtained in this process validation are not all displayed in the manuscript of this thesis. We have chosen to present an overview of the approach conducted to analyse the repeatability, reproducibility and fidelity of the nanostructure (homogeneity and size) and dimensional tolerances at the end of the process.

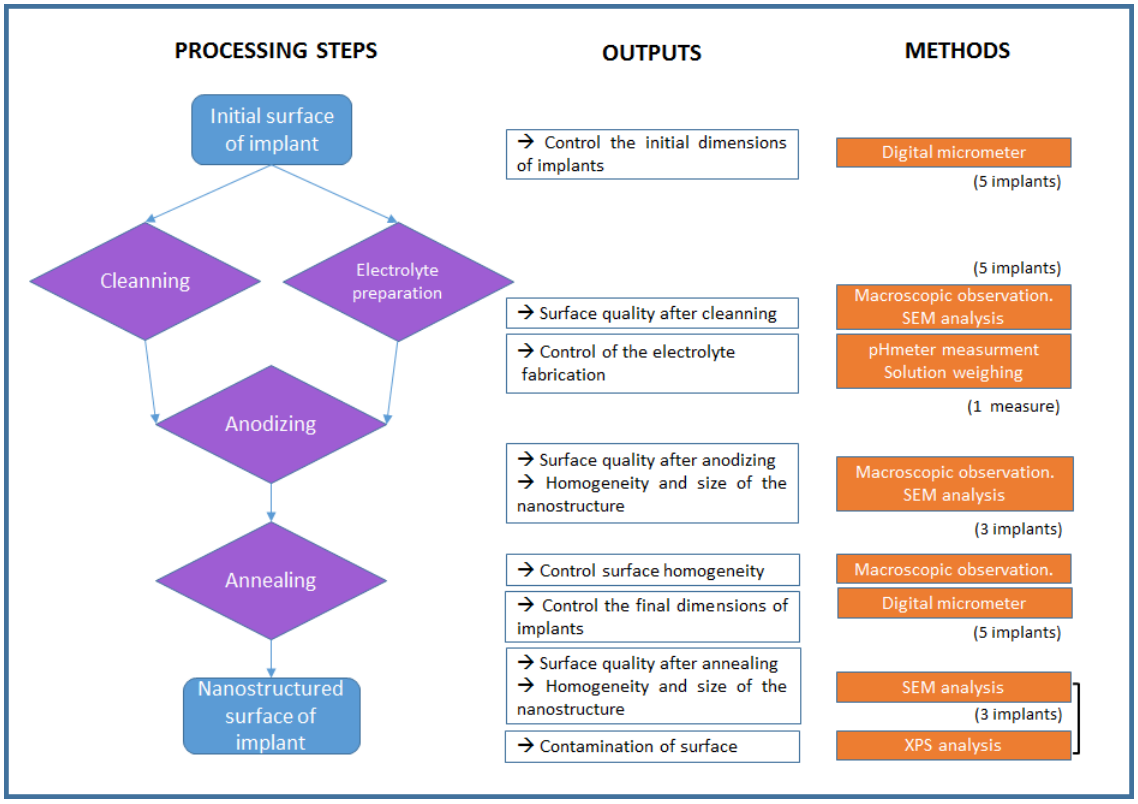

Figure 4.6: Flow chart of the validation process

- **Dimensional variations of the implant** – Five implants were randomly selected at the end of the process. The dimensional variations were measured using a digital micrometer using two dimensions: the diameter of the implant and its length. The different values obtained at the end of the treatment compared to the initial size prior to the treatment are displayed in **Table 4.4**. The upper and lower control limits which indicate the threshold at which the process output is considered statistically incorrect and possibly revelatory of a default in the process, are typically calculated at 3 standard errors from the mean. The control chart of the variations in diameter and the length of the implant are presented in **Figures 4.7(a)** and 4.7(b). The dispersions of the results for nanostructure size were calculated for a probability of 95 % at 3.7 μm and 15.9 μm for the diameter of the implant and its length respectively. Therefore, the dimensions of the implants mostly decreased after processing but the variations remained lower than the tolerance for the dimensions of the implants of 50 μm.

Table 4.4: Statistical analysis of the dimensions of the implants

Runs / Measures	1		2		3	
	$\Delta L(\mu m)$	$\Delta\phi(\mu m)$	$\Delta L(\mu m)$	$\Delta\phi(\mu m)$	$\Delta L(\mu m)$	$\Delta\phi(\mu m)$
1	4.00	-19.00	5.00	-21.00	-1.00	-9.00
2	7.00	-20.00	6.00	-21.00	-2.00	-18.00
3	5.00	-10.00	1.00	-17.00	4.00	-6.00
4	0.00	-17.00	2.00	-17.00	7.00	-11.00
5	2.00	-17.00	6.00	-20.00	4.00	-15.00
Mean	3.60	-16.60	4.00	-19.20	3.60	-11.80
SD (σ)	2.70	3.91	2.35	2.05	2.30	4.76
3 σ	8.11	11.73	7.04	6.15	6.91	14.29
High limit	11.71	-4.87	11.04	-13.05	10.51	2.49
Low limit	-4.51	-28.33	-3.04	-25.35	-3.31	26.10

- **Analysis of the size of the nanostructure** − The diameter of the nanotubes was measured on the SEM images at a magnification of 50,000 to 100,000 and imageJ software for the 3 RUNS. The results are given in **Table 4.5**. The statistical analysis was carried out using a Student's T-test (**Equation** (4.1)).

$$\bar{X} \pm t_\alpha \frac{\sigma(X)}{\sqrt{n}} \tag{4.1}$$

With t_α corresponding to the coefficient from the degree of confidence α

The dispersion of the results for nanostructure size was calculated for probability of 95 %. The confidence interval for the average of 56.25 nm on 6 measures is estimated at 1.57.

- **Controlling nanostructure homogeneity** −. The uniformity of the nanosurface was analysed at 2 locations on the same dental implants as the one used to determine the size of the nanostructure. These analyses were done at a lower magnification of 20,000 and imageJ analysis. The results are given in **Table 4.6**.

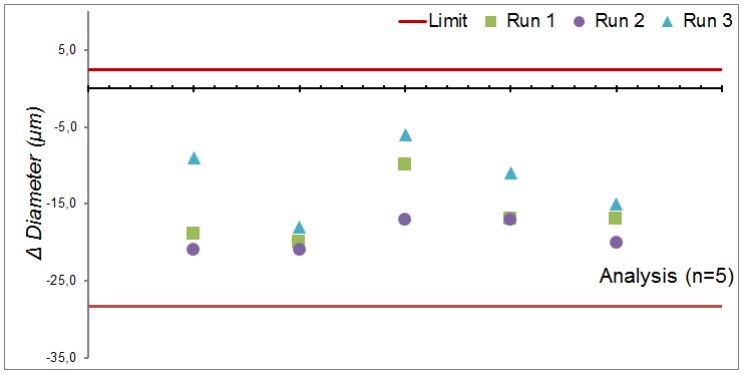

(a)

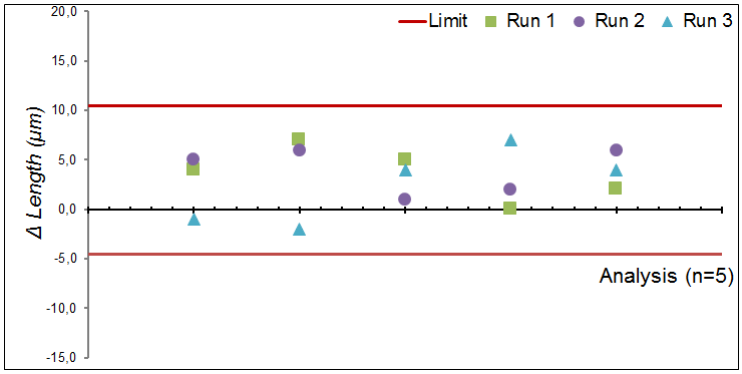

(b)

Figure 4.7: Control chart of the variations in diameter (a) and length(b)

The Cochran test was used to reveal aberrant results. The maximal variance obtained for the 3 Runs was 0.083. Thus the $T_{calculated}$ value of 0.5596 was lower than the $T_{threshold}$ value of 0.6161 for probability at 95%. Therefore the Cochran test was not significant and the data were considered homogeneous at a risk of 5 %.

Welch's t-test is an adaptation of Student's t-test and is used to test the hypothesis that two populations have equal means. It was calculated by comparing groups two by two using calculation of the difference. **Table 4.7** shows the results of the comparison of the 3 runs for the 3 pairs of

Table 4.5: Statistical analysis of the diameter of the nanotubes

Measures \ Runs	1 ϕ(nm)	2 ϕ(nm)	3 ϕ(nm)
1	54.97	50.21	54.75
2	55.75	51.35	53.08
3	48.65	47.42	51.49
4	55.64	51.91	52.86
5	52.98	50.57	53.18
6	46.40	55.44	56.31
Mean (nm)	52.40	51.15	53.61
SD (nm)	3.97	2.61	1.68
CV (%)	7.57	5.11	3.13
General Mean (nm)	52.39		
General SD (nm)	2.92		
General CV(%)	**5.58**		
General SD of the mean S_m (nm)	0.69		
General CV of the mean CV_m(%)	1.31		

groups (ddl = 10), $T_{calculated} < T_{threshold}$ at risk of 5 %. Therefore, the values obtained belong to the same population.

Repeatability and reproducibility:

$$S_r = \sqrt{\frac{\sum^p (\sigma)^2}{p}} \tag{4.2}$$

$$S_R = \sqrt{\frac{1}{p-1}\sum^p (X - \bar{X})^2 + \frac{n-1}{n}(S_r)^2} \tag{4.3}$$

The value of repeatability (s_r) was calculated at 0.21 (**Equation** (4.2)) and thus by the statistical evaluation of the inter-series data from the 3 runs. The value of reproducibility (S_r) was calculated at 0.20 (**Equation** (4.3)). The fidelity value is calculated by adding the value of reproducibility and the value of repeatability and thus was estimated at F=S_R+S_r=0.43. The process was found to be faithful.

Table 4.6: Statistical analysis of surface homogeneity

Runs / Measures	1 **Surface(%)**	2 **Surface(%)**	3 **Surface(%)**
1	100	99.9	99.3
2	100	99.9	99.9
3	100	99.7	99.8
4	99.4	99.8	99.5
5	99.9	99.9	100
6	99.9	100	100
Mean	99.87	99.87	99.75
SD	0.24	0.10	0.29
Variance	**0.055**	**0.011**	**0.083**
CV	0.23	0.10	0.29
General Mean (%)	99.83		
General SD (%)	0.22		
General CV(%)	**0.22**		
General SD of the mean S_m (%)	0.051		
General CV of the mean CV_m(%)	0.05		

Table 4.7: Statistical analysis of the reproductibility of the homogeneity of the nanotubes array

	Runs 1 & 2	Runs 2 & 3	Runs 1 & 3
Difference of the mean (d)	0	0.12	0.12
Standard deviation of d	0.104	0.125	0.151
$T_{calculated}$	0	0.93	0.77
$T_{threshold}$ (ddl=10)	2.23		

Other assays and conclusion − The rest of the results integrated into the worst case did not show any failing in the process. The analyses revealed a mean porosity of 29.3, 52.4 and 71.1 nm respectively for potential voltage of 5, 15 and 22 V. These results were predictable given the conclusion of chapter 3. Other characterisations were also carried out, such as controlling the electrolyte by weight and pH measurement, nanostructure morphology by calculating circularity and checking the absence of surface contaminants on the surface by XPS analysis.

All the results were stable and were shown to be in conformity with the stated objectives. The developed process has been mastered, is robust even in worst cases, and is reproducible. The validation process was conducted in September 2013 and successfully validated by G-MED, which gave the certification for the nanostructuring of single titanium implants for dental and orthopaedic applications.

4.2 Nanostructuration of tracheal prostheses for soft tissue integration

4.2.1 Context and generalities regarding tracheal prostheses

Laryngeal cancer develops in the larynx, or voice box. It mainly originates in the glottis (the area containing the vocal cords) but can also originate in an area above or below the glottis (supraglottis or subglottis). The risk factors for this cancer are mainly the consumption of tobacco or alcohol, but also include congenital reasons or environmental exposure [140]. The treatment for laryngeal cancer consists in removing the cancerous cells from the larynx by means of surgery, stopping the growth of cancer cells using chemotherapy and/or killing the cancer cells with radiation (radiotherapy). Depending on the severity of the cancer, some patients may require a partial or complete laryngectomy (removal of the larynx). The number of people with tracheal or more specifically laryngeal cancer each year is around a few thousand and every year around 1,800 patients require a total laryngectomy [140, 141].

Despite a satisfactory survival rate of 36 % to 57 % of people in at least the 10 years following diagnosis, depending on the kind of cancer [142], laryngectomy in patients implies the reduction of a certain ability to perform vital and/or everyday life tasks such as breathing, eating, or speaking. Patients who have undergone a total laryngectomy need a permanent tracheotomy to breathe and sometimes a gastrostomy tube to deliver nutrition directly to the stomach. Regarding speech, some patients may have vocal rehabilitation using different methods, such as oesophageal speech. However, this way of speaking cannot be achieved by all patients.

For these reasons, Protip has developed implantable artificial trachea called *ENTegral*® to partially replicate natural functions without enduring a tracheotomy tube. Patients could thus once again be able to breathe in a natural manner. The procedure consists in implanting the temporary closed prosthesis

during the laryngectomy procedure (**Figure 4.8(a)**). Then, after a few weeks of healing, the temporary cap is replaced by the removable part and the tracheotomy tube is removed (**Figure 4.8(b)**). This cap plays a protective role and has been specifically designed to allow normal breathing.

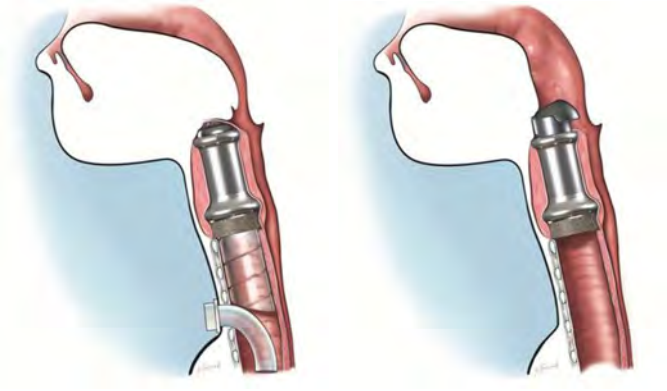

(a) (b)

Figure 4.8: Two-step surgical procedure for implantation of the *ENTegral*® : (a) First the tracheal prosthesis is implanted during the laryngectomy procedure. A temporary cap close the top of the prosthesis; (b) After a few weeks, the temporary cap is replaced by the removable part

Tracheal prosthesis devices are made of pure titanium and use the microbead technology patented by Protip [143]. Two sizes of implant are available, depending on the patient: a length of 50 mm and 65 mm respectively for small and normal prostheses with a maximum diameter of 29 mm. As presented in **Figure 4.13**, the medical device is composed of 3 parts: dense titanium and a sintered part combined with both dense and porous titanium. This structure is obtained from titanium beads of an average size of 500 μ formed by plasma arc technology. The beads are then connected to each other and to a compact titanium ring by electrofusion at a high pressure and temperature (up to 1000°C). The particularity of the sintered compact titanium is the observation of grain growth throughout the surface. Laser welding is used to link both the titanium compact part which forms the body of the prosthesis, and the sintered titanium. The porous titanium corresponds to the distal extremity and is designed to be sutured to the proximal trachea.

Although the product has obtained success in pre-clinical and the first clinical trials, titanium is an inert material and does not make possible adequate integration with the soft tissue. Thus, phenomena of fistulas or salivary flow

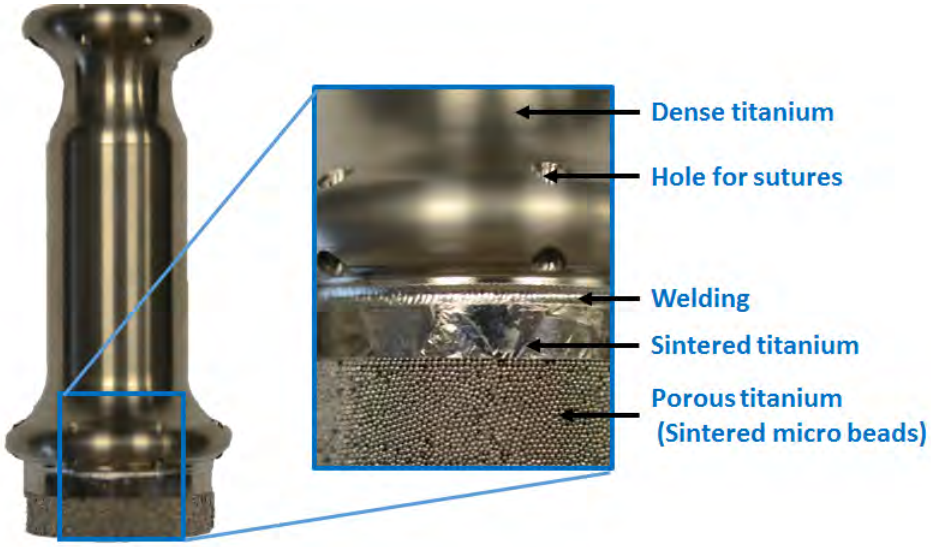

Figure 4.9: The tracheal prosthesis and its different surfaces

along the external surface of the prosthesis are observed due to poor soft tissue integration of the tracheal prosthesis [142].. In this context, the aim is to enhance the bioactivity of the surface by nanostructuration of the tracheal prosthesis.

4.2.2 Surface treatment of tracheal prothesis

Materials & Methods – The final design of the prothesis has widely changed since the beginning of the collaboration. It was at first wave-shaped mimicking the cartilage rings of the trachea as presented in **Figure 4.10(a)**. The first anodizing treatment tests were realised on template sample without the final design of the tracheal prothesis giving less expensive cost of production (**Figure 4.10(b)**). The particularity is that the tracheam template got same surface developped as the prothesis and thus, the current densities obtained during anodisation process were similar. Dimension of the template sample were about a diameter of 24 mm and a length of 58,0 mm (S=5400 mm^2) and 68,0 mm (S=6400 mm^2) respectively for the short and long template implant. Coupons composed with the 3 surface were treated simultaneously close to the prosthesis and used for quality control during the routine treatment of prosthesis (**Figure 4.10(c)**). Disk were also used and trated for surface analysis.

The manufacturers specifications did not require any specific nanostructure (nanopore or nanotubes). Nevertheless, the treatment should not reach the

(a) (b) (c) (d)

Figure 4.10: Picture of (a) the inital design of the tracheal prothesis , (b) the tracheal template, (c) the coupon and (d) the disk sample.

internal part of the implant in order to avoid tissue proliferation inside the tubular tracheal prosthesis. Thus, a prosthesis holder was designed to hide the interior part and bring current to the surface to the implant to treat (**Figures 27(a)** and **27(b)** in **appendix A page 185**). The manufacturer requested a uniform blue-green colour after processing the tracheal prosthesis.

Establishing the protocol was based on the conditions of the validation process of the surface treatment for dental implants. Differences were found in the volume of the solution used in the anodisation process which shift to a one litre bath due to the large size of the tracheal prosthesis.

Nanostructuration results– After several tests, the best holder and anodising conditions for homogeneity of colour and nanostructure were determined (**Figure 4.11**). The anodising treatment gives a homogeneous, shiny blue colour corresponding to the manufacturers specifications. Current density measured during anodisation was about 1.40 A while only 0.06 A was obtained for the dental implant. Thus, the increase in current density caused the solution to heat up to 36 $^{\circ}$C due to the electrical activity and chemical reaction.

Scanning electron microscopy and ImageJ image analysis were used to evaluate the characteristics of the nanostructure (diameter and circularity) at a magnification of $\times$ 20,000, as well as its homogeneity at a magnification of $\times$ 500 (area of 140 μm $\times$ 210 μm). These images consist of grey shades on which it is sometimes easy to discriminate between an oxide nanostructured titanium area which charges under the electron beam (light colour) and a non-nanostructured surface area or pollution which are mostly in a darker colour.

Figure ?? shows the sub-micrometric surface of the 4 different parts after anodising treatment: the dense titanium, welding and sinternd prosthesis elements. It revealed that in some parts, the nanostructuration was heterogeneous with visible scratches that destroyed the nanostructure. The welding and

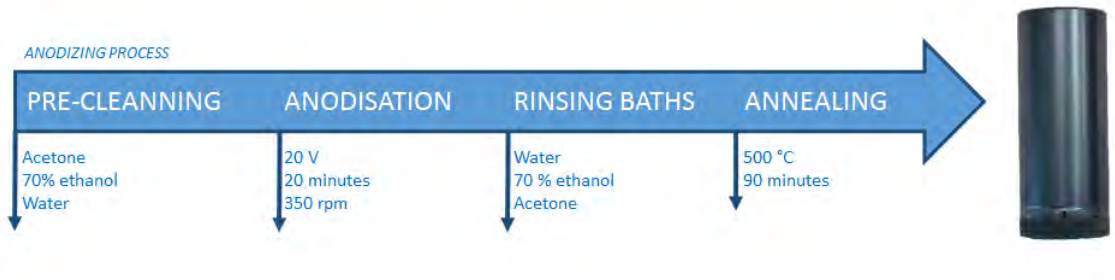

Figure 4.11: The different steps in the anodizing process with its parameters and its final blue-coloured appearance

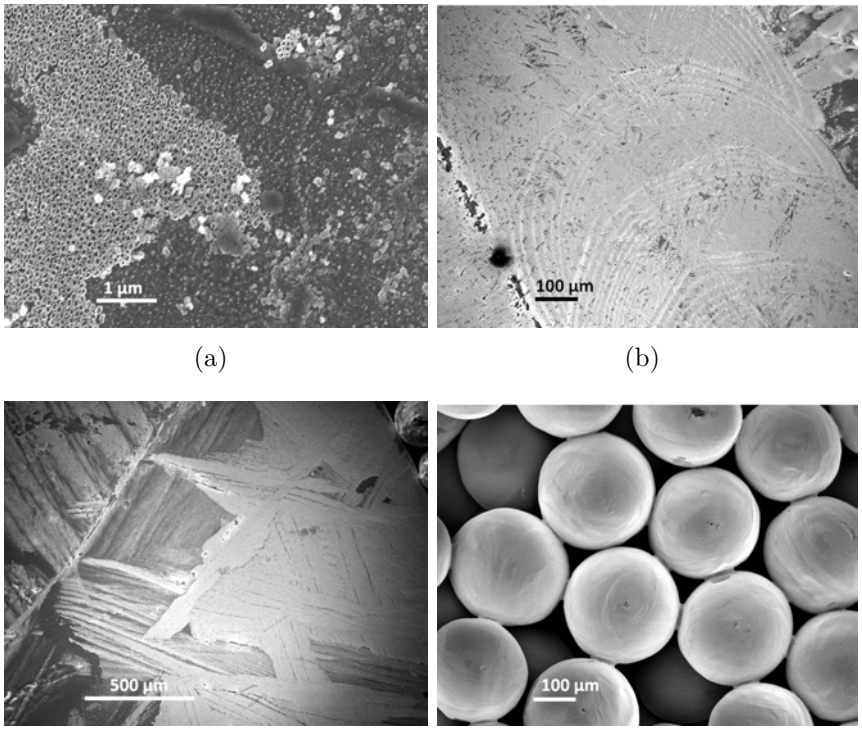

(a) (b)

(c) (d)

Figure 4.12: SEM micrographs of the nanostructure on the surface of the tracheal template sample on: (a) the compact titanium, (b) the welding, (c) the sintered titanium sintered and (d) the sintered beads

beads were more homogeneous. However, beads situated at the extremity of the prosthesis could be heterogeneous due to a lack of current connection between beads. The sintered compact titanium revealed heterogeneous nanoformation depending on the titanium grains.

Calculations regarding the repeatability of the treatment of the prosthesis revealed a high coefficient of variation of 50 % for surface homogeneity, while the nanotube diameter was homogeneous (**Table 4.8**). The surface treatment process for tracheal prostheses is not stable.

Table 4.8: Statistical analysis of the diameter and homogeneity of the nanotubes on tracheal template samples

Prosthesis analysed	ϕ of the Nano. Mean (μm)	surface homogeneity Mean [min-max](%)
1	0.07	84 [58-99]
2	0.07	73 [4-100]
3	0.07	81 [36-100]
4	0.07	73 [1-96]
5	0.07	6 [0-17]
6	0.06	11 [3-21]
7	0.07	67 [1-90]
8	0.07	83 [58-98]
9	0.07	75 [15-100]
Mean	0.07	61
SD	<0.01	30
Variance	**«0.01**	**932**
CV	5 %	50%

4.2.3 Delamination and optimisation of $TiO2$ nanostructures

In addition to the problems of heterogeneity in the surface treatment of the tracheal prosthesis, floating particles were observed in the first rinsing bath of water. After filtration of the solution and SEM observation, it was observed that these particles were individual nanotubes or plates of them that detached from the surface. **Figure 4.13(a)** shows the blue-coloured appearance of a prosthesis treated by anodisation presenting heterogeneous reflection. **Figures 4.13(b)**

confirmed that these traces/spots correspond to areas where the heterogeneity is more important and reinforces the idea of delamination of the TiO_2 nanotube layer. This delamination occurs by sheet, aggregate or by individual nanotubes.

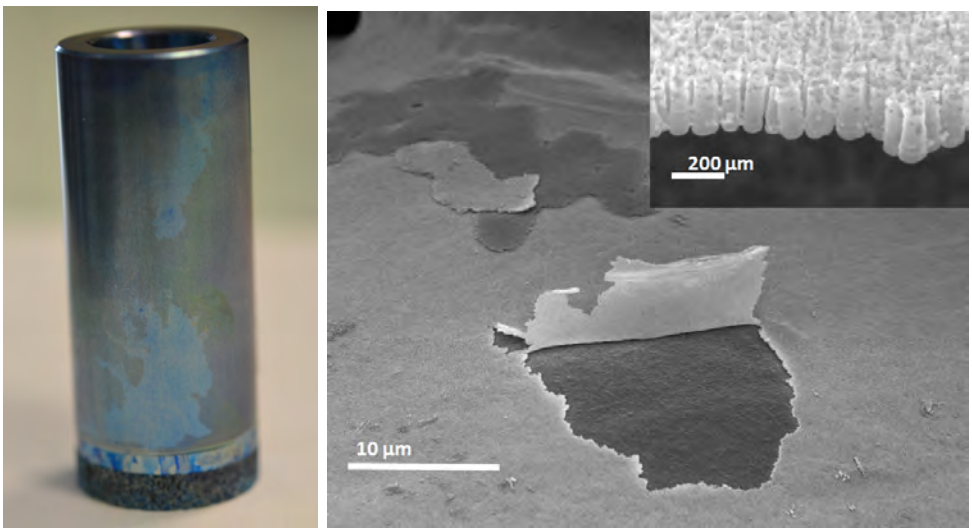

(a) (b)

Figure 4.13: (a)Tracheal template presenting surface heterogeneity ; (b) SEM micrographs of nanostructure peeling from the surface and called delamination

The results of oxide layer detachment were compared to the literature, however authors often censor this kind of problem. Only a few authors evoke the problem of weak adhesion of the nanotubes to the substrate. As explained, fluor ions (F^+) contained in the solution migrate through the oxide layer till the metal / oxide interface (**Figure 4.14(a)**) to recombine with the Ti^{4+} ions and form $[TiF_6]^{2-}$ [144]. However this species is soluble in water (**Figure 4.14(b)**)[145, 26, 146]. Thus, crack formation in the porosity network or its delamination result in the dissolution of the fluoride-rich layer [147]. One of the solutions proposed is to rinse the fresh anodic sample in pure ethanol to avoid dissolution of the fluorinated species.

In addition, some authors have suggested reducing the concentration of the fluoride by heat treatment or completely lose it at 500 °C. Annealing lead to evaporation of TiF_4 and also increase the hardness of the nanostructure [99, 30, 27]. New assays were carried out using the pure ethanol rinsing bath method. The results showed a more visually homogeneous prosthesis with less microscopic heterogeneity 4.15. **No particles could be seen by the naked eye in the rinsing bath**. However, delamination of the surface could occur from the micro-scale to the nano-scale levels. Although the SEM technique

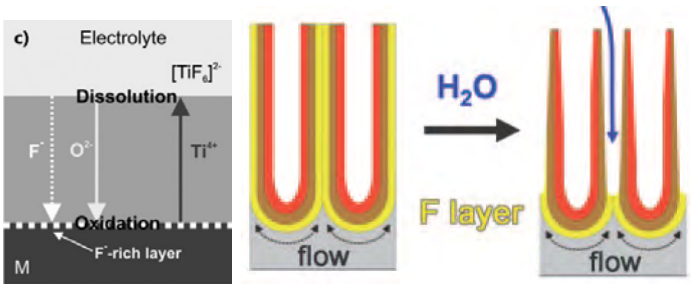

(a) (b)

Figure 4.14: (a) Schematic drawing showing field-aided transport of fluoride ions through the oxide layers: rapid fluoride migration leads to accumulation at the metal/oxide interface ; (b) Selective dissolution of fluoride-rich layers by H_2O

makes it possible to determine the homogeneity, it cannot be used to confirm the absence of delamination. The following part presents the LIBD technique used to detect very tiny particle delamination into a liquid solution and a mechanical test to check the origin of the weak mechanical adhesion of our TiO_2 nanostructure on its titanium substrate.

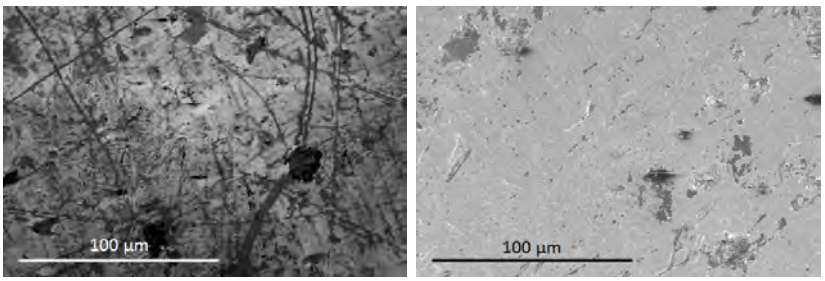

(a) (b)

Figure 4.15: SEM micrographs of the surface at low magnification : (a) after rinsing in water and (b) after rinsing in pure ethanol

4.2.4 Characterisation of TiO_2 nanostructure adhesion

Despite a visible improvement in surface homogeneity by changing the rinsing bath from water in the process to pure ethanol, the non-delamination is uncertain. In this subsection, detection of the presence or absence of delamination was performed using a more appropriate technique called laser induced breakdown detection (LIBD). The mechanical test, scratch test and tribology testing

was carried out to quantify the mechanical adhesion of the surface treatment on the titanium substrate.

4.2.4.a Nanoparticules released by LIBD

Laser induced breakdown detection (LIBD) is a very sensitive method for detecting small colloids down to a diameter of 1 nm contained in liquids by using plasma emission. Thus, determining delamination could not be performed by analysing the rinsing bath of ethanol. As the $[TiF_6]^{2-}$ species is soluble in water, delamination could also occur in human biological fluids containing water. This study aims to check TiO_2 nanostructure adhesion by soaking in a physiological solution of phosphate buffered saline (PBS).

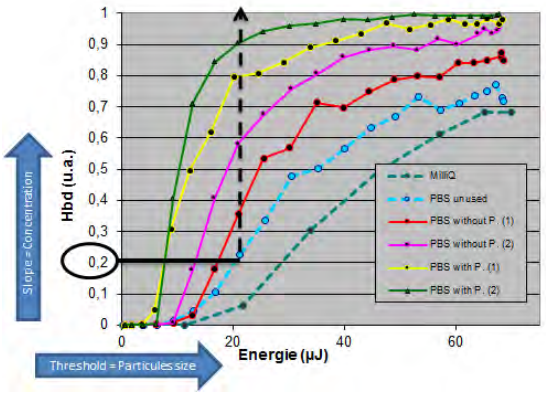

Figure 4.16: Breakdown probability (BDP) as a function of laser pulse energy for 6 different analyses : Milli-Q water (MQ-Water), PBS taken directly from the bottle (PBS-Unused), PBS handled in beakers as two test-solutions (PBS-without prothesis) and PBS solution in which anodized tracheal templates were soaked (PBS-With prothesis)

Assays were carried out on two template samples of tracheal prostheses. After the anodisation process (cleaning, anodising, rinsing, annealing), the **samples were soaked in PBS solution for 10 minutes** (called the Test-ENT). The LIBD analysis used 3 types of solution as controls: Milli-Q water (MQ-Water), PBS taken directly from the bottle (PBS-Unused) and PBS handled in beakers as two test-solutions (PBS-without prothesis).

Figure ?? shows the breakdown probability (BDP) measured as a function of the laser pulse energy (denoted as "s-curve")) for the 6 solutions analysed. The information obtained by LIBD measurements are **particle size**, which is defined as breakdown threshold energy, the minimum laser pulse energy required to generate a laser-induced plasma, and **particle concentration**

defined by the slope of the curve.

First of all, we observed a constant involved in the breakdown probability of the initial solution of Milli-Q water while more colloidal particles were present in the PBS in the bottle. If we considered a fixed colloidal concentration of the PBS solution with a breakdown probability of 20 %, the results showed that only the handling of the PBS solution (Test-PBS) led to the contamination of the solution (i.e. dust). However, after soaking anodised template prothesis in PBS solution, the results exhibited a sharp increase of particle size and concentration of 35%. The result thus suggested that anodised template samples, rinsed in pure ethanol and annealed up to 500 ° C, still induced delamination by soaking in a water-content solution.

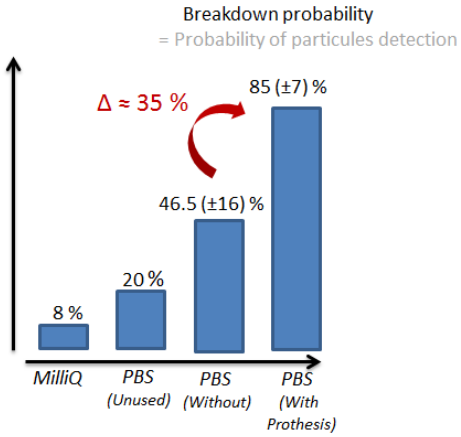

Figure 4.17: LIBD results if we considered a fixed colloidal concentration of the unused PBS solution at a breakdown probability of 20 % : the breakdown probability increase of 35% after soaking anodised template prothesis in PBS solution

4.2.4.b First results of mechanical adhesion and wear

Although surface heterogeneity and the lack of mechanical adhesion have been observed in treatments of tracheal prostheses and templates, it was not noticed in the treatment of dental implants. The aim of this part was to compare the mechanical strength of the titania nanostructure surface obtained on tracheal templates and dental implants. Nano-tribology tests were thus carried out to study the behaviour of the surface with regard to wear.

The first assays of the scratch test measurement were performed on two types of tracheal template (coupon rinsed in water and disks rinsed in an ethanol bath) and two types of dental implant (Ti cp and TA6V), both rinsed into

water-baths after anodisation. SEM observation of the surface sample before the scratch test showed the presence of delamination on one of the template samples rinsed in water.

Scratch tests were carried out 3 to 5 times/sample under an increasing load from 0 to 25 mN, or from 0 to 100 mN. **Figure 4.18** and **Table 4.9**, respectively show the SEM observations of the surface of Ti cp disks after the scratch test and summarising the critical load measurements.

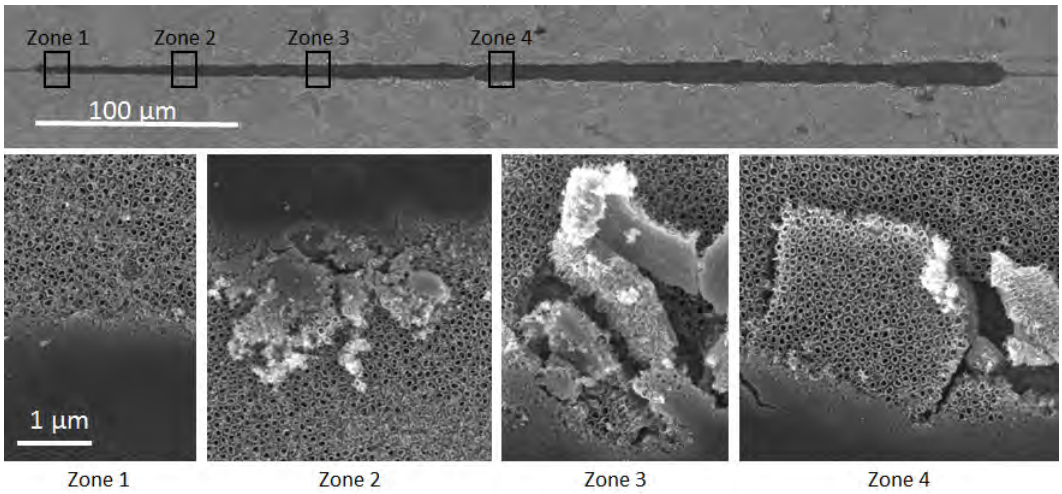

Figure 4.18: SEM micrographs of a scratch of the nanotubular surface on a Ti40 disk formed at 20 V for 20 minutes. The surface presented crushing (zone 1), cracks (zone 2) and trackside delamination (zone 3),as well as plate detachment (zone 4)

Table 4.9: Critical load obtained by microscopic analysis of the scratch test

Sample	Dental implants		Tracheal template	
	Ti cp	**TA6V**	**Ti cp**	
Rinsing bath	Water			Ethanol absolute
Mean CL	22.5 ±1.5	23.9 ±1.1	18.7 ±1.7	20 ±3.0

CL = Critical Load

The results indicate only a slightly difference with a critical load between the 4 groups. The oxide layer is first crushed, then cracks are observed followed

by trackside delamination and plate detachment. These measurements show similar adhesion, while delamination is only visible on the tracheal template. The values obtained are difficult to compare with those in the literature because they are specific to a given layer length. However, critical values found in the literature varied around 400 to 4000 mN for oxide layer thickness of 800 to 7000 nm [148, 146].

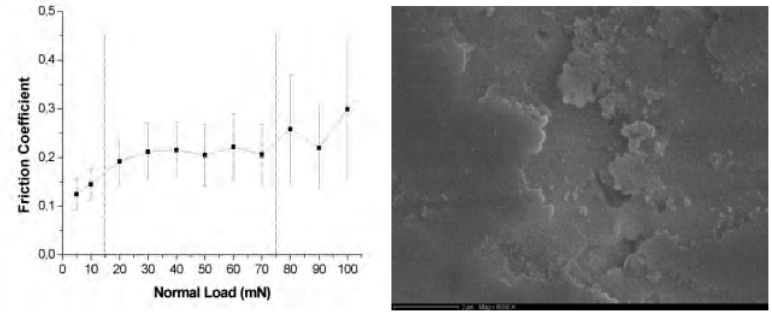

(a) (b)

Figure 4.19: (a) Evolution of the friction coefficient in function of the normal load; (b) SEM micrographs of surface condition at the end of the test of 1000 cycles

The tribology test was used to study the wear behaviour using normal load ranges from 5 to 100 mN with the same nanotribological setup as Stempfle [149]. **Figure 4.19(a)** reveals 3 tribological behaviours on the surface. The zones were observed for normal loads of less than 15 mN and up to 70 mN, which correspond respectively to the nondamaged surface and seizure of the surface leading to delamination. An intermediate zone between 20 and 60 mN showed a stable coefficient of friction (COF) of about 0.2. Similar results were observed for nanosculptured chromium thin films of 850 nm [149]. However the mechanical properties of the nanotube surfaces were carefully studied by Descamps *et coll.* by using orthopaedic implants screwed into the bone. Their results showed a COF of approximately 1 for a 450 nm-thick oxide layer and that the TiO_2 nanotube layers remained mainly intact while it underwent minimal mechanical damage after screwing and unscrewing the screw in the bone samples [28]. This observation was also found on dental implants from comparative studies on the femoral epiphysis of rabbits.

Figure 4.19(b) shows the nanostructured surface behaviour after a test of 1000 cycles. The results after 100 cycles showed no degradation of the surface, while testing with longer times (1000 cycles) induced scuffing or traces of rubbing. It was found that wear of the TiO_2 nanotube layer occurred by the detachment of "plates" from the surface.

To conclude, although the first results of surface treatment optimisation were promising, the mechanical properties of our nanosurface should be studied further and enhanced.

4.2.5 Soft tissue integration study in rats

Titanium is widely known and studied for bone integration. However, it is also used in soft tissue as stents and now artificial trachea. This latter prosthesis combines both the technology of porous titanium, composed of microbeads of 300 to 500 μm in diameter sintered between them, and a plane titanium surface. It has two advantages: the smooth surface of the beads which may favour fibroblast cell adhesion, and the micro-porosities for tissue penetration, thus creating a tight seal between the soft tissue and the titanium implant. Only a few publications evoke the soft tissue integration of titanium but they mainly focus on the abutment or neck of dental implants. Surface treatments of titanium for medical applications are also widely published but mainly for osseointegration or using implants that are not as complex as dental implants (cylindrical with threading).

The aim of this study was thus to understand and evaluate soft tissue integration with and without surface treatment on the complex shape of microbead implants. Three different surfaces were compared: machined non treated surfaces (NT), acid-etched in HCl (HCl) and nanostructured surfaces (anodised) with and without adding serum. The study was carried out in two steps. The first concerned the *in vivo* study of cylindrical porous implants using a subcutaneous rat implantation model for 2 weeks. The effects on the surface were measured using image analysis of the tissue coverage on the implants.

The second step concerned the *in vitro* study of a single bead using three different cell culture configurations in order to correlate cell behaviour with the *in vivo* results. The beads were placed on tissue culture polystyrene (TCPS), on non-cell adhesive plastic or encapsulated in cell-laden gelatin hydrogels to mimic cell movement from the surrounding soft tissue. Human fibroblast cells were evaluated using different staining methods.

My role in this project was to carry out the surface treatment by anodisation on titanium pellets and microbeads. The results of this study were recently published in the journal Nanoscale. This article N° 3 is entitled “Controlled implant/soft tissue interaction by nanoscale surface modifications of 3D porous titanium implants”.

4.2.5.a Article N° 3 : Controlled implant/soft tissue interaction by nanoscale surface modifications of 3D porous titanium implants

Nanoscale

PAPER

Cite this: *Nanoscale*, 2015, **7**, 9908

Controlled implant/soft tissue interaction by nanoscale surface modifications of 3D porous titanium implants†

Elisabeth Rieger,[a,b,c] Agnès Dupret-Bories,[a,c,d] Laetitia Salou,[e,f] Marie-Helene Metz-Boutigue,[a,b] Pierre Layrolle,[e] Christian Debry,[a,c] Philippe Lavalle[a,b] and Nihal Engin Vrana*[a,g]

Porous titanium implants are widely employed in the orthopaedics field to ensure good bone fixation. Recently, the use of porous titanium implants has also been investigated in artificial larynx development in a clinical setting. Such uses necessitate a better understanding of the interaction of soft tissues with porous titanium structures. Moreover, surface treatments of titanium have been generally evaluated in planar structures, while the porous titanium implants have complex 3 dimensional (3D) architectures. In this study, the determining factors for soft tissue integration of 3D porous titanium implants were investigated as a function of surface treatments *via* quantification of the interaction of serum proteins and cells with single titanium microbeads (300–500 μm in diameter). Samples were either acid etched or nanostructured by anodization. When the samples are used in 3D configuration (porous titanium discs of 2 mm thickness) *in vivo* (in subcutis of rats for 2 weeks), a better integration was observed for both anodized and acid etched samples compared to the non-treated implants. If the implants were also pre-treated with rat serum before implantation, the integration was further facilitated. In order to understand the underlying reasons for this effect, human fibroblast cell culture tests under several conditions (directly on beads, beads in suspension, beads encapsulated in gelatin hydrogels) were conducted to mimic the different interactions of cells with Ti implants *in vivo*. Physical characterization showed that surface treatments increased hydrophilicity, protein adsorption and roughness. Surface treatments also resulted in improved adsorption of serum albumin which in turn facilitated the adsorption of other proteins such as apolipoprotein as quantified by protein sequencing. The cellular response to the beads showed considerable difference with respect to the cell culture configuration. When the titanium microbeads were entrapped in cell-laden gelatin hydrogels, significantly more cells migrated towards the acid etched beads. In conclusion, the nanoscale surface treatment of 3D porous titanium structures can modulate *in vivo* integration by the accumulative effect of the surface treatment on several physical factors such as protein adsorption, surface hydrophilicity and surface roughness. The improved protein adsorption capacity of the treated implants can be further exploited by a pre-treatment with autologous serum to render the implant surface more bioactive. Titanium microbeads are a good model system to observe these effects in a 3D microenvironment and provide a better representation of cellular responses in 3D.

Received 23rd February 2015,
Accepted 21st April 2015

DOI: 10.1039/c5nr01237f

www.rsc.org/nanoscale

[a]*Institut National de la Santé et de la Recherche Médicale, INSERM Unité 1121, 11 Rue Humann, 67000 Strasbourg, France*
[b]*Faculté de Chirurgie Dentaire, Université de Strasbourg, 1 Place de l'Hôpital, 67000 Strasbourg, France*
[c]*Hôpitaux Universitaires de Strasbourg, Service Oto-Rhino-Laryngologie, 67098 Strasbourg, France*
[d]*Institut Universitaire du Cancer de Toulouse, 1 avenue Irène Joliot Curie 31059, Toulouse, France*
[e]*Inserm, UMR957, Lab. Pathophysiology of Bone Resorption, Faculty of Medicine, University of Nantes, France*
[f]*Biomedical Tissues SAS, IRTUN, 8 Quai Moncusu, 44008 Nantes, France*
[g]*Protip Medical, 8 Place de l'Hopital, 67000 Strasbourg, France.*
E-mail: e.vrana@protipmedical.com; Fax: +33 388329209

†Electronic supplementary information (ESI) available: 6 supplementary figures Fig. S1–S6. See DOI: 10.1039/c5nr01237f

1. Introduction

Titanium is a commonly used biomaterial especially in hard tissue replacement applications.[1] Most of the studies on titanium focused on its interaction with bone tissue cells or stem cells with an aim to convert them to osteoblasts. However, recently there have been attempts to use titanium implants in other medical indications, particularly for tracheal replacement.[2–5] These efforts necessitate a better understanding of the interaction of titanium surfaces with soft tissues. The behaviour of different cell types in contact with titanium can be distinctly different. One such example is the interaction

of gingival epithelial cells with dental titanium implants where epithelial cells prefer polished titanium to sandblasted titanium.[6] Cell/implant interactions have another aspect in otorhinolaryngology, as unlike in the case of dental implants where most of the patients are healthy otherwise, the tracheal implants are designed particularly for patients with recent cancer and surgical history. Hence, it is even more important to optimize surface properties for improved implant tissue integration.

We have recently reported the first successful clinical application of a titanium based artificial larynx system after total laryngectomy.[7] Removal of larynx is a necessity for late stage laryngeal cancer patients and it results in considerable problems for patients due to the presence of a tracheostomy (the trachea is attached to the skin of the neck to re-establish breathing). The most important consequences are due to the shunting of the aerodigestive upper tract: breathing with the tracheostomy (and not with the nose or the mouth), and difficulties in speaking (the patient has to learn oesophageal voice, or a small valve between the trachea and the oesophagus can be placed during the surgery). An artificial larynx system that can replace the functions of the larynx after total larynx resection would significantly improve the life quality of these patients. A system composed of a removable valve system and a permanent titanium implant part (ENTegral®, Protip Medical), can restore several functions of larynx and provides patients with a means to breathe without a tracheostomy. Titanium was selected because the mechanical properties of titanium prevent the possible collapse of the airway, which is a common risk in tracheal implants. In order to ensure the proper integration between the implant and the trachea, a macroporous, microbead based system was utilized. However, due to the physical properties of the titanium, the connection between the titanium and the surrounding tissue might not be rapidly established. This would further lengthen the inflammatory process. Thus, it is important to mediate the interaction of the implant with the surrounding soft tissue *via* surface modifications without compromising the bulk properties of the implant.

Surface properties are the most dominant aspect of non-degradable, implantable biomaterials[8] and are widely used to improve metallic implant's bioactivity. For example, it has been shown that acid etching of orthopaedic implants resulted in better osseointegration as quantified by the increased torque force to remove the implants *in vivo*.[9] Many methods, such as hydroxyapatite coating, polymer adsorption, etching, covalent bonding, and anodization have been used to achieve beneficial effects.[10,11] However quantification of these effects is generally limited to 2D, planar surfaces. This approach cannot fully capture the possible *in vivo* outcomes for complex implants, particularly porous implants. Moreover, all these modifications simultaneously change several parameters such as surface roughness, hydrophilicity and protein adsorption capacity, which makes it even harder to pinpoint the exact reasons behind the improvements in cellular behaviour.

In the dental implants field, the general understanding is that a rough titanium surface is better for bone attachment, whereas a smooth surface helps the gingival fibroblast adhesion. However, these conclusions are based on a structure where the interaction of the cells with the implant surface is planar. How the surface properties of titanium in a 3D configuration affect the cellular interaction with the implant surface is still an open question. These effects are difficult to quantify in metal foams as the pore shapes are irregular and the distribution of the pore sizes is widespread. Thus, a model in which the geometrical control over the components of the porous structure can be achieved, is desirable.

Microbead based macroporous titanium implants (Fig. S1†) provide a 3D system where it is possible to study the effects of surface modification on the building blocks of the system.[12] We have recently shown that just by changing the size of microbeads, extensive changes in the *in vivo* integration process can be observed.[13] It has been previously shown that hydrochloric acid (HCl) etching of porous titanium implants improves their osseoinductivity.[14] Also, effects of anodization on osseointegration and osteogenic differentiation of mesenchymal stem cells have been demonstrated.[15,16] In this study, the effects of the surface modifications on *in vivo* soft tissue migration into the porous implants were observed by using a rat subcutaneous implantation model for 2 weeks. In order to elucidate the reasons for the beneficial effects of nanoscale surface treatments on *in vivo* integration, we have used single titanium microbeads of 300–500 μm in diameter to study the effect of surface modifications on human fibroblast cell behaviour with respect to several parameters which are known to effect cell attachment, namely surface hydrophilicity, roughness and serum protein adsorption. The nature and content of proteins adsorbed was quantified by high performance liquid chromotography (HPLC) separation and subsequent protein sequencing to better understand the interaction between surface property changes and protein retention. Different cell culture configurations were used to mimic different *in vivo* conditions, such as mimicking cell in-growth from surrounding soft tissues by encapsulation of single titanium beads in cell-laden gelatin hydrogels.

2. Results and discussion

2.1 Results

The surface treatments had profound effects on the integration of the implants *in vivo* (Fig. S2†). After two weeks of subcutaneous implantation in rats, the extent of tissue formation around the implants was considerably higher in surface treated samples. Scanning Electron Microscopy (SEM) images demonstrated that both on the surface and in the cross-section, there was considerably more cell presence and extracellular matrix deposition for both anodized and HCl treated samples (Fig. 1). Particularly, the amount of tissue in the cross-section was significantly higher ($p < 0.05$). We also observed an increased expression of Interleukin-10 (IL-10) and Tissue

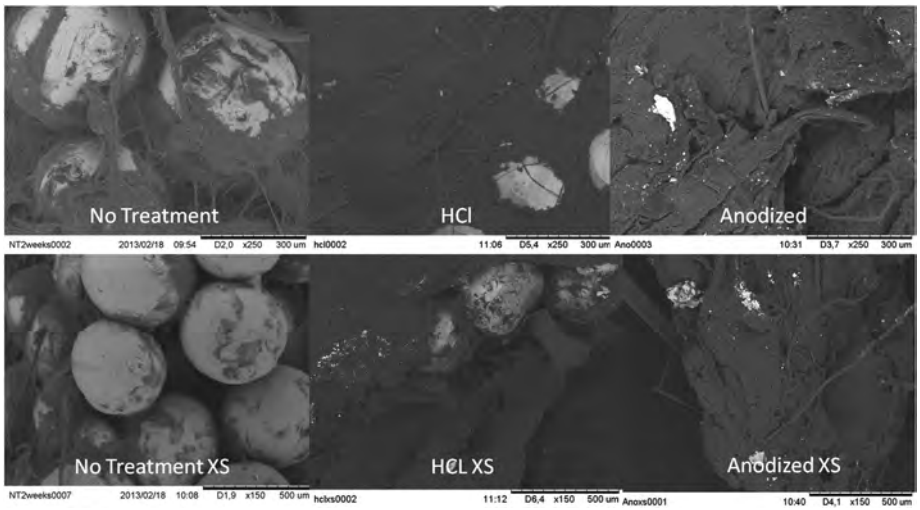

Fig. 1 SEM micrographs of explanted porous titanium implants after subcutaneous implantation.

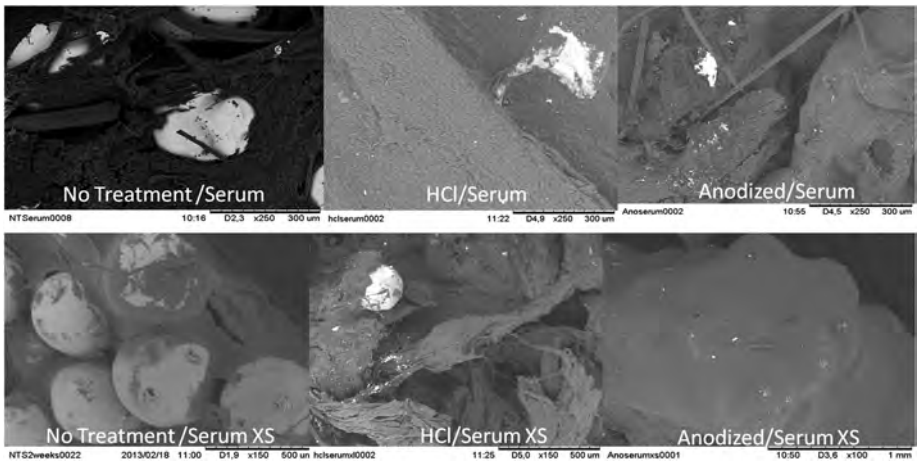

Fig. 2 SEM micrographs of explanted porous titanium implants after subcutaneous implantation with prior rat serum treatment.

Inhibitor of Matrix Metalloprotease 1 (TIMP-1) by the reverse transcription polymerase chain reaction (RT-PCR) in anodized samples which are anti-inflammatory markers, whereas there was no significant difference in the expression of the other genes checked between the groups. We also tried to introduce rat serum onto the implants prior to the implantation as a means of inducing protein adsorption and subsequent facilitation of the tissue integration. This treatment not only improved the colonization of non-treated implants but also resulted in additional amelioration of the treated surfaces, with significantly more colonization (Fig. 2). When the total area covered by tissue for both the surface and the cross-section of the implants was quantified, we observed that the treated implants had significantly more coverage in all configurations ($p < 0.05$) (Fig. 3). Also, in treated samples there was a significantly higher amount of collagen secretion (Fig. S3†).

Anodization locally induced microlevel changes but its effect was mainly at the nanometer level with the production of a regular array of titanium oxide nanotubes (Fig. S4†). The size of nanotubes was 50 ± 16 nm, having a size suitable for deposition of proteins. We have selected HCl etching due to the milder conditions of etching (Fig. 4). Utilization of different acids led to different surface morphologies for the beads, for example, hydrofluoric acid (HF) resulted in considerable changes in bead morphology within a short period (90 s), whereas HCl and sulfuric acid (H_2SO_4) treatments were mainly limited to the surface changes (Fig. S5†).

The topographical changes observed caused an increase in the roughness of the surfaces. As in the case of morphological changes, HF (R_a = 82.4 ± 14.8 nm) and H_2SO_4 (R_a = 43.6 ± 30.4 nm) treatments cause rougher surfaces, whereas HCl (R_a = 17.5 ± 6.0 nm) and anodization (R_a = 16.4 ± 2.6 nm) only resulted in slight but significant increases in surface rough-

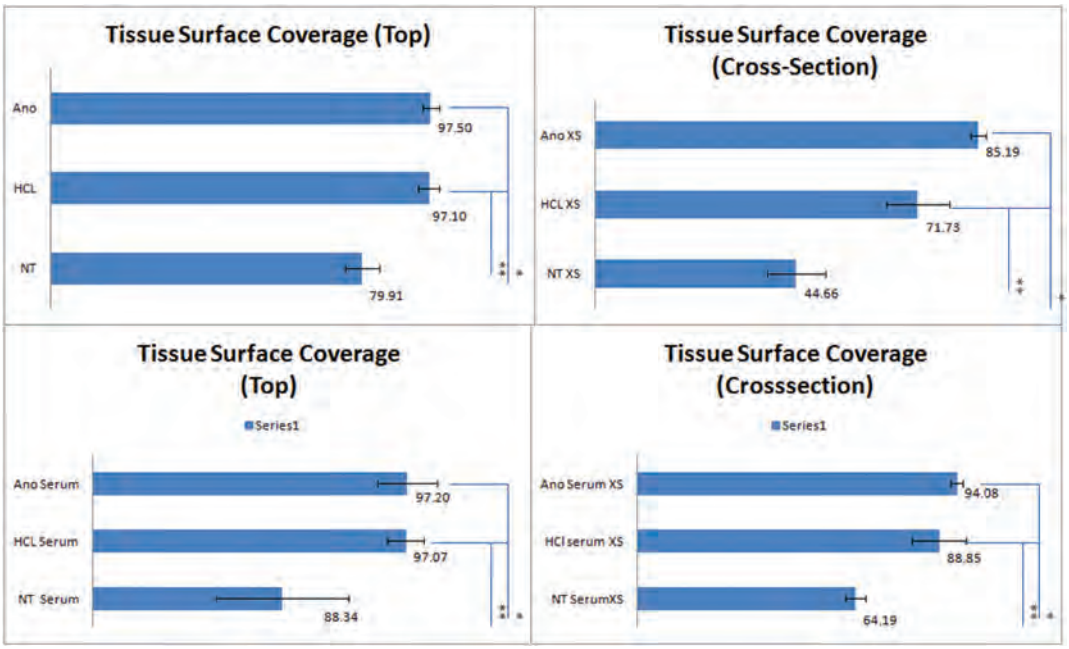

Fig. 3 Quantification of the tissue coverage of the explanted implants with image analysis. Surface treatments resulted in a significantly higher coverage particularly in the cross-section ($p < 0.05$).

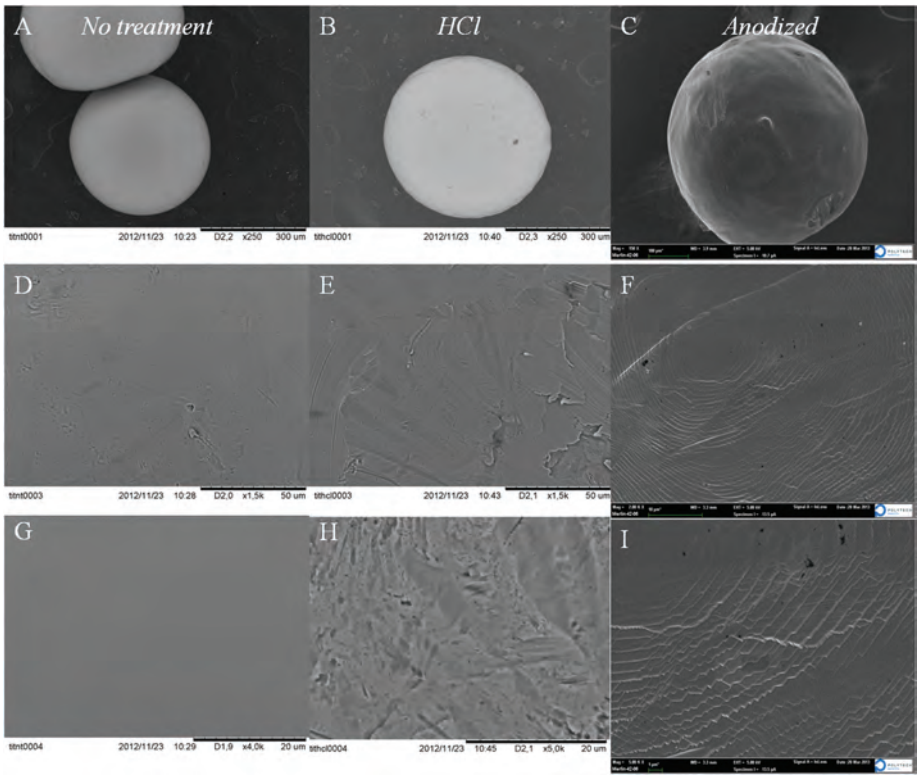

Fig. 4 SEM micrographs. Surface morphology of single titanium beads after surface treatments.

ness (compared to the roughness of untreated titanium (R_a = 8.4 ± 0.3 nm); however it should be noted that the nanotubes are closely packed with a diameter which is difficult to visualize with Atomic Force Microscopy (AFM). This might be the reason for the small change in roughness for anodized samples (Fig. 5).

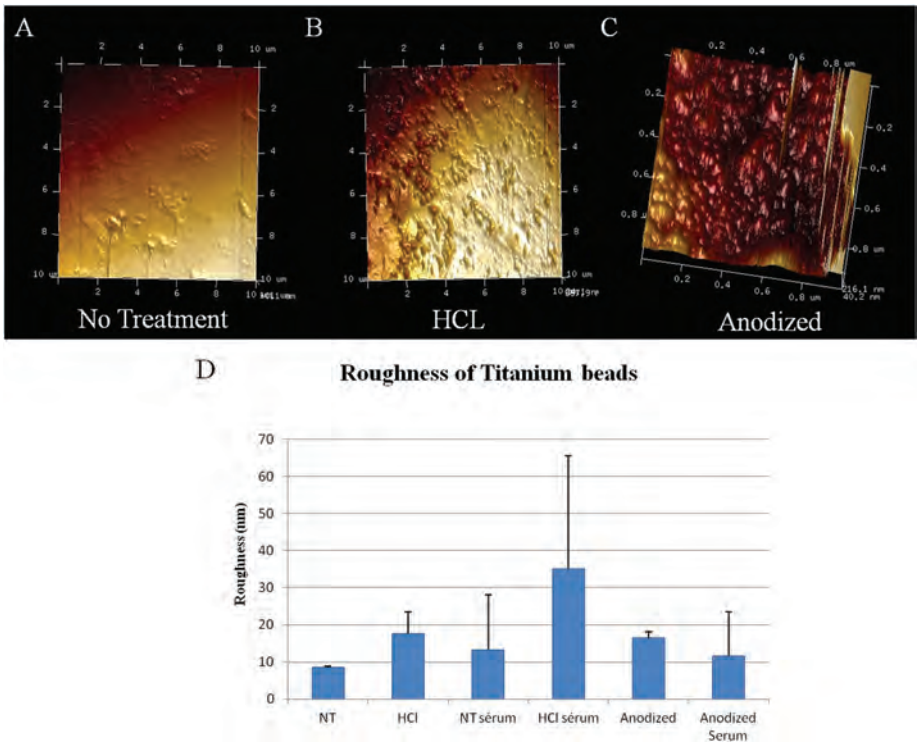

Fig. 5 AFM micrographs and surface roughness. Effect of different surface treatments on the surface topography and roughness of the titanium beads.

Surface treatments improved the hydrophilicity of pure titanium which had a contact angle of 66.2 ± 3.6°. Both anodization and acid etching decreased the contact angle, *i.e.* increased the hydrophilicity (Fig. S6†). This had a direct effect on protein adsorption on the microbeads also. We have quantified the adsorption of proteins from human serum. When human serum was directly used, acid etched samples adsorbed more proteins as quantified by HPLC (Fig. 6). The main proteins that have been adsorbed were albumin, transferrin, apolipoprotein A, alpha 1 antitrypsine and vitamin D binding protein. After depletion of IgG and albumin, again there was a significant difference in the absorption of apolipoprotein and alpha 1 antitrypsine. For anodized samples the adsorption trend was similar although the adsorption was less compared to HCl treated surfaces.

When the beads were placed on tissue culture polystyrene (TCPS), there was no statistical difference in the attachment of cells between different treatments (Fig. 7, TCPS); however when the beads were placed on non-cell adhesive surfaces, treated beads attracted significantly more cells ($p < 0.05$) (Fig. 7, No TCPS). In the case of encapsulated cells, the presence of the beads had no cytotoxic effect, so the cell numbers were comparable (Fig. 7, in gel), but the cells over 5 days preferred to move towards treated beads compared to non-treated beads.

After 5 days of culture, the surface of the treated beads was mostly covered by cells in suspension culture, whereas the non-treated beads had less cells due to the lack of initial attachment (Fig. 8, top row (only bead)). For gel culture,

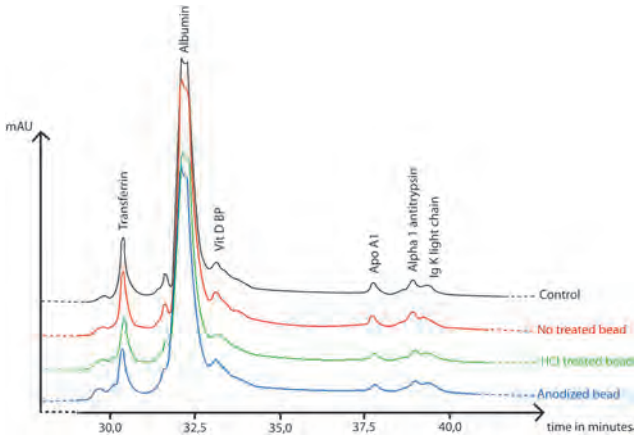

Fig. 6 HPLC and protein sequencing. Comparison of the human serum before and after being in contact with the treated or non-treated titanium beads and the main proteins adsorbed from the serum.

cells preferentially moved towards the beads, most probably due to its stiffness. This cell migration was more pronounced in the cases of anodized and HCl treated beads (Fig. 8, middle row (in gel)). In the case of TCPS surfaces, the cells became confluent and the beads were covered in all cases (Fig. 8, bottom row (beads + substrate)). When analysed by confocal microscopy the superior cell coverage on treated samples was more apparent under all conditions except for TCPS (Fig. 9).

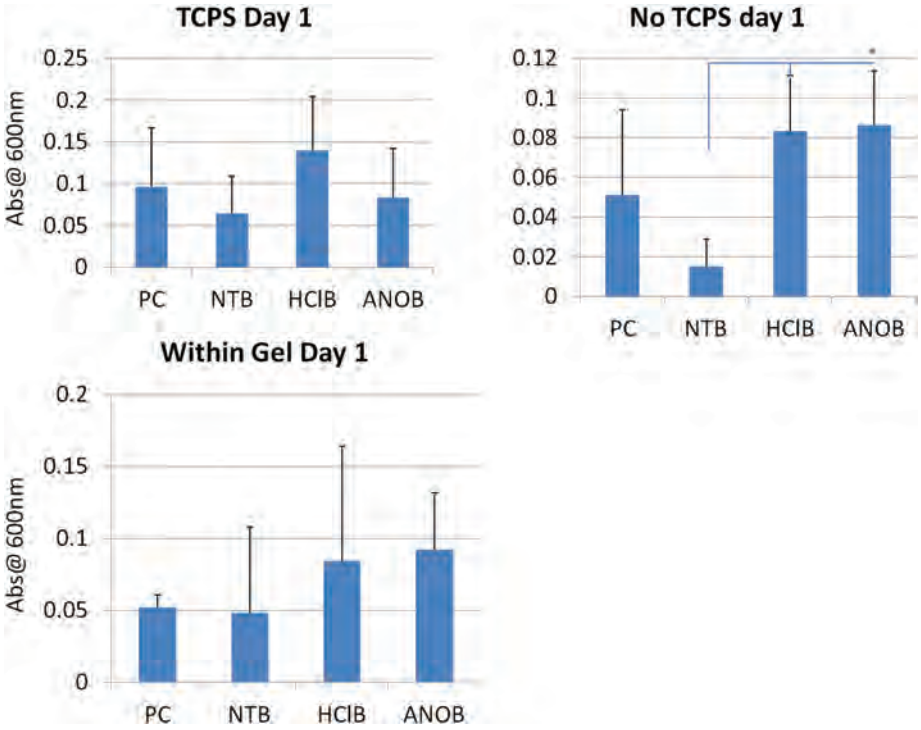

Fig. 7 Attachment of human gingival fibroblasts (HGF) to treated or non-treated beads and the effect of beads on cell viability within gelatin hydrogels.

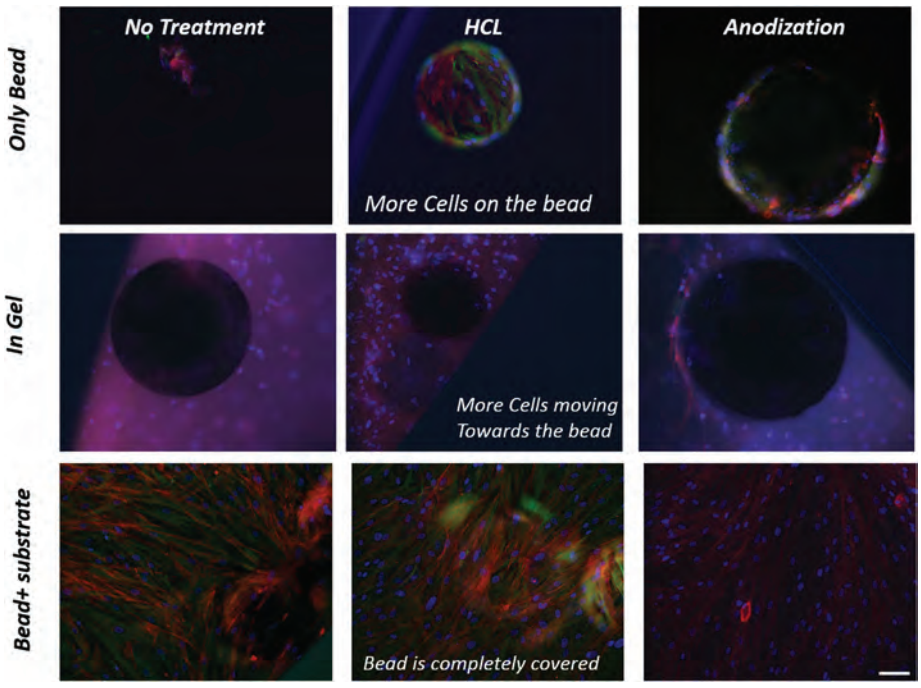

Fig. 8 FM micrographs. Hoechst/Phalloidin/Vimentin staining of cells after 5 days of culture in 3 different culture configurations. Scale bar = 100 μm.

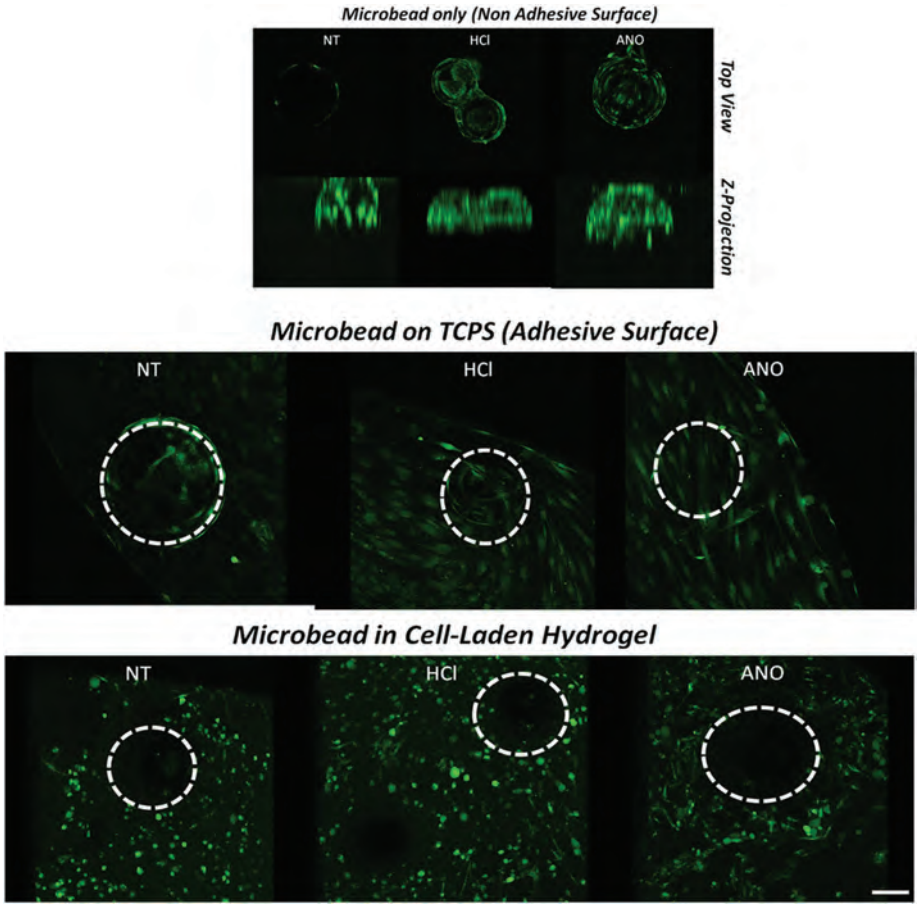

Fig. 9 Confocal micrographs. 3D reconstruction of HGF cells cultured on titanium beads in different configurations. Scale bar = 100 μm.

2.2 Discussion

One of the primary effects of both etching and anodization is the alteration of titanium surface topography at both nano- and micro levels. Topographical changes even at the level of 10 nm can affect cell behaviour. It has been recently shown that the presence of surface micro- and nanotopographies can downregulate the inflammatory response[17] with a significant decrease in both polymorphonuclear and mononuclear cells in rat subcutaneous implantation experiments. The decrease in the initial response due to the surface structuration might contribute to the faster integration of 3D porous structures too. For stem cells, it has been shown that the presence of nanoscale cues might be enough by itself for successful commitment of cells to a specific differentiated cell type.[18] Nanoscale cues can also provide surfaces with different preferences to bacterial and mammalian cell attachment.[19] For osteoblasts, the positive effect of both acid etching and anodization is well recorded and a recent study has shown that while both anodized and acid etched surfaces resulted in up-regulation of osteoblast differentiation related genes, anodized surfaces also caused an increase in cell adhesion related genes.[20] Thus, the presence of the nanoscale cues on the surfaces of the titanium beads can provide a better surface for cell attachment.

At the coating level, it has been shown that rough titanium surfaces can decrease fibroblast activity while increasing osteoblast activity.[21] But for bulk materials, especially surface modified materials, the effect is not only related to the roughness, thus the fibroblast behaviour is more varied. For example, as the roughness results for the acid etched and anodized beads shown before and after serum incubation, the changes in surface topography affects the protein adsorption and protein adsorption in return affects the surface roughness. For HCl etched beads due to the increased protein adsorption, there was an increase in the surface roughness, whereas most probably due to the filling of the nanotubes the effect was reversed for anodized samples. These might result in differential integrin clustering due to the distribution of the proteins on the implant surface. But even though the anodized samples have lower protein adsorption and roughness compared to acid etched samples, the size of the nanotubes exerts additional and more precise effects on the cell/surface interaction. Also, the anodisation directly forms the nanotubes on the surface of the titanium oxide layer, whereas acid etching physically etches the surface, which then forms an oxide layer upon

contact with air. The protein adsorption process goes through the filling of the nanotubes and it has been shown that with pores greater than 100 nm this may not be achieved, but for pores of 50 nm they can be completely filled.[22] Also, it should be noted that the due to the movement restrictions of the AFM tip the roughness of anodized samples can be lower than their actual values.

The method and nature of nano/micro structuration is also an important determinant. For example, laser assisted structuration methods can result in highly hydrophobic surfaces, even though the surface is highly hydrophilic immediately after the treatment,[23] due to the regular nature of the surface topography, without a chemical change at the interface level (where the chemical effect of the treatment is only applicable in the direct treatment areas with the laser). The effect of surface treatment on surface hydrophilicity is also treatment dependent; the hydrophobicity of untreated titanium surfaces is largely due to the presence of contaminants and both acid etching and anodization can remove them.[24] Dynamic contact angle analysis of microstructured titanium surfaces has shown an improved wettability following the first immersion cycle.[25] Thus, it is not feasible to describe the biological activity of the surface with respect to its initial contact angle. For the bulk materials, protein adsorption seems to be a more determinant factor than surface roughness. For example, if the roughness is obtained by grounding the reverse effect and improved fibroblast response has been reported.[26] Moreover, in a planar surface it is easier to single out the effect of roughness as the cells interact only with the surface from the top. For human gingival fibroblasts, formation of a hydride layer was shown to be an effective way of improving attachment,[27] however, again it was not possible to distinguish the source of this effect with respect to surface roughness or contact angle. It was suggested that the effect of the hydride layer is to improve the protein adsorption. In this study, we have also shown that the surface treatments are able to increase the protein adsorption on the porous titanium surfaces. The quantification of the specific proteins that are preferentially adsorbed onto a given surface can control the initial phases of tissue response to the implant.[28] Formation of an initial serum albumin layer on implants is a common occurrence due to the relative abundance of serum albumin. *In vitro*, this can decrease the adsorption of less abundant proteins like fibronectin, and vitronectin which are more relevant to cell attachment. However, the extent of this initial layer can facilitate the adsorption of other proteins *in vivo*, thus a higher serum albumin adsorption can be advantageous, as in the case of treated surfaces in this study. For example, one of the proteins identified in this study, apolipoprotein, has been implicated in having an effect on regeneration and also on cell growth and proliferation,[29] but it has been also related to inhibition of endothelial cell growth. Whereas, alpha 1 antitrypsin is a protease inhibitor that can increase the retention time of the other adsorbed proteins due to its anti-protease activity.[30]

Most of the studies on the effect of surface properties on cells are done on planar surfaces which are hard to convert into information in 3D configurations. In 3D metallic foams cells are exposed to significantly curved surfaces which have been shown to effect their ability to move and spread by affecting the contractile forces exerted by the cell cytoskeleton.[31] Moreover, analysis of the 3D titanium structures especially with conventional methods is difficult. Titanium microbeads are small enough to be visualized by fluorescence microscopy or confocal microscopy, which provides an opportunity to observe the cellular behaviour in a more 3D microenvironment. Moreover, bead based structures are advantageous as they provide macroscopically smooth surfaces that interact with the surrounding tissue unlike many metallic foams which have sharp edges that can damage the tissues in vicinity. Also, physical properties such as porosity or pore size can be easily modified by using the mixture of beads with different granulometries. Previously, polymeric beads have been used in delivery and immunoisolation of the cells as they provide an excellent surface : volume ratio and a beneficial effect on mass transfer limitations.[32] As our clinical practice showed that 3D structures composed of titanium microbeads can be integrated easily *in vivo*, 3D microbead-based titanium structures can be beneficial for filing load-bearing defects with an openly porous material with good mechanical properties.

The effects of surface treatments *in vivo* were much more pronounced compared to *in vitro* results. This is due to the incremental effects of increased hydrophilicity and roughness and resulting protein adsorption. As the biomaterial interaction within the body is mainly governed by the initial interaction with the body fluids, mainly blood, and subsequent protein adsorption it is important for *in vivo* application to utilize this interactions beforehand. The blood in the surgery area is in direct contact with wounded endothelial cells and will most probably contain high amounts of pro-inflammatory signals; thus, its adsorption on the surface of the implant not only triggers coagulation but also results in a more pro-inflammatory initial response. However, if the implant has already been partially coated with autologous serum from peripheral blood, then this effect can be diminished. As the surface treatments increase the protein adsorption, this would be a good way to boost the colonization also. Our *in vivo* tests showed that under all conditions application of serum caused a significant increase in colonization.

3. Experimental

3.1 Materials

Pure medical grade titanium beads (Ti40) were purchased from Nyco SA (Paris, France). All chemicals were purchased from Sigma-Aldrich (Germany) unless otherwise stated. Primary vimentin antibody was purchased from Santa-Cruz (California, USA). The Vybrant cell adhesion assay was purchased from Life Technologies (USA). An RNeasy mRNA extraction kit was purchased from Qiagen (The Netherlands) and iScript Reverse transcription Supermix for RT-qPCR was

obtained from Bio-Rad. The Apoptotic/Necrotic/Live cell assay was purchased from PromoKine (Heidelberg, Germany).

3.2 Methods

3.2.1 Surface treatments. Surface modification of the single titanium beads, plain titanium and 3D porous titanium samples (discs of 10 mm diameter and 2 mm of thickness) were done as described below (Table 1). For anodized samples at 20 V an annealing treatment for 1 h at 500 °C was carried out to stabilize the nanotubes. After the treatment, the samples were washed with distilled water and air-dried.

3.2.2 *In vivo* tests. 9 male Wistar rats weighing 300 g were implanted. Approval for these experiments was obtained from the Regional Committee of Ethics for Animal Experiments of Strasbourg. The implantation procedure was carried out under general anaesthesia, obtained with intraperitoneal injection of a mixture prepared with 90 mg kg^{-1} of ketamine and 10 mg kg^{-1} of xylazine. Local anaesthesia of the skin of the back was performed (1% lidocaine). Implants were placed subcutaneously at the back of the animals. The skin was stitched up with several stitches. Each animal except for one received four implants two at each side of the spinal column, where one side has the treated implants while the other side has the controls. In total, 6 implants for each condition without serum treatment and 3 implants for each condition with serum treatment were implanted. Animals were daily observed to ensure their well-being and whether there were any signs of infection at the operation area. Two weeks after the implantation procedure, animals were anaesthetised and the implants were explanted.

Macrophotographies of the implants were done and fixed in 4% Formol for 24 hours. Cross-sections of the implants were obtained by freeze-etching using liquid nitrogen. Afterwards, implants were coated with a 10 nm gold layer to be observed with SEM, the total coverage after 2 weeks on the surface and in the cross-section for each condition was quantified using the Image J image analysis program. The total amount of protein and collagen was quantified by semi-quantitative Fast Green-Sirius Red staining. Explants with the in-grown tissue were immersed in 30 mg ml^{-1} protease solution in sterile MilliQ water (origin of protease was *Streptomyces griseus*). For total digestion of the in-grown tissues, up to 48 hours of incubation was necessary. mRNA was achieved by using a RNeasy kit as per the instructions of the provider. The amount of extracted RNA and its quality were measured by using a Nanodrop spectrometer system (Thermo Scientific). The reverse transcription of the complementary DNA was done by reverse transcription Supermix for RT-qPCR (Bio-Rad), by the following cycle configuration: 5 min at 25 °C, 30 min at 42 °C and 5 min at 85 °C. The PCR amplication was done with the following reaction solution composition: 4 μL de supermix at 5 M, 0.1 μL of forward primer 0.1 μL of reverse primer, 0.2 μL of Taq polymerase (iTaq DNA polymerase, Bio-Rad), 4 μL of Betaine at 5 M, 1 μL of DMSO, 9.6 μL filtered MilliQ water and 1 μL complementary DNA. The amplification cycle was as follows: 1 min at 94 °C, 1 min at 60 °C, then 1 min at 72 °C for 35 times. The primers were designed by using the primer design tool of the primer provider (Eurofins MWG, Operon). The expression levels of the following genes were checked: interleukin-10 (IL-10), tissue inhibitor of matrix metalloprotease 1 (TIMP-1), von Willebrand factor (vWF), vascular endothelial growth factor A (VEGF A), tumor necrosis factor alpha (TNF-α), cadherin 1 (Cdh-1), vascular cell adhesion molecule 1 (VCAM-1), interferon gamma (IF-γ), transforming growth factor beta (TGF-β1), glyceraldehyde-3-phosphate dehydrogenase (GAPDH), and beta actin (β-actin) with the aim of comparing if there is a significant difference in the pro- and/or anti-inflammatory and vascularisation related markers.

3.2.3 Surface characterization. The surfaces of the titanium beads were characterized for the morphology, roughness, topography and surface hydrophilicity. The effect of the treatment on the bead morphology was characterized by visualization of single beads by Scanning Electron Microscopy (SEM, Hitachi TM-1000). The effect of the treatments on surface roughness was quantified by AFM in contact mode in 10 micron × 10 micron fields (Multimode Nanoscope VI, Bruker (Santa Barbara, CA, USA)). Surface roughness was calculated from an average of 6 images. Contact angle measurements of the treated and non-treated surfaces were done by using contact angles for a 10 microliter water droplet. Protein adsorption was initially quantified by the BCA assay and further characterization was done as described below.

3.2.4 Quantification of serum protein adsorption *via* HPLC and sequencing. In order to quantify the amount of protein adsorbed, single beads (which correspond to a ~8×10^5 μm^2 surface area with an average bead diameter of 500 μm) of each condition were incubated with human serum at room temperature for 1 hour. After the incubation the serum was removed and introduced into the HPLC system to quantify the missing amount of protein components which have been adsorbed. For the baseline human serum was directly introduced into the HPLC system.

3. 2.4.1 RP-HPLC purification. The proteins present in samples (100 μL) were separated at 40 °C using a Dionex HPLC system (Ultimate 3000; Sunnyvale, CA USA) on a Vydac 208TP C8-column (particle size, 5 μm; 150 mm × 2.1 mm; Grace, Vydac, Interchim, Montluçon, France) with a pre-column heater of 2 μL and an internal diameter of 0.13 mm (Inter-

Table 1 Titanium surface treatments

Type of treatment/ abbreviation	Concentration	Duration	Temperature
Hydrochloric acid/HCl	10 M	1 hour	Room temperature
Anodization/ANO	1% HF (wt%) and 1M glacial acetic acid	20 minutes	Room temperature
Fetal bovine serum	—	1 hour	Room temperature

chim, Montluçon, France). Absorbance was monitored at 214 nm, and the solvent system consisted of 0.1% (v/v) TFA in water (solvent A) and 0.09% (v/v) TFA in 70% (v/v) acetonitrile–water (solvent B). Elution was performed at a flow rate of 200 μL min^{-1} with the following solvent B gradient: 0% B for 5 min, 0% B to 100% B for 45 min and 100% B for 10 min. Fractions containing peaks were manually collected and concentrated until 20 μL by evaporation using a speed-vac.

3. 2.4.2 Automatic Edman sequencing of peptides. The N-terminal sequence of purified peptides was determined by automatic Edman degradation analysis on a Procise bi-cartridge microsequencer (Applied Biosystems, Courtaboeuf, France). Samples purified by HPLC were loaded on polybrene-treated glass-fibre filters. Phenylthiohydantoin-amino acids (Pth-Xaas) were identified by chromatography on a C18 column (PTH C-18, 2.1 mm Å–200 mm) and by comparison with the profile of the Pth-Xaas standard.

3.2.4.3 Identification of the isolated proteins. The sequence of the protein obtained after sequencing is compared with protein sequences included in the data bank UniProtKB by using http://web.expasy.org/blast/.

3.2.5 Cell Culture. Primary human gingival fibroblasts isolated from the University of Strasbourg Dental Faculty with patient consent were used at passages 3–6. The medium was DMEM low glucose with 10% Foetal Bovine Serum (FBS) and 1% Pen/Strep. Cells were passaged regularly and fed every other day. Trypsinized cells were seeded on single beads which were sterilized by UV treatment. For bead suspension experiments non-adhesive cell culture plates were used (NUNC). 1×10^5 cells were seeded on each bead. For encapsulation 5% porcine gelatin solution was used. 1.2×10^5 cells were encapsulated within the gel of 80 μl in 96 well plates which contains a single titanium bead inside by introduction of transglutaminase to crosslink gelatin (6 : 1 v : v ratio).

3.2.6 Cell culture configurations. Cell culture experiments were performed in 3 configurations as described in Fig. 10 in 96 well plates. First, to see the competitive attachment of the cells, cells were seeded on beads on TCPS where they can attach both to the well and to the titanium bead. In the second configuration, to see the preference of the cells to be attached to the beads, a non-adhesive plate was used, so that the cells can only attach to the beads. The third configuration was the encapsulation of the beads in a cell laden enzymatically degradable hydrogel (gelatin) to mimic the movement of the cells from the surrounding tissue to the implant.

3.2.7 Cell viability, morphology and distribution. Initial cell attachment and viability over 5 days was tested with TOX-8 (a resazurin based cell metabolic activity test). Cellular morphology and cell distribution were either observed by Calcein-AM staining or Hoechst/Phalloidin/Vimentin staining. 3D imaging of single beads in every configuration was done by using a confocal microscope after Calcein-AM staining. The total cell area and total cell numbers for each condition were determined by the Image-J image analysis program (NIH, USA).[33]

3.3 Statistical analysis

The experiments are performed at least in triplicates (for cell culture and protein adsorption in sextuplicates) and the results presented are the results of at least 3 independent experiments and they are reported as mean ± SD. The comparison between, non-treated, acid etched and anodized conditions was done by one-way ANOVA analysis at a statistical significance level of $p < 0.05$, followed by Tukey's test to determine the differences between samples.

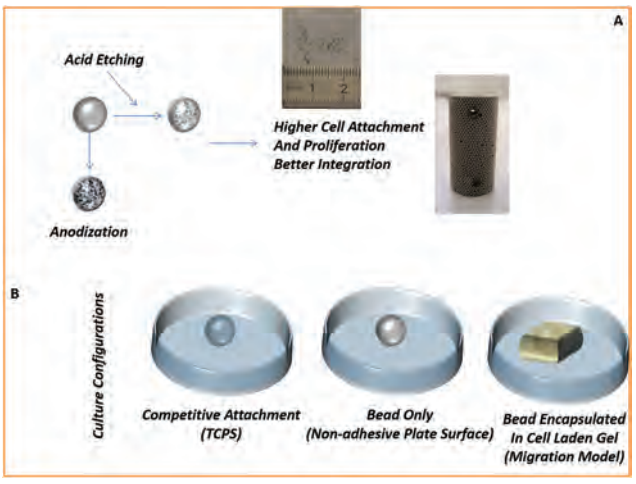

Fig. 10 The treatments and the cell culture configurations utilized.

4. Conclusions

The effects of two surface modification techniques, acid etching and nanotube formation *via* anodization, were quantified in a 3D model. The sum of all effects of surface treatments that are beneficial for cell attachment such as increased surface roughness, and improved protein adsorption has been shown to have an exponential impact on the *in vivo* integration. The ability to test the single components of an implant *in vitro* to understand the *in vivo* behaviour is an advantage of modular systems such as microbead-based porous titanium implants. These treatments are tested for the improvement of colonization of porous titanium tracheal connectors in artificial larynx implants.

Acknowledgements

This project has received funding from the European Union's Seventh Framework Programme for research, technological development and demonstration under grant agreement no. 606624 (NanoTi). This study has been partially funded by Protip Medical, Fédération de Médecine Translationnelle de Strasbourg (FMTS), Université de Strasbourg, France, and Ligue contre le cancer Alsace, France.

Notes and references

1 J. P. Li, P. Habibovic, M. van den Doel, C. E. Wilson, J. R. de Wijn, C. A. van Blitterswijk and K. de Groot, *Biomaterials*, 2007, **28**, 2810–2820.

2 N. E. Vrana, A. Dupret-Bories, C. Bach, C. Chaubaroux, C. Coraux, D. Vautier, F. Boulmedais, Y. Haikel, C. Debry, M.-H. Metz-Boutigue and P. Lavalle, *Biotechnol. Bioeng.*, 2012, **109**(8), 2134–2146.

3 L. M. Janssen, G. J. V. M. van Osch, J. P. Li, N. Kops, K. de Groot, L. Feenstra and J. A. U. Hardillo, *J. Tissue Eng. Reg. Med.*, 2010, **4**, 395–403.

4 A. Dupret-Bories, P. Schultz, N. E. Vrana, P. Lavalle, D. Vautier and C. Debry, *J. Rehabil. Res. Dev.*, 2011, **48**, 851–863.

5 A. A. Gaafar, A. A. El-Daly and H. A. Gaafar, *J. Laryngol. Otol.*, 2008, **122**, 391–396.

6 G. Lauer, M. Wiedmann-Al-Ahmad, J. E. Otten, U. Hübner, R. Schmelzeisen and W. Schilli, *Biomaterials*, 2001, **22**, 2799–2809.

7 C. Debry, A. Dupret-Bories, N. E. Vrana, P. Hemar, P. Lavalle and P. Schultz, *Head Neck*, 2014, **36**(11), 1669–1673.

8 F. Variola, F. Vetrone, L. Richert, P. Jedrzejowski, J.-H. Yi, S. Zalzal, S. Clair, A. Sarkissian, D. F. Perepichka, J. D. Wuest, F. Rosei and A. Nanci, *Small*, 2009, **5**, 996–1006.

9 S.-A. Cho and K.-T. Park, *Biomaterials*, 2003, **24**, 3611–3617.

10 G. Zhao, Z. Schwartz, M. Wieland, F. Rupp, J. Geis-Gerstorfer, D. L. Cochran and B. D. Boyan, *J. Biomed. Mater. Res., Part A*, 2005, **74A**, 49–58.

11 K. Mustafa, J. Wroblewski, B. S. Lopez, A. Wennerberg, K. Hultenby and K. Arvidson, *Clin. Oral Implants Res.*, 2001, **12**, 515–525.

12 N. E. Vrana, A. Dupret-Bories, C. Chaubaroux, E. Rieger, C. Debry, D. Vautier, M.-H. Metz-Boutigue and P. Lavalle, *JoVE*, 2013, e50533.

13 N. E. Vrana, A. Dupret-Bories, P. Schultz, C. Debry, D. Vautier and P. Lavalle, *Advanced Healthcare Materials*, 2014, **3**(1), 79–87.

14 M. Takemoto, S. Fujibayashi, M. Neo, J. Suzuki, T. Matsushita, T. Kokubo and T. Nakamura, *Biomaterials*, 2006, **27**, 2682–2691.

15 S. Lavenus, M. Berreur, V. Trichet, P. Pilet, G. Louarn and P. Layrolle, *Eur. Cell Mater.*, 2011, **22**, 84–96.

16 S. Lavenus, V. Trichet, S. Le Chevalier, A. Hoornaert, G. Louarn and P. Layrolle, *Nanomedicine*, 2012, **7**, 1045–1066.

17 A. Palmquist, A. Johansson, F. Suska, R. Brånemark and P. Thomsen, *Clin. Implant Dent. Relat. Res.*, 2013, **15**, 96–104.

18 L. E. McNamara, R. J. McMurray, M. J. P. Biggs, F. Kantawong, R. O. C. Oreffo and M. J. Dalby, *J. Tissue Eng.*, 2010, **1**(1), 120623.

19 Y. Wang, G. Subbiahdoss, J. Swartjes, H. C. van der Mei, H. J. Busscher and M. Libera, *Adv. Funct. Mater.*, 2011, **21**, 3916–3923.

20 S. Sista, A. Nouri, Y. Li, C. Wen, P. D. Hodgson and G. Pande, *J. Biomed. Mater. Res., Part A*, 2013, **101**(12), 3416–3430.

21 A. Cohen, P. Liu-Synder, D. Storey and T. J. Webster, *Nanoscale Res. Lett.*, 2007, **2**, 385–390.

22 K. S. Brammer, S. Oh, C. J. Frandsen and S. Jin, in *Biomaterials Science and Engineering*, ed. R. Pignatello, 2011, ch. 9, ISBN: 978-953-307-609-6.

23 H. Kenar, E. Akman, E. Kacar, A. Demir, H. Park, H. Abdul-Khaliq, C. Aktas and E. Karaoz, *Colloids Surf., B*, 2013, **108**, 305–312.

24 C. J. Oates, W. Wen and D. W. Hamilton, *Materials*, 2011, **4**, 893–907.

25 F. Rupp, L. Scheideler, D. Rehbein, D. Axmann and J. Geis-Gerstorfer, *Biomaterials*, 2004, **25**, 1429–1438.

26 E. Eisenbarth, J. Meyle, W. Nachtigall and J. Breme, *Biomaterials*, 1996, **17**, 1399–1403.

27 R. Xing, L. Salou, S. Taxt-Lamolle, J. E. Reseland, S. P. Lyngstadaas and H. J. Haugen, *J. Biomed. Mater. Res., Part A*, 2014, **102**(5), 1389–1398.

28 K. Nakanishi, T. Sakiyama and K. Imamura, *J. Biosci. Bioeng.*, 2001, **91**, 233–244.

29 R. W. Mahley, *Science*, 1988, **240**, 622–630.

30 P. G. W. Gettins, *Chem. Rev.*, 2002, **102**, 4751–4804.

31 J. A. Sanz-Herrera, P. Moreo, J. M. García-Aznar and M. Doblaré, *Biomaterials*, 2009, **30**, 6674–6686.

32 A. Khademhosseini, M. H. May and M. V. Sefton, *Tissue Eng.*, 2005, **11**, 1797–1806.

33 M. D. Abràmoff, P. J. Magalhães and S. J. Ram, *Biophotonics Int.*, 2004, **11**, 36–43.

4.2.5.b Addtional discussion

In this study, we demonstrated the effects of surface treatments on soft tissue integration in the technology of titanium microbeads. Three different surfaces were compared: machined non-treated surfaces (NT), acid-etched in HCl (HCl), and nanostructured surfaces (anodized) with and without adding serum. The results showed extensive tissue formation on the treated surface after implantation in a subcutaneous rat model. Both cell numbers and extracellular matrix deposits were higher for the anodised and HCl treated samples. However, only the anodised samples showed an increase in the anti-inflammatory markers (IL 10, TIMP-1). The addition of human serum to the implant induced protein adsorption and tissue integration. These effects were in addition to the effects of the surface treatment. Other comparisons were carried out using three *in vitro* models with quantification of the human serum proteins adsorbed and the attachment of the fibroblast cells. Higher protein quantification was obtained for the HCl treated surface in comparison to the others. The HCl and anodised surfaces attracted the cells over 5 days of culture compared to the non-treated beads. This study also revealed the non-cytotoxic effect of the titanium beads on the cell. To resume, it was observed that the surface treatment initially made possible the attachment of the cells on the surface and increased tissue integration. Anodised surfaces may also reduce the inflammation that appears with the implantation of new titanium devices into the body.

The integration of this titanium microbead technology with soft tissue was previously studied by the same research team using other surface treatments and different multilayer films associated with peptide treatments for a tracheal application [150]. The application was related to dental implants. The objective was to improve the adhesion of gingival epithelial tissue and to constitute the first barrier against infection. They combined porous titanium made of 125 to 500 μm beads mounted with multilayered polyelectrolyte films (MPFs) with and without functionalisation by a laminin-5-derived adhesion peptide. These polypeptidic proteins are involved in the structural scaffolding of epithelial tissues [5]. The study showed that porous titanium is a material which is very well colonised by soft tissues both *in vitro* and *in vivo*. Bioactive peptides could thus enhance soft tissue integration.

The enhancement of soft tissue integration of the dental abutment was also a topic that I studied during an internship in Oslo and was published by Xing *et coll.* [113]. This paper reports on experiments using an electrochemical process of cathodic polarisation in organic acids, while the anodisation process was used to form nanostructures. The treatment modified the roughness but also produced surface hydride (H^-). It has been found that acetic acid under a specific current density produced more surface hydride than oxalic and tartaric

acid. This hydride content was positively correlated to the proliferation rate of human gingival fibroblasts (HGF) while no statistically significant difference was related to surface topography and hydrophilicity. Hydride implementation created by cathodisation on Ti surfaces may be another potential means for nanostructured surfaces to promote connective tissue growth and act as a barrier against bacteria.

In this study, we propose the reverse treatment of cathodisation named anodisation which makes it possible to create TiO_2 nanotubes. It has been shown in several studies that nanostructures stimulate the soft tissue response as well as osseointegration both *in vitro* and *in vivo*. However, process treatments applied to tracheal prostheses have been observed by SEM to peel off from the titanium substrate. This weak adhesion between the substrate and the newly-formed oxide layer is rarely discussed. This weakness is due to the presence of a fluoride rich TiO_2 layer at the interface. Yu *et coll.* have recently proposed a method to improve this adhesion of the nanostructure to the surface by carrying out additional anodisation in a fluoride-free electrolyte [146]. Thus, an additional compact layer was formed instead of the floride-rich layer. The results obtained show an increase of 300 % in the adhesion of the nanostructure. This method could be a research possibility for the application of nanostructured surfaces on tracheal prostheses.

To conclude, several surface treatments of titanium could be used to improve soft tissue integration. This study makes it possible to demonstrate that anodised beads can improve soft tissue integration. However, the mechanical strength of the oxide layer is mitigated and requires optimisation of the adhesion by deleting the fluoride-rich layer.

4.3 Scaling up of the surface treatment on medical devices

The nanosurface has been shown to have the bioactive properties required for medical application such as dental implants, orthopaedic or tracheal prostheses. In the case of dental and orthopaedic implants, an industrial treatment process should be able to treat a large quantity of implants in the same batch. For instance, for an SME the lowest range of dental implants could produce approximately 500 implants/batch while a large range could have up to 1,500 implants/batch.

The process is currently in the developmental stage for future industrialisation (**Figure 4.20**). To adapt the laboratory setup used into an industrial process, two different approaches are possible (**Figure 4.21**). Numbering up

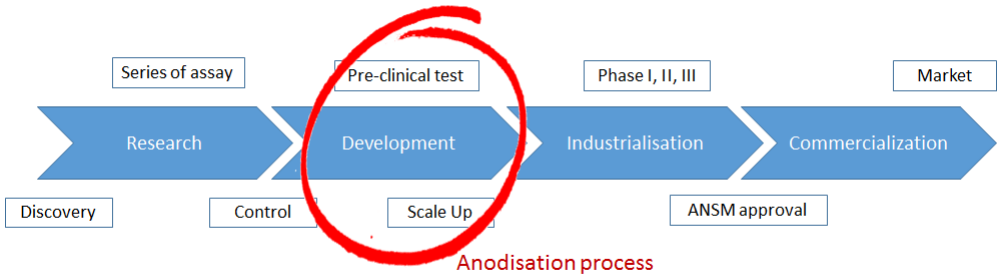

Figure 4.20: Process: from the research to the industrial tool

consists in increasing the number of the electrochemical cell without changing any dimensions. This method increases production costs and is less relevant in cases of large batches of implants. Scaling up consists in adapting the size of the electrochemical cell process to fit the treatment of several implants simultaneously. It makes it possible to reduce the costs and may even make it possible to automate the process in cases of large batches of implants.

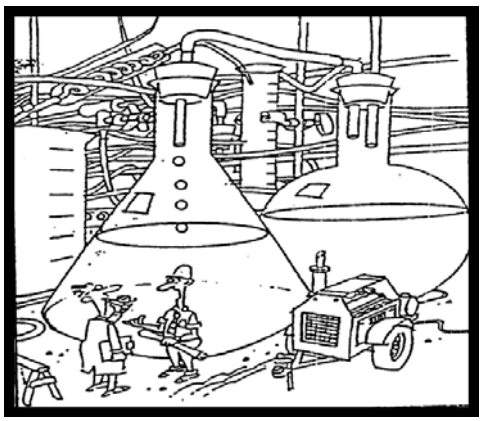

Figure 4.21: Humoristic picture of scaling up : "We've got a few problems going from lab scale up to full scale commercial"

The extrapolation consists in adjusting the operating conditions (i.e. electrolyte, voltage, current, stirring, temperature). It is necessary to ensure the formation of nanotubes by changing from the laboratory scale to the industrial scale. The objective is to obtain the same performances from different conditions. For this reason, it is necessary to carry out a progressive increase in scale by creating intermediate steps representative of the real system and called the pilot. Due to the composition of the electrolyte (acetic acid and hydrofluoric acid) the choice of materials for tanks or holders are restricted (**Table 4.10**).

Teflon is one of the rare and most appropriate materials for good resistance to these two acids. However, this soft material is easily deformable and has weak properties in terms of wear by screwing.

Table 4.10: Chemical compatibility of the materials with the acids

Material \ **Acid**	Acetic acid	hydrofluoric acid
Aluminium	+	0
Copper	+	0
Polypropylene (PP)	+	-
Polyethylene (PE)	-	-
PTFE	+	+
PVC	0	-
Stainless steel 316	+	0
Titanium	+	0
Silicone	0	0

+ = high; - = limited; 0 = not compatible

In the case of the nanostructuration of dental implants, the pilot scale was to create a first holder that could treat 12 implants in a same batch (**Figure 4.22(a)**). The holder was made of titanium, for current feeding of the implant, covered with a PTFE cover to protect the metal from the acid electrolyte. Implants are screwed onto the holder using screw holders. Treatment tests were carried out in both potentiostatic and galvanostatic mode (**Table 4.11**).

Table 4.11: Input and output parameters obtained in both potentiostatic and galvanostatic mode

Mode	Potentiostatic	Galvanosatic
Input parameters	20 V / 20 min	I = 0.57 A
Output parameters	I = 0.50 -> 0.96 A	9.2 V / 20 min

Nanoporous array formation was only observed on the implant surface using the galvanostatic method. The batches of implants obtained were homogenous in nanostructure and in surface colour (**Figure 4.22(b)**). The potentiostatic mode only produced an acid-etched surface with a heterogeneous coloured surface. Although nanoformation was observed in one method, it was found to be not reproducible in terms of variation of output voltage. Moreover, it was observed that the electrolyte solution changed colour too, and the bath temperature increased during the treatment.

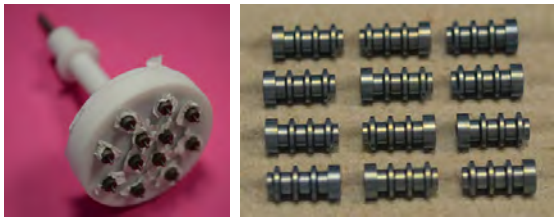

(a) (b)

Figure 4.22: (a) 12-implant holder for dental implant treatmenst; (a) Macroscopic appearance of 12 implants nanostructured in galvanostatic mode

In the case of ENT applications, the artificial larynx prostheses are not yet commercialised but the quantity of implants expected for the sale is low. Thus, the scaling up mainly concerns increasing the dimension of the electrolytic cell for unit treatments of tracheal prostheses.

As presented in the previous section, the first assays for tracheal prosthesis treatments have been carried out. In addition to adhesion problems, the results have shown a process that is not stable in terms of current density and bath temperature. The variations in current density have been shown to increase with increasing bath temperature and vice versa, leading to a snowball effect (**Table 4.12**). For high conditions (temperature and current density), colour changes in the electrolyte were noticed and revealed modification to the composition of the electrolyte.

To avoid a modification of the bath parameter, the temperature might also be directly controlled using cooling apparatus. In addition to this device, it is necessary to use bigger tanks so that small changes in the solution are insignificant with regard to the bath volume. Then, because of the changing bath volume, bath stirring is thus impacted. A recent study published in 2015 by Allonneau *et coll.* described transfers generated by magnetic bars [151]. The

Table 4.12: Evolution in the output current density and bath temperature for anodisation of tracheal templates in potentiostatic mode

Sample	1	2	3	4
Initial temperature T_0 ($^\circ$C)	22	23	26	30
Initial intensity I_0 (A)	0.85	0.98	1.29	1.40
Final temperature T_f ($^\circ$C)	27	29	36	50
Final intensity I_f (A)	0.95	1.12	2.30	4.00

two following equations (**Equation** (4.4) and (4.5))make it possible to evaluate the dissipated power (P) in relation to the stirring speed (N) and stirring diameter (D) in the only case of geometric similarity between the two systems [152].

$$P = N^3 \times D^2 \tag{4.4}$$

$$\frac{h}{H} = \frac{d}{D} = \frac{l}{L} \tag{4.5}$$

h,l,d and H,L,D are the height and width of the tank, and the length of the magnetic bar respectively for both the electrolytic cell and its extrapolated cell. The first assays carried out under control of bath temperature used cooling stirring. Nevertheless the minimum limit of agitation of the cooling stirring was about 400 rpm while the stirring calculated following the dissipated power equation was about 230 rpm. The results have shown higher homogeneity than the nanostructure obtained before however a few trace of delamination are still noticeable by SEM analysis. Others experiments are currently in progress.

4.4 Conclusion

This chapter is devoted to the medical applications of this nano-surface produced using the anodising process. Dental implant applications have been performed with success and show promising results for *in vivo* osseointegration. In addition, the unit treatment process was validated in 2013 by a certified organisation (G-MED) for nanostructuring for both dental and orthopaedic applications. Although this surface treatment has also demonstrated good results for soft tissue integration experimentation on tracheal prostheses has nevertheless

revealed the issue of mechanical adhesion of the nanostructured layer to the titanium substrate.

GENERAL DISCUSSION

This thesis consisted in developing an innovative surface treatment for medical titanium implant applications. Two *in vivo* studies performed in rabbits have shown that our TiO_2 honeycomb surface may enhance bone healing quality than non-treated surfaces. Moreover, our rough nano-surface provided similar biolocal responses as the rougher conventional surfaces used in dentistry, made by grit-blasting and acid-etching (0.5 *vs* 1.5 μm). Thus, nano-surfaces could be an alternative to excessively rough surfaces which are difficult to clean up for bacterial decontamination as in the case of peri-implantitis on dental implants [67, 153].

Nowadays, infection is the most severe complication associated with the use of biomaterials and causing implant failures. In the dental field, peri-implantitis is observed at 14% after 5 years and the rate increases with time and the first septic failure [154]. In orthopaedics, percutaneous fixation implants have a high risk of colonisation by the bacteria naturally present at the skin-implant interface and virulent bacteria (i.e. Staphylococcus aureus) can lead to high complications [8, 9, 155]. Although the ideal surface for achieving rapid osseointegration has still not been found, it cannot derogate from the constraints of biological healing limits. Recently, research has also been oriented towards the bacterial infection problem by providing bactericidal or bacteriostatic surfaces for titanium implants. There are many strategies for introducing antibacterial agents on to the titanium surface: metal doping [156], growth a TiO2 layer doped [157] or realized a doped coating [158].

Titania nanotube surfaces have been shown to reduce bacterial attachment by TiO_2 high photocatalytic activity under UV light [[159]. However, other methods have been looked at for antibacterial performances without using the

photocatalytic property. As has already been discussed in the additional discussion of Article N° 2, titania nanostructures are suitable as reservoirs for storing growth factor as well as antibacterial agents. Moom Sinn also suggested covering the nanoporosity using chitosan film in order to encapsulate the drug in order to achieve longer release times [160].

Optimising nanostructured surfaces for antimicrobial activity has also been proposed by using the incorporation of elements. There are several "antibacterial metals", such as silver ions as well as mercury, copper, cobalt, vanadium, iron, lead, zinc, and aluminium. Silver nanoparticles have demonstrated antibacterial effects and are potentially less toxic than the others. These nanoparticles are already widely used in antiseptic dressings, antibacterials for catheters as well as surface coatings. For instance, Medicoating already manufactures antibacterial hydroxyapatite powders containing silver particles, known for their antibacterial properties and lesser toxicity. This powder is intended to be used for coatings using the plasma spraying technique or surface blasting producing respectively a prolonged or flash antibacterial effect. Incorporation of silver elements into the surface have also already been been performed using ions implantation, hydrothermal, soaking, sputtering or directly include in electrolyte of anodisation [161, 162, 163, 164, 165, 166].

The applications for Zn-incorporated biomaterials in tissue engineering are currently developing. Zinc has the particularity of being both antibacterial by Zn^{2+} release and stimulation of osseointegration [33, 34]. Zinc ions are the cofactor for matrix metalloproteinase [35] leading to anabolic effects on bone metabolism by stimulating osteoblast proliferation and mineralisation [167, 168, 169, 170]. However, the effects are dose-dependent. An overdose of the element can be cytotoxic. Its minimum inhibitory concentration (MIC) and the Lethal Doses 50 are about 768 $\mu g/ml$ and 3.6×10^{-3} respectively for Zn^{2+} to 2000-5000$\mu g/ml$ reported for ZnO nanoparticles [171].

Zinc element have been already incoporated into titania nanostructure using mainly a two-step method of anodisation and hydrothermal treatment [33, 172, 34]. As proposed by Ghicov *et coll.*, phosphorous species have been successfully incorporate by the simple method of adding phosphorous components into the electrolyte bath during nanotubes formation [173]. Thus, the insertion of this zinc element in our nanostructure have been tried using both ways of incorporation by electrolyte modification, and dip coating. The aim of this second surface treatment was to obtain the highest zinc concentration in the TiO_2 nanostructure with an easy industrial process as compared to the hydrothermal method. ZnO nanoparticles are soluble in acid solutions, but zinc incorporation during the synthesisation of titania nanotubes could be a mean of forming the oxide layer with zinc titanate compounds of $ZnO - TiO_2$ such

as the $ZnTiO_3$ phase which is formed by heating at 500 $^\circ$C [174, 175].

The first assays were carried out by incorporating zinc into the electrolyte adding 0.1, 0.25, 0.50 and 1M of zinc acetate powder. XPS analysis of the surface did not make ZnO /Zn readily perceivable and thus the determination of the presence of zinc titanate compounds. However, the nanostructure formed revealed a heterogeneous nanostructure as well as distribution of the zinc **??**. Heterogeneity of element repartition has also been observed by Zhao et al. which found silver incorporation from 1.24 at % near the surface while only 0.2 at % was obtained at a depth of 3 μm [163]. However, though zinc acetate did not change the chemical composition of the bath, it interacted with the HF leading to the formation of ZnF_2 species and an increase in the pH of the electrolytes. Thus, the thickness of the oxide layer formed was 5 times higher than in standard conditions (150 nm vs 700 nm) leading to a weaker adhesion nanostructured layer on the titanium substrate. This observation seems to go against Crawford et al. The theory that delamination only occurred in films thinner than 600-650 nm [176].

However it is not proven that zinc element is not linked to this mechanical instability like fluoride species [146, 26]. Zinc release was studied on titania disks treated with both zinc incorporation into the electrolyte and dip-coating into a solution of zinc acetate followed by annealing.

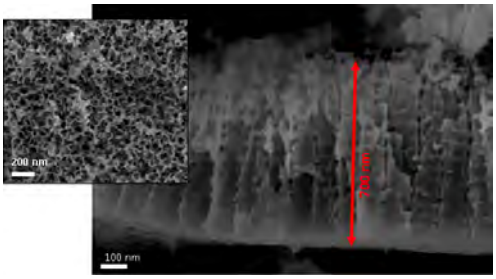

Figure 4.23: SEM micrographs of the top and the cross section of the nanostructure obtained by adding in 1M zinc acetate into the electrolyte

The results show a total release of zinc before 24h with a total amount of 208 ($\pm$10) $\mu g/L$ while the minimum inhibitory concentration (MIC) was about 800 $\mu g/L$ [171]. The disadvantage is that zinc required higher concentrations to induce antibacterial effects while only ppm are necessary for silver nano-particles. Silver efficiency has been confirmed by Mei *et coll.*, and Zhao *et al.* respectively incorporated silver by ion implantation at 1kV into titania nanostructures and by soaking in $AgNO_3$ solutions after the anodising and annealing treatment [161, 163].

Although silver nano-particles are generally low risk to humans via exposure

by inhalation, oral, subcutaneous or intravenous consumption, it is currently a widely controversial issue as fundamental research has shown the potential of this nanomaterial to produce cytotoxic effets. There are new fears of sanitary problems regarding the exponential increase in advanced new nanotechnology. Their application is multidisciplinary and is particularly relevant in the field of medicine with an expected growth rate of 14% per year [177]. The field of medical devices has been regulated for more than 20 years by the European Directives 93/42/CE (medical devices) and 90/385/CE (active implantable medical devices). Thus, according to Directive 93/42/CE, medical devices are classified according to the level of risk (period of use, invasiveness, active device, etc.) into four classes : Class I for low risk, class IIa and IIb for high risk (i.e. dental implants) and class III for high risk and contact with the central nervous system or incorporating a therapeutic substance such as silver nanoparticles. In few, European Directive 93/42 will be replaced by a new regulation from the European Parliament and the Council on medical matters including the new issue of medical devices incorporing nanomaterial. A nanomaterial was defined by *the official journal of european union* of 2011 as "A natural, incidental or manufactured material containing particles, in an unbound state or as an aggregate or as an agglomerate and where, for 50 % or more of the particles in the number size distribution, one or more external dimensions is in the size range 1 nm - 100 nm". This definition includes nano-particule and material that is incorporated and structured at the nanometric scale such as our nanostructured surface created via anodisation treatment. Rule 19 of the new Europeenne regulation stipulates that all medical devices incorporating nanomaterials or are made now will be part of class III and shall not be exempt from clinical investigation [178].

This new regulation may be an obstacle for the development and marketing of this nano-surface treatement, which mainly interests dental implant manufacturers. Nanostructured dental implants should be switched from class IIb to class III, requiring further clinical investigation and therefore a higher cost as compared to other micrometric surface treatments with similar biolocal responses. However, rule 19 also has some exclusion clauses such as the nanomaterial that is encapsulated or attached and cannot be released into the body of the patient or user when the device is used for its intended purpose.

Although our current surfaces have mechanical adhesive problems, the solution for avoiding the potential problems associated with Rule 19 would be to improve the mechanical properties of nanostructured oxide layers, thus limiting particle emissions as much as possible. Besides that, abrasion of the untreated implant surface is unavoidable. Particle emissions from wear in non-treated implants have already been noted and are mentioned in the SCENIHR (Scientific

Committee on Emerging and Newly Identified Health Risk, Procedure adopted in January, 2015) guide [179].

It may also be possible that manufactured medical devices which do not contain nanomaterials may also switch directly into class III because they can leach particles. For instance, the wear rate of the polyethylene is generally of the order of 100 microns / year, generating billions of particles of a few micrometers. Metal debris is smaller, between 10 and 90 nm and is released at a rate ranging from 10^{12} -10^{14} particles per year in a metal-on-metal implant [180]. In the case of dental implants, there is no metal couple, however surface particles could be emitted during implant insertion even with a non-treated implant and might explained some implants failures [181, 182, 183]. Finally, the current issues will be to know the tests recommended by the regulation for demonstrating the attachment of the nanosurface to the implants. Unfortunately, it is very premature to know with any certainty if it will be possible for us to derogate from rule 19 with as the law has not yet been adopted and probably will not be for another few months.

GENERAL CONCLUSION & PERSPECTIVES

This thesis focused on surface treatments for titanium implants used for both soft and hard tissues integration in the aim of offering an innovative surface treatment for better clinical success. This work have been supported financially by the company Biomedical Tissues and the "Association Nationale de la Recherche et de la Technologie"(ANRT).

This manuscript first centred on briefly presenting the titanium material as well as its applications in the field of medicine associated with integration issues leading to implant failure. The processes and limitations of micrometric surface modifications currently commercialised were then described and made it possible to introduce a new approach to surface treatment by means of nanoscale modification. Nano-modification of surfaces mimics bone architecture and may modulate cell behaviour by the phenomenon of mechanotransduction. The book chapter inserted in the first chapter of this thesis gives the state of the art on anodising surface treatments, which despite its simplicity in terms of equipment reveals wide complexity in terms of the influences of parameters on the nanostructure formation and morphology. Thus, in the second chapter, process configuration and fixed parameters (i.e. electrolytes) were displayed. As titanium is used as a biomaterial, it required multi-scale characterisation from both materials science - for the surface characterization techniques used (SEM, CA, RAMAN,XPS, AFM) and for the different issues related to measurement of the mechanical adhesion of the nanostructured oxide layer - and biology for biocompatibility using an *in vivo* study.

The electrochemical process of anodisation using first generation electrolytes

with 1 % wt. HF made it possible to rapidly grow a nanostructured titanium dioxide layer of titanium substrate. This structure presented an easily controllable pore size, good uniformity, a thickness of around 150 nm and did not change the initial roughness of the titanium surface. By modifying the voltage (potentiostatic mode), it is possible to control the colour of the surface and form nanopore arraya at 10 V or nanotubes aligned perpendicularly at 20 V. These two structures show different wettability behavioura, as well as crystalline structure composition (anatase, rutile) after the annealing treatment. XPS analysis showed migration of fluoride ions through the porous layer of the titanium dioxide induced by anodisation. This fluoride-rich layer could have been an asset for bone healing, but these fluoride titanium species are responsible for the weak adhesion of nanostructures in aqueous solution. The annealing treatment at 500 ° C reduced fluoride insertion but was not enough to avoid particle release and ensure mechanical strength and wear as shown in chapter 4.

Part of this thesis also included biological characterisation by comparison of osseointegration using two studies carried out in a rabbit model. Both studies were carried out using homemade samples and dental implants have shown promising biocompatibility results similar to those of conventional grit-blasted and acid-etched surfaces and higher bone anchorage than machined surfaces. The optimisation of the nanostructured surfaces has been evoked to reduce bacterial infection, which is the cause of most implant failures. Zinc combines both antibacterial activity and anabolic effects on bone metabolism. The first results of zinc incorporation into titania nanostructures did not make possible a sufficient concentration for it to be a minimum inhibitor for bacterial concentration but it could still be a promising surface for medical applications.

From an industrial point of view, this surface treatment has been applied in dental and tracheal implants with more or less success. The unit treatment process was validated in 2013 by a certified organisation (G-MED) for nanostructuring for both dental and orthopaedic applicatiosn while delamination of the nanosized oxide layer was observed for anodised tracheal implants. Although an improvement in the mechanical strength of the surface is possible, the new European regulation regarding medical devices including nanomaterials could be a restriction for the use of this treatment in medical applications.

In the short term, it would be interesting to study other nanostructures. Although we have shown relatively good results of biocompatibility and bioactivity, the optimal nanostructure have not been find. As shown by Menon *et al.*, at the nanoscale, different nano-design could induce different cells behavior [29]. Moreover, others perspectives concern the optimization the nano-surface.

As shown in several studies, crystal structure of TiO_2 play a role on surface bioactivity [30, 31]. Thus, it could be interesting to study the best composition or mixture of crystalline structure (anatase, brookite, rutile) to enhance implant integration with hard and soft tissues. Then, Kim *et coll.*,have shown zeta potential of TiO_2 nanotubes could depend on the pH of the electrolyte [32]. Using a third generation electrolyte, they found a positive surface charge at pH 3 while at higher pH values, the surface charge was negative. A negative charge on implants surface may attrack positive ions required for bone formation such as calcium, phosphorus, zinc, etc. Thus the combination of nano-surface design, crystal structure, surface charge and composition (antibacterial agents) may be a new line of research for inducing long-term clinical implant success.

The second outlook for this work is to understand the lack of mechanical adhesion of TiO_2 nanostructures on titanium substrates. Probably related to the mechanical properties, the process should be improved to take under control all the anodic parameters and thus facilitate scaling up to an industrial scale.

Finally, the long-term prospects are difficult to identify in view of the regulations which are currently evolving. The use of this process for medical applications may become more complex, expensive and dependent on demand: no client, no development. Moreover, as noticed during the three years of this thesis, nanosurfaces inspire either interest and curiosity for implant manufacturers, or fear. Although, this innovative surface is a marketing asset, no one wants to be the first to take risks. This attitude may be to the result of the previous sanitair scandal (i.e. PIP prostheses, hydroxyapatite coatings). Companies thus prefer to improve current surface treatment technology rather than use new possibilities. However, with time and pre-clinical trials, things may change.

Appendices

APPENDIX A

Materials and Methods : Basic work principle of methods for surface characterisation

Basic work principle of Scanning Electron Microscope (SEM) – A focused electron beam scans across the surface of the sample and generates secondary electrons (SE), backscattered electrons (BSE) and characteristic X-rays. The secondary electrons (SE) are obtained by inelastic collisions between primary electrons (the beam) and the sample. It produces a topographical image of the sample. Unlike secondary electrons, backscattered electrons (BSE) originate from elastic interaction of the beam with the nucleus of an atom in the specimen analysed. Because the number of backscattered electrons is proportional to the atomic number of the elements (Z), the image obtained depicts a high resolution compositional map: high Z elements appear brighter than those with low Z. The X-rays produced are used for analysis of the composition by means of EDX microanalysis.

Basic work principle of Atomic Force Microscopy (AFM) – Atomic Force Microscopy (AFM), a non destructive technique, provides a better topography contrast than SEM images and topographical quantification. A tip, usually made from Si, is mounted at the end of a flexible cantilever. It scans the surface of the sample following different modes. The bending movement of the cantilever is measured using a laser reflexion method and thus provides a nanoscale 3D profile of the surface. The main limitation of this technique is that it depends on the sharpness of the tip. The AFM images reflect the interaction of the probe with the sample surface and not the true sample topography: this is called tip convolution. In addition, the small-sized area that is scanned is not representative of the analysed area.

Basic work principle of roughness tester – Roughness tester is a less precise technique, but more representative of the surface than AFM analysis. This non destructive measurement is performed by moving a diamond probe along a straight line on the sample surface. The device measures the height variations of the arm holding the tip that moves on the surface along a longitudinal line

to determine basic roughness parameters (see 2.2.2).

Basic work principle of wettability measured by contact angle – Contact angle (CA) measurement is a basic technique for the characterising surface treatment no matter the field of application. It reports the aptitude of liquid to be spread over a surface by wettability. The method consists of measuring the angle between the tangent from the profile of a drop deposited on the substrate, with the substrate surface itself: the angle is called the contact angle (θ). Using water it is possible to determine the hydrophilic (θ <90 $^\circ$) or hydrophobic nature (θ >90 $^\circ$) of the surface. It is also possible to calculate the surface energy of a solid surface by a liquid, with physical units characterised using the Young equation (**Equation** (6)).

$$-\gamma_(SV) + \gamma_(SL) + \gamma_(LV)\cos(\theta) = 0 \tag{6}$$

The components $\gamma_(SV)$, $\gamma_(SL)$ and $\gamma_(LV)$ are interfacial tension computable using liquids with different polar, non-polar and dispersive components depending on the selected model resolution to determine the unknown in the Young equation (Neumann, Owens and Wendt, Van Oss Good).

Basic work principle of X-ray photoelectron spectroscopy (XPS) – In XPS, the sample is irradiated with monochromatic X-rays in an ultrahigh vacuum. The ionisation of its atoms by photoelectric effect caused by this solicitation leads to the production of photoelectrons. E_K The kinetic energy of these photoelectrons is measured and, knowing the initial photon energy $h\nu$, the binding energies E_B of the photoelectrons EB can be plotted on a spectrum using the Einstein **Equation** (7). Peak XPS are characteristic of the atom, and its chemical environment (e.g. oxidation) can be observed as a variation of energy (displacements of the XPS peak).

$$E_K = h\nu - E_B \tag{7}$$

This technique is used to analyse the chemical composition of a surface sample to a depth ranging from 1 nm to 10 nm. The nature of the chemical bonds and the atomic percentages are obtained by data processing. All elements except hydrogen and helium are detectable. This analysis technique is non-destructive, except in case of ionic erosion used to obtain a depth profile thicknesses of the micrometer long. The main advantage of this device is that it makes it possible to precisely identify the elements with a relative concentration of less than 0.1 atomic%. However, the drawback of this technique is that it is difficult to access and it has large spot analysis (300 x 700 μm^2) which

does not make possible to target the analysis.

Basic work principle of Raman spectroscopy – Raman spectroscopy makes it possible to characterise the molecular structure and chemical composition of solid, liquid or gaseous samples, without destruction or any need for special preparation. The irradiation of a sample with a monochromatic light (laser) causes an elastic and inelastic scattering of photons. The resulting spread spectrum is mainly composed of the same frequency as the incident beam (Rayleigh scattering). However a part of the spread spectrum corresponds to network of modified spectra called the Raman spectrum (stokes lines to create vibrations, anti-stokes for destroying vibrations).

APPENDIX B

ImageJ : Semi-automatic calculation of histomorphometric parameters

(Return to chapter 2)

We have created a macro for semi-automatic calculation of histomorphometry calculation using ImageJ software. By thresholding bone (in light grey) and implant (in white) included in resin (in dark grey), it makes it possible to directly calculate the percentages of bone growth (% BG) and bone surface at 0.5 mm around the implant (% BS/TS 0.5 mm) (**Figure ??**)

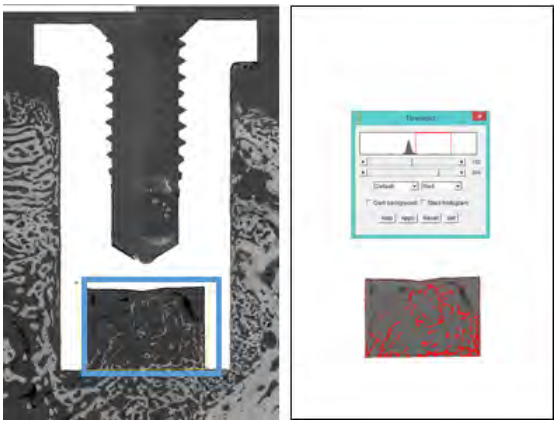

Figure 24: Principle of calculation of the percentages of bone growth (% BG) in the growth chamber using the semi-automatic macro created on ImageJ software

Calculation of the percentages of bone to implant contact (% BIC) is carried out by the ratio for calculating the length (for 1 pixel wide, perimeter= length/2) of the edge of the implant and the contact of the bone (**Figure 26** and **Table 13**)

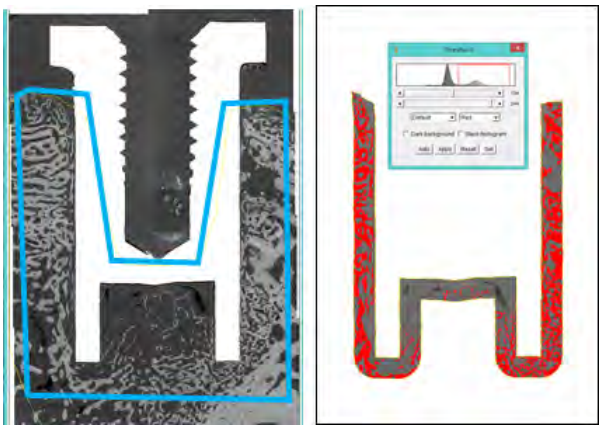

Figure 25: Principle of calculation of the percentage of bone surface at 0.5 mm around the implant (% BS/TS 0.5 mm) using the semi-automatic macro created on ImageJ software

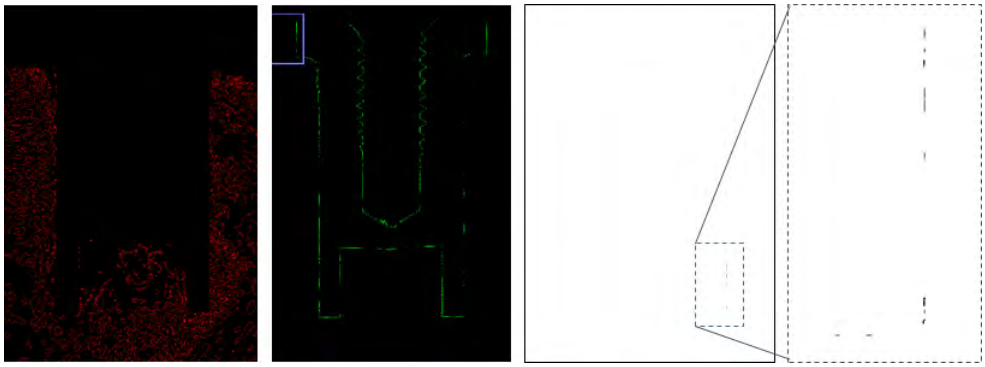

Figure 26: Principle of calculation of the percentage of bone to implant contact (% BIC) using the semi-automatic macro created on ImageJ software

Table 13: calculation of the percentage of bone to implant contact

Output datas			**Calculation**	
Image	count (C)	Perimeter (P)	Total length (L) $= \frac{P \times C}{2}$	BIC
Total Implant	2	12192	12192	21 %
Contact B/I	40	129	2572	

```
//Selection of the INPUT and OUTPU DATAS
path=getDirectory("Select the folder of  data to be analysed");
list=getFileList(path);
savepath=getDirectory("Select the folder to save the analysis");

for(i=0;i<list.length;i++){
open(path+list[i]);

//Improvement of  the image quality
run("8-bit");
run("Enhance Contrast...", "saturated=0.4");
run("Set Measurements...", "area perimeter area_fraction display redirect=None decimal=3");
run("Set Scale...", "distance=0 known=0 pixel=1 unit=pixel global");
setTool("freehand");

//Creation of the element for measurement
run("Select None");
run("Duplicate...", "title=implant");
run("Duplicate...", "title=BG");
run("Duplicate...", "title=BS/TS0.5mm");
run("Duplicate...", "title=BIC");

//Selection of the implant
selectWindow("implant");
setTool("wand");
run("Wand Tool...", "mode=Legacy tolerance=30");
beep();
title = "Selection de l'implant";
message = "Select the implant and click on OK";
waitForUser(title,message);
roiManager("Add");

// Selection of the growth chamber
selectWindow("implant");
run("Select None");
setTool("polygon");
beep();
title = " Growth chamber ";
message = "Select the growth chamber and click on OK";
waitForUser(title,message);
roiManager("Add");

// Quantification of BG
selectWindow("BG");
roiManager("Select", newArray(0,1));
roiManager("AND");
roiManager("Add");
run("Select None");
roiManager("Select", newArray(1,2));
roiManager("XOR");
roiManager("Add");
selectWindow("BG");
roiManager("Select", 3);
run("Clear Outside");
run("Select None");
run("Threshold...");
title = "Threshold";
msg = "If necessary, use the \"Threshold\" tool to\nadjust the threshold, then click \"OK\".";
waitForUser(title, msg);
 selectWindow("BG");
 getThreshold(lower, upper);
  if (lower==-1)
     exit("Threshold was not set");
run("Convert to Mask");
run("Close-");
run("Erode");
run("Erode");
run("Dilate");
run("Dilate");
roiManager("Select", 3);
run("Set Measurements...", "area area_fraction display redirect=None decimal=3");
run("Measure");
selectWindow("BG");
close();

// Quantification of Bone surface at 0.5mm
selectWindow("implant");
roiManager("Select", 0 );
run("Enlarge...", "enlarge=185");
roiManager("Add");
run("Select None");
selectWindow("implant");
setTool("freehand");
beep();
title = "Zone of interest ";
message = " Select the zone of interest (the portion of the implant inserted into bone) and click on OK";
waitForUser(title,message);
roiManager("Add");
selectWindow("BS/TS0.5mm");
roiManager("Select", 0 );
run("Clear", "slice");
run("Select None");
roiManager("select", 4);
setBackgroundColor(255, 255, 255);
run("Clear Outside");
roiManager("Select", newArray(4,5));
roiManager("AND");
```

```
roiManager("Add");
roiManager("Select", newArray(0,6));
roiManager("AND");
roiManager("Add");
roiManager("Select", newArray(7,6));
roiManager("XOR");
roiManager("Add");
run("Clear Outside");
roiManager("Select", 8 );
run("Threshold...");

// Image threshold
title = "Threshold";
msg = "If necessary, use the \"Threshold\" tool
to\nadjust the threshold, then click \"OK\".";
waitForUser(title, msg);
 selectWindow("BS/TS0.5mm");
 getThreshold(lower, upper);
  if (lower==-1)
     exit("Threshold was not set");
run("Convert to Mask");
run("Close-");
run("Erode");
run("Erode");
run("Dilate");
run("Dilate");
roiManager("Select",8 );
roiManager("Measure");
selectWindow("BS/TS0.5mm");
close();

// Saving data
name = "Results"+list[i]+".xls";
 selectWindow("Results");
  saveAs("Results", savepath+name);
            if (isOpen("Results")) {
        selectWindow("Results");
        run("Close" );}

//  Calculation of Bone to Implant Contact
selectWindow("BIC");
run("Select None");
run("Duplicate...",
"title=implant_contact_Enlarge");
run("Duplicate...","title=os_contact");
run("Duplicate...", "title=implant_contact_Dilate");
selectWindow("BIC");
close();

// To remove the effect of resin embedding :
#METHOD1- Enlarge the implant
selectWindow("implant_contact_Enlarge");
roiManager("Select", 0 );
run("Enlarge...", "enlarge=1");
run("Fill", "slice");
run("Clear Outside");
run("Select None");
run("Find Edges");
roiManager("Select", 5 );
run("Make Inverse");
run("Fill", "slice");
run("Select None");
roiManager("Select", 3);
run("Fill", "slice");
run("Select None");
run("Green");
run("Invert");
run("Set Measurements...", "area perimeter
area_fraction display redirect=None decimal=3");
run("Analyze Particles...", "size=0-Infinity
circularity=0.00-1.00 show=Nothing summarize");
selectWindow("implant_contact_Enlarge");
run("Duplicate...",
"title=implant_contact_enlargebis");
selectWindow("implant_contact_enlargebis");
run("Invert");

// To remove the effect of resin embedding :
#METHOD2- Dilate the implant
selectWindow("implant_contact_Dilate");
roiManager("Select", 0 );
run("Fill", "slice");
run("Clear Outside");
run("Select None");
run("Find Edges");
roiManager("Select", 5 );
run("Make Inverse");
run("Fill", "slice");
run("Select None");
roiManager("Select", 1 );
run("Fill", "slice");
run("Select None");
run("Green");
run("Invert");
setOption("BlackBackground", false);
run("Dilate");
run("Set Measurements...", "area perimeter
area_fraction display redirect=None decimal=3");
run("Analyze Particles...", "size=0-Infinity
circularity=0.00-1.00 show=Nothing summarize");
selectWindow("implant_contact_Dilate");
run("Duplicate...",
"title=implant_contact_dilatebis");
selectWindow("implant_contact_dilatebis");
run("Invert");
```

// Bone threshold and Find edge

```
selectWindow("os_contact");
run("Select None");
roiManager("Select", 0 );
run("Clear", "slice");
run("Select None");
run("Threshold...");
//open Threshold tool
title = "Threshold";
msg = "If necessary, use the \"Threshold\" tool
to\nadjust the threshold, then click \"OK\".";
waitForUser(title, msg);
 selectWindow("os_contact");
 getThreshold(lower, upper);
  if (lower==-1)
     exit("Threshold was not set");
run("Convert to Mask");
run("Close-");
run("Erode");
run("Erode");
run("Dilate");
run("Dilate");
roiManager("Select", 5);
run("Make Inverse");
run("Clear", "slice");
run("Select None");
run("Find Edges");
run("Red");
```

// BIC measurement

```
imageCalculator("Multiply create",
"implant_contact_enlargebis","os_contact");
run("Invert");
run("Analyze Particles...", "size=0-Infinity
circularity=0.00-1.00 show=Nothing summarize");

imageCalculator("Multiply create",
"implant_contact_dilatebis","os_contact");
run("Invert");
run("Analyze Particles...", "size=0-Infinity
circularity=0.00-1.00 show=Nothing summarize");
```

// Saving data

```
name = "Summary"+list[i]+".xls";
 selectWindow("Summary");
  saveAs("Results", savepath+name);
            if (isOpen("Summary")) {
        selectWindow("Summary");
        run("Close" ); }
```

// Close windows

```
selectWindow("implant_contact_Enlarge");
close();
selectWindow("implant_contact_enlargebis");
close();
selectWindow("os_contact");
close();
selectWindow("implant");
close();
selectWindow("ROI Manager");
run("Close");
selectWindow("Threshold");
run("Close");
selectWindow("implant_contact_Dilate");
close();
selectWindow("implant_contact_dilatebis");
close();
selectWindow("Result of
implant_contact_enlargebis");
close();
close();
close();}
```

APPENDIX C

Medical applications : Holder for anodisation of tracheal template and prothesis

(Return to chapter 4)

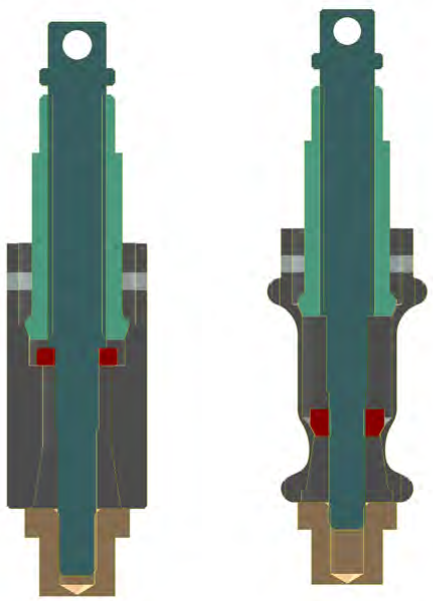

(a) (b)

Figure 27: Diagram of the holder used for treatment of anodisation on tracheal templates and prostheses. It consists of the assembly of several components: tracheal templates and prostheses (in grey) are sealed at both extremities with two pieces of Teflon (in green and brown) and electrically connected using a titanium washer (in red) all mounted on a titanium threaded rod (in blue) that can be adjusted in relation to the sample size (small or normal)

LIST OF FIGURES

LIST OF TABLES

BIBLIOGRAPHY

[1] HAUTE AUTORITE DE SANTE (HAS). Rapport d'évaluation : Prothèses de hanche, phase contradictoire suite à la révision d'une catégorie de dispositifs médicaux. 2014.

[2] HAUTE AUTORITE DE SANTE (HAS). Rapport d'évaluation : Implants articulaires du genou, révision des descriptions génériques de la liste des produits et prestations remboursables. 2012.

[3] HAUTE AUTORITE DE SANTE (HAS). Conditions de realisation des actes d?implantologie orale : environnement technique. 2008.

[4] Hua Ling Sun, Cui Huang, Yan Ru Wu, and Bin Shi. Failure rates of short dental implants and factors influencing their failure: a systematic review. *The International Journal of Oral & Maxillofacial Implants*, 26(4):816–825, August 2011.

[5] Carlos Nelson. Factors Affecting the Success of Dental Implants. In Ilser Turkyilmaz, editor, *Implant Dentistry - A Rapidly Evolving Practice*. InTech, August 2011.

[6] P. I. Branemark, R. Adell, U. Breine, B. O. Hansson, J. Lindstram, and A. Ohlsson. Intra-osseous anchorage of dental prostheses. I. Experimental studies. *Scandinavian Journal of Plastic and Reconstructive Surgery*, 3(2):81–100, 1969.

[7] Yasuyuki Shibuya, Masaki Kobayashi, Junichiro Takeuchi, Tomoko Asai, Maho Murata, Masahiro Umeda, and Takahide Komori. Analysis of 472 Branemark system TiUnite implants:a retrospective study. *The Kobe Journal of Medical Sciences*, 55(3):E73–81, 2009.

[8] Davide Campoccia, Lucio Montanaro, and Carla Renata Arciola. A review of the clinical implications of anti-infective biomaterials and infection-resistant surfaces. *Biomaterials*, 34(33):8018–8029, November 2013.

[9] R. Branemark, O. Berlin, K. Hagberg, P. Bergh, B. Gunterberg, and B. Rydevik. A novel osseointegrated percutaneous prosthetic system for the treatment of patients with transfemoral amputation: A prospective study of 51 patients. *The Bone & Joint Journal*, 96-B(1):106–113, 2014.

[10] Tung Nguyen-Hieu, Alain Borghetti, and Gerard Aboudharam. Peri-implantitis: from diagnosis to therapeutics. *Journal of Investigative and Clinical Dentistry*, 3(2):79–94, 2012.

[11] Rolando A. Gittens, Rene Olivares-Navarrete, Alice Cheng, David M. Anderson, Taylor McLachlan, Ingrid Stephan, JÃ$\frac{1}{4}$rgen Geis-Gerstorfer, Kenneth H. Sandhage, Andrei G. Fedorov, Frank Rupp, Barbara D. Boyan, Rina Tannenbaum, and Zvi Schwartz. The Roles of Titanium Surface Micro/Nanotopography and Wettability on the Differential Response of Human Osteoblast Lineage Cells. *Acta biomaterialia*, 9(4):6268–6277, April 2013.

[12] L Le GuÃ©hennec, A Soueidan, P Layrolle, and Y Amouriq. Surface treatments of titanium dental implants for rapid osseointegration. *Dental materials: official publication of the Academy of Dental Materials*, 23(7):844–854, 2007.

[13] C M Stanford. Surface modifications of dental implants. *Australian dental journal*, 53 Suppl 1:S26–33, June 2008.

[14] Rudiger Junker, Athanasios Dimakis, Maurice Thoneick, and John A Jansen. Effects of implant surface coatings and composition on bone integration: a systematic review. *Clinical oral implants research*, 20 Suppl 4:185–206, 2009.

[15] Rolando A. Gittens, Rene Olivares-Navarrete, Zvi Schwartz, and Barbara D. Boyan. Implant osseointegration and the role of microroughness and nanostructures: lessons for spine implants. *Acta Biomaterialia*, 10(8):3363–3371, August 2014.

[16] John E. Davies. Bone bonding at natural and biomaterial surfaces. *Biomaterials*, 28(34):5058–5067, December 2007.

[17] John E. Davies. Understanding peri-implant endosseous healing. *Journal of Dental Education*, 67(8):932–949, August 2003.

[18] Z. Schwartz and B. D. Boyan. Underlying mechanisms at the bone-biomaterial interface. *Journal of Cellular Biochemistry*, 56(3):340–347, November 1994.

[19] Rowena McBeath, Dana M. Pirone, Celeste M. Nelson, Kiran Bhadriraju, and Christopher S. Chen. Cell shape, cytoskeletal tension, and RhoA regulate stem cell lineage commitment. *Developmental Cell*, 6(4):483–495, April 2004.

[20] Matthew J. Dalby, Nikolaj Gadegaard, Rahul Tare, Abhay Andar, Mathis O. Riehle, Pawel Herzyk, Chris D. W. Wilkinson, and Richard O. C. Oreffo. The control of human mesenchymal cell differentiation using nanoscale symmetry and disorder. *Nature Materials*, 6(12):997–1003, December 2007.

[21] Lucie Bacakova, Elena Filova, Martin Parizek, Tomas Ruml, and Vaclav Svorcik. Modulation of cell adhesion, proliferation and differentiation on materials designed for body implants. *Biotechnology advances*, 29(6):739–767, December 2011.

[22] Jung Park, Sebastian Bauer, Klaus von der Mark, and Patrik Schmuki. Nanosize and vitality: TiO2 nanotube diameter directs cell fate. *Nano Letters*, 7(6):1686–1691, June 2007.

[23] Seunghan Oh, Karla S. Brammer, Y. S. Julie Li, Dayu Teng, Adam J. Engler, Shu Chien, and Sungho Jin. Stem cell fate dictated solely by altered nanotube dimension. *Proceedings of the National Academy of Sciences*, page pnas.0813200106, January 2009.

[24] Ingela Petersson, Kristina Junemo-Bostrom, Gunilla Johansson-Ruden, Fredrik Andersson, Stig Hansson, and Jan-Eirik Ellingsen. An implant and a method for treating an implant surface, 01 2004.

[25] ; Yao Chang Webster, Thomas J. A method for producing nanostructures on a surface of a medical implant, 03 2009.

[26] Poulomi Roy, Steffen Berger, and Patrik Schmuki. TiO2 Nanotubes: Synthesis and Applications. *Angewandte Chemie International Edition*, 50(13):2904–2939, 2011.

[27] B. Yang, C. K. Ng, M. K. Fung, C. C. Ling, A. B. Djuria, and S. Fung. Annealing study of titanium oxide nanotube arrays. *Materials Chemistry and Physics*, 130(3):1227–1231, 2011.

[28] Stephane Descamps, Komla O. Awitor, Vincent Raspal, Matthew B. Johnson, Roshan S. P. Bokalawela, Preston R. Larson, and Curtis F. Doiron. Mechanical Properties of Nanotextured Titanium Orthopedic Screws for Clinical Applications. *Journal of Medical Devices*, 7(2):0210051–0210055, 2013.

[29] Lakshmanan Vinoth-Kumar V V Divya Rani. Osteointegration of titanium implant is sensitive to specific nanostructure morphology. *Acta biomaterialia*, 8(5):1976–89, 2012.

[30] W. Q. Yu, Y. L. Zhang, X. Q. Jiang, and F. Q. Zhang. In vitro behavior of MC3t3-E1 preosteoblast with different annealing temperature titania nanotubes. *Oral Diseases*, 16(7):624–630, 2010.

[31] A. Mazare, M. Dilea, D. Ionita, I. Titorencu, V. Trusca, and E. Vasile. Changing bioperformance of TiO2 amorphous nanotubes as an effect of inducing crystallinity. *Bioelectrochemistry (Amsterdam, Netherlands)*, 87:124–131, October 2012.

[32] Youngji Kim, Hyunku Joo, Namguk Her, Yeomin Yoon, Chang-Ha Lee, and Jaekyung Yoon. Self-rotating photocatalytic system for aqueous Cr(VI) reduction on TiO2 nanotube/Ti mesh substrate. *Chemical Engineering Journal*, 229:66–71, August 2013.

[33] Elmy Elizabeth, Gaurav Baranwal, Amit G. Krishnan, Deepthy Menon, and Manitha Nair. ZnO nanoparticle incorporated nanostructured metallic titanium for increased mesenchymal stem cell response and antibacterial activity. *Nanotechnology*, 25(11):115101, March 2014.

[34] Yong Li, Wei Xiong, Chengcheng Zhang, Biao Gao, Hanfeng Guan, Hao Cheng, Jijiang Fu, and Feng Li. Enhanced osseointegration and antibacterial action of zinc-loaded titania-nanotube-coated titanium substrates: In vitro and in vivo studies. *Journal of Biomedical Materials Research Part A*, 102(11):3939–3950, 2014.

[35] Keith A. McCall, Chih-chin Huang, and Carol A. Fierke. Function and Mechanism of Zinc Metalloenzymes. *The Journal of Nutrition*, 130(5):1437S–1446S, January 2000.

[36] Tomas Albrektsson Per-Ingvar Branemark, George Albert Zarb. Tissue-integrated prostheses : osseointegration in clinical dentistry. *SERBIULA*.

[37] Bjrn Klinge, Margareta Hultin, and Tord Berglundh. Periimplantitis. *Dental Clinics of North America*, 49(3):661–676, vii–viii, July 2005.

[38] L. Ponsonnet, K. Reybier, N. Jaffrezic, V. Comte, C. Lagneau, M. Lissac, and C. Martelet. Relationship between surface properties (roughness, wettability) of titanium and titanium alloys and cell behaviour. *Materials Science and Engineering: C*, 23(4):551–560, June 2003.

[39] Sandrine Lavenus, Jean-Charles Ricquier, Guy Louarn, and Pierre Layrolle. Cell interaction with nanopatterned surface of implants. *Nanomedicine (London, England)*, 5(6):937–947, August 2010.

[40] Sandrine Lavenus, ValÃ©rie Trichet, SÃ©bastien Le Chevalier, Alain Hoornaert, Guy Louarn, and Pierre Layrolle. Cell differentiation and osseointegration influenced by nanoscale anodized titanium surfaces. *Nanomedicine (London, England)*, 7(7):967–980, 2012.

[41] Karla S. Brammer, Christine J. Frandsen, and Sungho Jin. TiO2 nanotubes for bone regeneration. *Trends in Biotechnology*, 30(6):315–322, June 2012.

[42] Naside Gozde Durmus and Thomas J Webster. Nanostructured titanium: the ideal material for improving orthopedic implant efficacy? *Nanomedicine (London, England)*, 7(6):791–793, June 2012.

[43] Young-Taeg Sul. Electrochemical growth behavior, surface properties, and enhanced in vivo bone response of TiO2 nanotubes on microstructured surfaces of blasted, screw-shaped titanium implants. *International Journal of Nanomedicine*, 5:87–100, 2010.

[44] Jae-Kwan Lee, Dong-Soon Choi, Insan Jang, and Won-Youl Choi. Improved osseointegration of dental titanium implants by TiO2 nanotube arrays with recombinant human bone morphogenetic protein-2: a pilot in vivo study. *International Journal of Nanomedicine*, 10:1145–1154, February 2015.

[45] Frederick J. Schoen Jack E Buddy D. Ratner, Allan S. Hoffman. Biomaterials science: An introduction to materials in medicine. *Academic Press*, 1996.

[46] M. Niinomi. Recent research and development in metallic materials for biomedical, dental and healthcare products. *Mater. Sci.*, pages 193–200, 2007.

[47] Harun H. Bayraktar, Elise F. Morgan, Glen L. Niebur, Grayson E. Morris, Eric K. Wong, and Tony M. Keaveny. Comparison of the elastic and yield properties of human femoral trabecular and cortical bone tissue. *Journal of Biomechanics*, 37(1):27–35, January 2004.

[48] R. Valiev C.N. Elias, J.H.C. Lima and M.A. Meyers. Biomedical applications of titanium and its alloys. *Journal of the Minerals, metals, and Materials Society*, pages 46–49, 2008.

[49] http://www.arcam.com/wp-content/uploads/arcam-astm-f75-cobalt-chrome.pdf.

[50] http://www.goodfellow.com.

[51] Dorian A. H. Hanaor and Charles C. Sorrell. Review of the anatase to rutile phase transformation. *Journal of Materials Science*, 46(4):855–874, December 2010.

[52] P. I. Branemark, B. O. Hansson, R. Adell, U. Breine, J. Lindstram, O. Hallan, and A. Ohman. Osseointegrated implants in the treatment of the edentulous jaw. Experience from a 10-year period. *Scandinavian Journal of Plastic and Reconstructive Surgery. Supplementum*, 16:1–132, 1977.

[53] S. Anil, P.S. Anand, H. Alghamdi, and J.A. Janse. Dental Implant Surface Enhancement and Osseointegration. August 2011.

[54] E. Ruoslahti. RGD and other recognition sequences for integrins. *Annual Review of Cell and Developmental Biology*, 12:697–715, 1996.

[55] Sangeetha Raghavendra, Marjorie C. Wood, and Thomas D. Taylor. Early wound healing around endosseous implants: a review of the literature. *The International Journal of Oral & Maxillofacial Implants*, 20(3):425–431, June 2005.

[56] T. Albrektsson, E. Dahl, L. Enbom, S. Engevall, B. Engquist, A. R. Eriksson, G. Feldmann, N. Freiberg, P. O. Glantz, and O. Kjellman. Osseointegrated oral implants. A Swedish multicenter study of 8139 consecutively inserted Nobelpharma implants. *Journal of Periodontology*, 59(5):287–296, May 1988.

[57] Giuseppe Corinaldesi, Francesco Pieri, Licia Sapigni, and Claudio Marchetti. Evaluation of survival and success rates of dental implants placed at the time of or after alveolar ridge augmentation with an autogenous mandibular bone graft and titanium mesh: a 3- to 8-year retrospective study. *The International Journal of Oral & Maxillofacial Implants*, 24(6):1119–1128, December 2009.

[58] JohnD Stroncek and MontyW Reichert. *Overview of Wound Healing in Different Tissue Types*. Frontiers in Neuroengineering Series. CRC Press, December 2007.

[59] Evandro Scligliano Amarante, Leandro Chambrone, Roberto Fraga Moreira Lotufo, and Luiz A. Lima. Early dental plaque formation on toothbrushed titanium implant surfaces. *American Journal of Dentistry*, 21(5):318–322, October 2008.

[60] M. Gomez-Florit, R. Xing, J. M. Ramis, S. Taxt-Lamolle, H. J. Haugen, S. P. Lyngstadaas, and M. Monjo. Human gingival fibroblasts function is stimulated on machined hydrided titanium zirconium dental implants. *Journal of Dentistry*, 42(1):30–38, January 2014.

[61] Satoru K. Nishimoto, Miyako Nishimoto, Sang-Won Park, Kwang-Min Lee, Hyun-Seung Kim, Jeong-Tae Koh, Joo L. Ong, Yongxing Liu, and Yunzhi Yang. The effect of titanium surface roughening on protein absorption, cell attachment, and cell spreading. *The International Journal of Oral & Maxillofacial Implants*, 23(4):675–680, August 2008.

[62] Nathalia Marin-Pareja, Emiliano Salvagni, Jordi Guillem-Marti, Conrado Aparicio, and Maria-Pau Ginebra. Collagen-functionalised titanium surfaces for biological sealing of dental implants: effect of immobilisation process on fibroblasts response. *Colloids and Surfaces. B, Biointerfaces*, 122:601–610, October 2014.

[63] Hans-Peter Weber and David L. Cochran. The soft tissue response to osseointegrated dental implants. *The Journal of Prosthetic Dentistry*, 79(1):79–89, 1998.

[64] D. Buser, T. Nydegger, T. Oxland, D. L. Cochran, R. K. Schenk, H. P. Hirt, D. Snativy, and L. P. Nolte. Interface shear strength of titanium implants with a sandblasted and acid-etched surface: a biomechanical study in the maxilla of miniature pigs. *Journal of Biomedical Materials Research*, 45(2):75–83, May 1999.

[65] A. Wennerberg, A. Ektessabi, T. Albrektsson, C. Johansson, and B. Andersson. A 1-year follow-up of implants of differing surface roughness placed in rabbit bone. *The International Journal of Oral & Maxillofacial Implants*, 12(4):486–494, August 1997.

[66] Toshihiro Hara, Kaichi Matsuoka, Kenichi Matsuzaka, Masao Yoshinari, and Takashi Inoue. Effect of surface roughness of titanium dental implant placed under periosteum on gene expression of bone morphogenic markers in rat. *The Bulletin of Tokyo Dental College*, 53(2):45–50, 2012.

[67] Ana Mellado-Valero, Pedro Buitrago-Vera, Maria F. Soli¡-Ruiz, and Juan C. Ferrer-Garcia. Decontamination of dental implant surface in peri-implantitis treatment: A literature review. *Medicina Oral, Patologa Oral y Ciruga Bucal*, 18(6):e869–e876, November 2013.

[68] Wim Teughels, Nele Van Assche, Isabelle Sliepen, and Marc Quirynen. Effect of material characteristics and/or surface topography on biofilm development. *Clinical Oral Implants Research*, 17 Suppl 2:68–81, October 2006.

[69] Zieliski Andrzej and Sobieszczyk Sylwia. CORROSION OF TITANIUM BIOMATERIALS, MECHANISMS, EFFECTS AND MODELISATION.

[70] Maxim Goldman, Gintaras Juodzbalys, and Valdas Vilkinis. Titanium Surfaces with Nanostructures Influence on Osteoblasts Proliferation: a Systematic Review. *Journal of Oral & Maxillofacial Research*, 5(3), October 2014.

[71] Hui Wang Liwen Lin. Enhanced osteointegration of medical titanium implant with surface modifications in micro/nanoscale structures. *Journal of Orthopaedic Translation*, 2(1):35–42, 2014.

[72] Marco Annunziata, Adriana Oliva, Antonietta Buosciolo, Michele Giordano, Agostino Guida, and Luigi Guida. Bone marrow mesenchymal stem cell response to nano-structured oxidized and turned titanium surfaces. *Clinical Oral Implants Research*, 23(6):733–740, June 2012.

[73] Webster TJ. Lu J. Reduced immune cell responses on nano and submicron rough titanium. *Acta Biomaterialia.*, (16):223–231, 2015.

[74] Rolando A. Gittens, Rene Olivares-Navarrete, Taylor McLachlan, Ye Cai, Sharon L. Hyzy, Jennifer M. Schneider, Zvi Schwartz, Kenneth H. Sandhage, and Barbara D. Boyan. Differential Responses of Osteoblast Lineage Cells to Nanotopographically-Modified, Microroughened Titanium-

Aluminum-Vanadium Alloy Surfaces. *Biomaterials*, 33(35):8986–8994, December 2012.

[75] Rama Krishna Alla, Kishore Ginjupalli, Nagaraja Upadhya, Mohammed Shammas, Rama Krishna Ravi, and Ravichandra Sekhar. Surface Roughness of Implants: A Review. *Trends in Biomaterials and Artificial Organs*, 25(3):112–118, May 2011.

[76] Alexander Kolb, Georg Reinisch, Manuel Sabeti-Aschraf, Alexander Grabl, and Reinhard Windhager. Contamination of surfaces for osseointegration of cementless total hip implants by small aluminium oxide particles: analysis of established implants by use of a new technique. *Journal of Orthopaedic Science: Official Journal of the Japanese Orthopaedic Association*, 18(2):245–249, March 2013.

[77] A. Schuh, U. Holzwarth, W. Kachler, J. Gaske, and G. Zeiler. [Surface characterization of Al2o3-blasted titanium implants in total hip arthroplasty]. *Der Orthopade*, 33(8):905–910, August 2004.

[78] KD Beaty. Implant surface preparation, 03 1999.

[79] Sally R. Frenkel, Jordan Simon, Harold Alexander, Michael Dennis, and John L. Ricci. Osseointegration on metallic implant surfaces: effects of microgeometry and growth factor treatment. *Journal of Biomedical Materials Research*, 63(6):706–713, 2002.

[80] Rolando A. Gittens, Taylor McLachlan, Rene Olivares-Navarrete, Ye Cai, Simon Berner, Rina Tannenbaum, Zvi Schwartz, Kenneth H. Sandhage, and Barbara D. Boyan. The effects of combined micron-/submicron-scale surface roughness and nanoscale features on cell proliferation and differentiation. *Biomaterials*, 32(13):3395–3403, May 2011.

[81] Omid Mashinchian, Lesley-Anne Turner, Matthew J Dalby, Sophie Laurent, Mohammad Ali Shokrgozar, Shahin Bonakdar, Mohammad Imani, and Morteza Mahmoudi. Regulation of stem cell fate by nanomaterial substrates. *Nanomedicine*, 10(5):829–847, March 2015.

[82] Sandrine Lavenus. *Etude des interations entre cellules souches et surface implantaires nanostructurees*. PhD thesis, University of Nantes, 2010.

[83] Gopal K. Mor, Maria A. Carvalho, Ooman K. Varghese, Michael V. Pishko, and Craig A. Grimes. A room-temperature TiO2-nanotube hydrogen sensor able to self-clean photoactively from environmental contamination. *Journal of Materials Research*, 19(02):628–634, 2004.

[84] Joop G. C. Wolke, Jan-Paul C. M. van der Waerden, Christel P. A. T. Klein, and John A. Jansen. Bone Sectioning Using a Modified Inner Diamond Saw. In Yuehuei H. An MD and Kylie L. Martin BSc, editors, *Handbook of Histology Methods for Bone and Cartilage*, pages 253–263. Humana Press, 2003.

[85] Gopal K. Mor, Oomman K. Varghese, Maggie Paulose, Karthik Shankar, and Craig A. Grimes. A review on highly ordered, vertically oriented TiO2 nanotube arrays: Fabrication, material properties, and solar energy applications. *Solar Energy Materials and Solar Cells*, 90(14):2011–2075, September 2006.

[86] Dawei Liu Peng Xiao. Electrochemical and photoelectrical properties of titania nanotube arrays annealed in different gases. *Sensors and Actuators B-chemical - SENSOR ACTUATOR B-CHEM*, 134(2):367–372, 2008.

[87] Viswanathan S. Saji, Han Cheol Choe, and William A. Brantley. An electrochemical study on self-ordered nanoporous and nanotubular oxide on Ti35Nb5Ta7Zr alloy for biomedical applications. *Acta Biomaterialia*, 5(6):2303–2310, July 2009.

[88] Yongsheng Chen Satoshi Kaneco. Fabrication of uniform size titanium oxide nanotubes: Impact of current density and solution conditions. *Scripta Materialia*, (5):373–376, 2007.

[89] S Van Gils, P Mast, E Stijns, and H Terryn. Colour properties of barrier anodic oxide films on aluminium and titanium studied with total reflectance and spectroscopic ellipsometry. *Surface and Coatings Technology*, 185(2):303–310, 2004.

[90] Hsin-Jay Wu, Li-Ling Huang, Sinn-Wen Chen, Eric Jein-Wein Liou, and Yueh-Tse Lee. Surface characterization of anodized dental archwires and miniscrews. *Journal of the Taiwan Institute of Chemical Engineers*, 40(5):563–572, September 2009.

[91] Chiao-ling Yang, Feng ling Chen, and Sinn wen Chen. Anodization of the dental arch wires. *Materials Chemistry and Physics*, 100(2):268–274, December 2006.

[92] V. C. Anitha, Deepthy Menon, Shantikumar V. Nair, and R. Prasanth. Electrochemical tuning of titania nanotube morphology in inhibitor electrolytes. *Electrochimica Acta*, 55(11):3703–3713, April 2010.

[93] Rosales Leal. Effect of roughness, wettability and morphology of engineered titanium surfaces on osteoblast-like cell adhesion. *Colloids and Surfaces A Physicochemical and Engineering Aspects*, 365:222–229, 2010.

[94] Marzieh Abbasi-Firouzjah Fatemeh Rezaei. Investigation of antibacterial and wettability behaviours of plasma-modified PMMA films for application in ophthalmology. *Journal of Physics D Applied Physics*, 47(8), 2014.

[95] Rajini P. Antony, Tom Mathews, Sitaram Dash, Ashok K. Tyagi, and Baldev Raj. X-ray photoelectron spectroscopic studies of anodically synthesized self aligned TiO2 nanotube arrays and the effect of electrochemical parameters on tube morphology. *Materials Chemistry and Physics*, 132:957–966, February 2012.

[96] C. P. Ferreira, M. C. GonÃ§alves, R. Caram, R. Bertazzoli, and C. A. Rodrigues. Effects of substrate microstructure on the formation of oriented oxide nanotube arrays on Ti and Ti alloys. *Applied Surface Science*, 285, Part B:226–234, November 2013.

[97] Magdalena Jarosz, Kapusta-Ko&#x142, Joanna Odziej, Jasku&#x142, Marian A, and Grzegorz D. Sulka. Effect of Different Polishing Methods on Anodic Titanium Dioxide Formation. *Journal of Nanomaterials*, 2015:e295126, March 2015.

[98] Ning Liu, Kiyoung Lee, and Patrik Schmuki. Small diameter TiO2 nanotubes vs. nanopores in dye sensitized solar cells. *Electrochemistry Communications*, 15(1):1–4, February 2012.

[99] A. Jaroenworaluck, D. Regonini, C. R. Bowen, and R. Stevens. A microscopy study of the effect of heat treatment on the structure and properties of anodised TiO2 nanotubes. *Applied Surface Science*, 256(9):2672–2679, 2010.

[100] Jing Zhang, Meijun Li, Zhaochi Feng, Jun Chen, and Can Li. UV Raman Spectroscopic Study on TiO2. I. Phase Transformation at the Surface and in the Bulk. *The Journal of Physical Chemistry B*, 110(2):927–935, January 2006.

[101] Young-Taeg Sul. Electrochemical growth behavior, surface properties, and enhanced in vivo bone response of TiO2 nanotubes on microstructured surfaces of blasted, screw-shaped titanium implants. *International Journal of Nanomedicine*, 5:87–100, 2010.

[102] Cheul-Goo Kang, Young-Bum Park, Hyunmin Choi, Seunghan Oh, Keun-Woo Lee, Seong-Ho Choi, and June-Sung Shim. Osseointegration of implants surface treated with various diameters of tio_2 nanotubes in rabbit. *Journal of Nanomaterials*, 2015:e634650, January 2015.

[103] Young-Ah Yi, Young-Bum Park, Hyunmin Choi, Keun-Woo Lee, Sun-Jai Kim, Kwang-Mahn Kim, Seunghan Oh, and June-Sung Shim. The Evaluation of Osseointegration of Dental Implant Surface with Different Size of TiO_2 Nanotube in Rats. *Journal of Nanomaterials*, 2015:e581713, January 2015.

[104] A. Mazare, M. Dilea, D. Ionita, I. Titorencu, V. Trusca, and E. Vasile. Changing bioperformance of TiO2 amorphous nanotubes as an effect of inducing crystallinity. *Bioelectrochemistry*, 87:124–131, 2012.

[105] Kakoli Das, Susmita Bose, and Amit Bandyopadhyay. Surface modifications and cell & materials interactions with anodized Ti. *Acta Biomaterialia*, 3(4):573–585, July 2007.

[106] M. Mousny, X. Banse, L. Wise, E. T. Everett, R. Hancock, R. Vieth, J. P. Devogelaer, and M. D. Grynpas. The genetic influence on bone susceptibility to fluoride. *Bone*, 39(6):1283–1289, December 2006.

[107] A. L. Khandare, P. Suresh, P. Uday Kumar, N. Lakshmaiah, N. Manjula, and G. Shanker Rao. Beneficial Effect of Copper Supplementation on Deposition of Fluoride in Bone in Fluoride- and Molybdenum-Fed Rabbits. *Calcified Tissue International*, 77(4):233–238, September 2005.

[108] Lucas Makoto Shimoraha Flavia Godoy Iano Marcela Mitsuko Yanai Tania Mary Cestari Marilia Afonso Rabelo Buzalaf Rodrigo Cardoso de Oliveira Mileni da Silva Fernandes, Gisele Miyamura Martins. Fluoride effect on the process of alveolar bone repair in rats: evaluation of activity of mmp-2 and 9. *RSBO*, 9(3):229–237, July 2012.

[109] T. Berglundh, I. Abrahamsson, J.-P. Albouy, and J. Lindhe. Bone healing at implants with a fluoride-modified surface: an experimental study in dogs. *Clinical Oral Implants Research*, 18(2):147–152, April 2007.

[110] E.T. Everett. Fluorides Effects on the Formation of Teeth and Bones, and the Influence of Genetics. *Journal of Dental Research*, 90(5):552–560, May 2011.

[111] Cordova Jara Luis. *Microenvironnement osseux et ostéolyse: application au descellement aseptique des implants orthopédiques*. PhD thesis, University of Nantes, 2014.

[112] Preetinder Singh. Understanding peri-implantitis: A strategic review. *Journal of Oral Implantology*, 37(5):622–626, 2010.

[113] Rui Xing, Laetitia Salou, Sébastien Taxt-Lamolle, Janne E. Reseland, Stale P. Lyngstadaas, and Havard J. Haugen. Surface hydride on titanium by cathodic polarization promotes human gingival fibroblast growth. *Journal of Biomedical Materials Research. Part A*, 102(5):1389–1398, 2014.

[114] Manjeet Mapara, Betsy Sara Thomas, and K. M. Bhat. Rabbit as an animal model for experimental research. *Dental Research Journal*, 9(1):111–118, 2012.

[115] Laurent Le Guehennec, Eric Goyenvalle, Marco-Antonio Lopez-Heredia, Pierre Weiss, Yves Amouriq, and Pierre Layrolle. Histomorphometric analysis of the osseointegration of four different implant surfaces in the femoral epiphyses of rabbits. *Clinical Oral Implants Research*, 19(11):1103–1110, November 2008.

[116] Julie RozÃ©, Alain Hoornaert, and Pierre Layrolle. Correlation between primary stability and bone healing of surface treated titanium implants in the femoral epiphyses of rabbits. *Journal of Materials Science. Materials in Medicine*, 25(8):1941–1951, August 2014.

[117] Hans Jacob Ronold, Stale Petter Lyngstadaas, and Jan Eirik Ellingsen. A study on the effect of dual blasting with tio_2 on titanium implant surfaces on functional attachment in bone. *Journal of Biomedical Materials Research. Part A*, 67(2):524–530, November 2003.

[118] Jung-Woo Koh, Jae-Ho Yang, Jung-Suk Han, Jai-Bong Lee, and Sung-Hun Kim. Biomechanical evaluation of dental implants with different surfaces: Removal torque and resonance frequency analysis in rabbits. *The Journal of Advanced Prosthodontics*, 1(2):107–112, July 2009.

[119] Lars M Bjursten, Lars Rasmusson, Seunghan Oh, Garrett C Smith, Karla S Brammer, and Sungho Jin. Titanium dioxide nanotubes enhance bone bonding in vivo. *Journal of biomedical materials research. Part A*, 92(3):1218–1224, March 2010.

[120] L. Sennerby, P. Thomsen, and L. E. Ericson. A morphometric and biomechanic comparison of titanium implants inserted in rabbit cortical and cancellous bone. *The International Journal of Oral & Maxillofacial Implants*, 7(1):62–71, 1992.

[121] Sangeeta Dhir. Biofilm and dental implant: The microbial link. *Journal of Indian Society of Periodontology*, 17:5–11, 2013.

[122] Bey A Khan S Hadi SA, Ashfaq N. Biological factors responsible for failure of osseointegration in oralimplants. *Biology and Medicine*, 3(2):164–170, 2011.

[123] Cho-Tung Yip, Min Guo, Haitao Huang, Limin Zhou, Yu Wang, and Chuanjun Huang. Open-ended TiO2 nanotubes formed by two-step anodization and their application in dye-sensitized solar cells. *Nanoscale*, 4(2):448–450, January 2012.

[124] J. W. Vehof, A. E. de Ruijter, P. H. Spauwen, and J. A. Jansen. Influence of rhBMP-2 on rat bone marrow stromal cells cultured on titanium fiber mesh. *Tissue Engineering*, 7(4):373–383, 2001.

[125] Rozalia Dimitriou, Eleftherios Tsiridis, and Peter V. Giannoudis. Current concepts of molecular aspects of bone healing. *Injury*, 36(12):1392–1404, December 2005.

[126] S. D. Cook. Preclinical and clinical evaluation of osteogenic protein-1 (BMP-7) in bony sites. *Orthopedics*, 22(7):669–671, July 1999.

[127] L. Nordsletten and J. E. Madsen. The Effect of Bone Morphogenetic Proteins in Fracture Healing. *Scandinavian Journal of Surgery*, 95(2):91–94, June 2006.

[128] Wellington K. Hsu and Jeffrey C. Wang. The use of bone morphogenetic protein in spine fusion. *The Spine Journal*, 8(3):419–425, May 2008.

[129] Hongbo Wei, Shuyi Wu, Zhihong Feng, Wei Zhou, Yan Dong, Guofeng Wu, Shizhu Bai, and Yimin Zhao. Increased fibroblast functionality on CNN2-loaded titania nanotubes. *International Journal of Nanomedicine*, 7:1091–1100, 2012.

[130] Masahiro Asano, Satoshi Kubota, Tohru Nakanishi, Takashi Nishida, Tomoichiro Yamaai, Gen Yosimichi, Kazumi Ohyama, Tomosada Sugimoto, Yoji Murayama, and Masaharu Takigawa. Effect of connective tissue growth factor (CCN2/CTGF) on proliferation and differentiation

of mouse periodontal ligament-derived cells. *Cell Communication and Signaling*, 3(1):11, October 2005.

[131] H. P. Gerber, T. H. Vu, A. M. Ryan, J. Kowalski, Z. Werb, and N. Ferrara. VEGF couples hypertrophic cartilage remodeling, ossification and angiogenesis during endochondral bone formation. *Nature Medicine*, 5(6):623–628, June 1999.

[132] Nisarg J. Shah, Mara L. Macdonald, Yvette M. Beben, Robert F. Padera, Raymond E. Samuel, and Paula T. Hammond. Tunable dual growth factor delivery from polyelectrolyte multilayer films. *Biomaterials*, 32(26):6183–6193, September 2011.

[133] Sarabjeet S. Suri, Hicham Fenniri, and Baljit Singh. Nanotechnology-based drug delivery systems. *Journal of Occupational Medicine and Toxicology*, 2(1):16, December 2007.

[134] Tolou Shokuhfar, Suman Sinha-Ray, Cortino Sukotjo, and Alexander L. Yarin. Intercalation of anti-inflammatory drug molecules within TiO2 nanotubes. *RSC Advances*, 3(38):17380–17386, September 2013.

[135] Zhang Wang, Ping Li, Fei Luo, Dan Mao, and Xiu Feng Xiao. Titania nanotube arrays load with ibuprofen by solvothermal and its release behavior. In *Advanced Materials Research*, volume 1030, pages 2368–2371. Trans Tech Publ, 2014.

[136] Huiying Jia and Lei L. Kerr. Sustained ibuprofen release using composite poly(lactic-co-glycolic acid)/titanium dioxide nanotubes from Ti implant surface. *Journal of Pharmaceutical Sciences*, 102(7):2341–2348, July 2013.

[137] BaoHong Zhao, WeiMing Tian, HaiLan Feng, In-Seop Lee, and FuZhai Cui. Effects of RGD peptide grafting to titanium dental implants on the adhesion of human gingival fibroblasts and epithelial cells. *Current Applied Physics*, 5(5):407–410, July 2005.

[138] Xuezhong He, Junyu Ma, and Esmaiel Jabbari. Effect of grafting RGD and BMP-2 protein-derived peptides to a hydrogel substrate on osteogenic differentiation of marrow stromal cells. *Langmuir: the ACS journal of surfaces and colloids*, 24(21):12508–12516, November 2008.

[139] Yuanping Ma, Zhenting Zhang, Yiran Liu, Hongyi Li, Na Wang, Wenwen Liu, Wenjun Li, Lingling Jin, Jinshu Wang, and Su Chen. Nanotubes

Functionalized with BMP2 Knuckle Peptide Improve the Osseointegration of Titanium Implants in Rabbits. *Journal of Biomedical Nanotechnology*, 11(2):236–244, February 2015.

[140] Institut National du Cancer (INC) HAUTE AUTORITE DE SANTE (HAS). Tumeur maligne, affection maligne du tissu lymphatique ou hématopoïétique : Cancer des voies aérodigestives supérieures. 2009.

[141] P. T. Maddox and L. Davies. Trends in Total Laryngectomy in the Era of Organ Preservation: A Population-Based Study. *Otolaryngology – Head and Neck Surgery*, 147(1):85–90, July 2012.

[142] J. F. Regnard, P. Fourquier, and P. Levasseur. Results and prognostic factors in resections of primary tracheal tumors: a multicenter retrospective study. The French Society of Cardiovascular Surgery. *The Journal of Thoracic and Cardiovascular Surgery*, 111(4):808–813; discussion 813–814, 1996.

[143] Dispositif Ã clapets destine à etre implanté au sein d'un larynx dysfonctionnel ou d'une prothese de larynx. Classification internationale A61L27/14, A61M16/04, A61F2/20; Classification coopÃ©rative A61F2/203, A61M16/0468; Classification europÃ©enne A61F2/20B.

[144] Guohua Liu, Kaiying Wang, Nils Hoivik, and Henrik Jakobsen. Progress on free standing and flow through TiO2 nanotube membranes. *Solar Energy Materials and Solar Cells*, 98:24–38, 2012.

[145] Wei Wei, Steffen Berger, Christina Hauser, Karsten Meyer, Min Yang, and Patrik Schmuki. Transition of TiO2 nanotubes to nanopores for electrolytes with very low water contents. *Electrochemistry Communications*, 12(9):1184–1186, 2010.

[146] Dongliang Yu, Xufei Zhu, Zhen Xu, Xiaomin Zhong, Qunfang Gui, Ye Song, Shaoyu Zhang, Xiaoyuan Chen, and Dongdong Li. Facile Method to Enhance the Adhesion of TiO2 Nanotube Arrays to Ti Substrate. *ACS Applied Materials & Interfaces*, 6(11):8001–8005, 2014.

[147] Guoge Zhang, Haitao Huang, Yuanshuai Liu, and Limin Zhou. Fabrication of crack-free anodic nanoporous titania and its enhanced photoelectrochemical response. *Applied Catalysis B: Environmental*, 90:262–267, 2009.

[148] S. Baradaran, W. J. Basirun, E. Zalnezhad, M. Hamdi, Ahmed A. D. Sarhan, and Y. Alias. Fabrication and deformation behaviour of multilayer Al2o3/Ti/TiO2 nanotube arrays. *Journal of the Mechanical Behavior of Biomedical Materials*, 20:272–282, 2013.

[149] Philippe StempflÃ©, AurÃ©lien Besnard, Nicolas Martin, Anne Domatti, and Jamal Takadoum. Accurate control of friction with nanosculptured thin coatings: Application to gripping in microscale assembly. *Tribology International*, 59:67–78, 2013.

[150] Philippe Schultz, Dominique Vautier, Ludovic Richert, Nadia Jessel, Youssef Haikel, Pierre Schaaf, Jean-Claude Voegel, Joelle Ogier, and Christian Debry. Polyelectrolyte multilayers functionalized by a synthetic analogue of an anti-inflammatory peptide, alpha-MSH, for coating a tracheal prosthesis. *Biomaterials*, 26(15):2621–2630, 2005.

[151] Charline Allonneau, Eric Olmos, StÃ©phane Guyot, Eric Ferret, Patrick Gervais, and Ramy Cachon. Hydrodynamic characterization of a new small-scale reactor mixed by a magnetic bar. *Biochemical Engineering Journal*, 96:29–37, 2015.

[152] Scale-up et scale-down des bioreacteurs: methodologie et outils, journal = Cours PPT - ONIRIS, author = Eric Olmos, Université de Lorraine, year = 2014,.

[153] D. K. Dennison, M. B. Huerzeler, C. Quinones, and R. G. Caffesse. Contaminated implant surfaces: an in vitro comparison of implant surface coating and treatment modalities for decontamination. *Journal of Periodontology*, 65(10):942–948, October 1994.

[154] P. Andrew Norowski and Joel D. Bumgardner. Biomaterial and antibiotic strategies for peri-implantitis: A review. *Journal of Biomedical Materials Research Part B: Applied Biomaterials*, 88B(2):530–543, February 2009.

[155] W. Zimmerli. Clinical presentation and treatment of orthopaedic implant-associated infection. *Journal of Internal Medicine*, 276(2):111–119, August 2014.

[156] I. V. Sukhorukova, A. N. Sheveyko, Ph. V. Kiryukhantsev-Korneev, N. Y. Anisimova, N. A. Gloushankova, I. Y. Zhitnyak, J. Benesova, E. Amler, and D. V. Shtansky. Two approaches to form antibacterial surface: Doping with bactericidal element and drug loading. *Applied Surface Science*, 330:339–350, March 2015.

[157] Lidy E. Fratila-Apachitei Bogdan S Necula. In vitro antibacterial activity of porous tio2 ag composite layers against methicillin-resistant Staphylococcus aureus. *Acta biomaterialia*, 5(9):3573–80, 2009.

[158] Laurent Bedel Jitti Mungkalasiri. CVD elaboration of nanostructured Ag thin films with efficient antibacterial properties. *Chemical Vapor Deposition*, 16(1):477–484, 2010.

[159] Eugen Panaitescu Joanna Podporska-Carroll. Antimicrobial properties of highly efficient photocatalytic TiO2 nanotubes. *Applied Catalysis B: Environmental*, 176, 2015.

[160] Dusan Losic Moom Sinn Aw, Karan Gulati. Controlling drug release from titania nanotube arrays using polymer nanocarriers and biopolymer coating. *Journal of Biomaterials and Nanobiotechnology*, 2:477–484, 2011.

[161] Shenglin Mei, Huaiyu Wang, Wei Wang, Liping Tong, Haobo Pan, Changshun Ruan, Qianli Ma, Mengyuan Liu, Huiling Yang, Liang Zhang, Yicheng Cheng, Yumei Zhang, Lingzhou Zhao, and Paul K. Chu. Antibacterial effects and biocompatibility of titanium surfaces with graded silver incorporation in titania nanotubes. *Biomaterials*, 35(14):4255–4265, May 2014.

[162] Xianfeng Gao, Jianyang Li, Joel Baker, Yang Hou, Dongsheng Guan, Junhong Chen, and Chris Yuan. Enhanced photovoltaic performance of perovskite solar cells with freestanding tio2 nanotube array films. *Chemical Communications*, 50(48):6368–6371, June 2014.

[163] Lingzhou Zhao, Hairong Wang, Kaifu Huo, Lingyun Cui, Wenrui Zhang, Hongwei Ni, Yumei Zhang, Zhifen Wu, and Paul K. Chu. Antibacterial nano-structured titania coating incorporated with silver nanoparticles. *Biomaterials*, 32(24):5706–5716, August 2011.

[164] C. Gasqueres, G. Schneider, R. Nusko, G. Maier, E. Dingeldein, and A. Eliezer. Innovative antibacterial coating by anodic spark deposition. *Surface & coatings technology*, 206(15):3410–3414, 2012.

[165] Bogdan S. Necula, Lidy E. Fratila-Apachitei, Sebastian A. J. Zaat, Iulian Apachitei, and Jurek Duszczyk. In vitro antibacterial activity of porous TiO2-Ag composite layers against methicillin-resistant Staphylococcus aureus. *Acta Biomaterialia*, 5(9):3573–3580, November 2009.

[166] Paula Sfirloaga Carmen Lazau. Development of a novel fast-hydrothermal method for synthesis of Ag-doped TiO 2 nanocrystals. *Materials Letters - MATER LETT*, 65(2):337–339, 2011.

[167] Y. H. Gao and M. Yamaguchi. Zinc enhancement of genistein's anabolic effect on bone components in elderly female rats. *General Pharmacology*, 31(2):199–202, August 1998.

[168] Masayoshi Yamaguchi, Satoshi Uchiyama, Kaori Ishiyama, and Ken Hashimoto. Oral administration in combination with zinc enhances beta-cryptoxanthin-induced anabolic effects on bone components in the femoral tissues of rats in vivo. *Biological & Pharmaceutical Bulletin*, 29(2):371–374, February 2006.

[169] Xiupeng Wang, Atsuo Ito, Yu Sogo, Xia Li, and Ayako Oyane. Zinc-containing apatite layers on external fixation rods promoting cell activity. *Acta Biomaterialia*, 6(3):962–968, March 2010.

[170] D Chen, L C Waite, and W M Pierce, Jr. In vitro effects of zinc on markers of bone formation. *Biological trace element research*, 68(3):225–234, June 1999.

[171] Wen-Li Du, Shan-Shan Niu, Ying-Lei Xu, Zi-Rong Xu, and Cheng-Li Fan. Antibacterial activity of chitosan tripolyphosphate nanoparticles loaded with various metal ions. *Carbohydrate Polymers*, 75(3):385–389, February 2009.

[172] Kaifu Huo, Xuming Zhang, Hairong Wang, Lingzhou Zhao, Xuanyong Liu, and Paul K Chu. Osteogenic activity and antibacterial effects on titanium surfaces modified with Zn-incorporated nanotube arrays. *Biomaterials*, 34(13):3467–3478, April 2013.

[173] Andrei Ghicov, Hiroaki Tsuchiya, Jan M. Macak, and Patrik Schmuki. Titanium oxide nanotubes prepared in phosphate electrolytes. *Electrochemistry Communications*, 7(5):505–509, May 2005.

[174] Hyo Tae Kim Alex, er Golovchansky and Yoonho Kim. Zinc titanates dielectric ceramics prepared by sol-gel process. *J. Korean Phys.Soc.*, 32:1167–1169, 1998.

[175] Hyo Tae Kim, Yoonho Kim, Matjaz Valant, and Danilo Suvorov. Titanium Incorporation in Zn2Tio4 Spinel Ceramics. *Journal of the American Ceramic Society*, 84(5):1081–1086, 2001.

[176] G. A. Crawford, N. Chawla, K. Das, S. Bose, and A. Bandyopadhyay. Microstructure and deformation behavior of biocompatible TiO2 nanotubes on titanium substrate. *Acta Biomaterialia*, 3(3):359–367, 2007.

[177] http://www.leem.org/sites/default/files/1425.pdf.

[178] Nanomatériaux et médecine : des besoins nouveaux en termes de caractérisation.

[179] Scientific Committee on Emerging and Newly Identified Health Risks SCENIHR. Guidance on the determination of potential health effect of nanomaterials used in medical devices. January 2015.

[180] P. F. Doorn, P. A. Campbell, J. Worrall, P. D. Benya, H. A. McKellop, and H. C. Amstutz. Metal wear particle characterization from metal on metal total hip replacements: transmission electron microscopy study of periprosthetic tissues and isolated particles. *Journal of Biomedical Materials Research*, 42(1):103–111, October 1998.

[181] Plinio Senna, Altair Antoninha Del Bel Cury, Stephen Kates, and Luiz Meirelles. Surface Damage on Dental Implants with Release of Loose Particles after Insertion into Bone. *Clinical Implant Dentistry and Related Research*, November 2013.

[182] Kw Frisken, Gw Dandie, S. Lugowski, and G. Jordan. A Study of Titanium Release into Body Organs Following the Insertion of Single Threaded Screw Implants into the Mandibles of Sheep. *Australian Dental Journal*, 47(3):214–217, September 2002.

[183] TP Chaturvedi. Allergy related to dental implant and its clinical significance. *Clinical, Cosmetic and Investigational Dentistry*, 5:57–61, August 2013.

l'université nantes angers le mans
COMMUNAUTÉ D'UNIVERSITÉS ET ÉTABLISSEMENTS

UNIVERSITÉ DE NANTES

Thèse de Doctorat

Laëtitia SALOU

New bioactive surfaces for titanium implants

Research, characterisation and industrial development

Résumé

Biocompatible et résistant à la corrosion des fluides biologiques, le titane reste cependant un matériau inerte : il ne favorise pas de manière active l'intégration osseuse autour de l'implant. La modification de surface du titane à l'échelle nanométrique permet de moduler l'expression des gènes favorisant l'adhésion et la différentiation cellulaire par un mécanisme de mécano-transduction. Dans ces travaux de thèse, nous nous sommes donc attachés développer, caractériser et appliquer une surface nanostructurée directement sur des dispositifs médicaux.
Dans un premier temps, notre étude s'est concentrée sur la préparation et la caractérisation physicochimique. Après l'obtention de surface reproductible sur petits échantillons, nos recherches se sont axées sur la caractérisation biologique de la surface. Des études in-vivo réalisées chez le lapin ont permis de montrer une accroche osseuse renforcée et bonne ostéointégration de la surface nanostructurée en comparaison avec des surfaces couramment utilisées sur le marché. L'application de cette nouvelle surface sur pièce plus complexe comme les prothèses de trachée, nous a permis de rendre compte d'un phénomène de délamination de la couche de nanostructure. Nos recherches se sont donc orientées vers la problématique de tenue mécanique de la surface avec la réalisation de nano scratch-test et tribologie. Un sujet dans l'air du temps, puisqu'une nouvelle règlementation européenne concernant l'incorporation de nanomatériaux dans les dispositifs médicaux rentrera en vigueur en 2017.
En conclusion, ces travaux nous permettent de proposer une nouvelle surface améliorant l'intégration tissulaire interessante pour une application médicale.

Mots clés
Titane ; Nanostructure ; Anodisation ; Ostéointégration ; Dispositifs médicaux ; Mechanotransduction ; In vivo ; Propriétés mécaniques

Abstract

Biocompatible and corrosion resistant regarding biological fluids, titanium is still an inert material: it does not participate actively at the tissue-integration around the implant. Surface modification of titanium at nanoscale can promote cell adhesion and differentiation by modulate genes expression due to a phenomenon of mechano-transduction. In this thesis, we have focused on the development, the characterization and the direct application of our nanostructured surface of medical devices.
First of all, our study focused on the preparation and physicochemical characterization. After obtaining reproducible surfaces on small samples, our research has focused on the biological characterization of the surface. In-vivo studies conducted in rabbits have allowed us to show similar biomechanical attachment and good osseointegration of the nanostructured surface compared to commonly used surfaces on the market. The application of this new surface on more complex titanium implant such as tracheal prosthesis, has allowed us to observe delamination phenomenon of the nanostructure layer. Therefore, our research was oriented towards the problem of mechanical strength of the surface with the realization of nano scratch test and tribology. A topic in the zeitgeist, as a new EU regulation for medical devices which incorporate nanomaterials will take effect in 2017.
To conclude, this work enable to propose a nano-surface with promising results of tissues integration required for medical device.

Key Words
Titanium ; Nanostructure ; Anodisation ; Osteointegration ; Medical devices ; Mechanotransduction ; *In vivo* ; Mechanical properties